Investigating the Importance of Physiological Cell Culture Conditions in Modeling Cancer Metabolism and Metabolic Reprogramming

Georgina Louise Gardner, B.Sc. (Honours)

Submitted in partial fulfillment of the requirements for the degree of
Master of Science
Biological Sciences (Cell and Molecular Biology)

Faculty of Mathematics and Science
Brock University
St. Catharines, ON, Canada

ABSTRACT

Standard cell culture conditions do not mimic the physiological environment of cancer cells. Traditional culture media contain metabolites at concentrations that far exceed conditions measured *in vivo*, and oxygen is often unregulated, exposing cells to atmospheric oxygen concentrations (~18%), rather than the 0-3% O_2 measured in solid tumours *in vivo*. Recently, plasma-like media have been developed to address these limitations, aiming to improve culture conditions and maintain biologically relevant cancer phenotypes *in vitro*. However, these conditions remain unrepresentative of interstitial fluid in solid tumours. The goal of this thesis was to investigate how physiological culture conditions affect cancer cell behaviours, specifically cell metabolism and adaptive metabolic responses. In the first data chapter of this thesis, I explored nutrient exhaustion in physiological plasma-like medium (Plasmax) at 18% and 5% O_2, and the adaptive mechanisms by which cancer cells can maintain survival under metabolic stress conditions. Here, I found that glucose and amino acid depletion from Plasmax over 48 hours is associated with several adaptive mechanisms consistent with metabolic reprogramming *in vivo*. Given these responses, I hypothesized that a media formulation designed using metabolite concentrations from tumour interstitial fluid may modulate metabolic phenotypes in a similar manner, providing a more physiologically relevant culture model for cancerous cells. Data chapter 2 addresses this hypothesis, whereby I formulated a novel cell culture medium using quantitative metabolite data from murine pancreatic ductal adenocarcinoma (PDAC) tumour interstitial fluid, named Tumour Microenvironment Medium (TMEM), and investigated the effects of TMEM and 1.5% O_2 on an adapted murine PDAC cell line (KPCY). Importantly, I found that tumour-like conditions elicited a substantial transcriptional and functional response in cultured cells, modulating cell proliferation, migration, glucose utilization, and mitochondrial bioenergetics in ways relevant to *in vivo* cancer biology. Overall, the results of this thesis highlight the responsiveness of cultured cells to their environment, and the importance of representative culture conditions in the acquisition of biologically accurate experimental data.

KEYWORDS

Cell culture; media; oxygen; tumour microenvironment; cancer; physiological; physioxia; RNA-seq; bioenergetics; Plasmax; metabolism; metabolic remodelling

ACKNOWLEDGEMENTS

First, I would like to offer my greatest appreciation to my supervisor, Dr. Jeff Stuart, for showing me a world of scientific learning, critical thinking, and excitement that I never knew possible before starting in the lab. Dr. Stuart, I cannot thank you enough for the incredible mentorship and support that you have shown me over the past 3 years. The passion and care that you put into every project and every student goes unmatched. You have instilled in me an intrinsic need for knowledge and learning that will carry with me for my career. You have taught me to be a careful, humble, and eager scientist, and have granted me amazing opportunities to learn new skills and become confident in myself. Thank you.

I also would like to thank my thesis advisory committee, Dr. Gaynor Spencer and Dr. Rebecca MacPherson, for their feedback and support in the completion of this thesis project. Thank you for dedicating time to committee meetings and reviewing this manuscript. The faculty at Brock are incredible.

To my family, thank you for loving and supporting me at every stage of this degree. Thank you to my mum in particular, who has continued to push me to be my best in all aspects of my life. Thank you for being so understanding and encouraging. To Levi, I struggle to put into words how thankful I am to have your support. Without you, I would have been wreck to say the least! Thank you for your constant care, consideration, and love. To my friends for life, Alexis Clute and Daravan Phimmanao, thank you for always being amazing and constant lights in my life.

Next, I would like to thank all of the amazing friends and lab mates that I have made on the fifth floor of Cairns. Anel Turgambayeva and Marvel Megaly, thank you for being great friends and supports. I have truly cherished getting to know you both the past few years and have been so grateful to learn alongside incredible female scientists. Fereshteh Moradi and Olivia Bagshaw, the same sentiments go to you and beyond! Thank you for training and supporting me early in the lab and continuing to inspire me as amazing working women in STEM. Mariska Andrade and Jake Wiebe, thank you for being hilarious friends and lab mates (ish). Getting to know you both this year has been amazing. Lucas Maddalena, thank for everything, everywhere, all at once. You have taught me so much. Danielle Martin, thank you for being my only friend at Brock for the longest time. We are two peas in a pod. Finally, thank you to my amazing lab mate and best friend, Ricardo Alva. Ricardo, no words can describe how much meeting you has meant to me. We both know we needed each other to get to the end of this. I am thankful every day to know you.

CONTRIBUTIONS

I performed all experiments, statistical analysis, chapter writing, and figure/table presentation.

For RNA-seq experiments in Chapter 2 and 3, Novagene performed sample preparation, RNA library preparation, sequencing, reference genome data mapping, and differential gene expression analysis. I performed initial RNA quality control on samples, additional differential gene expression filtering with Novagene differential expression data, and all functional enrichment analysis.

Table of Contents

LIST OF FIGURES

Chapter 1

Chapter 2

Chapter 3

LIST OF TABLES

Chapter 1

Chapter 2

Chapter 3

LIST OF ABBREVIATIONS

4E-BP1	eukaryotic translation initiation factor 4E-binding protein 1
ACC1/2	Acetyl-CoA carboxylase 1/2
ADM	Adrenomedullin
ADP	Adenosine diphosphate
AFT2	Activating transcription factor 2
AMP	Adenosine monophosphate
AMPK	AMP-activated protein kinase
ANG	Angiogenin
ASCT2	Alanine-serine-cysteine transporter 2
ASL	Argininosuccinate lyase
ASS1	Argininosuccinate synthase 1
ATP	Adenosine triphosphate
BCAAT	Branched chain amino acid transporter
CAF	Cancer-associated fibroblast
CAMKK2	Calcium/calmodulin-dependent protein kinase kinase 2
COX	Cytochrome c oxidase
DMEM	Dulbecco's Modified Eagle Medium
EAAT3	Excitatory amino acid transporter 3
eEF2K	Eukaryotic elongation factor 2 kinase
eIF4E/2a	Eukaryotic translation initiation factor 4E/2a
EMS	Epithelial-to-mesenchymal transition
EMT	Epithelial-mesenchymal transition
ER	Endoplasmic reticulum
ETC	Electron transport chain
FADH2	Flavin adenine dinucleotide (reduced form)
FAK	Focal adhesion kinase
FDG	Fluorodeoxyglucose
GAP	GTPase-activating protein
GCN2	General control non-repressible 2
GEF	Guanine nucleotide exchange factor
GLUT	Glucose transporter
GTP	Guanosine triphosphate
HIF	Hypoxia-inducible factor
HPLM	Human Plasma-Like Medium
HRE	Hypoxia-response element
IFP	Integrated stress response
L-2HG	L-2-Hydroxyglutarate
LAT1	Large neutral amino acid transporter 1
LDH	Lactate dehydrogenase

LKB1	Liver kinase B1
MEM	Minimum Essential Medium
MFF	Mitochondrial fission factor
Mfn1/2	Mitofusin 1/2
mLST8	Mammalian lethal with sec-13 protein 8
mTOR	Mammalian target of rapamycin
mTORC1/2	Mammalian target of rapamycin complex 1/2
NADH	Nicotinamide adenine dinucleotide (reduced form)
OXPHOS	Oxidative phosphorylation
PDAC	Pancreatic ductal adenocarcinoma
PDK	Pyruvate dehydrogenase kinase
PFK	Phosphofructokinase
PFKFB2/3	6-phosphofructo-2-kinase/fructose-2,6-biphosphatase isoforms
PHD	Prolyl hydroxylase domain-containing protein
PHGDH	Phosphoglycerate dehydrogenase
PIKK	Phosphatidylinositol 3-kinase-related kinase
PKM2	Pyruvate kinase M2
PRPS	Phosphoribosyl pyrophosphate synthetase
pVHL	Von Hippel-Lindau tumor suppressor
SREBP	Sterol regulatory element-binding protein
TCA	Tricarboxylic acid cycle
TGF	Transforming growth factor
TIF	Transcription initiation factor
TMEM	Tumour microenvironment medium
TSC	Tuberous sclerosis complex
ULK1	Unc-51-like kinase 1
UMPS	Uridine monophosphate synthetase
VEGF	Vascular endothelial growth factor

Chapter 1: Introduction and Literature Review

1.1 GENERAL INTRODUCTION

Cell growth and function is dependent on the availability, uptake and utilization of metabolites from the extracellular environment. Energy acquisition through the catabolism of metabolic substrates is necessary for biological processes. Additionally, amino acids, carbohydrates, fatty acids, and nucleotides serve as biomass precursors. Thus, to maintain normal cell function and viability, metabolic demands must be met by the extracellular metabolome. If not, coordinated cellular responses are initiated to reduce metabolic demand and conserve energy stores. Conversely, if metabolites are in excess, as is the case for some metabolic diseases, metabolism may exceed normal demands, leading to oxidative stress.

Metabolic demand varies according to the functions and replication rates of cells (Elia, 1992; Schmidz-Nielsen 1982; Wang et al., 2010). Additionally, the capacity of cells to respond to metabolic stress is dependent on their flexibility in using different energy sources, the storage of energy reserves, and their ability to regulate energy-consuming processes. For example, while most cell types throughout the body are able to use glucose and fatty acids for energy production, neurons primarily utilize glucose, and are therefore more vulnerable to hypoglycemia (Auer et al., 1984; Graveling et al., 2013). On the other hand, hepatocytes, adipocytes, and myocytes store excess carbon as lipids and glycogen, making them increasingly tolerant to metabolic stress. Interestingly, cellular tolerance to hypoxia is in part related to the function of cells, in particular their reliance on ion-motive ATPases (Boutilier & St-Pierre, 2000). With ion pumping accounting for over 80% of ATP consumption in neurons, the essential excitability function of these cells again makes them more vulnerable to ATP depletion and cell death (Attwell & Laughlin, 2001). Alternatively, muscle cells, including cardiomyocytes, can modulate their function and reduce contractile activity for an extended period in response to low intracellular ATP levels, and are thus more tolerant to prolonged hypoxia exposure (Budinger et al., 1998).

To meet metabolic demands, mammalian cells have highly integrated mechanisms that sense energy and nutrient availability, and subsequently coordinate catabolic and anabolic processes. Overall, cell survival requires that net energy production and metabolic availability is sufficient to support basal energy consuming processes required for cell maintenance, repair and function. Specifically, ATP and biomass required for active transport, signal transduction and synthesis of biomolecules must be available, regardless of the proliferative, quiescent or post-mitotic state of the cell (Buttgereit & Brand, 1995; Palm & Thompson, 2017). Upon metabolic

stress, ATP synthesis must thus be coupled to essential cellular processes, with non-essential cellular processes inhibited.

In cancer cells, oncogenic regulation of cell growth and proliferation leads to increased metabolic demand that is often uncoupled from nutrient availability (reviewed in DeBerardinis & Chandel, 2016; Eisenberg et al., 2020). Thus, despite metabolic constraint within a solid tumour, cancer cells do not initially respond to metabolic stress by adopting a quiescent state. Instead, they adapt to utilize available fuel sources and conditionally flexible metabolic pathways to drive cell survival, tumorigenesis, and metastasis. The *in vivo* environment of solid tumours is thus a critical modulator of cancer cell biology. Furthermore, elucidating the specific mechanisms by which cancer cells remodel their metabolism to meet metabolic demands *in vivo* presents a promising avenue for anti-cancer therapeutics. With that said, current cell culture models do not maintain metabolic conditions consistent with *in vivo* tumours. Thus, the unique cellular mechanisms and vulnerabilities evoked by cancer cells *in vivo* are likely not modeled in standard culture, compromising the fidelity of basic research performed under such conditions.

1.2 CELLULAR METABOLISM

Cellular metabolism is a fundamental process used by cells to synthesize energy for normal cell function. Free energy produced from the oxidative breakdown of organic molecules is harnessed and stored in high energy bonds that are later hydrolyzed and used to drive energetically unfavourable reactions required by the cell (Dunn and Grider, 2022). Adenosine 5-triphosphate (ATP) is the 'energy currency' of cells, with its synthesis from ADP to ATP being coupled to most energy-yielding reactions, and its hydrolysis coupled to most energy-requiring reactions. Other molecules (e.g., NADH, FADH2, GTP) also store free energy in high-energy bonds for specific cellular processes and signaling pathways, however ATP is the primary energy source used in most biological reactions.

The generation of ATP is most commonly produced through glycolysis and oxidative phosphorylation (OXPHOS), with the primary fuel source being glucose (Lunt & Vander Heiden, 2011). Glycolysis, that being the catabolism of glucose to pyruvate within the cytosol of the cell, produces a net of two ATP, two NADH, and two pyruvate molecules per one molecule of glucose. Subsequently, the fate of pyruvate produced through glycolysis depends on the presence of oxygen. Under conditions of oxygen availability, pyruvate is used to drive mitochondrial respiration, whereby pyruvate is transported across the outer mitochondrial membrane by voltage-dependent anion channels (Huizing et al., 1996; Papa et al., 1971), converted into acetyl-CoA within the mitochondrial matrix, and fed directly into the tricarboxylic acid cycle (TCA). This cycle involves a series of chemical reactions that ultimately produce high energy-yielding carriers (3 NADH, 1 $FADH_2$) and one molecule of ATP or GTP. NADH and $FADH_2$ subsequently transfer stored electrons to specialized proteins localized in the inner mitochondrial membrane, which make up the electron transport chain (ETC). Here, aerobic respiration takes place, generating 36-38 molecules of ATP per glucose molecule. Alternatively, under conditions of low oxygen, anaerobic respiration takes place. Pyruvate is converted into lactic acid by lactate dehydrogenase (LDH), regenerating NAD^+ from NADH to drive glycolysis.

While the processes summarized above are seemingly straightforward metabolic mechanisms that begin with glucose input, the flux of metabolites into and out of these pathways are far more complex. Glucose input alone does not represent the only entry point into metabolism. Alternatively, lipids, amino acids and other carbohydrates can be incorporated into these pathways under conditions of metabolic stress or abundance. For example, the metabolic breakdown of fatty

acids and β-oxidation of fatty acyl-CoA within the mitochondria produces acetyl-CoA, NADH, and $FADH_2$, which can enter the TCA cycle and supply electrons to the ETC (Houten & Wanders, 2010). Acetyl-CoA produced through fatty acid oxidation may also undergo ketogenesis within the liver to produce ketone bodies (i.e. acetone, acetoacetate β-hydroxybutyrate), an alternative fuel source that is highly soluble, and thus easily transported throughout the body. Amino acids, particularly glutamate, can also be converted into intermediates of the TCA cycle, fueling ATP production (Chandel, 2021). Additionally, pyruvate can be generated from lactate, malate and three-carbon amino acids, rather than glucose (McCommis & Finck, 2015).

The contribution of flexible metabolic inputs allows cells to meet energetic demands given diverse metabolite availabilities. This flexibility is, however, carefully coordinated by nutrient and oxygen sensing pathways. Importantly, cancer cells are extremely proficient at this metabolic flexibility, owing to oncogenic metabolic adaptations. This enhances the utilization of available resources beyond non-cancerous metabolism, prolonging survival in nutrient constrained environments of the tumour.

1.3 MECHANISMS OF NUTRIENT AND OXYGEN SENSING

In mammalian cells, cell metabolism, growth, and proliferation are tightly integrated with sensing the availability of energy and nutrients (Efeyan et al., 2015; Fernandes & Demetriades, 2021; Sung et al., 2023). The regulation of cellular metabolism according to metabolite availability is achieved by the coordination of several signaling pathways, with metabolites themselves serving as signaling molecules. The master regulators of these pathways are AMP activated kinase (AMPK) and the target of rapamycin (TOR) complexes, whose functions are closely integrated (Figure 1.1). Furthermore, oxygen sensing is accomplished through hypoxia-inducible factor (HIF), a master regulator of the cellular transcriptional response to hypoxia. In the following section, the regulation and downstream effects of these mechanisms will be discussed in detail.

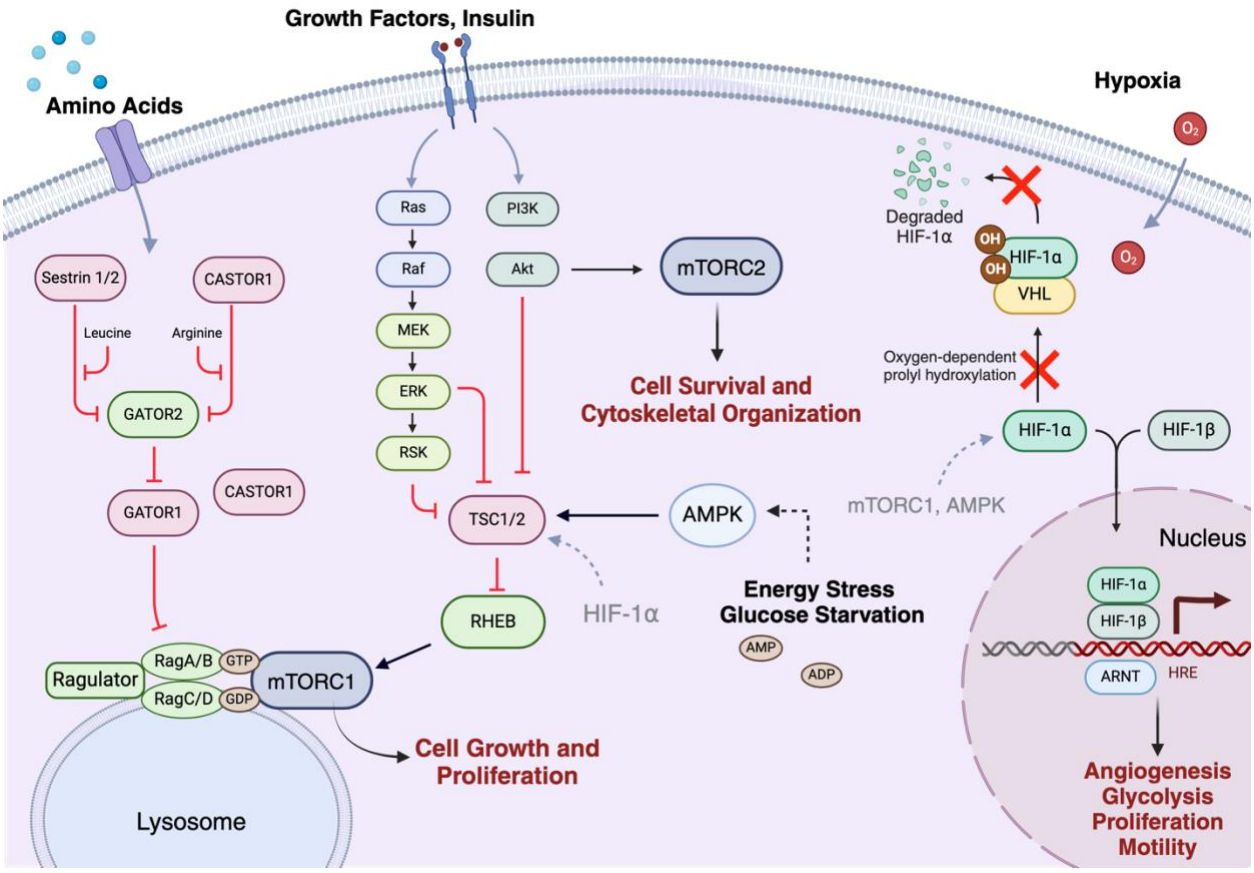

Figure 1.1: Integration of cellular energy status, nutrient availability, and oxygen level sensing through AMPK, mTOR, and HIF pathways. mTORC1/2 pathways are activated by amino acids and growth factor availability. AMPK signaling is activated by AMP/ADP accumulation. HIF signaling occurs under hypoxic conditions in which HIF-1α escapes oxygen-dependent hydroxylation and proteasomal degradation, allowing for HIF-1α stabilization and translocation into the nucleus. These pathways are closely integrated to maintain cellular homeostasis. AMPK and HIF-1α negatively regulate mTORC1 activity at TSC1/2. Both mTORC1 and AMPK regulate HIF-1α transcription and stability, creating a negative feedback mechanism on mTORC1 signaling. For mTORC1/2 pathway, mTORC promoting proteins are labeled in green, and mTORC inhibiting proteins labeled in red. Created with BioRender.com.

1.3.1 AMPK Pathway

The AMPK signaling pathway is a master metabolic regulator of energy homeostasis in eukaryotic cells. It is a highly conserved heterotrimeric protein complex composed of a catalytic α subunit, scaffolding β subunit, and regulatory γ subunit, that together function to sense and respond to reductions in cellular energy status resulting from imbalances between energy utilization and production (Hardie & Carling, 1997; Mihaylova & Shaw, 2011). In mammals, multiple isoforms of each subunit have been identified, including two α subunit isoforms (α1, α2),

two β subunit isoforms (β1,β2), and three γ subunit isoforms (γ1, γ2, γ3). Together, these subunits enable AMPK to sense fluctuations in intracellular energy levels and orchestrate appropriate responses to restore energy homeostasis.

AMPK primarily senses changes in cellular energy status by the binding of adenosine nucleotides (AMP, ADP, ATP) to the γ-subunit of the complex. Under conditions of energy abundance, AMPK is inactive and bound to free ATP. However, under conditions of energy stress, during which ATP stores become depleted and AMP/ADP accumulate, allosteric activation of AMPK by AMP/ADP binding increases (Cantó & Auwerx, 2010; Mihaylova & Shaw, 2011). This activation induces a conformational change in the AMPK complex, exposing phosphorylation sites along the activation loop of the catalytic subunit to kinases. Thr172 within this region is then phosphorylated by upstream AMPK kinases such as LKB1 and CAMKK2, further activating the catalytic function of AMPK. The active state of the phosphorylated threonine residue is maintained so long as AMPK remains bound to AMP/ADP. This shields the Thr172 from phosphatases, while allowing the continual phosphorylation of Thr172 by upstream kinases.

When activated, AMPK functions to directly and indirectly regulate numerous downstream targets to promote ATP generating catabolic pathways. AMPK activation stimulates glucose uptake through GLUT1 and GLUT4 by promoting GLUT transporter trafficking to the plasma membrane (Barnes et al., 2002; Kurth-Kraczek et al., 1999; Pehmøller et al., 2009), and inhibiting reuptake of transporters by endocytosis (O'Donnell & Schmidt, 2019). It also promotes glycolysis by activating PFKFB2 and PFKFB3, 6-phosphofructo-2-kinase/fructose-2,6- biphosphatase isoforms that produce fructose-2,6-bisphosphate (F2,6BP), a potent activator of glycolytic enzyme 6-phosphofructo-1-kinase (PFK) (Marsin et al., 2000, Marsin et al., 2002). Moreover, AMPK promotes fatty acid oxidation by inactivating acetyl-CoA carboxylase-2 (ACC2), and thus reducing the production of malonyl-CoA, an inhibitor of mitochondrial fatty acid uptake via the carnitine shuttle (Thomson & Winder, 2009).

In addition to catabolic effects, AMPK inhibits energy consuming anabolic pathways. Fatty acid and cholesterol synthesis is inhibited by AMPK through the inactivation of acetyl-CoA carbocylase-1 (ACC1) and HMG-CoA reductase (Hardie et al., 1989). Glycogen synthesis, protein synthesis, nucleotide synthesis are also inhibited by the phosphorylation and inactivation of glycogen synthase, elongation factor-2 kinase (eEF2K), and phosphoribosyl pyrophosphate synthase (PRPS), respectively (Johanns et al., 2017; Jørgensen et al., 2004; Qian et al., 2018).

Furthermore, chronic AMPK activation promotes mitochondrial biogenesis, *GLUT4* transcription, and oxidative metabolism through the phosphorylation of mitochondrial regulating transcriptional coactivator, PGC-1α (Jäger et al., 2007). AMPK activation also promotes mitophagy through phosphorylation of autophagy activating ULK1 (Egan et al., 2011), and mitochondrial fusion/fission through phosphorylation of mitochondrial membrane proteins, including mitochondrial fission factor (MFF) and mitofusin 1/2 (Mfn1/2) (Ducommun et al., 2015; Toyama et al., 2016).

In addition to metabolic processes, AMPK activation can suppress cell proliferation and arrest cell cycle in G1 phase (Imamura et al., 2001). Moreover, in cancer cells, AMPK phosphorylates integrins, focal adhesion kinases (FAKs), and epithelial-mesenchymal transition (EMT) regulating transcription factor, Twist1, to promote cell motility, adhesion, and invasion, (Crosas-Molist et al., 2023; Saxena et al., 2018; Schaffer et al., 2015). Thus, AMPK tunes a wide array of metabolic and biologic processes to environmental conditions.

1.3.2 mTOR Pathway

The mammalian target of rapamycin (mTOR) is a master regulator of cell growth and survival, integrating nutritional and environmental signals into downstream anabolic targets (Battaglioni et al., 2022; Saxton & Sabatini, 2017; Shaw, 2008; Zou et al., 2020). mTOR is a serine/threonine protein kinase of the phosphatidylinositol kinase-related kinase (PIKK) family that forms two structurally and functionally distinct multiprotein complexes, mTOR complex 1 (mTORC1) and mTOR complex 2 (mTORC2). These complexes are differentially regulated and allow mTOR to bind and phosphorylate unique targets in response to nutrients and growth factors (Kim et al., 2008; Sancak et al., 2008). mTORC1 is a regulator of cell growth and metabolism, while mTORC2 compliments its function as a regulator of cell proliferation and survival.

In mammals, mTORC1 is a homodimeric complex of heterotrimers composed of mTOR, Raptor (regulatory-associated protein of mTOR), and mLST8 (mammalian lethal with SEC13 protein 8) (Hara et al., 2002; Kim et al., 2002). While mTOR contains the kinase catalytic domain, Raptor facilitates the recruitment and binding of mTORC1 substrates to mTOR. Alternatively, mLST8 stabilizes kinase activity by binding to the kinase domain of mTOR. Similar to mTORC1, mTORC2 contains mTOR and mLST8; however, Rictor (rapamycin insensitive companion of mTOR) serves as the recruitment subunit rather than Raptor (Jacinto et al., 2004; Sarbassov et al., 2004).

Activation of mTORC1 is accomplished through the association of the complex with two mTORC1-interacting GTPase classes: Rag and Rheb. Rag GTPases (Ras-related small GTP-binding proteins) are a family of heterodimer forming proteins that are activated when amino acids are present in abundance within the cell (Kim et al., 2008; Sancak et al., 2008). Active Rag GTPases function to bind cytosolic mTORC1 and anchor it to the lysosomal surface, specifically to Ragulator (Rag GTPase regulator) scaffolding (Sancak et al., 2010). Rheb GTPases (Ras homolog enriched in brain) are similar small GTP-binding proteins localized to lysosomal surfaces that are activated following growth factor signaling. Rheb functions to activate mTORC1 by binding the mTOR subunit and allosterically inducing a conformational change that promotes kinase activity (Long et al., 2005; Parmar & Tamanoi, 2010; Yang et al., 2017). In contrast, mTORC2 activation is primarily regulated by insulin/PI3K signaling whereby insulin signaling inhibits mSin1, a phosphoinositide-binding mTORC2 inhibitory subunit, allowing mTORC2 activation to take place (Liu et al., 2015).

Regulation of the nucleotide state and activity status of Rag and Rheb GTPases are mediated by GTPase-activating proteins (GAPs) (e.g. GATOR1, FLCN-FNIP2, TSC1/2) and guanine exchange factors (GEFs) (e.g. Ragulator) (Bar-Peled et al., 2012; Chantranupong et al., 2014; Inoki et al., 2003; Tsun et al., 2013). In general, GAPS promote the intrinsic hydrolysis of GTP to GDP, inactivating Rag GTPases, while GEFs promote the exchange of GDP for GTP to activate Rag GTPases. Importantly, GAP and GEF regulating proteins, of which over 26 have been identified, make up the nutrient-sensing component of this pathway.

Amino acids activate mTORC1 signaling through amino acid sensors, SESTRIN2 and CASTOR1, which both regulate GAP activity. When amino acids are present and readily bind sensors, these proteins indirectly promote GAP inhibition, and subsequent mTORC1 signaling (Chantranupong et al., 2014; Wolfson et al., 2016). Alternatively, growth factors activate mTORC1 through the inhibition Tuberous Sclerosis Complex (TSC), a GAP that binds and inactivates Rheb when growth factor signaling is low. Growth factor extracellular binding (i.e. Insulin, IGF-1,Wnt, TNFα) and subsequent PI3K-Akt signaling converge on TSC to inactivates it. This allows mTORC1 activation through Rheb, similar to mTORC2 activation (Dan et al., 2002; Garami et al., 2003; Inoki et al., 2002).

When activated mTORC1/2 phosphorylate several effectors to promote anabolic mechanisms (Laplante & Sabatini, 2013; Sun et al., 2023). mTORC1 activation promotes protein

synthesis through the phosphorylation and inactivation of eukaryotic translation initiation factor (eIF4E) binding protein (4E-BP1), and activation S6 kinase 1 (S6K1), a substrate that promotes the translation of mRNA encoding elongation factors and ribosomal proteins (Blommaart et al., 1995; K. Hara et al., 1998). Lipid synthesis is also promoted by mTORC1 activation through positive regulation of sterol-regulatory-element-binding proteins (SREBPs), transcription factors that regulate the expression of lipogenic genes, including those involved in fatty acid synthesis and cholesterol biosynthesis (Le Bacquer et al., 2007; S. Li et al., 2010). Furthermore, mTORC1 inhibits fatty acid oxidation and ketogenesis through the inactivation of PPARα, a nuclear receptor that regulates the expression of genes required for lipid catabolism (Sengupta et al., 2010). Both mTORC1 and mTORC2 promote cell proliferation, growth and survival through the activation of transcription factor STAT3, and protein kinase B (AKT), respectively (Kim et al., 2009). Additionally, mTORC1/2 negatively regulates autophagy (Codogno & Meijer, 2005; Mammucari et al., 2007).

1.3.3 HIF Signalling

Hypoxia inducible factor (HIF) is an intracellular oxygen sensor that regulates a multitude of intracellular activities in response to hypoxia (Semenza & Wang, 1992). It is a heterodimeric protein, composed of α and β subunits, that serves as a transcription factor when stabilized. Three isoforms of HIF-α have been identified (HIF-1α, HIF-2α, HIF-3α) (Y. Z. Gu et al., 1998; Semenza & Wang, 1992; Tian et al., 1997), however only one isoform of HIF-β (HIF-1β/ARNT) exists (Chhipa et al., 2018; Dodd et al., 2015; Land & Tee, 2007).

Oxygen sensing is accomplished by oxygen-sensitive post-translational modifications of HIFα that lead to its rapid degradation. Under normoxia (~18% O_2), HIFα is hydroxylated by oxygen-dependent prolyl-4-hydroxylases (PHDs) and subsequently recognized and bound by von Hippel-Lindau tumour suppressor protein (pVHL), a ubiquitin ligase (Huang et al., 1998). This results in the ubiquitination of HIF-α, and subsequent proteasomal degradation. Therefore, HIFα:HIFβ dimers do not form when oxygen levels are high. However, when oxygen is limited in hypoxia, PHD hydroxylation activity is suppressed, allowing HIF-α to accumulate and translocate into the nucleus. There, HIF-α may dimerize with constitutively active HIF-β to form the active HIF complex (Semenza & Wang, 1992). Upon activation, HIF transcriptional regulation

is initiated, whereby HIF binds to hypoxia response elements (HREs) of gene targets, promoting gene expression.

Transcriptionally active HIF complexes directly induce the expression of hundreds of genes involved in cellular adaptation and survival under low oxygen supply (Reviewed in Dengler et al., 2014). Importantly, HIF-α isoforms (HIF-1α and HIF-2α) confer differential gene target selectivity to HIF-1, HIF-2, HIF-3 complexes (Downes et al., 2018; Zhang et al., 2014). Generally, HIF-1 is more transcriptionally active following acute hypoxia (<24h), regulating glycolytic responses, whereas HIF-2 is more transcriptionally active following chronic hypoxia (>24h), regulating angiogenesis, vasodilation, stemness, proliferation and migration. However, there is overlap in target genes. While less is known regarding HIF-3 function, genes distinct to HIF-3 have been identified in zebrafish embryos (*sqrdl, mclb, zp3v2*) (Zhang et al., 2014), as well as those involved in HIF1/2 suppression in human kidney cells (Hara et al., 2001).

Erythropoietin (EPO), vascular endothelial growth factor A (VEGF-A), angiopoietin 2 (ANG2), and adrenomedullin (ADM) are among a few of the genes transcriptionally activated by HIF-1/2 that serve to rescue oxygen supply by stimulating angiogenesis (Forsythe et al., 1996; Semenza & Wang, 1992). Moreover, to maintain energy levels, HIF mediates a shift in metabolism to increase glucose fermentation and reduce OXPHOS. HIF-1 suppresses TCA cycle metabolism by activating pyruvate dehydrogenase kinase 1 (PDK1), which subsequently inactivates pyruvate dehydrogenase (PDH), the enzyme that irreversibly produces acetyl-CoA from pyruvate (Kim et al., 2006; Papandreou et al., 2006). HIF-1 also increases lactate dehydrogenase (LDH) expression, the enzyme that converts pyruvate to lactate (Semenza et al., 1996). Moreover, glucose transporters (GLUT-1, GLUT-3), glycolytic enzymes, and positive glycolysis regulator PFKFB are upregulated by HIF-1, increasing glucose uptake and utilization to compensate for reduced oxidative metabolism (Iyer et al., 1998). HIF-1 also induces remodeling of cytochrome c oxidase (COX) to optimize ETC efficiency, and limit ROS generation (Fukuda et al., 2007). Indeed, cytochrome c oxidase subunit 4 isoform (COX4) transcription is modulated by HIF-1, increasing COX4-2 expression, while degrading COX4-1 via Lon protease expression. More recent findings suggest COX4-2 decreases the affinity of COX to oxygen, limiting ETC function at low oxygen levels (Pajuelo Reguera et al., 2020).

Genes involved in proliferation, motility, EMT, extracellular matrix remodelling, immune evasion, and apoptosis are also regulated by HIF1/2 (Dengler et al., 2014). Importantly, these roles

are integral to cancer cell biology, and have largely been characterized in cancer models. For this reason, HIF-regulated genes implicated in tumorigenesis will be discussed in more detail in later sections.

1.3.4 Integration of Nutrient Sensing Pathways

AMPK, mTOR and HIF signaling pathways efficiently sense and coordinate appropriate responses to distinct changes in cellular homeostasis through crosstalk between their mechanisms. Active AMPK regulates mTORC1 by allosterically inactivating the complex via direct phosphorylation of Raptor and TSC2 (Gwinn et al., 2008), subsequently increasing TSC GAP activity to Rheb (Inoki et al., 2002). Furthermore, both AMPK and mTORC1 signaling increase HIF1α transcription and enhance HIF-1 stability (Chhipa et al., 2018; Dodd et al., 2015; Land & Tee, 2007). This suggests HIF activity is increased in response to energy stress, thus facilitating increased glycolytic energy production and angiogenesis, as well as in response to nutrient abundance, facilitating the expression of metabolic machinery. However, in hypoxic conditions, HIF-1α has a negative feedback function on mTORC1, inhibiting mTORC activation through the activation of TSC complex (Brugarolas et al., 2004).

When coordinated metabolic response pathways are unable to meet energy and biomass demands, cellular stress responses are initiated. The integrated stress response (ISR) pathway is a common mechanism used by cells to sense disruptions in cellular homeostasis, and subsequently coordinate appropriate effector responses (Hu & Zhang, 2021; Pakos-Zebrucka et al., 2016). The eukaryotic translation factor 2 kinase (eIF2α kinase) family, including GCN2, PERK, PKR, and HIR, are regulators of this pathway, responding to amino acid deprivation, endoplasmic reticulum (ER) stress, viral infection, and heme deprivation, respectively. Under stress conditions, active eIF2α kinases converge on eukaryotic translation factor 2 (eIF2α), inactivating it through phosphorylation. In doing so, global protein synthesis is reduced, while select mRNA ISR effectors undergo a preferential increase in translation by phosphorylated eIF2α, including activating transcription factor 4 (AFT4) (B'chir et al., 2013). Importantly, ISR effectors regulate the expression of stress responsive genes, including those involved in amino acid transport, biosynthesis, redox regulation, protein folding, and autophagy (Reviewed in Kalinin et al., 2023; Neill & Masson, 2023). Furthermore, when conditions cannot be mitigated by IRS effectors, and AFT4 expression is prolonged, the IRS induces pro-apoptotic genes (Teske et al., 2013)

In summary, AMPK, mTOR and HIF pathways are critical regulators of cellular activities. AMPK serves as a sensor of cellular energy levels, activating catabolic pathways to restore energy homeostasis when ATP availability is limited. Conversely, mTOR regulates cell growth and metabolism, promoting anabolic metabolism when nutrients and growth factors are in abundance. HIF responds to oxygen availability, transcriptionally reprogramming cells under hypoxic conditions. Moreover, when cellular stress exceeds the regulatory capacities of these pathways, the ISR reduces non-essential protein translation and promotes expression of essential homeostatic genes.

1.4 CANCER DEVELOPMENT

Cancer is a disease that often arises from genetic alterations in specific genes known as proto-oncogenes and tumour suppressor genes. In normal cells, these genes serve as regulators of cell survival, growth, division and apoptosis (Sanchez-Vega et al., 2018; Vicente-Dueñas et al., 2013). However, mutations in these genes lead to unregulated cell proliferation, and suppression of normal apoptotic pathways. Proto-oncogene mutations are considered “gain of function” that result in increased cell growth and proliferation (Kontomanolis et al., 2020). Alternatively, tumour suppressor gene mutations are considered “loss of function” that result in the inability of cells to perform programmed cell death pathways, repair damaged DNA, and monitor cell cycle checkpoints. Mutations in these genes, whether by point mutation, gene amplification or chromosomal translocation, ultimately lead to unregulated cell replication and inhibition of cell death. Tumour development occurs through continued neoplastic replication resulting in the formation of a solid cellular mass. This cellular niche is distinct from surrounding healthy tissue.

To date, over 250 oncogenes and tumour suppressor genes have been identified, with considerable variation existing in the specific genes and pathways affected between cancer type, stage, and individual (Sinkala, 2023). Several commonly altered oncogenes and tumour suppressor genes, including KRAS, MYC, and P53, are critical modulators of cell proliferation and likely represent the initial drivers of cancer development. However, as tumorigenesis progresses, genetic alterations continue to accumulate in cancerous cells, contributing to their survival in increasingly hostile metabolic environments established within the tumours. Interestingly, many of the shared genetically altered signalling pathways between different cancers mediate metabolic response pathways (Eisenberg et al., 2020). For example, oncogenes KRAS, BRAF, and PIK3CA are gene members of PI3K/AKT/mTOR and RTK/RAS pathways. Overexpression or constitutive

activation of these genes increase pathway signaling without growth factor or metabolite signaling, promoting anabolic processes.

1.5 THE TUMOUR MICROENVIRONMENT

Solid tumours are complex structures composed of an array of cell types and constituents that support cancer cell survival. At a basic level, the components of a solid tumour are organized into two compartments: the parenchyma (i.e., cancerous cells) and the stroma (i.e., extracellular matrix, blood and lymph vessels, interstitial fluid) (Connolly et al., 2003). Generally, the architecture of the tumour involves a compact cancerous core, surrounded and infiltrated by fibroblasts and immune cells (Fu et al., 2021; Ribeiro Franco et al., 2020). Extracellular matrix (ECM) composed of proteoglycans, glycoproteins and collagen provides a support scaffold for the tumour, as well as having a functional role in processes such as cell migration, growth, and differentiation (Popova & Jücker, 2022). Blood and lymphatic vessels extend within the tumour to provide oxygen and nutrients and remove waste. Tumour interstitial fluid surrounds the cells, ECM, and vasculature of the tumour, and contains soluble nutrients, waste products, and cellular secretions between neighbouring cells and vessels (Baronzio et al., 2012; Wagner & Wiig, 2015) (Figure 1.2). Together, these components make up the tumour microenvironment.

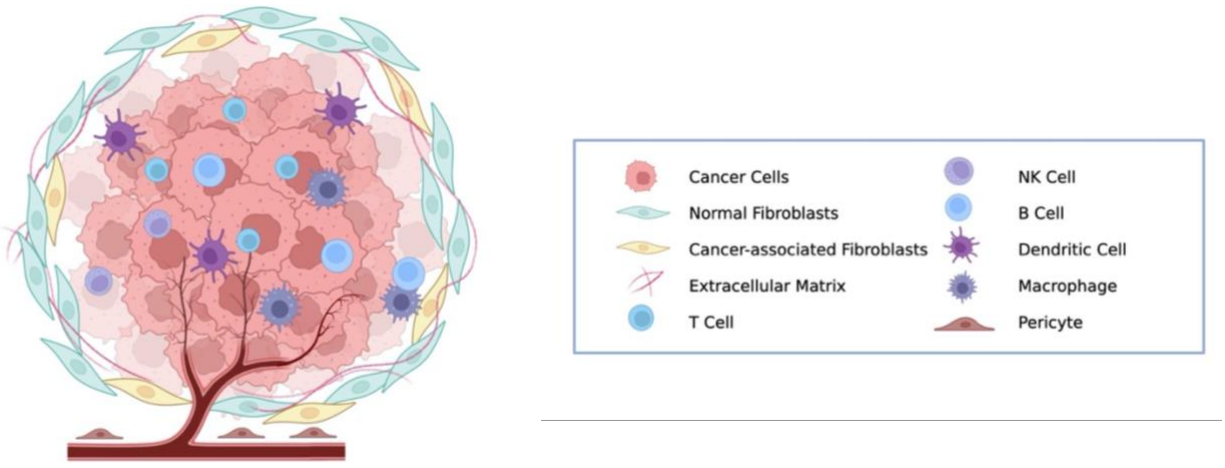

Figure 1.2: Illustration of the intricate organization of solid tumours. The tumorous mass is composed of cancerous cells, immune cells, fibroblasts, structural matrix, and vasculature. These components make up the tumour microenvironment. NK=natural killer; T/B Cell = T and B lymphocyte; B Cell = Bone Lymphocyte. Created with BioRender.com

1.5.1 Tumour Vasculature

Tumour vasculature tends to be highly disorganized, and immature compared to normal tissue. This is due to the overproduction of local pro-angiogenic factors (i.e., VEGF-A, ANG, TGFα, IL-8), and inhibition of angiogenic inhibitors (i.e., TSP-1) by cancer and stromal cells during tumorigenesis (Reviewed in Lugano et al., 2020). In general, the spatial distribution of vasculature throughout the tumour is heterogeneous. Additionally, blood flow through this vasculature is impaired by abnormal branching patterns and inconsistent changes in vessel diameter (Bernabeu et al., 2020; Konerding et al., 2001; Pries et al., 2009; Yuan et al., 1994). Moreover, the blood vessels are leaky, having increased fenestrations, large endothelial cellular junctions, and poorly developed basement membranes (Gerlowski & Jain, 1986; Yuan et al., 1994).

Poor tumour vascularization affects the interstitial fluid pressure (IFP) within the tumour. IFP is the pressure exerted by interstitial fluid on the cells and vessels of the tumour. In solid tumours, IFP is elevated compared to normal tissue, and positive relative to intravascular pressure (Fukumura & Jain, 2007; Gutmann et al., 1992; Roh et al., 1991). High blood vessel permeability, low venous and lymphatic drainage, and compact cell density contribute to this phenomenon. Accumulation of hyaluronan, a polysaccharide able to absorb water, also contributes to increased IFP in some tumours (e.g. pancreatic cancer) (Provenzano et al., 2012; Voutouri et al., 2016). Overall, this feature further reduces the function of blood vessels, particularly in regions more internal to the tumour, where blood flow, perfusion, and concentration of solutes within the vessel are lower (Jain, 1988). This leads to gradients in haemodynamic delivery, and heterogeneity in hemoglobulin and oxygenation status throughout the tumour (Li et al., 2020; Stamatelos et al., 2019). Moreover, nutrient delivery and metabolic waste removal are impaired, likely in a similar heterogenous manner as oxygen. Due to the poor fluid dynamics and reduced vascular coverage (Jain, 1988), the extracellular environment within the tumour is generally considered hypoxic and metabolically constrained.

1.5.2 Oxygen Availability within the Tumour Microenvironment

Poor vascularization within the tumour is associated with tumour hypoxia *in vivo*. This is a hallmark feature of solid tumours that has been well characterized over the last 60 years (reviewed by Vaupel et al., 1989, Vaupel et al., 2021). In general, median oxygen conditions ranging from 0.3 to 4.3% O_2 can be expected within solid tumours (McKeown, 2014) (Table 1.1).

However, the specific oxygen saturations found within the tumour microenvironment vary within individual tumours, and between tumour stages, cancer types, and patients (Li et al., 2020; Pandkar et al., 2021; Stamatelos et al., 2019). Moreover, oxygen concentrations fluctuate cyclically, over hours and days, coinciding with fluctuations in perfusion (Brurberg et al., 2005; Panek et al., 2017; Pigott et al., 1996; K. Wang et al., 2009). This results in heterogeneity in oxygenation within the same tumour region.

Table 1.1: Oxygenation status in solid tumours and associated normal tissue.

	Tumour % O_2	Normal Tissue % O_2	Reference
Brain	1.7	3.4	(Vaupel et al., 2007)
Head and Neck	1.3	5.3-6.7	(Vaupel et al., 2007)
Lung	1.9	5.6	(Falk et al., 1992)
Breast	1.3	6.8	(Vaupel et al., 2003)
Cervical	1.2	5.5	(Vaupel et al., 2007)
Pancreatic	0.7	3.9-5.3	(Carlsson et al., 1998; Koong et al., 2000)
Prostate	0.8	2.8-4.1	(Movsas et al., 1999)

Note: Data provided at median, unless range available.

Hypoxia within the tumour microenvironment is associated with HIF-1α stabilization and subsequent transcriptional regulation of cell metabolism, as described earlier. In addition to these targets, HIF signaling promotes the acquisition of malignant phenotypes in cancer cells. Indeed, transcriptional regulators of cell migration and metastasis are direct targets of HIF-1. In pancreatic, colon, brain, and gastric cancers, HIF-1 directly induces EMT through the transcription of TWIST and ZEB, transcriptional repressors that downregulate epithelial-like genes (Chen et al., 2016; Chen et al., 2017; Joseph et al., 2015; Yang et al., 2017). Cell migration, invasion, and ECM remodelling are also upregulated by HIF signaling in colon, breast, ovarian, liver, and non-small cell lung cancer (Cheng et al., 2013; Feng et al., 2018; X.-Z. Gao et al., 2019; Hoffmann et al., 2018; X. Liu et al., 2018). Moreover, HIF-1/2α overexpression is associated with metastasis and poor prognosis of cancers *in vivo* (Baba et al., 2010; Gao et al., 2017; Zhong et al., 1999). Thus, while hypoxia is generally unfavourable in normal tissue, hypoxia within the tumour microenvironment promotes adaptive migratory responses that contribute to metastasis and disease aggression.

1.5.3 Nutrient Availability within the Tumour Microenvironment

Tumour interstitial fluid (TIF) supplies cells of the tumour with nutrients delivered by the vasculature. The metabolic availability within the tumour microenvironment can thus be estimated by the isolation and metabolomic analysis of TIF. However, very few studies that quantify TIF metabolite concentrations are currently available. Rather than isolate TIF, most metabolomics studies quantitatively characterize the metabolic landscape of solid tumours and adjacent tissue using homogenized tumour specimens that include cytosols. Metabolomic data from these studies is thus representative of a culmination of intra- and extra-cellular metabolic constituents, rather than the extracellular, interstitial microenvironment of the cells. Although successful at demonstrating the extent to which the metabolome of tumorous and healthy tissue differ (Hirayama et al., 2009; Kamphorst et al., 2015; Kinoshita & Yokota, 1997; Tokunaga et al., 2018), as well as the metabolic heterogeneity between cancer types (Reznik et al., 2018), this approach fails to delineate the specific nutrient constraints experienced by cells proliferating within these microenvironments. It is thus necessary to perform metabolomic analysis on TIF to achieve an appropriate estimation of the metabolic availability within the tumour microenvironment. Nonetheless, TIF isolation proves difficult due to the risk of cell rupture, vasculature contamination, and inflammation associated with sampling techniques (i.e., implanted wicks, catheters, micro dialysis, centrifugation) (Reviewed in Wiig & Swartz, 2012). Importantly, while TIF isolation methods have been increasingly refined over the last 25 years, almost all studies that isolate TIF aim to characterize the proteomic landscape of samples, rather than metabolomic. Moreover, those that do perform extensive metabolomic analysis, typically do not provide absolute concentrations of metabolites, nor fold changes from plasma levels that may be used to approximate TIF concentrations (Vecchio et al., 2021; Wibom et al., 2010). While occasionally glucose, lactate, pyruvate, glutamate, and glycerol TIF measurements are available for some human cancers (Table 1.2), more extensive metabolite concentrations are generally not available.

Table 1.2: Nutrient composition (mM) of human plasma and tumour interstitial fluid.

	TIF Sampling Technique	Glucose	Lactate	Pyruvate	Glutamate	Glutamine	Glycerol	References
Human Plasma	N/A	4.6-5.3	1.1-1.9	9-60	32-140	420-720	331-532	(Ackermann & Tardito, 2019)
Renal cell carcinoma	Tumour resection and centrifugation	3.36	9.05	N/A	N/A	0.44	N/A	(Reinfeld et al., 2021)
Head and Neck								
Larynx	Microdialysis	N/A	2.280	0.0506	N/A	N/A	N/A	(Schroeder et al., 2013)
Oral cavity	Microdialysis	N/A	1.677	0.0443	N/A	N/A	N/A	(Schroeder et al., 2013)
Hypopharynx	Microdialysis	N/A	2.657	0.0476	N/A	N/A	N/A	(Schroeder et al., 2013)
Oropharynx	Microdialysis	N/A	3.397	0.0960	N/A	N/A	N/A	(Schroeder et al., 2013)
Glioma*	Microdialysis	2.16 (2.68)	8.760 (3.82)	137.86 (95.71)	40.52 (74.4)	N/A	39.89 (21.83)	(Roslin et al., 2003)

Data are median concentrations from multiple biological replicates, except '*' data represents mean (SD).

To date, only one group has performed a comprehensive metabolic analysis of TIF sampled from solid tumours (Sullivan et al., 2019). In this study, the metabolite composition of TIF isolated from end-stage autochthonous LSL-$Kras^{G12D/+}$, $Trp54^{flox/flox}$, Pdx-1-Cre (KP-/-C) murine pancreatic ductal adenocarcinoma (PDAC) tumours was measured using liquid chromatography/mass spectrometry (LC/MS). Over 118 metabolites were quantified in TIF, representing the best approximation for the tumor metabolome existing to date. Results of this quantification showed that the composition of TIF does indeed differ significantly from plasma.

In agreement with other measurements that suggest TIF glucose is 2-9 times lower than in plasma, Sullivan et al., (2019) found glucose to be 2-fold less abundant in TIF compared to paired plasma measurements. Most essential amino acids were also significantly reduced in TIF (i.e. tryptophan, arginine, lysine, and tyrosine), among other metabolites (i.e. pyruvate, sarcosine, succinate, α-ketoglutarate). Conversely, several non-essential and conditionally essential amino acids (i.e. glutamate, glycine, aspartate, hypoxanthine, serine, ornithine) were found to accumulate within TIF.

In addition to amino acids, Sullivan et al., (2019) found lactate accumulated in PDAC TIF, consistent with other cancers (Table 1.2). Importantly, extracellular acidity can be expected to increase alongside lactate. While not measured in this study, average pH of 6.8-7.0 have been measured in the tumour microenvironment of other cancers *in vivo* 5/23/2024 2:32:00 PM. Importantly, lactate accumulation and acidification of the tumour microenvironment impacts many aspects of cell physiology (Kato et al., 2013; Rauschner et al., 2021). In cancerous cells, lactate itself is associated with inhibition of anti-tumour innate immune responses through immunosuppression of T lymphocytes and macrophages (El-Kenawi et al., 2019; Fischer et al., 2007), and impaired monocyte migration (Goetze et al., 2011). More recently, an epigenic role of lactic acid was also shown, suggesting that lactic acid can regulate gene expression through histone modifications (Zhang et al., 2019).

Cellular consumption and excretion rates cannot be interpreted using *in vivo* extracellular metabolite levels as contributions from microvascular circulation and non-cancerous cells cannot be factored into the interpretation. With that said, the poor circulation within the tumour microenvironment may allow for some interpretation of metabolic utilization based on TIF composition, however, this should be considered cautiously. In this case, the TIF data acquired by Sullivan et al. (2019), suggests essential amino acids are consumed, while non-essential and conditionally essential amino acids are produced. Moreover, glucose depletion and lactate accumulation suggest glycolytic metabolism within the tumour microenvironment. Interestingly, differential abundance of metabolites involved in the urea cycle and arginine biosynthesis pathway are consistent with arginosuccinate synthase (ASS1) deficiency associated with bladder cancer, glioblastomas, myxofibrosarcoma, nasopharyngeal carcinoma, breast cancer, and PDAC (Allen et al., 2014; Huang et al., 2013; Liu et al., 2017; Qiu et al., 2014; Syed et al., 2013). However, once again, these interpretations should be taken cautiously. Non-cancerous cells of the tumour microenvironment also contribute to changes in TIF, alongside unknown changes attributed to circulation.

In summary, the metabolite availability within the tumour microenvironment is constrained. Glucose and many essential amino acids are limited, while several metabolite intermediates are increased. Considering the mechanisms used by cells to sense and respond to nutrient availability previously discussed, these conditions present a distinct metabolic

environment that likely modulates the anabolic and catabolic function of cells in ways unique from plasma.

1.5.4 Non-malignant cells in the Tumour Microenvironment

Due to the dense nature of solid tumours, interaction between cancer cells and their surroundings is both inevitable and essential to the growth and metastasis of tumours. Cancer associated fibroblasts (CAFs), for example, are activated fibroblasts within the tumour microenvironment that both send and receive signals with neighbouring cancer cells. Initially activated by cytokine and growth factors released by cancer and immune cells, CAFs exhibit cancer-promoting effects through the release of CAF-derived cytokines, chemokines and growth factors that enhance cancer cell proliferation (Mao et al., 2021). Moreover, co-culture of CAFs with colon and breast cancer cells, promotes single cell migration and invasion through the binding of cancer cells fibronectin outgrowths on CAFs (Miyazaki et al., 2020). Similarly, in 3D coculture of lung squamous carcinoma with CAFs, CAFs were observed to promote migration and invasion of cancer cells, and enhance cell hyperplasia (Chen et al., 2018). In cervical cancer, the ability of CAFs to regulate cell invasion, migration and growth was associated with transforming growth factor (TGF) β1 and stromal cell-derived factor 1 overexpression (Xiao et al., 2022). Interestingly, CAFs were also found to regulate angiogenesis in murine colorectal tumour through STAT3 activation (Heichler et al., 2020). Thus, it is clear that non-malignant fibroblasts found within the tumour microenvironment promote tumorigenesis and metastasis.

Immune cells of both the adaptive and innate immune system are also well characterized to have regulatory roles within the tumour microenvironment. Interestingly, rather than immune cells solely working to combat the growing tumour, some immune cells can be converted to pro-tumorigenic tumour-associated cells. For example, in glioblastomas, chemokine signaling molecules produced in the tumour microenvironment suppress anti-tumour immune responses in tumour-associated macrophages (TAMs) through mTOR-dependent upregulation of STAT3 and NF-kB (Dumas et al., 2020). Active TAMs produce pro-inflammatory cytokines, however lack the ability to stimulate T cell activation. Additionally, TAMs enhance glycolytic metabolism and lactate production in cancer cells through the release of extracellular vesicles containing HIF-1α-stabilization long noncoding RNA (Chen et al., 2019). Cross talk between cancerous cells and immune cells thus promotes immune escape and regulates cancer cell metabolism.

1.6 METABOLIC HALLMARKS IN CANCER PROGRESSION

Metabolic reprogramming is a hallmark feature of cancer that involves the enhancement or suppression of conventional metabolic pathways to support cancer survival, proliferation and metastasis. This is driven by a combination of mutational factors intrinsic to tumour development, as well as metabolic availability within the tumour.

1.6.1 The Warburg Effect

The earliest proposed example of metabolic reprogramming in cancer cells suggests that tumours are highly glycolytic, favouring glucose fermentation over OXPHOS, even under conditions of oxygen availability (Warburg, 1956). This phenomenon, termed the 'Warburg Effect', has since dominated the attention of cancer biologists in discussion surrounding cancer metabolism. Indeed, extensive research suggests that glycolytic metabolism is a metabolic feature shared amongst most cancer types *in vivo*. Glucose uptake, measured using 18F-fluorodeoxyglucose (FDG), consistently indicates increased glucose metabolism in tumours *in vivo* (Courtney et al., 2018; Jadvar et al., 2009; Martinez et al., 2018; Momcilovic et al., 2018; Ong et al., 2008). Additionally, GLUT transporter and LDH-A expression is frequently elevated in the tumours of cancer patients (Dong et al., 2017; Koukourakis et al., 2003, 2008; Mohtasham et al., 2019; Rong et al., 2013). Early studies attribute the Warburg effect to defective mitochondrial function in cancer cells (Pelicano et al., 2006). This was initially supported by the identification of mutations in TCA cycle enzymes, including succinate dehydrogenase, fumarate hydratase, and isocitrate dehydrogenase (Ricketts et al., 2008; Sjöblom et al., 2006; Tomlinson et al., 2002). However, more recent evidence suggests that mitochondrial function is intact in most cancers, and in fact cancer cells readily switch between oxidative and glycolytic glucose fates depending on oxygen and nutrient availability (Moradi, et al., 2021; Vaupel & Mayer, 2012). Furthermore, increased glucose fermentation is now understood to be a metabolic strategy employed by rapidly proliferating cells in general, not specifically cancer cells (Ghashghaeinia et al., 2019; Sun et al., 2019).

The longstanding hypothesis behind the 'Warburg effect' suggests that increased glucose uptake provides carbon mass for macromolecule biosynthesis (Vander Heiden et al., 2009). However, recent work involving isotope tracing of glucose and glutamine utilization suggests that amino acids primarily contribute to cell mass, rather than glucose (Hosios et al., 2016). Alternatively, others have hypothesized that NAD^+ demands in proliferating cells exceed the

regenerative capacity achieved through OXPHOS, thus requiring glucose fermentation to meet demands. Recent work by Luengo et al. (2021) provides evidence for this hypothesis, indicating that the ETC is thermodynamically inhibited during 'Warburg metabolism' *in vitro*. Indeed, ATP is not hydrolyzed to ADP at a rate sufficient to drive continuous ATP synthase activity in proliferating cells, preventing mitochondrial NAD^+ regeneration. Rather, ATP production through glycolysis alone is sufficient to meet energy demands and produce continuous NAD^+ through the fermentation of pyruvate to lactate. Furthermore, Wang et al., (2022) demonstrate that cytosolic NAD^+ regeneration through the malate aspartate and glycerol phosphate shuttle systems, which shuttle electrons into the mitochondrial matrix and the intermembrane space, respectively, is saturated during 'Warburg metabolism'. Oxidative phosphorylation thus becomes a bottleneck for NADH oxidation, necessitating a metabolic shift to fermentation to meet NAD^+ demands.

Of note, the majority of research elucidating the 'Warburg effect' is performed in culture, using media with high glucose, or unspecified glucose contributions. Glucose is thus present in abundance, with concentrations up to 5-fold greater than in plasma. Under physiological tumor-like glucose conditions, it may be that glucose availability is not sufficient to overdrive glycolysis to the same extent, thereby abolishing the saturation observed. This is one example of how cell culture conditions can potentially introduce artifact into experimental results. This will be discussed in more detail in Section 1.8.

1.6.2 Intrinsic and Environmental Regulation of Cancer Metabolism

While the Warburg effect is not a metabolic remodeling mechanism specifically employed by cancer cells, increased glucose uptake and glycolytic metabolism remains a hallmark feature of cancer metabolism *in vivo*. Notably, cancer cells remain proliferative and metabolically active even when faced with metabolic constraints. This paradoxical behaviour may be best explained by considering the influence of oncogenic and environmental stimuli within the tumour microenvironment.

Most oncogenes commonly dysregulated in cancer belong to the PI3K-AKT-mTOR pathway (Reviewed by Lee & Muller, 2010). Overexpression or constitutive activation of oncogenes belonging to this pathway thus regulate growth promoting processes in a manner uncoupled from canonical pathway stimulation. Rather than requiring growth factors or amino acid signaling to activate mTORC, cancerous cells with this oncogenic signature increase activation of growth promoting processes in a self-sufficient manner (Ho et al., 2012; Wang et al.,

2019). KRAS, PI3K, AKT and RAF are among those oncogene proteins involved in this process, all of which inactivate TSC, promoting mTORC1 activation. In addition to oncogenes, several tumour suppressor gene products also belong to this signaling pathway, and similarly converge on TSC (i.e., PTEN, NF1, LKB1); however, to promote TSC activity. Loss of function of these genes in mutated cancers promotes mTORC1 activation (Corradetti et al., 2004; Johannessen et al., 2005; Ma et al., 2005). Additionally, Myc, a transcription factor overexpressed in many cancer types, regulates metabolism and proliferation downstream of various signaling pathways, including Ras/Raf/ERK and Wnt/β-catenin (Gurel et al., 2008; Qu et al., 2017). Myc overexpression promotes the expression of glycolytic enzymes, GLUT transporters, and monocarboxylate transporters in cancer cells, enhancing glycolytic metabolism (Dang et al., 2006; Gan et al., 2016; Guo et al., 2000; Kim et al., 2004; Osthus et al., 2000). Oncogenic mutations intrinsic to cancer development thus increase metabolic activity independent of canonical nutrient and growth factor signaling. Furthermore, in cancers in which Myc is overexpressed, glycolytic metabolism may be genetically favoured from cancer onset.

In addition to oncogenic regulation, environmental conditions within the tumour may also contribute to glycolytic metabolism hallmarks. As described earlier, hypoxia, a common feature of tumours *in vivo*, promotes glycolytic metabolism through HIF-1 signaling. Furthermore, specific metabolites that accumulate within the tumour microenvironment, known as oncometabolites, can also promote HIF-α stabilization through the inhibition of PHD2. Indeed, oncometabolites such as succinate, fumarate, and 2-hydroxyglutarate (2-HG) are produced in some cancers due to mutations in succinate dehydrogenase (SDH), fumarate hydratase (FH), and isocitrate dehydrogenase (IDH), respectively (Hoekstra & Bayley, 2013; Schmidt et al., 2021; Xu et al., 2011). These metabolites competitively inhibit α-ketoglutarate binding at PHD2, thereby promoting HIF-α stability (Burr et al., 2016; Isaacs et al., 2005; Selak et al., 2005). Normally, α-ketoglutarate facilitates HIF-1α degradation by enhancing the oxygen-dependent activity of prolyl hydroxylases; however, the presence of oncometabolites disrupts this process. Notably, both fumarate and 2-HG were increased in PDAC TIF measurements performed by Sullivan et al., (2019), with absolute concentrations provided.

1.6.3 Metabolic Flexibility

In nutrient limiting conditions, cancer cells must adapt their metabolic utilization strategies to sustain intrinsic growth-promoting signals. Critically, while glucose uptake and PI3K-AKT-

mTOR activation is increased by oncogenes, extracellular nutrient availability is not unlimited *in vivo*. Consequently, cancer cells adapt by enhancing the uptake and utilization of available metabolites and macromolecules. This adaptation is most often accomplished by upregulating the expression of transporters and enzymes.

Amino acid transporters are highly expressed in many tumours to increase uptake for proteinogenic, signaling and metabolic functions. This is regulated downstream of GCN2/AFT cellular stress pathways. For example, large amino acid transporter (LAT1), encoded by *SLC7A5*, is highly expressed in breast cancer, glioblastomas, and pulmonary pleomorphic cancer (An et al., 2016; Ansari et al., 2018; Kaira et al., 2019). Overexpression of this transporter increases the import of branched chain amino acids (BCAA) whose metabolism drives several cancer promoting processes. Indeed, BCAA can fuel TCA cycle through their conversion to glutamine by branched chain amino acid transaminase 1/2 (BCAT1/2), with BCAT itself being overexpressed in glioblastomas, breast cancer and leukemia (Hattori et al., 2017; Tönjes et al., 2013; Zhang & Han, 2017). Glutamine directly replenishes TCA cycle intermediate α-ketoglutarate, namely via glutaminase, whose protein levels are again overexpressed in several cancers (Huang et al., 2014). Furthermore, BCAA are used for de novo nucleotide and amino acid synthesis as they can supply nitrogen and carbon skeletons to biosynthesis reactions (Peng et al., 2020).

Additionally, excitatory amino acid transporter 3 (EAAT3) essential for glutamate and cysteine import, encoded by *SLC1A1*, is overexpressed in lung cancer (W. Guo et al., 2021). Additionally, neutral amino acid transporters of alanine, serine, and cysteine (ASCT1/2), encoded by *SLC1A4* and *SLC1A5*, are overexpressed in virtually all cancers, including prostate, lung, breast, cervical, esophageal, ovarian, renal, brain and hepatic cancers (Scalise et al., 2017). Moreover, the expression of amino acid transporters is associated with tumor grade and prognosis in many of these cancers. Thus, the upregulation amino acid import is a critical adaptive mechanism used by cancerous cells to drive anaplerotic and biosynthetic pathways.

1.7 CELL CULTURE

Cell culture is a fundamental tool used in biomedical research to study the behavior, physiology and molecular mechanisms of mammalian cells. This technique is employed amongst most medical and biotechnology industries, with applications in drug discovery and development, regenerative medicine, vaccine development, and basic research. It is an indispensable tool.

To successfully culture mammalian cells, conditions that support cell growth, viability, and function must be established. Conditions are often tailored to promote specific biological phenotypes, such as replicative growth, differentiation, stemness, and metabolic adaptations. However, little emphasis has been made in the development of culture conditions that accurately replicate the *in vivo* environment of cells. Standard commercial media formulations, such as DMEM and RPMI, frequently contain some constituents at concentrations that far exceed those found in blood plasma, while lacking other components present in extracellular fluid. Moreover, the regulation of oxygen levels in cell culture is frequently overlooked, resulting in cultured cells being exposed to atmospheric levels of ~18% O_2, rather than the 2-11% O_2 levels measured *in vivo*.

1.7.1 Timeline of Cell Culture Advancements

The first instance of vertebrate cell culture can be traced back to experiments performed by German developmental theorist Wilhelm Roux in 1885, during which cells isolated from the neural plate of chick embryos were sustained for several days in a saline buffer solution. In 1910, research exploring the use of natural tissue components to promote cell survival identified key factors present in *in vivo* cellular environments that may improve cell viability *in vitro*. Characterization of these factors later found glucose to be essential to cell survival (Lewis, 1922), proteins and amino acids necessary for cell growth and proliferation (Baker & Carrel, 1926; Carrel & Baker, 1926), and hormones and vitamins important factors in several different cellular processes and interactions (Vogelaar & Erlichman, 1933). Considering these factors, the development of synthetic media that incorporate growth promoting components began. This contributed to the establishment of the first mammalian cell lines using mouse fibroblasts in 1943 (Earle et al., 1943), and the later establishment of the first human continuous cell line from cervical cancer cells, HeLa cells (Gey et al., 1952).

In 1955, Harry Eagle determined the minimum media constituent concentrations required by cells in culture, and thus developed a Minimum Essential Medium (MEM). This medium included 13 amino acids, 8 vitamins, glucose, protein serum, and 6 inorganic salts (Eagle, 1955a, Eagle, 1955b). In 1959, Dulbecco & Freeman modified MEM to increase the concentration of glucose, amino acids and vitamins four-fold, thus creating an excess of these constituents. This increase ultimately ensured that cells in culture had an excess of nutrients, eliminating the need to perform frequent media changes. This media, termed Dulbecco's Modified Eagle's Medium

(DMEM), was soon adopted by many researchers. Currently, DMEM continues to be the most widely used media today with over 28,000 Google Scholar research papers citing its use in 2023.

Although the use of media with an excess of nutrients has become the standard cell culture approach over the past 50 years, recent research conducted through the human metabolome project indicates that these media largely misrepresent *in vivo* cellular environments (Psychogios et al., 2011; Wishart et al., 2008). DMEM provides cells with supraphysiological concentrations of components such as glucose, pyruvate, amino acids and vitamins when compared to human serum (Table 1.3). For instance, many formulations of DMEM contain glucose at concentrations as high as 25mM, while only being present at 5mM in human plasma. Additionally, there are numerous components present in human serum that are not provided in many commercial media, like DMEM. DMEM is also formulated with only ~35 components, while over 220,000 metabolites have been identified in the human body (Human Metabolome Project).

The recognition of the impact of using non-physiological media in cell culture has recently initiated a movement among a small population of researchers toward producing and using physiological media. This initially began with researchers adjusting individual constituent concentrations within traditional media to achieve more physiologic levels, as was seen in the formulation of Serum-like Modified Eagle's Medium (SMEM) by Tardito et al., (2015). In this case, plasma-like glucose, pyruvate and amino acid concentrations were achieved by manipulating existing commercial media. However, the non- physiological levels of the remaining constituents were not ideal, thus the need for a physiological media remained. In response to such demands, Jason Canter and colleagues formulated the first physiological growth media in 2017, containing over 31 metabolites, growth factors and hormones at physiological plasma-like concentrations. This medium was termed Human Plasma-Like Medium (HPLM). In 2019, a second physiological culture media known as Plasmax was developed to further improve physiological culture conditions beyond what was established with HPLM (Vande Voorde et al., 2019). Plasmax was formulated with 66 organic components, including many micronutrients significant to cellular functions that were missing in HPLM (Table 1.3).

In addition to media constituent considerations that have arisen over the last decade, regulation of oxygen to physiological levels has long since been considered. Molecular oxygen is essential for cell survival and function as it plays an important role in several oxygen-consuming processes within the cell, the most obvious being aerobic metabolism. Oxygen is delivered to

tissues and cells via diffusion and convection of atmospheric O_2 at the lungs and through the circulatory system. Oxygen partial pressures drop off from atmospheric levels as the oxygen is dispersed, with the final oxygen concentrations experienced by cells typically ranging from 1-11%, compared to the ~18-21% in the atmosphere (Physoxia Database from Keeley & Mann, 2019). Thus, to maintain physiological culture conditions for cells, oxygen levels must be regulated using O_2-regulating incubators. Nonetheless, in most published research O_2 is not regulated (Abbas et al., 2021). Rather, the use of atmospheric O_2 conditions continues to be common cell culture practice.

Importantly, when regulating oxygen in culture, pericellular oxygen must be considered (Maddalena et al., 2017; Pettersen et al., 2005). While oxygen is regulated in the headspace (gas phase) of oxygen regulating incubators, diffusion of oxygen from headspace (gas phase) to the media (liquid phase), along with the 0.5-1cm distance from the media surface to the cell monolayer (pericellular), is limited (Reviewed in Place et al., 2017). Consequently, in static culture, cellular respiration depletes pericellular oxygen availability, establishing oxygen gradients within the media. Thus, to regulate oxygen to specific partial pressure, pericellular oxygen levels should be considered.

Table 1.3: Metabolite concentrations (uM) in Human Plasma and PDAC TIF compared to a commercially available Plasmax and DMEM. A 3-point colour scale on concentration difference (log fold change) between average TIF and Plasmax was applied. Red colours represent increased concentration in TIF (up to log fold change = 2). Blue colours represent increased concentration in Plasmax (up to log fold change = -2). Green colours represent metabolites quantified in TIF, but not present in Plasmax or DMEM. Yellow colours represent Human Plasma and TIF range, and are not part of the colour scale.

	Human Plasma#	PDAC TIFψ	TIF Average ψ	Plasmax#	DMEM#
Proteinogenic Amino Acids					
L-Alanine	230 – 510	637.1 – 1458	1122	510	N/A
L-Arginine	13 – 64	0.9 – 5.2	2.1	64	398
L-Asparagine	45-130	63 – 146	115	41	N/A
L-Aspartate	0 – 6	246 – 519	399	6	N/A
L-Glutamate	32 – 140	789 – 1300	1054	98	N/A
L-Glutamine	420 – 720	434 – 1330	821	650	4000
L-Glycine	170 – 330	368 – 626	483	330	400

L-Histidine	26 – 120	53 – 117	94	120	200
L-Isoleucine	42 – 100	92 – 198	130	140	802
L-Leucine	66 – 170	204 – 426	289	170	802
L-Lysine	150 – 220	73 – 214	139	220	798
L-Methionine	16 – 30	35 – 107	74	30	201
L-Phenylalanine	41 – 68	54 – 106	80	68	400
L-Proline	110-360	71 – 164	122	360	N/A
L-Serine	56 – 140	55 – 115	88	140	400
L-Threonine	92 – 240	145 – 314	252	240	798
L-Tryptophan	44.8 – 64.2	18 – 71	31	78	78
L-Tyrosine	45 – 74	36 – 111	60	74	399
L-Valine	150 - 310	121 – 222	150	230	803
Non-Proteinogenic Amino Acids					
α-Aminobutyrate	15 – 41	4.7 – 13*	2.93	41	N/A
Arginosuccinate	N/A	0.2 – 1.3	0.75	N/A	N/A
Homocitrulline	N/A	0.4 – 2.2*	0.72	N/A	N/A
L-Citrulline	16 - 55	44 – 119	73	55	N/A
L-Cystine	30 - 65	16 – 111	51	65	201.3
L-Homocysteine	6.1 - 12.1	N/A	N/A	9	N/A
Methionine Sulfoxide	N/A	35 – 107	3.17	N/A	N/A
L-Ornithine	27 - 80	161 - 485	312	80	N/A
N,N,N-Trimethyllysine	N/A	0.9 - 1.7	1.20	N/A	N/A
Sarcosine	N/A	0.9 - 9.4*	0.22	N/A	N/A
Amino Acid Derivatives					
Acetyl carnitine	2.5 - 8.6	19.6 - 34.9*	25	5	N/A
Acetylglutamate	N/A	0.6 - 4.5	1.40	N/A	N/A
N-Trimethylglycine (Betain)	49.6 - 94.4	84 - 219.9*	94	72	N/A
Glutathione (reduced)	32.2 - 41.8	5.4 - 80.8*	22	37	N/A
L-a-Aminoadipate	N/A	10.7 - 21.9	15	N/A	N/A
L-Carnitine	34.1 - 57.3	27 - 54.6*	40	46	N/A
L-Carnosine	5.5 - 7.5	0.6 – 3*	0.49	6	N/A

N-Acetyl-L-aspartate	N/A	2.3 - 6.1*	1.13	N/A	N/A
N-Acetylglycine	69.7	0.1 - 1.8*	23	70	N/A
N,N-dimethyl-L-Arginine (ADMA)	N/A	1.4 - 2.4*	0.84	N/A	N/A
Taurine	45 - 130	1742 - 3070.4	2326	130	N/A
Other Components					
Acetate	26.8 - 57	N/A	350	42	N/A
Allantoin	N/A	59.7 - 191.2*	63	N/A	N/A
Carbamoyl aspartate	N/A	0.3 - 2.2	0.78	N/A	N/A
cis Aconitate	N/A	1.4 - 5.5	2.97	N/A	N/A
Citrate	87.2 - 141.2	164.8 - 585.3	339	114	N/A
Creatine	8.4 – 6	N/A	N/A	37	N/A
Creatinine	60.5 - 87.7	5.5 - 27.3*	12.6	74	N/A
Cytidine	N/A	8.4 - 12.7*	4.60	N/A	N/A
5'-Deoxy-5'-methylthioadenosine	N/A	0.0429 – 0.0831	0.0612	N/A	N/A
D-Glucose	4599 - 5344	808 - 10096	2304	5560	25000
Glycerol	331 - 532	N/A	179	82	N/A
2-hydroxybutyrate	23.5 - 39.1	N/A	84	31	N/A
3-hydroxybutyrate	10.6 - 143.2	12 - 218.5	81	77	N/A
Hypoxanthine	4.5 - 5.3	50 - 152	10	5	N/A
L-Kynurenine	N/A	0.3 - 1.9	1.01	N/A	N/A
Lactate	1118 - 1861	2009 - 6754	3794	500	N/A
Malate	N/A	105.1 - 208.8	156	N/A	N/A
Orotate	N/A	0.5 - 1	0.702	N/A	N/A
Pyruvate	9.3 - 60	10.5 - 100.6	42	100	1000
Sorbitol	N/A	0.6 - 2	1.34	N/A	N/A
Succinate	23.5	69.7 - 164.9*	106	23	N/A
Urea	3920 - 8229	N/A	N/A	3000	N/A
Uric Acid	229 - 315	N/A	N/A	270	N/A
Uridine	1.8 - 4.4	25.8 - 102.5*	61	3	N/A
Xanthine	N/A	4.7 - 13.2*	0.894	N/A	N/A
Vitamins					
Ascorbate	57.9 - 67.3	117.8 - 182.5*	145.7	62	N/A
Choline	9.2 - 19.8	169.1 - 275.2	227.8	7.1	28.6

D-Biotin	0.0006 - 0.0019	0.028 - 0.089	0.0616	4.2	0.53
D-pantothenate	4.5 - 5.3	1.7 - 5.8	3.74	2.1†	8.4
Pyridoxal	0.007 - 0.060	0.1 - 0.3	0.0033	4.9	19.4

TIF=tumour interstitial fluid
PDAC=pancreatic ductal adenocarcinoma
N/A = not applicable as metabolite not present in formulation.
* Semi-quantitative quantification
ψ PDAC TIF metabolomics data source (Sullivan et al., 2019). Ranges shown are minimum and maximum measurements from 7 TIF samples and 5-18 plasma samples. Averages shown are an average of all measurements > 0 uM.
#Plasmax and DMEM media formulations from (Ackermann & Tardito, 2019)

1.8 EFFECTS OF NON-PHYSIOLOGICAL CONDITIONS IN CELL CULTURE

Growing evidence suggests that culture in non-physiological media and oxygen alters numerous aspects of cell biology. Processes such as proliferation, glucose utilization, oxygen consumption, mitochondrial morphology, redox states, and response to drugs exhibit notable changes depending on culture condition.

1.8.1 High Glucose DMEM in Cell Culture

Early evidence that non-physiological media alters biological responses can be found in research performed using traditional DMEM formulations (high glucose) versus 'physiological' DMEM (low glucose). For example, proliferation rates measured in human pancreatic cancer cells cultured in DMEM with glucose concentrations ranging from 5.5mM to 50mM for 12, 24, or 48 show a dose dependent increase in proliferation with increasing concentrations (Han et al., 2011). Similarly, high glucose DMEM (25mM) increases proliferation and viability in non-small-cell lung cancer, breast cancer, and endometrial cancer compared to low glucose DMEM (5mM) (Ding et al., 2018; Han et al., 2015; Hou et al., 2017). In human umbilical vein endothelial and osteosarcoma cells, basal oxygen consumption rates are reduced in high glucose DMEM (25mM) following 6-9 day, and 2-day adaptations, respectively (Balsa et al., 2019; Koziel et al., 2012). Similarly, maximum oxygen consumption and spare respiratory capacity is reduced in C2C12 myoblasts in high glucose DMEM (27.7mM) (Elkalaf et al., 2013). In human skeletal muscle cells, high glucose DMEM (20mM) promotes glucose fermentation, increasing basal glycolytic rate and lactate production (Lund et al., 2019). ROS generation is significantly increased in pancreatic cancer cells cultured in high glucose (25mM) for 24 hours (Luo et al., 2018), and hydrogen peroxide production is increased in a cell-line specific manner (Fonseca et al., 2018). This activates

oxidative stress responses, including the Nrf2/ARE cascade. Finally, high glucose DMEM (25mM) also induces Drp1-dependent mitochondrial fragmentation and impairs mitochondrial membrane potential in primary neonatal rat ventricular cardiomyocytes following 72h exposure (Wu et al., 2021).

In summary, glucose concentration alone is sufficient to alter multiple aspects of cell biology. Supraphysiological glucose concentrations increase cell proliferation, drive glycolytic and non-oxidative metabolism, and increase oxidative stress in cultured cells. Interestingly, these alterations are consistent with Warburg metabolism, suggesting the 'Warburg Effect' may be an artifact of non-physiological cell culture conditions.

1.8.2 Effects of HPLM and Plasmax in Cell Culture

Given the effect of DMEM glucose concentration on cell metabolism, it is unsurprising that media containing physiological concentration of all constituents will have a significant effect on cells *in vitro*. Indeed, both HPLM and Plasmax have been shown to profoundly alter the metabolic landscape of cultured cells compared to RPMI and DMEM, respectively.

Cantor et al. (2017) demonstrate that culture in HPLM has a substantial effect on cellular metabolism. While glycolytic flux did not differ between HPLM and RPMI cultured cells, a cell line specific reduction in basal OCR was measured. Moreover, the fate of glucose differed in HPLM. Using carbon-13 labeled glucose and nitrogren-15 labeled glutamine, they find that in HPLM cultured cells, glucose does not feed into the TCA cycle to the same capacity as in RPMI. Instead, they suggest that exogenous glucose is used for lipid synthesis. Moreover, the fate of glutamine for the biosynthesis of amino acids was increased in HPLM. The most notable finding by Cantor et al., (2017) was that exogenous uric acid present in HPLM but not RPMI, is a direct inhibitor of uridine monophosphate synthase (UMPS). Moreover, 5-fluorouracil, an antimetabolite therapeutic drug that induces cytotoxic effects when metabolized into fluorouridine triphosphate by UMPS, is less effective in UMPS-inhibited cells. Thus, culture in HPLM allowed for the role of an endogenous metabolite, uric acid, to be elucidated. This work also demonstrates the effect of culture media on modulating the effectiveness of drugs.

Vande Voorde et al., (2019) demonstrate that culture in Plasmax has broad effects on cell proliferation, morphology, and gene expression in human triple negative breast cancer cell lines. Importantly, sodium selenite present in Plasmax increased colony formation in cultured cells by maintaining glutathione peroxidase activity, reducing lipid peroxidation, and preventing

ferroptosis. Additionally, following differential gene expression analysis, DMEM-F12 was found to upregulate expression of HIF target and stabilize HIF-1α levels, inducing a pseudohypoxia state in cultured cells at atmospheric conditions. Pyruvate, present at concentrations 10-fold greater than in Plasmax, was identified as the metabolite responsible for HIF-1α stabilization and subsequent HIF signaling. Finally, Vande Voorde et al., (2019) found supraphysiological levels of arginine in DMEM-F12 reverse the activity of argininosuccinate lyase (ASL) in the urea cycle, producing an metabolic rewiring process not relevant to *in vivo* biology.

Since the publication of Plasmax and HPLM, several other research groups have investigated the role of media formulation in cell metabolism. Golikov et al., (2022) show that culture in Plasmax increases basal and maximal mitochondrial respiration, but not glycolysis in Huh, A549, HeLa, and Vero E6 cell lines adapted for 7 days in their respective condition. Moreover, Plasmax increased mitochondrial networking, but not mitochondrial mass or turnover. Thus, Plasmax improves mitochondrial efficiency and OXPHOS, in part by rearranging mitochondrial network. Moradi, et al., (2021a) also show that Plasmax increases basal, maximal and spare OCR, in four cancer cell lines (MCF7, SaOS2, LNCaP, Huh7) at the same atmospheric oxygen conditions used by Golikov et al., (2022). Cell line specific increases in mitochondrial networking was also observed in these conditions. In contrast, while Golikov et al., (2022) found no effect of media on glycolytic metabolism, Moradi, et al., (2021a) show extracellular acidification rate (ECAR), a proxy for glycolytic metabolism, is increased in all cell lines cultured in DMEM. This agrees with the glycolytic results comparing high and low glucose DMEM described above.

Furthermore, Moradi, et al., (2021a) investigate the effect of physiological oxygen (5%) in combination with media composition. While ECAR was increased in all DMEM cultured cells regardless of oxygen, cell-line- and oxygen-dependent effects on OCR were noted. However, in all cell lines except SaOS2, 18% O_2/DMEM had the lowest OCR, consistent with increased glycolytic metabolism in these conditions. In general, OCR was increased in Plasmax at 5% and 18% O_2, with the exception of SaOS2 which was decreased at 18% O_2, and LNCaP, which was decreased at 5% O_2 relative to 5% O_2/DMEM and 18% O_2/Plasmax. Thus physiological media and oxygen culture condition generally promote OXPHOS, with some cell lines decreasing glycolytic and oxidative metabolism all together. In agreement with Golikov et al., (2022), media composition had no effect on mitochondrial abundance at 18% O_2. Further, the specific effect on

mitochondrial network was found to be cell-line specific, with increased mitochondrial networking observed in Plasmax and 5% O_2.

In a separate study, Moradi, et al., (2021b) show similar findings in C2C12 myoblast cells, with Plasmax increasing mitochondrial networking. In contrast to cancer cell lines, 18% O_2 and Plasmax were found to increase mitochondrial abundance in C2C12, with Plasmax reducing basal and maximal respiration regardless of oxygen. Physiological conditions of 5% O_2 and Plasmax showed the lowest OCR of all conditions. 18% O_2 increased basal, maximal and spare respiratory capacity in both media. Thus, while Plasmax increases OCR in cancer cells in a cell line specific manner, the opposite is seen in myoblasts.

In addition to metabolism, several recent publications have also emphasized the role of physiological culture media in promoting conditionally essential processes and vulnerabilities in cancer cells. Using CRISPER/Cas9 genome-wide loss of function genetic screening, Rossiter et al., (2021) identify genes conditionally essential to cells according to media composition, including those encoding glycolytic enzymes and metabolite transporters. Further, a preprint from Flickinger et al., (2023) identify HPLM-sensitive drug treatments that are conditionally lethal depending on drug-nutrient interactions within the media. Conditionality of the chemotherapeutics examined was attributed to the availability of nucleotide salvage pathway substrates present in HPLM. Along these lines, Abbott et al. (2023) demonstrate the differential response of hundreds of metabolism-targeting drugs with culture in non-physiological (RPMI) versus serum-derived culture medium.

1.8.3 Effects of Supra-Physiological Oxygen in Cell Culture

With oxygen regulation having been performed since the 1950s, the effects of supra-physiological oxygen on cultured cells have been characterized and reviewed extensively. The first observations illustrating the effect of oxygen on cells were performed by Cooper et al. (1958), whereby oxygen levels regulated below atmosphere were found to increase growth rate of embryo kidney cells. Since then, an abundance of evidence has been published, suggesting the effects of hyperoxia are rather broad (Reviewed in Alva, Gardner, et al., 2022). Indeed, several other publications suggest that reduced oxygen tensions increase proliferation and replicative lifespan of cultured cells, owing to hyperoxia inducing oxidative damage and replicative senescence in cells (Packer & Fuehr, 1977; Scaffa et al., 2021). Moreover, the effect of supraphysiological oxygen on mitochondrial function appears to be cell-line specific, increasing OXPHOS in human stem cells (Estrada et al., 2012), while reducing OXPHOS in most cancerous and non-stem cell

lines (Moradi, Moffatt, et al., 2021; Timpano et al., 2019). Conversely, there is unanimous agreement that supraphysiological oxygen increases the production of ROS in multiple cell lines, leading to oxidative stress (Estrada et al., 2012; Maddalena et al., 2017; Tiede et al., 2011). Finally, culture in atmospheric oxygen versus 5% O_2 has cell line specific effects on gene expression, with HIF targets commonly enriched at 5% O_2 conditions in all cell lines (Alva, Moradi, et al., 2022).

1.9 CHALLENGES AND LIMITATIONS OF PHYSIOLOGICAL MEDIA

Advancements in physiological cell culture conditions certainly alter many aspects of cell biology. Perhaps most importantly, evidence suggests that cells cultured in physiological media exhibit phenotypes that more closely correlate with those observed *in vivo* (Alva, 2024; Vande Voorde et al., 2019). Nonetheless, maintaining cells in physiological plasma-like media presents two major challenges.

First, plasma-like media are formulated with nutrient contributions substantially lower than in standard media. While successful at establishing metabolic conditions that are physiologically relevant, the longevity of such media over the course of an experiment has not been defined, at least not prior to this thesis. Consequently, cells cultured in Plasmax for prolonged periods may be vulnerable to starvation. In standard cell culture practice using DMEM, cultures can be left for 2-4 days before the media must be replenished. For Plasmax and HPLM, it is likely that similar practices would leave cells nutritionally starved. This problem circles back to the initial motivation behind the development of DMEM from MEM. Importantly, many publications that cite the use of Plasmax or HPLM either do not indicate frequency of media exchange (Coronel et al., 2022; Torres-Quesada et al., 2022), or perform exchanges every 2+ days (MacPherson et al., 2022; Wang et al., 2022a, 2022b). Thus, defining culture practices that ensure intended physiological conditions are maintained throughout experiments is critical.

Second, while plasma-like media, particularly Plasmax, is described as a physiological media for ‘cancer models', cancerous cells from solid tumour are not directly exposed to circulating plasma. Instead, they are bathed in tumour interstitial fluid. Moreover, Plasmax differs quite substantially from TIF (Table 1.3), and ultimately does not effectively model the tumour microenvironment. Thus, to improve cancer cell culture models, physiological media formulated using TIF nutrient concentrations must be achieved.

1.10 THESIS OBJECTIVE AND OUTLINE

The main objective of this thesis was to enhance our understanding of how the nature of *in vitro* models affects cancer cell biology and therefore experimental outcomes. Specifically, I investigated how physiological culture conditions affect cancer cell metabolism. In Chapter 2, I explore nutrient exhaustion in physiological plasma-like medium (Plasmax), and the adaptive mechanisms by which cancer cells can maintain survival under metabolic stress conditions. Here, I found that glucose and amino acids are rapidly depleted from Plasmax following a standard culture period of 48 hours. Notably, a transcriptional response suggestive of adaptive metabolic stress pathways was observed, including enrichment of terms association with amino acid biosynthesis and uptake. While results suggested that media replenishment may ameliorate metabolic stress responses in physiological culture practices, the adaptive mechanisms were consistent with metabolic reprogramming that would be expected in depleted tumour environments. I thus hypothesized that the conditions established in nutrient depleted Plasmax evoke adaptive metabolic responses representative of *in vivo* hallmarks. In Chapter 3, I developed a novel cell culture medium using tumour interstitial fluid metabolomics data to explore this, named Tumour Microenvironment Medium (TMEM). I established nutrient and oxygen culture conditions representative of the murine PDAC microenvironment in a PDAC cell line, and investigated the adaptive phenotypes acquired by cultured cells compared to plasma-like conditions. Importantly, I found that culture conditions representative of the tumour microenvironment modulate numerous hallmark features of cancer cells. Cell migration, proliferation, glucose consumption and utilization, and mitochondrial bioenergetics were each altered in ways relevant to *in vivo* cancer biology. Overall, these findings highlight the importance of representative culture conditions in the acquisition of biologically accurate experimental data.

Chapter 2: Rapid Nutrient Depletion to Below the Physiological Range by Cancer Cells Cultured in Plasmax

This chapter is published as: Gardner, G. L., Moradi, F., Moffatt, C., Cliche, M., Garlisi, B., Gratton, J., Mehmood, F., & Stuart, J. A. (2022). Rapid nutrient depletion to below the physiological range by cancer cells cultured in Plasmax. *American Journal of Physiology-Cell Physiology*, *323*(3), C823-C834.

Author contributions

I performed all experiments and manuscript writing. MC, BG, JG and FM assisted with some cell culture experiments. CSM assisted with Seahorse assays. JAS contributed to manuscript editing.

2.1 ABSTRACT

Mammalian cell culture is a fundamental tool used to study living cells. Presently, the standard protocol for performing cell culture involves the use of commercial media that contain an excess of nutrients. While this reduces the likelihood of cell starvation, it creates non-physiologic culture conditions that have been shown to 're-wire' cellular metabolism. Recently, researchers have developed new media like Plasmax, formulated to approximate the nutrient composition of human blood plasma. Although this represents an improvement in cell culture practice, physiologic media may be vulnerable to nutrient depletion. In this study I directly addressed this concern by measuring the rates of glucose and amino acid depletion from Plasmax in several cancer cell lines (PC-3, LNCaP, MCF-7, SH-SY5Y) over 48 hours. In all cell lines, depletion of glucose from Plasmax was rapid such that, by 48h, cells were hypoglycemic (<2mM glucose). Most amino acids were similarly rapidly depleted to sub-physiological levels by 48h. In contrast, glucose and most amino acids remained within the physiological range at 24h. When the experiment was done at physiological oxygen (5%) versus standard (18%) with LNCaP cells, no effect on glucose or amino acid consumption was observed. Using RNA sequencing, I show that this nutrient depletion is associated with enrichment of starvation responses, apoptotic signaling, and endoplasmic reticulum stress. A shift from glycolytic metabolism to mitochondrial respiration at 5% O_2 was also measured using Seahorse analysis. Taken together, these results exemplify the metabolic considerations for Plasmax, highlighting that cell culture in Plasmax requires daily media exchange.

2.2 INTRODUCTION

Cell culture is a widely utilized technique that has been vital to improving our understanding of the cellular, molecular, and biochemical properties of living cells. With well-established practices and commercially available material produced throughout the world, cell culture serves as an accessible and efficient approach in cell biology. Current cell culture practices have their origins in the mid-19th century, with the first commercial medium for mammalian cell culture being later developed by Harry Eagle in the 1950s (Eagle, 1955b; Eagle 1955a; Eagle, 1959). This medium, termed Minimum Essential Medium (MEM), included 13 amino acids, 8 vitamins, 6 inorganic salts, glucose, and protein serum. In 1959, Dulbecco and Freeman modified MEM by increasing the concentrations of amino acids approximately four-fold, to avoid their depletion over time in static culture (Dulbecco & Freeman, 1959). Dulbecco's Modified Eagle's Medium (DMEM) has since been widely adopted by researchers and is currently the most widely used mammalian cell culture medium, with over 23,000 Google Scholar research papers citing its use in 2020.

Although the use of media like DMEM has been incorporated into a standard cell culture workflow, there is a growing awareness of how its failure to mimic the *in vivo* cellular environment impacts cell biology (Cantor et al., 2017; Psychogios et al., 2011; Vande Voorde et al., 2019; Wishart et al., 2018). Non-physiological culture media can drive changes in cell phenotypes that cause cellular activities to diverge from their *in vivo* states (Gui et al., 2016; Maeda & Khatami, 2018; McKee & Komarova, 2017; Muir et al., 2017; Poulsen et al., 2014). In recognition of this limitation of commercial media, Canter et al. (2017) developed Human Plasma-Like Medium (HPLM), which is modeled after the human blood serum metabolome, containing over 31 metabolites, growth factors, and hormones at concentrations within their physiological ranges. In 2019, a second physiological culture medium, Plasmax (Vande Voorde et al., 2019), was formulated with 66 organic components, including many micronutrients that are not found in HPLM. In the breast cancer cell lines used to characterize the effects of Plasmax, the medium was found to influence proliferation, morphology, colony formation, gene expression, and the intracellular metabolome (Vande Voorde et al., 2019).

These observations point to the need for cell culturists to adopt increasingly physiologic cell culture conditions, including the use of media like Plasmax. However, since Plasmax does not contain nutrients in excess, it is vulnerable to nutrient depletion by cells in static culture,

particularly where media exchange is performed every other day. Here I directly addressed this concern by determining the rates of nutrient uptake in four commonly studied cancer cell lines (PC-3, LNCaP, MCF-7 and SH-SY5Y) over a 48h culture period in Plasmax. The experiments were performed at physiological (5% O_2), and standard (18% O_2) oxygen conditions. In both oxygen environments, I found rapid depletion of glucose from Plasmax in all four cell lines such that, by 48h, typically only ~20% of the initial glucose remained (~1.5 mM versus ~6 mM at time = 0h). Similar rapid depletion was found for most amino acids, most of which had fallen below the range reported in human blood plasma by 48h. RNA sequencing performed on LNCaP cells cultured for 48h in depleting media indicates that nutrient exhaustion initiates extensive starvation-mediated stress responses. Similarly, Seahorse metabolic flux analysis suggests that nutrient depletion is associated with oxygen-dependent metabolic reprogramming in LNCaP cells.

2.3 MATERIALS AND METHODS

2.3.1 Cell Culture

PC-3, LNCaP, MCF-7 and SH-SY5Y cell lines were purchased from the American Type Culture Collection (Manassas, VA, USA). All cell lines were cultured in Plasmax media supplemented with 2.5% FBS and penicillin (50 I.U./mL) / streptomycin (50 μg/mL). Plasmax was formulated according to the protocol outlined by Vande Voorde et al. (2019), with adjustments made to produce 5L Plasmax batches.

Plates were initially maintained in humidified 5% CO_2 atmosphere at 37 °C inside Forma 3110 water-jacketed incubators (ThermoFisher, Waltham, MA, USA). Cell lines were seeded from frozen stocks onto 100mm cell culture plates and cultured in Plasmax continuously for two weeks prior to the initiation of the experiment to allow cells to equilibrate to the medium (they had previously been cultured in DMEM). Cells were incubated using either a standard cell culture O_2 level (~18% O_2; superphysiologic) or physioxia (5% O_2). All media were conditioned in the corresponding incubator for 24hr prior to use to ensure equilibration with the ambient condition. Media changes were performed daily, with cell passaging performed when plates reached ~80% confluency. After this two-week equilibration period, the experiments were initiated.

For all experiments, cells were counted using a hemocytometer and seeded between 300,000 and 1,000,000 cells per 100mm culture plate. Two plates were seeded per cell line and oxygen condition. 20mL of Plasmax was added to each plate, and cells were incubated for 48h. At

0h, two 1mL media samples were collected directly from the fresh Plasmax bottle. At 24h and 48h, two 1mL media samples were collected from each plate. No media changes were performed throughout the 48-hour period. The experiment was repeated three times per oxygen condition, for a total of six samples per cell line for each O_2 level.

2.3.2 Media Glucose and Amino Acid Analysis

Two 1mL samples were collected per plate per condition and centrifuged at 200g for two minutes to separate media from any cell debris. The supernatant was transferred to cryovials, snap frozen in liquid nitrogen, and stored at -80°C for up to eight months. Glucose concentration of samples was determined using a GlucCell (CESCO Bioengineering, Taichung, Taiwan, R.O.C) measurement device. A glucose standard curve was established using 1.25, 2.5, 5, and 10mM glucose standards in Plasmax medium. Each sample and standard was tested 2-3 times.

2.3.3 Liquid Chromatography – Mass Spectrometry Amino Acid Analysis

Amino acids were identified and quantified essentially as in Huang et al., 2018 and Ozcan & Senyuva, 2006. The samples were analyzed using Agilent LCMS 1260 Infinity II in atmospheric pressure chemical ionization mode (APCI). The system consisted of the Agilent 1260 Multicolumn Thermostat (Cat #G7116A), Vialsampler (Cat #G7129C), Flexible Pump (Cat #G7104C), and MSD (Cat #G6125C) equipped with APCI interface. The software for data analysis and acquisition was Agilent_OpenLab CDS. Data acquisition was performed in SIM mode using the interface parameters: gas temperature at 320°C, vaporizer temperature of 425°C, nebulizer pressure of 55 psi, and gas flow of 4 L/min. Ions monitored for 15 underivatized amino acids using the Quantifying Ions (m/z) and Internal Standard Quantifying ions (m/z) listed in Supplemental Table 2.1.

The chromatographic separations were performed with the Agilent InfinityLab Poroshell 120 HILIC-Z (2.1x100mm) column using 20mM ammonium formate in water at pH=3 (Mobile Phase A), and 20mM aqueous ammonium formate at pH=3 in 9:1 acetonitrile/water. The injection volume was 5uL, with a flow rate of 0.5mL per minute. A gradient of Mobile Phase A and Mobile Phase B was applied as follows: from 0-11.5min isocratic elution with 100% B; from 11.5-12min, 70% B and 30% A; from 12-25 100% B; from 25min, maintained at 100% B for 5 minutes for re-equilibration.

Media samples were thawed from –80°C storage within 30 minutes of sample preparation. Samples were vortexed and sonicated for 5 seconds each before being transferred to Agilent 2mL

glass vials. 475uL of sample and 25uL of internal standard solution containing the following deuterated amino acids from CDN Isotopes were added to each vial: L-Alanine-3,3,3-d_3 (Cat. #D-1297), L-Aspartic-2,3,3-d_3 Acid (Cat. #D-0898), L-Glutamic-2,4,4-d_3 Acid (Cat. #D-8010), Glycine-2,2-d_2 (Cat. #D-0064), L-Leucine-d_7 (iso-propyl-d_7), L-Lysine-3,3,4,4,5,5,6,6-d_8 (Cat. #D-2555), L-Methionine-d_3 (Cat. #D-1292), and L-Phenyl-d_5-alanine-2,3,3-d_3 (Cat. #D-1241). Vials were inverted and vortexed before being placed in the loading dock. Six samples were run at a time, with two vials per sample, for a total of 12 vials. Samples were analyzed at room temperature, with each run taking ~6 hours to complete. Time 0h samples served as control concentrations for each run.

Quantitative analysis of amino acid concentrations within the samples was accomplished using a 5-point calibration curve of Amino Acid Standard analytical standards diluted with HPLC LC-MS grade water against the retention factor (Rf, a ratio of the analyte ion area to internal standard ion area). A minimum R^2 value of 0.96 was ensured for each curve prior to proceeding to sample analysis. Sample amino acids were also compared against closely eluting deuterated internal standards.

OpenLab CDS Data Analysis (version 2.4) was used to analyze chromatographs obtained from sample readings. Amino acid and deuterated internal standard peaks were manually processed according to retention times provided by Huang et al., (2018). The area under the curve (AOC) for each peak was then automatically integrated, and amino acid and internal standard quantifying ion integrations were compared to determine the Rf. The Rf was then used to calculate the concentration of the main acid based on the linear calibration equation.

*2.3.4 Consumption/Cell*Hour Calculation*

To calculate the nutrient consumption rate, I used a cell*hour calculation to estimate the number of cells and the time over which they were present throughout the experiment. Exponential growth equations were calculated in Excel using the 0h and 48h cell counts. The equation was used to estimate the number of cells present over each 1h period from 0h to 48h. Nutrient consumption after 48 hours was then divided by the sum of the number of hours each newly proliferated cell was present for. Using this cell hour approach to nutrient consumption allowed for the exponential increase in cells throughout the study period to be accounted for, whilst also considering the number of hours each new cell was present and thus metabolically active.

2.3.5 Presens Oxodish Procedure

24-well disposable Oxodish plates (OD24; PreSens, Regensburg, Germany) were used to monitor pericellular oxygen levels in cells cultured under 5% O_2 to monitor pericellular hypoxia. The number of cells seeded and the final volume of media in each well was adjusted to maintain the same cell density and media column height of a typical 100mm culture. Pericellular O_2 levels were measured at 10-minute intervals for 50 hours.

2.3.6 RNA Extraction

Total RNA was extracted from LNCaP cells cultured in Plasmax for 48 hours with either A) a media change performed after 24h or B) with no media change performed. This was repeated at both 18% and 5% O_2. The Qiagen RNAeasy Mini Plus kit (Hilden, Germany) was used for this extraction. RNA samples from three replicates per experimental condition were then pooled into one sample. RNA purity and concentration were evaluated using a 260/280 ratio measured using a nanodrop spectrophotometer (ThermoFisher Scientific, MA, USA). RNA degradation and integrity was assessed using 1% agarose gel electrophoresis. Pooled samples were then snap frozen in liquid nitrogen and stored at –80 C until before being sent to Novogene Incorporated (Sacramento, CA, USA) for RNA sequencing.

2.3.7 Library Preparation and Sequencing

All RNA samples received by Novogene underwent additional quality control (QC) tests prior to sequencing to assess RNA integrity and purity. These included Nanodrop spectrophotometry and Agarose Gel Electrophoresis. After successfully passing the initial QC assessment, the RNA library was constructed for the samples. mRNA within the total RNA samples were enriched using poly-T oligo-attached magnetic isolation beads that selected for the polyA tails of mRNA, thus purifying the mRNA from total RNA. The cDNA was then synthesized from the mRNA template using random hexamer primers, a custom second-strand synthesis buffer (Illumina), dNTPs, RNase H and DNA polymerase I. A tailing, sequencing adaptor ligation and end-terminal repair were performed, followed by size selection and PCR enrichment to produce the completed double-stranded cDNA library. QC was performed on the RNA library using Qubit 2.0 for preliminary concentration measurements, Agilent 2100 for insert size analysis, and qPCR for precise library concentration quantification. mRNA sequencing of the completed cDNA library was performed by Novogene on the Illumina NovaSec 6000 Sequencing System with a pair-end 150bp read length and a read-depth of >20 million reads per sample.

2.3.8 RNA Seq Data Analysis

To improve analysis quality and reliability, raw sequenced read filtering was performed in which reads containing adaptors, N>10% (N=bases that cannot be determined), and low quality Qscores of <=5 in over 50% of the bases (Qscore=Quality value) were removed. Reads were aligned to the reference genome (*Homo sapiens* GRCh38) using Hisat2 v2.0.5. Gene expression was estimated using the FPKM (Fragments per Kilobase of transcript sequence per Millions base pairs sequenced) of each gene. Differentially expressed gene lists were provided by Novogene, comparing gene expression with no media change versus media change at T24h. These DEGs were reduced to genes with a *p*-value < 0.05, log2(FC) ≥1 (equal to FC ≥ 2), and FPKM value to be a minimum of 5 in at least one of the two samples in the comparison to ensure the genes observed were strongly affected.

2.3.9 Functional Enrichment Analysis

Functional enrichment analysis was performed using Database for Annotation, Visualization, and Integrated Discovery (DAVID) version 6.8 with default settings. The reduced DEG lists were imputed, using *Homo sapiens* as the reference species. Enriched GO Terms, KEGG Pathways, and Reactome Pathways were reduced to terms with either a p-value <0.05 or a Benjamini adjusted p-value <0.05, as indicated.

2.3.10 Cellular Respiration

Cellular respiration was evaluated in LNCaP cells cultured in Plasmax. Oxygen consumption rate (OCR) and extracellular acidification rate (ECAR) were measured using a Seahorse Extracellular Flux Analyzer XFe24 Mito Stress test (Agilent, Santa Clara, CA). To encourage cell adherence, Seahorse XFe24 plates were coated with Poly-D-lysine hydrobromide (Sigma-Aldrich, MO, USA) the night before seeding. Cells were seeded 48h prior to measurement, with media change performed on half the wells after 24h. One hour before the Mito Stress test, all wells were replaced with Plasmax media free of serum, sodium bicarbonate and penicillin/streptomycin supplementation, and moved to a CO_2 free incubator. One final wash using the same media was performed directly before the assay. For the Mito Stress Test, 1uM oligomycin A, 1 uM FCCP and 0.5uM rotenone/antimycin A were sequentially added by the Flux Analyzer, according to standard protocol. Hoechst 33342 nuclear staining dye (Sigma-Aldrich, MO, USA) was added to the final injection to visualize, image and count the cells. Cells were imaged using a Zeiss Axio Observer 7 (Oberkochen, Germany) and counted using an ImageJ cell counter plugin.

2.3.11 Statistical Analysis

Statistical analyses were performed using Microsoft Excel version 15.38 software and Prism 8.4.3 (San Diego, CA). For glucose concentration experiments, two-way ANOVA and Tukey-Kramer Post Hoc tests were performed to test for effect of oxygen level (5% vs. 18%) and time (0h, 24h, 48h) on media glucose concentration for each cell line. For glucose uptake rate experiments, unpaired t-tests (two-tailed) between 18% and 5% oxygen conditions were performed for each cell line. For oxygen consumption experiments, two-way ANOVA and Tukey-Kramer Post Hoc tests were performed to test for effect of oxygen level (5% vs 18%) and media exhaustion (media change vs. no media change) on OCR and ECAR. Statistical significance was established at p-value ≤ 0.05 unless otherwise stated for RNA sequencing. All averaged data was presented with standard error of means [SEM].

2.4 RESULTS

Cell lines were seeded on 100mm culture plates with 300,000 to 1,000,000 cells to mimic seeding densities typical of a cell culture-based experiment. At confluence, plates of this size hold close to ten million cells, so for an experiment lasting 48h, this was not a particularly high density. Cells were cultured in 20mL of medium, which is greater than some recommendations (ThermoFisher Cell Culture Protocols), and within the recommended 1mL/100,000 cells/day provided by Vande Voorde et al., (2019). Nonetheless, I saw appreciable nutrient depletion under these conditions that could affect the integrity of multi-day experiments that do not incorporate daily media changes.

Target fasting blood glucose concentrations in healthy adults is <5.6 mM (Imran et al., 2018), with biochemical hypoglycemia diagnosed when glucose concentrations fall below 3.0 mM (International Hypoglycaemia Study Group, 2017). Plasmax is formulated with 5.56 mM glucose, using Human Serum Metabolome measurements for reference (Psychogios et al., 2011). I used the Plasmax formulation reported by Vande Voorde et al., (2019), which is supplemented with 2.5% FBS. Although the glucose concentration of FBS is variable, average glucose contributions of ~17 mM have been reported across different FBS batches (Owens & Kind, 2008). Our 0h glucose measurements in Plasmax supplemented with 2.5% FBS averaged 6.0 +/- 0.1 mM **(Table 2.1)**, which is consistent with the above values.

Table 2.1: Media glucose concentrations for PC-3, SH-SY5Y, MCF-7 and LNCaP cells cultured in cultured at 18% or 5% O_2 for 48h. Blue colours represent the fold-change depletion of glucose in reference to the lower limit of the physiological range. A 5-point cut-off on the colour scale was applied to the fold change to assign the colour. Yellow cells represent concentrations above the lower limit of the physiologic range.

Oxygen Condition	Sampling Time	Mean Glucose Concentration [mM] (SEM)			
		LNCaP	PC-3	SH-SY5Y	MCF-7
18% O_2	0h	**5.9** (0.1)	**6.2** (0.1)	**5.8** (0.1)	**5.8** (0.3)
	24h	**3.1** (0.2)	**4.0** (0.3)	**3.4** (0.3)	**4.5** (0.5)
	48h	**1.1** (0.1)	**1.4** (0.1)	**1.7** (0.6)	**1.8** (0.3)
5% O_2	0h	**6.2** (0.1)	**5.9** (0.2)	**5.7** (0.1)	**6.2** (0.5)
	24h	**2.6** (0.8)	**2.9** (0.9)	**3.8** (0.3)	**5.8** (0.7)
	48h	**1.3** (0.2)	**1.9** (0.4)	**1.4** (0.2)	**2.3** (0.6)

Values are in mM and are **means** (SEM), n=3, except for time 0h which is n=6.

Significant glucose depletion from Plasmax was observed over 48h in culture in all cell lines and in all experimental conditions **(Table 2.1, Supplementary Figure 2.1)**. At 24h, the media glucose concentration averaged across all four cell lines was 3.8 +/- 0.3 mM at 18% O_2 and 3.8 +/- 0.7 mM at 5% O_2. Although not considered hypoglycemic, these concentrations were below healthy adult human plasma ranges (Psychogios et al., 2011). At 48h, glucose concentrations had fallen below 2mM in most cell lines, averaging 1.5 +/- 0.2 mM at 18% O_2 and 1.7 +/- 0.2 mM at 5% O_2. Thus, all cell lines were experiencing hypoglycemic conditions following 48h continuous culture in Plasmax, with O_2 level having no measurable effect on this outcome. I used Presens Oxodish technology to measure pericellular O_2 levels at 5% O_2, since hypoxia can develop under these conditions (Maddalena et al., 2017). However, pericellular O_2 remained above 3.7% for all cell lines cultured at 5% **(Figure 2.1)**, confirming no pericellular hypoxia.

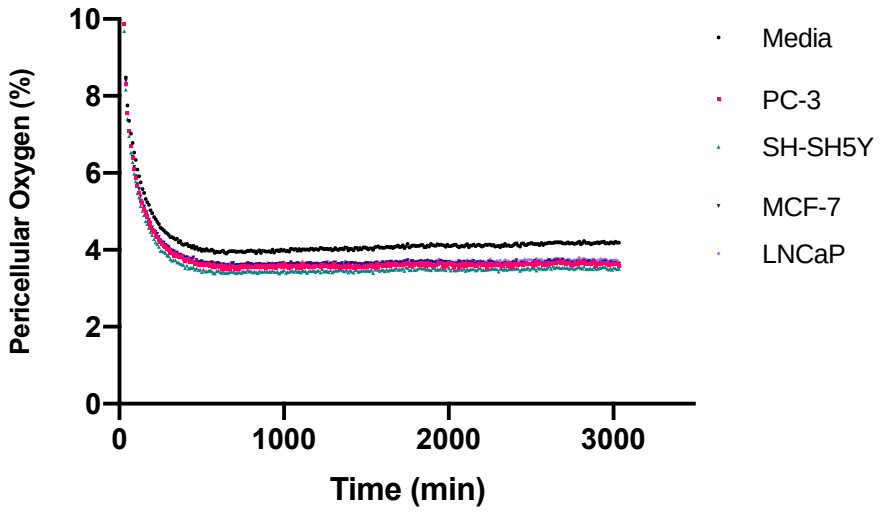

Figure 2.1: PreSens Oxodish Pericellular Oxygen Readings for LNCaP, PC-3, SH-SY5Y, MCF-7, and control media over 3000 minutes. All cell lines observed to maintain pericellular oxygen levels above 3.7% O_2 for the entirety of the test period. Date shows means of 4-5 technical replicates within one PreSens Oxodish.

Specific glucose consumption rates were calculated for all cell lines. Rates of glucose consumption were standardized to cell*hour to account for exponential growth over each 48h experiment **(See Supplemental Figure 2.2 and 2.3 for growth curves**). The glucose consumption rates calculated using this method ranged from 740-2312 fmol/cell*h across cell lines **(Table 2.2)**. No significant differences were found between rates of glucose consumption at 5% versus 18% O_2 of any cell line, with the exception of SH-SY5Y cells, which consumed glucose at faster rates at 5% O_2, despite showing no signs of pericellular hypoxia.

Table 2.2: Glucose consumption rates of cells lines in Plasmax and standard culture media. Data include results of present study and published values.

Cell Line	Glucose Consumption Rate	Conditions	Reference
MCF-7	759 ± 46.7 fmol/cell*h	Plasmax, 18% O_2	Present Study
	742 ± 68.1 fmol/cell*h	Plasmax, 5% O_2	Present study
	280 fmol/cell*h	RPMI-1640, 21% O_2 (10mM Glucose, 2mM Lactate, 10% heat inactivated FBS)	(Prado-Garcia et al., 2020)

	438 fmol/cell*h	DMEM (5mM Glucose, 20% FBS)	(Mazurek et al., 1997)
	208 fmol/cell/h	IMEM (11mM Glucose, 10% FBS)	(Kaplan et al., 1990)
PC-3	1903 ± 552.3 fmol/cell*h	Plasmax, 18% O_2	Present Study
	1821 ± 642.63 fmol/cell*h	Plasmax 5% O_2	Present Study
	208 fmol/cell/h	RPMI 1640 (11.11mM Glucose, 10% FBS, atmosphere with 5% CO_2)	(Vaz et al., 2012)
	729 fmol/cell/h	Complete RPMI-1640 (10% FBS)	(Fu et al., 2010)
LNCaP	1772 ± 105.6 fmol/cell*h	Plasmax, 18% O_2	Present Study
	2159 ± 315.5 fmol/cell*h	Plasmax, 5% O_2	Present Study
	208 fmol/cell/h	RPMI 1640 (11.11mM Glucose, 10% FBS, atmosphere with 5% CO_2)	(Vaz et al., 2012)
SH-SY5Y	1095 ± 205.1 fmol/cell*h (#)	Plasmax, 18% O_2	Present Study
	2312 ± 75.8 fmol/cell*h	Plasmax, 5% O_2	Present Study
H1299	300 fmol/cell*h	RMPI-1640 or DMEM, 21% O2, 10% heat inactivated FBS	(Hosios et al., 2016)
A-549	200 fmol/cell*h	RMPI-1640 or DMEM, 21% O2, 10% heat inactivated FBS	(Hosios et al., 2016)
	155 fmol/cell*h	RPMI-1640, 21% O2 (10mM Glucose, 2mM Lactate, 10% heat inactivated FCS	(Prado-Garcia et al., 2020)
MDA-468	204 fmol/cell*h	IMEM with 11mM Glucose (10% FCS)	(Kaplan et al., 1990)
A-427	700 fmol/cell*h	RPMI-1640, 21% O2 (10mM Glucose, 2mM Lactate, 10% heat inactivated FCS)	(Prado-Garcia et al., 2020)

DU145	687.5 fmol/cell/h	Complete DMEM (10% FBS)	(Fu et al., 2010)

Rates presented in fmol/cell*h and fmol/cell/h due to differences in reporting glucose uptake measurements. # represents significantly different from rate at 5% O_2. Significance measured by unpaired student t-test (two-tailed) between 18% and 5% oxygen conditions.

Comparison with published values for glucose consumption rates shows considerable variability between reported literature values **(Table 2.2).** The glucose consumption rates of MCF-7 cells in our experiments were 2-4 times greater than published values for MCF-7 cells in a variety of media. Indeed, glucose consumption rates reported in the literature are not consistent between publications and it is unclear whether this is due to differences in media and/or FBS concentrations, or other factors. Controlled comparisons of glucose consumption by the same cell line in different media will be required to address these discrepancies.

Concentrations of amino acids in fresh Plasmax were at the high end of the physiological range reported in blood plasma or healthy humans for most measurements (Ackermann & Tardito, 2019). Unfortunately, I could not find data reporting typical concentrations of individual amino acids in FBS, thus serum contributions within our measurements could not be compared. Our 0h values for individual amino acids reflect the sum of Plasmax and FBS concentrations. Importantly, at the beginning of these experiments, all amino acids were within the range reported for human blood plasma, or slightly above **(Tables 2.3-2.6, Supplementary Figure 2.4)**.

Table 2.3: Amino acid concentrations (uM) in media at 0, 24, and 48h following cell seeding for LNCaP cells cultured in Plasmax and incubated at 5% CO_2 and either 5% or 18% O_2. Blue colours represent the fold change depletion of each amino acid in reference to the lower limit of the physiological range. A 5-point cut-off on the colour scale was applied to the fold change to assign the colour. Yellow cells represent concentrations above the lower limit of the physiologic range.

Amino Acid	**Human Plasma Range** (uM)	**Time**				
		0h	**24h**		**48h**	
			5% O_2	**18% O_2**	**5% O_2**	**18% O_2**
Alanine	230-510	**615.5** (6.1)	**377.8** (10.9)	**355.0** (35.0)	**194.9** (51.9)	**192.9** (16.6)
Arginine	13-64	**72.2** (0.004)	**18.6** (2.2)	**17.1** (4.0)	**9.2** (1.0)	**7.9** (4.0)
Aspartic Acid	0-6	**6.6** (0.6)	**5.3** (0.5)	**4.5** (1.2)	**1.6** (0.6)	**1.1** (0.2)
Glutamic Acid	32-140	**99.0** (2.0)	**66.5** (0.9)	**59.6** (8.2)	**33.8** (6.0)	**38.1** (2.2)
Glycine	170-330	**245.6** (6.9)	**187.3** (8.6)	**172.4** (17.1)	**98.0** (22.5)	**89.0** (3.8)
Histidine	26-120	**146.3** (0.005)	**79.7** (15.6)	**78.9** (21.4)	**41.1** (4.3)	**49.4** (5.3)
Lysine	150-220	**143.7** (2.6)	**103.0** (4.7)	**95.5** (7.1)	**54.7** (12.1)	**52.7** (3.9)
Methionine	16-30	**22.3** (0.4)	**14.5** (1.0)	**12.9** (1.3)	**5.0** (2.2)	**4.8** (0.7)
Phenylalanine	41-68	**55.3** (0.5)	**38.2** (1.6)	**35.2** (2.8)	**16.5** (6.0)	**15.1** (1.6)
Proline	110-360	**264.9** (16.8)	**192.9** (14.3)	**188.9** (20.8)	**105.9** (29.1)	**105.9** (7.7)
Serine	56-140	**89.7** (3.7)	**66.8** (7.8)	**62.0** (0.8)	**35.3** (11.6)	**27.7** (3.3)
Threonine	92-240	**153.2** (5.8)	**115.6** (20.6)	**110.0** (17.8)	**63.2** (18.8)	**45.7** (3.8)
Tryptophan	45-64	**64.6** (1.0)	**53.3** (2.1)	**50.9** (3.1)	**38.2** (4.1)	**38.4** (1.5)
Tyrosine	45-74	**59.2** (1.9)	**48.3** (2.2)	**47.0** (4.7)	**33.2** (2.9)	**33.6** (1.8)
Valine	150-310	**195.4** (13.2)	**149.2** (14.8)	**153.4** (35.5)	**73.5** (16.7)	**78.6** (18.6)

Values are in µM and are **means** (SEM), n=3 for each oxygen condition, except for time 0h which is n=6. Human Plasma Ranges for individual amino acids were taken from Ackerman and Tardito (2019).

Table 2.4: Amino acid concentrations in media at 0, 24, and 48h following cell seeding for PC-3 cells cultured in Plasmax. Blue colours represent the percent depletion of each amino acid in reference to the lower limit of the physiological range. A 5-point cut-off on the colour scale was applied. Yellow cells represent concentrations above the lower limit of the physiologic range.

Amino Acid	**Human Plasma Range** (uM)	**Time**		
		0h	**24h**	**48h**
Alanine	230-510	**589.4** (5.0)	**249.7** (70.2)	**155.2** (6.1)
Arginine	13-64	**57.2** (1.7)	**10.4** (2.9)	**7.0** (0.2)
Aspartic Acid	0-6	**5.9** (0.3)	**2.6** (0.1)	**2.1** (0.3)
Glutamic Acid	32-140	**97.8** (3.9)	**47.0** (10.5)	**29.8** (0.1)
Glycine	170-330	**283.4** (6.2)	**132.8** (34.4)	**76.4** (2.3)
Histidine	26-120	**139.0** (4.9)	**46.5** (8.0)	**36.4** (0.6)
Lysine	150-220	**164.9** (1.8)	**71.3** (22.7)	**42.8** (1.3)
Methionine	16-30	**26.7** (0.2)	**7.6** (4.2)	**2.6** (0.4)
Phenylalanine	41-68	**66.1** (0.9)	**25.2** (10.0)	**12.2** (1.4)
Proline	110-360	**289.6** (9.4)	**135.8** (40.3)	**85.8** (0.7)
Serine	56-140	**109.4** (3.4)	**55.4** (16.3)	**30.2** (0.3)
Threonine	92-240	**175.1** (4.8)	**82.9** (26.8)	**48.7** (0.5)
Tryptophan	45-64	**77.5** (1.5)	**43.4** (8.0)	**34.4** (1.0)
Tyrosine	45-74	**72.2** (1.2)	**41.0** (7.4)	**31.4** (0.9)
Valine	150-310	**269.2** (11.3)	**111.9** (37.1)	**67.9** (1.1)

Values are in µM and are **means** (SEM), n=2 from pooled 18% O_2 and 5% O_2 measurements. Human Plasma Ranges for individual amino acids were taken from Ackerman and Tardito (2019).

Table 2.5. Amino acid concentrations in media at 0, 24, and 48h following cell seeding for SH-SY5Y cells cultured in Plasmax. Blue colours represent the percent depletion of each amino acid in reference to the lower limit of the physiological range. A 5-point cut-off on the colour scale was applied to the fold change to assign the colour. Yellow cells represent concentrations above the lower limit of the physiologic range.

Amino Acid	**Human Plasma**			
		Time		
	Range (uM)	**0h**	**24h**	**48h**
Alanine	230-510	**598.8** (7.1)	**373.3** (40.9)	**254.0** (79.2)
Arginine	13-64	**57.6** (1.5)	**15.3** (0.5)	**10.9** (5.1)
Aspartic Acid	0-6	**7.3** (0.6)	**5.5** (0.1)	**3.4** (1.0)
Glutamic Acid	32-140	**89.5** (14.6)	**67.5** (2.5)	**43.6** (13.1)
Glycine	170-330	**279.8** (1.3)	**181.0** (23.0)	**131.0** (36.4)
Lysine	150-220	**167.4** (3.3)	**102.1** (6.1)	**67.4** (19.7)
Methionine	16-30	**25.1** (0.6)	**13.8** (1.5)	**7.4** (3.9)
Phenylalanine	41-68	**66.0** (0.3)	**38.3** (4.3)	**22.8** (9.2)
Proline	110-360	**329.5** (7.0)	**204.4** (21.5)	**136.1** (39.4)
Serine	56-140	**101.1** (1.1)	**68.3** (0.9)	**43.0** (10.5)
Threonine	92-240	**180.1** (9.3)	**108.3** (8.3)	**75.5** (18.4)
Tryptophan	45-64	**73.7** (2.4)	**51.6** (3.0)	**40.4** (5.4)
Tyrosine	45-74	**66.0** (2.9)	**48.0** (1.9)	**36.5** (4.9)
Valine	150-310	**252.1** (0.9)	**163.0** (13.1)	**95.7** **(30.1)**

Values are in µM and are **means** (SEM), n=2 from pooled 18% O_2 and 5% O_2 measurements. Human Plasma Ranges for individual amino acids were taken from Ackerman and Tardito (2019).

Table 2.6: Amino acid concentrations in media at 0, 24, and 48h following cell seeding for MCF-7 cells cultured in Plasmax.
Blue colours represent the percent depletion of each amino acid in reference to the lower limit of the physiological range. A 5-point cut-off on the colour scale was applied. Yellow cells represent concentrations above the lower limit of the physiologic range.

Amino Acid	**Human Plasma Range** (uM)	**Time**		
		0h	**24h**	**48h**
Alanine	230-510	**687.8** (70.5)	**489.4** (28.1)	**350.3** (98.4)
Arginine	13-64	**69.9** (0.8)	**18.0** (0.8)	**11.4** (2.8)
Aspartic Acid	0-6	**8.2** (0.1)	**4.9** (0.7)	**2.6** (0.7)
Glutamic Acid	32-140	**115.3** (9.4)	**89.5** (5.7)	**64.6** (16.1)
Glycine	170-330	**299.8** (7.8)	**252.2** (13.9)	**168.0** (49.2)
Histidine	26-120	**134.3** (6.5)	**82.4** (5.8)	**54.0** (12.7)
Lysine	150-220	**186.2** (19.9)	**137.2** (5.0)	**92.0** (26.5)
Methionine	16-30	**31.2** (4.7)	**19.8** (1.8)	**11.1** (4.5)
Phenylalanine	41-68	**73.5** (9.2)	**50.7** (2.1)	**33.0** (10.8)
Proline	110-360	**328.1** (41.6)	**233.4** (17.1)	**170.5** (45.5)
Serine	56-140	**107.6** (3.1)	**85.5** (5.8)	**59.9** (17.2)
Threonine	92-240	**185.1** (7.3)	**139.9** (0.5)	**88.8** (13.4)
Tryptophan	45-64	**80.2** (6.8)	**59.8** (2.5)	**48.0** (7.9)
Tyrosine	45-74	**76.8** (8.3)	**61.1** (3.1)	**45.9** (7.3)
Valine	150-310	**263.1** (33.9)	**201.7** (20.9)	**124.4** (37.9)

Values are in µM and are **means** (SEM), n=2 from pooled 18% O_2 and 5% O_2 measurements. Human Plasma Ranges for individual amino acids were taken from Ackerman and Tardito (2019).

Initial experiments with LNCaP cells were performed at both 5% and 18% O_2, with media sampled at 24h and 48h. At 24h, substantial depletions of individual amino acids were noted, but only lysine, methionine and phenylalanine fell slightly below the lower limit of the physiological

range **(Table 2.3, Supplementary Figure 2.4).** By 48h, however, the concentrations of almost all amino acids were below the physiological range. As observed for glucose concentrations, no significant differences were detected between 5% and 18% O_2 conditions. Given the absence of O_2 effects observed in the above experiments, for measurements of amino acid depletion in PC-3, SH-SY5Y, and MCF-7 cells, I did not compare high and low oxygen.

Amino acid depletion from Plasmax by PC-3 **(Table 2.4)**, SH-SY5Y **(Table 2.5)**, and MCF-7 **(Table 2.6)** cells was similar to LNCaP cells. In all three cell lines, most amino acid concentrations had fallen below their physiological range by 48h. By comparison, most 24h concentrations remained within this range. However, lysine, methionine and phenylalanine were again exceptions to this trend, with concentrations falling below the physiological range by 24h for all cell lines except MCF-7 (only lysine). Rates of amino acid consumption per cell*h were calculated for all cell lines **(Table 2.7).** Interestingly, while these were similar in LNCaP, PC-3, and SH-SY5Y cells, the rates were lower by about 50% in MCF-7 cells. This, however, was not assessed statistically. I do not have an explanation for this difference beyond cell line specific heterogeneity in metabolic function. Glucose consumption rates by MCF-7 cells were similar to the other cell lines in this study.

Table 2.7: Amino acid consumption rates by LNCaP, PC-3, SH-SY5Y and MCF-7 cell lines.

Amino Acid	LNCaP	PC-3	SH-SY5Y	MCF-7
Alanine	**150.30**	**128.82**	**120.18**	**62.93**
	(15.95)	(7.48)	(5.57)	(4.64)
Arginine	**24.03**	**14.72**	**18.61**	**12.40**
	(2.34)	(0.54)	(3.95)	(0.05)
Aspartic Acid	**2.24**	**0.94**	**1.34**	**0.49**
	(0.26)	(0.04)	(0.24)	(0.13)
Glutamic Acid	**22.61**	**21.51**	**16.69**	**9.08**
	(10.38)	(3.68)	(5.30)	(1.31)
Glycine	**68.06**	**59.81**	**50.53**	**23.01**
	(7.40)	(1.65)	(0.14)	(8.58)
Histidine	**36.25**	**29.26**	**25.12**	**15.70**
	(3.42)	(1.52)	(1.20)	(0.97)
Lysine	**40.47**	**35.60**	**48.84**	**17.56**
	(4.01)	(1.42)	(9.26)	(0.97)
Methionine	**7.79**	**7.03**	**6.46**	**3.98**
	(0.71)	(0.29)	(0.56)	(0.13)
Phenylalanine	**17.57**	**16.29**	**15.40**	**7.74**
	(1.84)	(0.17)	(0.61)	(0.14)
Proline	**68.04**	**63.67**	**67.02**	**29.34**
	(6.60)	(7.67)	(0.63)	(0.26)
Serine	**26.43**	**22.55**	**20.45**	**8.45**
	(3.35)	(3.79)	(2.26)	(2.91)
Threonine	**44.74**	**37.12**	**36.08**	**17.98**
	(4.73)	(5.78)	(0.57)	(0.74)
Tryptophan	**12.47**	**12.91**	**10.88**	**5.74**
	(1.21)	(0.97)	(0.01)	(0.10)
Tyrosine	**11.64**	**11.93**	**9.47**	**5.43**
	(1.40)	(0.93)	(0.38)	(0.34)
Valine	**50.87**	**64.87**	**55.35**	**25.89**
	(6.50)	(1.35)	(4.20)	(0.47)

Values are in fmol/cell*h and are **means** (SEM) of 5-6 measurements (LNCaP) or 2 measurements (PC-3, SH-SY5Y, MCF-7).

Due to the substantial nutrient depletion measured in all cell lines cultured without media exchange for 48h, I next evaluated the effect on nutrient depletion from Plasmax on gene expression using RNAseq. These experiments were performed in LNCaP cells, which were cultured at 18% O_2 or 5% O_2 for 48 hours, either with or without media exchange at 24h. In cells cultured without media replacement, 132 differentially expressed genes (DEGs) were enriched at 18% O_2, and 52 DEGs at 5% O_2. Of these enriched DEGs, 37 were shared between the oxygen conditions **(Supplemental Figure 2.5)**. GO term enrichment analysis performed using DAVID

identified biological processes, cellular components, and molecular functions related to nutrient deprivation and cellular stress as being enriched in cells that did not receive media replenishment at 24h. At 18% O_2, DEGs were most significantly associated with amino acid import and biosynthesis **(Figure 2.2a, Supplemental Figure 2.6).** At 5% O_2, DEGS were associated with unfolded protein response (UPR) pathways, RNA transcription regulation, and endoplasmic reticulum (ER) stress response **(Figure 2.2b, Supplemental Figure 2.6)**. KEGG and Reactome analysis revealed that at both 18% and 5% O_2, pathways associated with metabolite starvation, ER stress, and intrinsic apoptotic signaling were enriched **(Figure 2.3).**

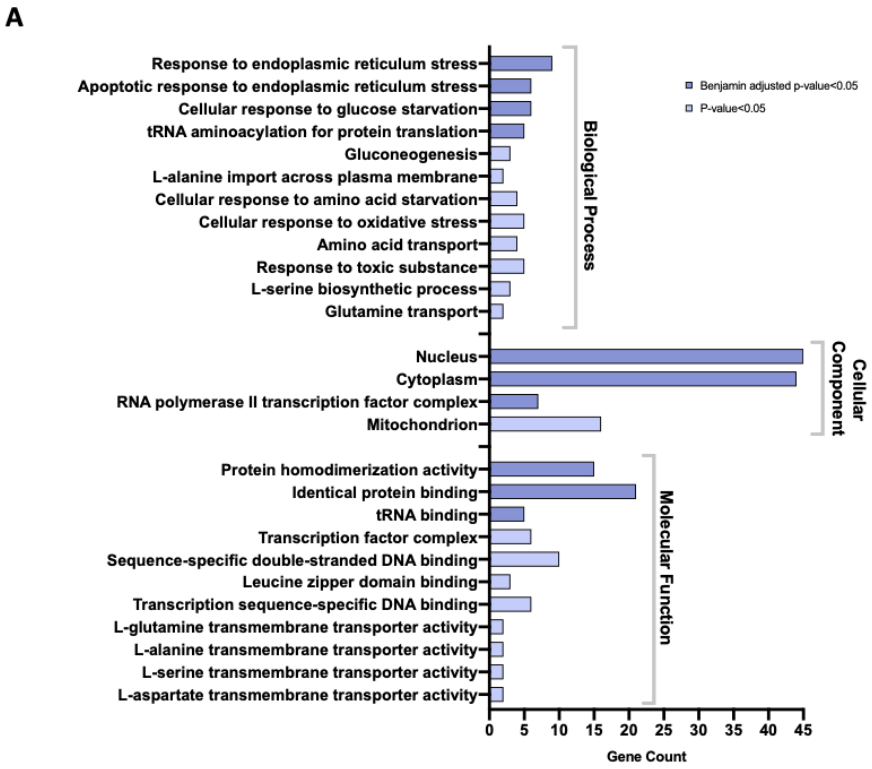

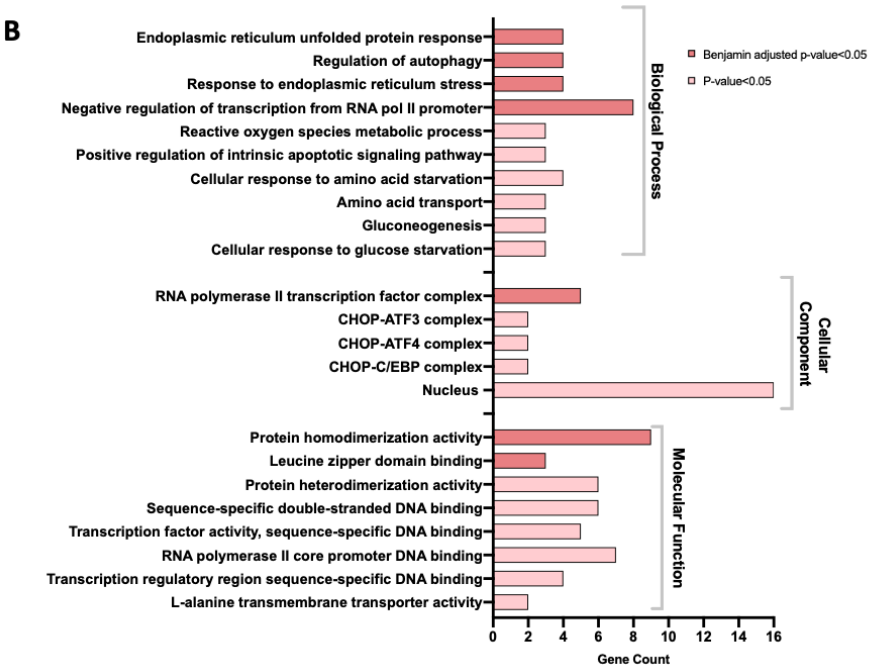

Figure 2.2: Enriched GO terms for LNCaP cells cultured for 48 hours with no media change at a) 18% O_2 and b) 5% O_2. DEG lists for this analysis were reduced to genes with a *p*-value ≤ 0.05, log2(FC) ≥1 (equal to FC ≥ 2), and a minimum FPKM value of 5 in at least one of the two samples

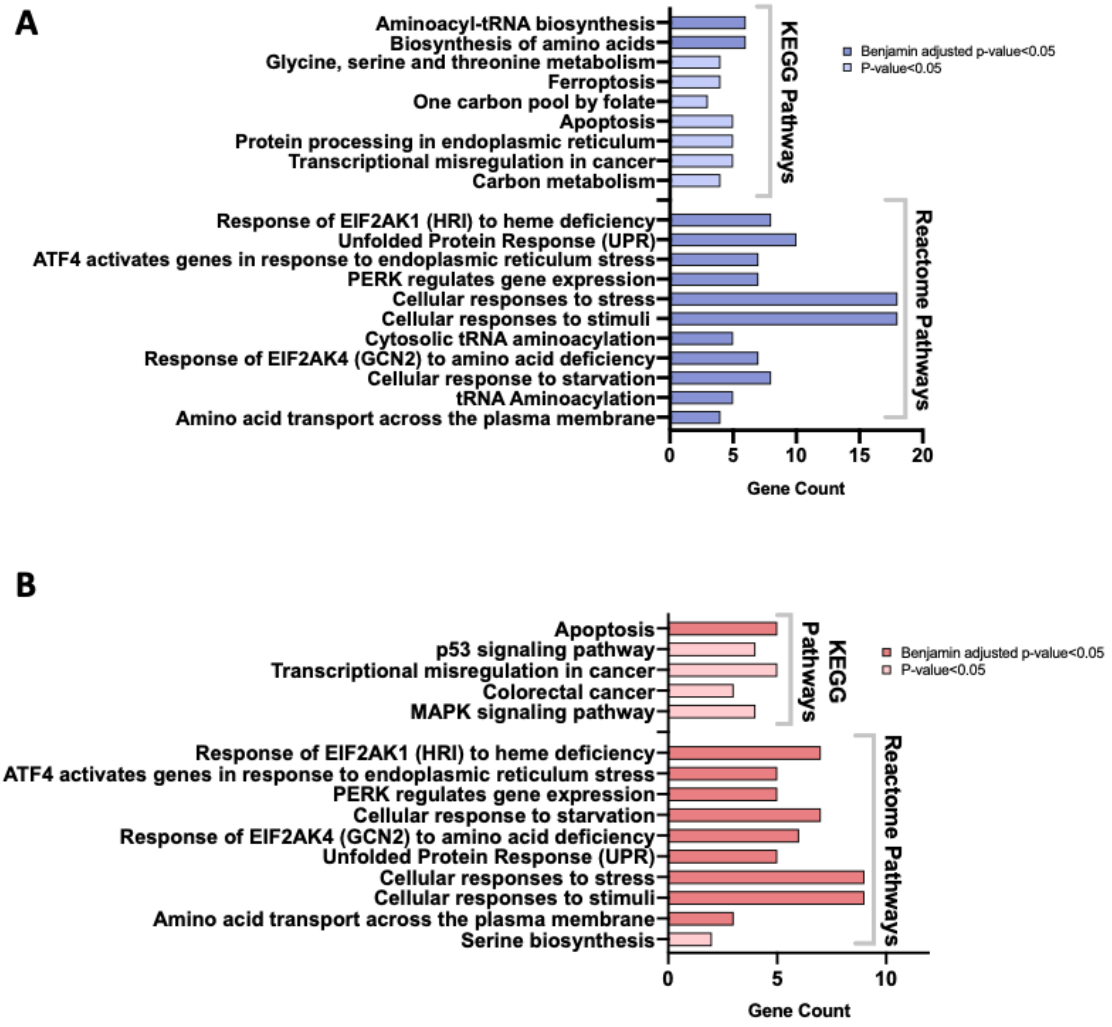

Figure 2.3: Enriched KEGG and Reactome pathways in LNCaP cells cultured for 48 hours with no media change at A) 18% O_2 and B) 5% O_2. DEG lists for this analysis were reduced to genes with a *p*-value ≤ 0.05.

When media exchange was performed at 24h, 100 transcripts were enriched at 18% O_2 and 16 at 5% O_2. Of these, only 2 DEGs were shared between the oxygen conditions **(Supplemental Figure 2.7)** At 18% O_2, these were associated with DNA replication and cell proliferation, with the nucleus being the most strongly affected cellular component **(Figure 2.4a, Supplemental Figure 6)**. KEGG and Reactome pathways associated with cell cycle and DNA replication processes were also enriched at 18% O_2 **(Figure 2.4b).** At 5% O_2, 16 DEGs were enriched with the media exchange, however no GO terms, KEGG or Reactome pathways were identified. Taken together these data indicate that media exchange after 24h promotes cellular proliferation though, interestingly, this is O_2 dependent.

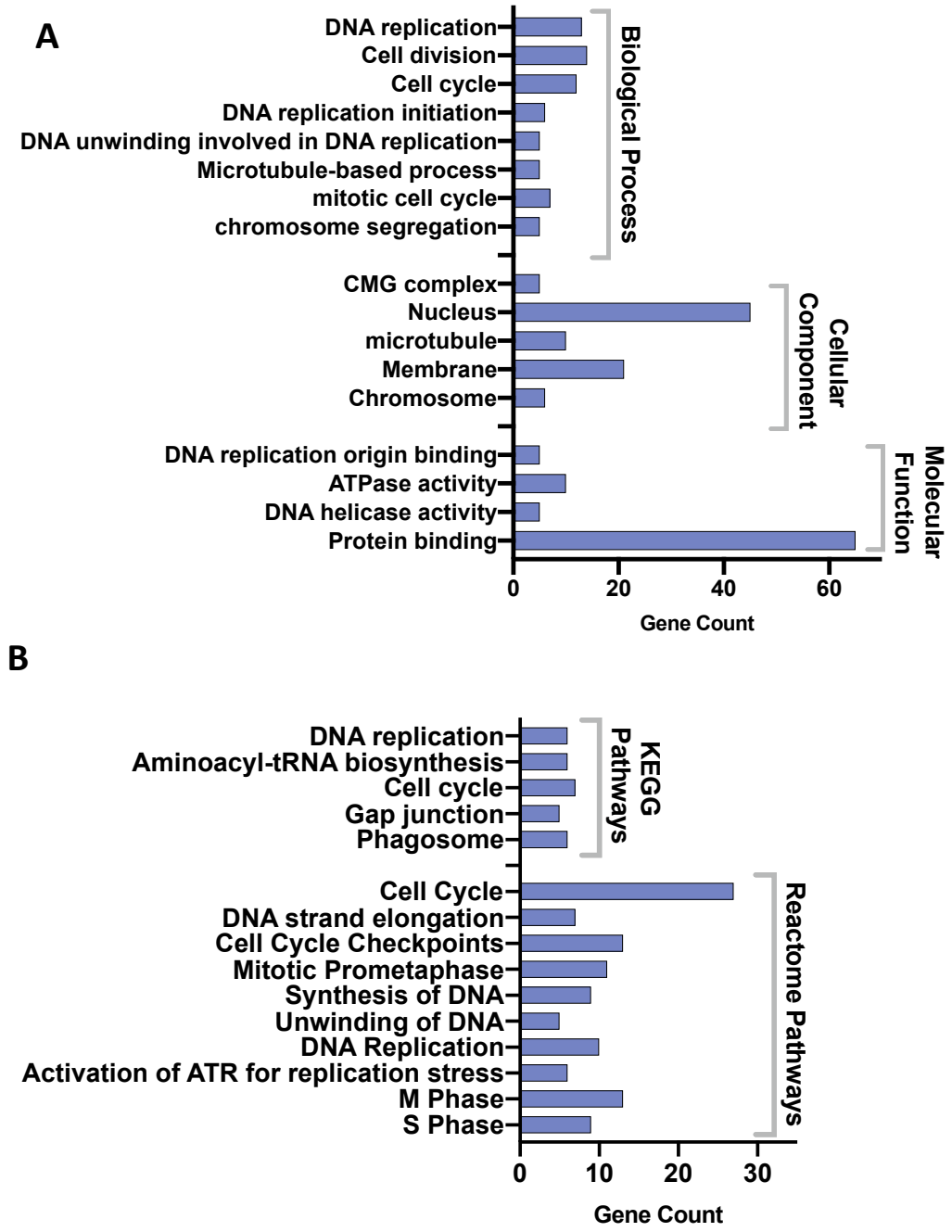

Figure 2.4: Differentially expressed genes, GO terms and KEGG/Reactome pathways in LNCaP cells cultured for 48h with a media change performed at T24h. (a) Enriched GO terms associated with media replacement at 18% O_2. (b) Enriched KEGG and Reactome pathways associated with media replacement at 18% O_2. DEG lists for this analysis were reduced to genes with a P value ≤ 0.05.

To determine whether nutrient depletion affected cellular bioenergetics and mitochondrial metabolism, a Seahorse XF Cell Mito Stress Test was performed on LNCaP cells, again cultured

for 48h either with or without a 24-hour media exchange. At 18% O_2, nutrient depletion had no significant effect on basal oxygen consumption rate (OCR), with proton leak-linked OCR and ATP production-linked OCR being largely unaffected **(Figure 2.5a).** Extracellular acidification rate (ECAR) was also not different between media treatment groups (Figure 2.5b). In contrast, nutrient depletion in cells cultured under 5% O_2 conditions resulted in measurable changes to energy metabolism. Basal OCR was significantly increased when no media change was performed, with ATP production-linked OCR being the most significant contributor **(Figure 2.5a).** Concurrently, ECAR was significantly greater in cells with a 24-hour media change performed when compared to nutrient depleted cells and cells cultured at 18% O_2 **(Figure 2.5b).** This suggests that nutrient abundance favours glycolytic metabolism over mitochondrial respiration at physiologic oxygen. It was also noted that basal OCR was significantly lower at 5% O_2 compared to 18% O_2, suggesting respiration rates are reduced at physiological oxygen saturations in LNCaP cells.

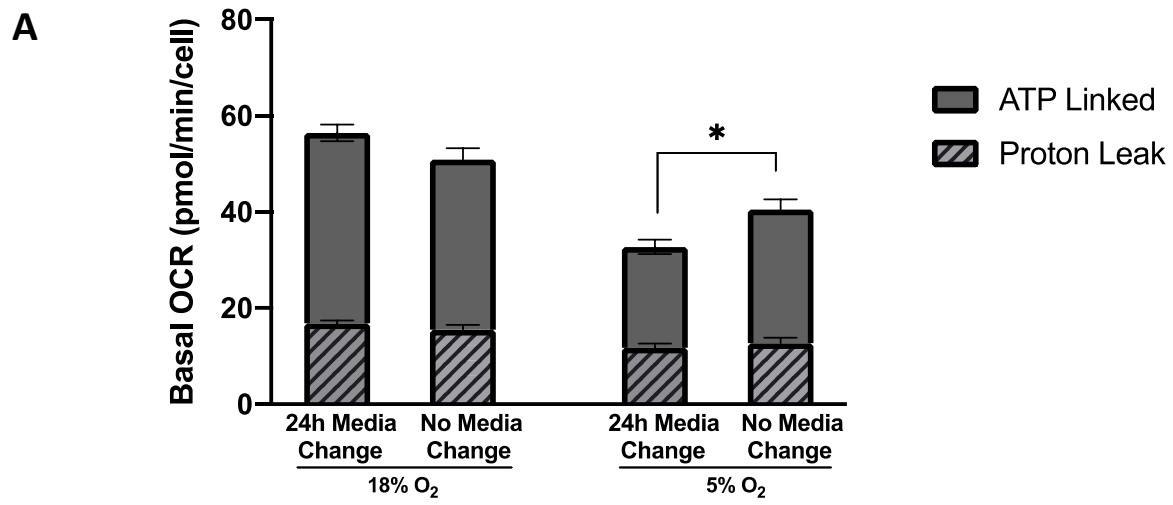

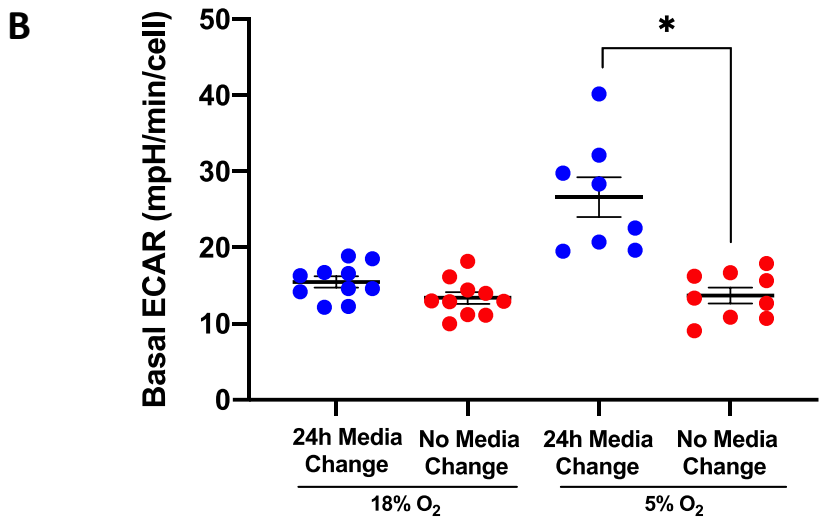

Figure 2.5: Basal oxygen consumption rates (OCR) and extracellular acidification rates (ECAR) of LNCaP cells cultured for 48h with media exchange versus cells without media exchanged at T24. (A) OCR measured using Seahorse extracellular flux at 18% O_2 and 5% O_2 indicate an oxygen-dependent effect of nutrient depletion on basal respiration. Similarly, (B) ECAR is differentially affected by media exhaustion. Statistical significance determined by two-way ANOVA and Tukey-Kramer Post Hoc tests '*' *P*-value ≤ 0.05. N=8-10 wells from one Seahorse plate.

2.5 DISCUSSION

The importance of maintaining physiologic conditions in cell culture has been extensively demonstrated (Ackermann & Tardito, 2019; Cantor et al., 2017; Cooper,P.D et al., 1958; Fu et al., 2010; Kashiwagura et al., 1984; Packer & Fuehr, 1977; Pahl & Baeuerle, 1994; Tiede et al., 2011; Vande Voorde et al., 2019). The composition of Plasmax is based on the human blood plasma metabolome for the purpose of maintaining a physiologic environment. However, since the majority of mammalian cell culture uses static systems in which the medium is not continuously exchanged, the composition will change over time such that nutrient depletion is possible. In Plasmax, most nutrient concentrations are near the upper limits of the physiological range, which can alleviate this problem. Nonetheless, rapidly consumed metabolites are susceptible to exhaustion. Our glucose concentration data highlight the extent of this problem in Plasmax. While [glucose] remained close to the normoglycemic range over the first 24h (3.8 mM vs 4.6-5.3 mM), concentrations had fallen well below this range by 48h in all cell lines such that hypoglycemic conditions were experienced by cells. The Plasmax formulation used here, supplemented with 2.5% FBS, is based on the recommendation of Vande Voorde et al. (2019) and contains ~6 mM glucose. The un-supplemented HPLM formulation contains 5 mM glucose (Cantor et al., 2017). Based on our findings, I suggest adjusting the Plasmax and HPLM formulations to increase glucose concentrations. In adult humans, although fasting blood glucose concentrations of < 5.6mM are considered healthy, they can reach up to 10 mM following a meal (Imran et al., 2018; International Hypoglycaemia Study Group, 2017). Thus, a starting concentration of 7 mM glucose would slow the development of hypoglycemia to beyond 24h, making it easier to stay within the physiological range.

The same pattern of rapid nutrient depletion was observed for amino acids. Most amino acids are present in Plasmax near the high ends of their concentration ranges reported in human plasma. Nonetheless, virtually all amino acids had been depleted to well below these ranges by 48h. Since it would be counterproductive to increase Plasmax amino acid concentrations to values above their normal range, this issue is probably best addressed by performing media exchanges once per day. Vande Voorde et al. (2019) emphasize this logic, demonstrating that physiological concentrations of arginine in Plasmax prevent the reversal of the argininosuccinate lyase catalyzed urea cycle reactions observed with supraphysiologic arginine exposure. However, sub-physiological concentrations of arginine, along with many other amino acids, likely present a host

of new problems, and this works against the intent behind physiological media. Thus, more frequent media exchanges is the obvious solution. Interestingly, cancer cells growing in solid tumours will experience nutrient-poor environments that could be similar to a depleted Plasmax, but the development of a defined nutrient-poor medium will be a more reproducible way to provide this environment.

To facilitate comparisons to published values, I calculated specific glucose and amino acid consumption rates (Table 2.2). Our rates were generally higher than most published values: glucose consumption ranged between 796 and 1984 fmol/(cell*h) in our four cell lines, whereas published values range from below 208 (not included in Table 2) to 729 fmol/(cell*h). It is important to note that the published calculations are not standardized, nor in some instances, provided. This is particularly true regarding the calculation of cell number as it changes over time due to proliferative growth. I used an exponential growth equation and estimated the area under that curve to calculate cell*h. Other approaches will change this value in the denominator of the fraction, driving the values up or down depending on how the calculation is done. In general, it seems that glucose consumption rates of cells in Plasmax are comparable to rates in other culture media.

Of equal importance to using culture media with physiologically relevant nutrient composition is the use of physioxic conditions. Almost all cells in mammalian tissues experience O_2 levels corresponding to 2-8% O_2, rather than the ~18% O_2 of standard cell culture. I included some measurements of glucose and amino acid uptake in both O_2 environments but did not detect differences. It is important to note that 5% O_2 is not 'hypoxic', but rather at the high end of O_2 concentrations that most cells, particularly cancer cells, will be exposed to. 5% O_2 is not, for example, sufficiently low to limit oxidative phosphorylation and necessitate glucose fermentation. Our research group have previously reported measurements of pericellular O_2 under conditions used here (Maddalena et al., 2017). I also performed pericellular O_2 measurements using the Presens SDR Oxodish system and found that O_2 levels remained in the physioxic range throughout a 48h experiment. I thus conclude that broadly similar nutrient uptake rates occur in both oxygen environments.

The significance of this nutrient depletion was evident in the transcriptomic data, where multiple pathways and processes relating to nutrient starvation, endoplasmic reticulum stress, and apoptosis were observed in LNCaP cells experiencing nutrient depletion. Although the details of

these responses differed between the two O_2 levels, enrichment of amino acid starvation processes and ER stress responses were present at both 18% and 5% O_2. Transcripts implicated in amino acid transport and biosynthesis (*ATF4, SLC6A9, SLC7A11, SLC1A4, SLC1A5*) via the amino acid response (AAR) pathway were one such response noted (Chen et al., 2014; Verma et al., 2020). Additionally, genes indicative of ER stress and downstream apoptotic unfolded protein response (UPR) pathways were also upregulated (*AFT3, AFT4, DDIT3/CHOP, SENS2, STC1, DDIT4, TRIB3, EIF3CL*) (Chantranupong et al., 2014; X. Huang et al., 2008; Mungrue et al., 2009; Ohoka et al., 2005; Park et al., 2014; Yamaguchi & Wang, 2004; Zhang et al., 2017). These results suggests that amino acid depletion exceeded the capacity of the early AAR to restore intracellular stores, resulting in reduced transcription and cell cycle arrest. Corroborating our observations that nutrient availability directly influences cellular proliferation pathways, the transcriptomic data of LNCaP cells treated with a 24h media exchange suggests that maintaining nutrient availability within the physiological range is associated with the upregulation of cell-cycle promoting genes at 18% O_2 (*CSAG2, SLC29A1, MT-TE, TUBA4A*) (Yang & Potts, 2020; S. Y. M. Yao et al., 2011).

Nutrient starvation pathways are understood to have regulatory effects on energy production. Indeed, increased mitochondrial respiration is a well-characterized adaptive response associated with survival in cells experiencing ER stress (Johnson et al., 2014; Knupp et al., 2019). This agrees with our Seahorse Mito Stress test findings where nutrient depletion was associated with increased mitochondrial respiration at 5% O_2 in LNCaP cells. Conversely, cells in which nutrient availability was maintained due to the 24h media exchange had enhanced glycolysis. I have no definitive explanation as to why this occurs only at 5% O_2, especially considering oxygen had no effect on nutrient consumption rates, media replacement had no effect on transcripts related to proliferation at 5% O_2, and no hypoxia was observed in Seahorse control wells. A more in-depth characterization of cellular respiration in LNCaP cells would be required to determine this. Regardless, the agreement between our RNA transcriptome data and Seahorse bioenergetic conclusions suggest that nutrient deprivation associated with 48h Plasmax use without media exchange is sufficient to alter cell physiology such that cellular stress and survival pathways are prioritized.

Conclusion

We have shown that the rates of glucose and amino acid uptake from Plasmax growth media are similar to those reported for other media and sufficient to induce a state of nutrient

deprivation within 48h of continuous static culture. This was observed at relatively modest seeding densities and a relatively high volume of medium in all four cell lines investigated here. I found similar trends when cells were cultured in physioxia and standard cell culture O_2 levels. This observed nutrient depletion was associated with the induction of endoplasmic reticulum stress and apoptotic pathways, as well as metabolic adjustments. Given these observations, Plasmax (and presumably other physiologic media) is clearly quite susceptible to nutrient depletion, which necessitates media exchanges at least once per day to maintain nutrient levels within the physiological range. The movement towards physiological cell culture design is important and will aid in translating cell culture results into the clinic. Nonetheless, it will require careful attention to the maintenance of targeted nutrient concentrations.

2.6 APPENDIX

Supplemental Table 2.1: Underivatized amino acid quantifying ions and internal standard quantifying ions used for mass spectrometry.

Underivatized Amino Acid	Deuterated Internal Standard	Underivatized Quantifying Ion (m/z)	Internal Standard Quantifying Ion (m/z)
Alanine	Alanine-D_3	90	93
Aspartic Acid	Aspartic Acid-D_3	134	137
Glutamic Acid	Glutamic Acid-D_3	148	151
Glycine	Glycine-D_2	76	78
Lysine	Lysine-D_8	147	155
Methionine	Methionine-D_3	150	153
Phenylalanine	Phenylalanine-D_8	166	174
Proline	Leucine-D_7	116	139
Serine	Glycine-D_2	106	78
Threonine	Glycine-D_2	120	78
Tyrosine	Phenylalanine-D_8	182	174
Valine	Leucine-D_7	118	139
Arginine	Lysine-D_8	175	155
Histidine	Lysine-D_8	156	155
Tryptophan	Phenylalanine-D_8	205	174

A

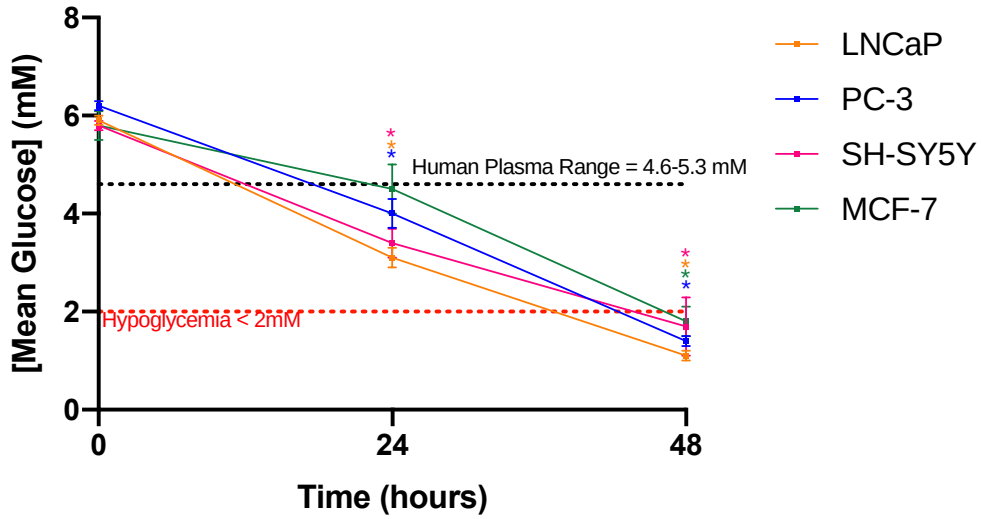

B

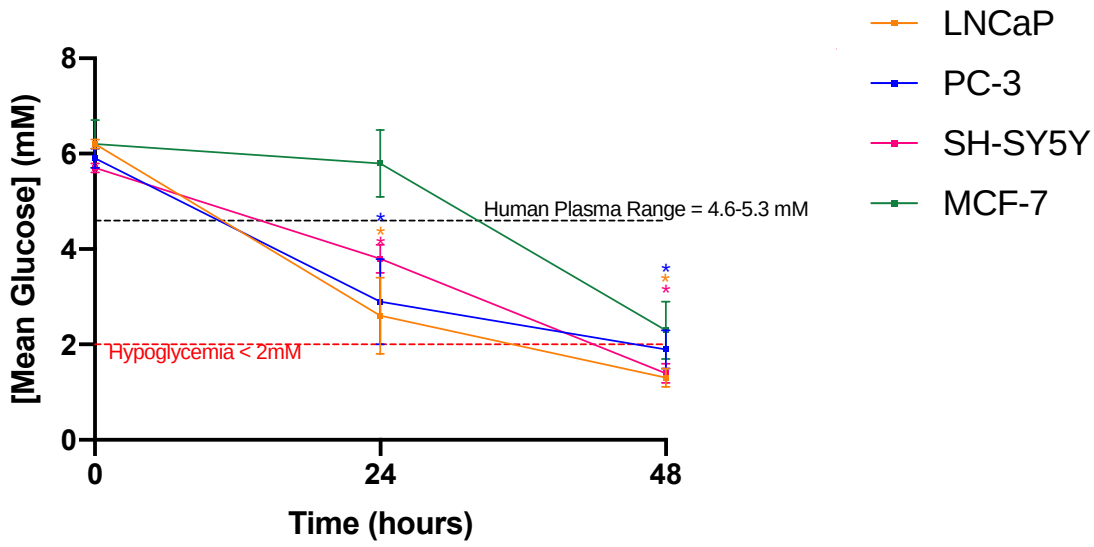

Supplemental Figure 2.1: Mean glucose concentration (mM) over 48 hours for LNCaP, PC-3, SH-SY5Y and MCF-7 cell lines cultured at a) 18% O_2 and b) 5% O_2. Glucose measurements performed at T0h, 24h and 48h. Means expressed ± SEM. N=3 independent experiments. Statistical significance determined by two-way ANOVA followed by Tukey-Kramer post hoc means comparisons to test for effect of time and oxygen level (18% vs 5%) in each cell line. *P*-value ≤ 0.05. No significance measured between oxygen conditions. '*' Indicates significant difference in concentration from 0h measurement for each cell line and condition.

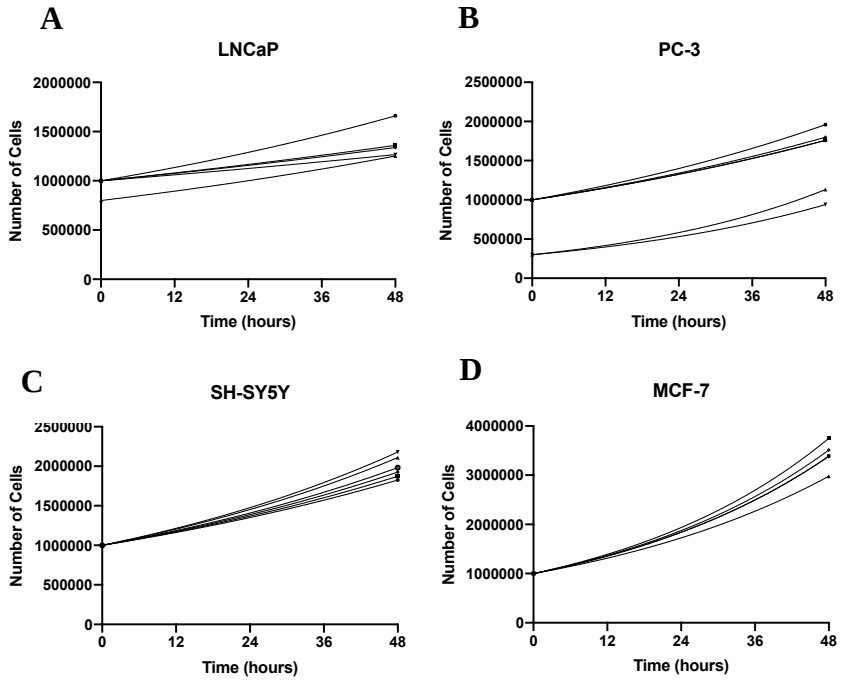

Supplemental Figure 2.2: Growth curves for a) LNCaP b) PC-3 c) SH-SY5Y and d) MCF-7 cells lines cultured for 48h at 18% O_2 with no media replacement at T24h. Cell counts performed and T0h and T48h. N=5-6 experimental replicates per cell line.

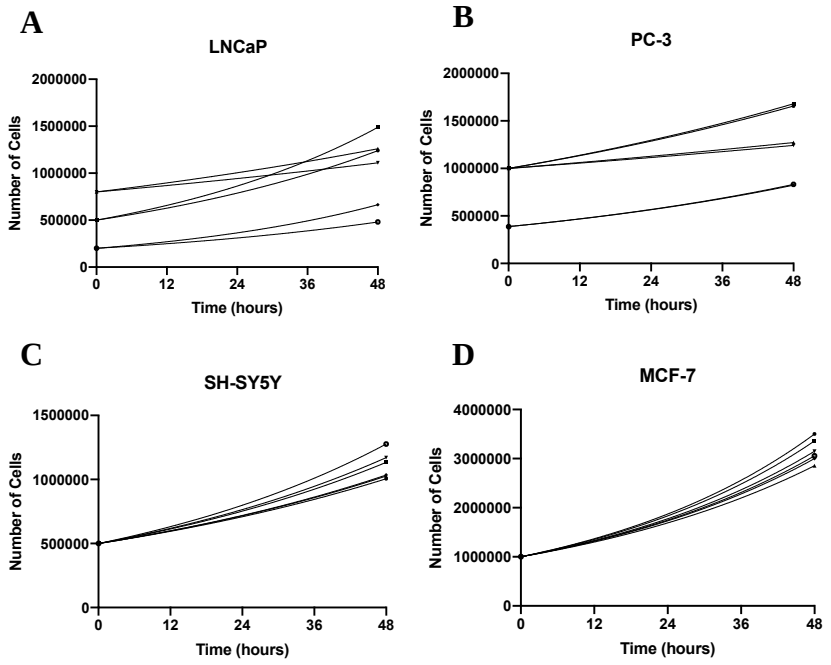

Supplemental Figure 2.3: Growth curves for a a) LNCaP b) PC-3 c) SH-SY5Y and d) MCF-7 cells lines cultured for 48h at 5% O_2 with no media replacement at T24h. Cell counts performed and T0h and T48h. N=5-6 experimental replicates per cell line

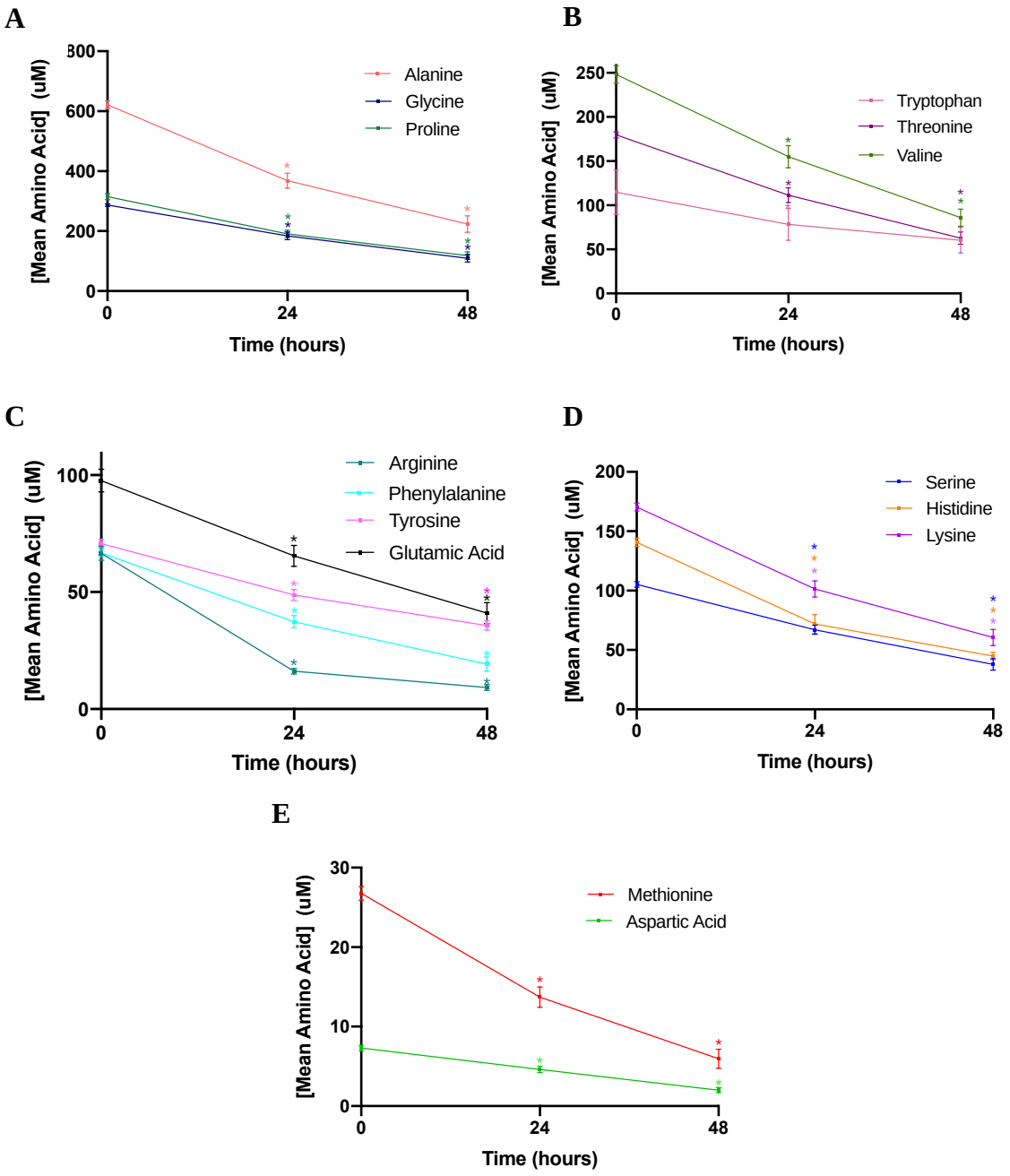

Supplemental Figure 2.4: Mean amino acid concentrations (uM) over 48 hours from pooled LNCaP, PC-3, SH-SY5Y and MCF-7 media measurements. Media measurements performed at T0h, 24h and 48h. Means expressed ± SEM. N=12 from pooled independent experiments. Statistical significance determined by one-way ANOVA followed by Tukey-Kramer post hoc to compare individual amino acid concentrations and time. *P*-value ≤ 0.005. '*' Indicates significant difference from 0h measurement.

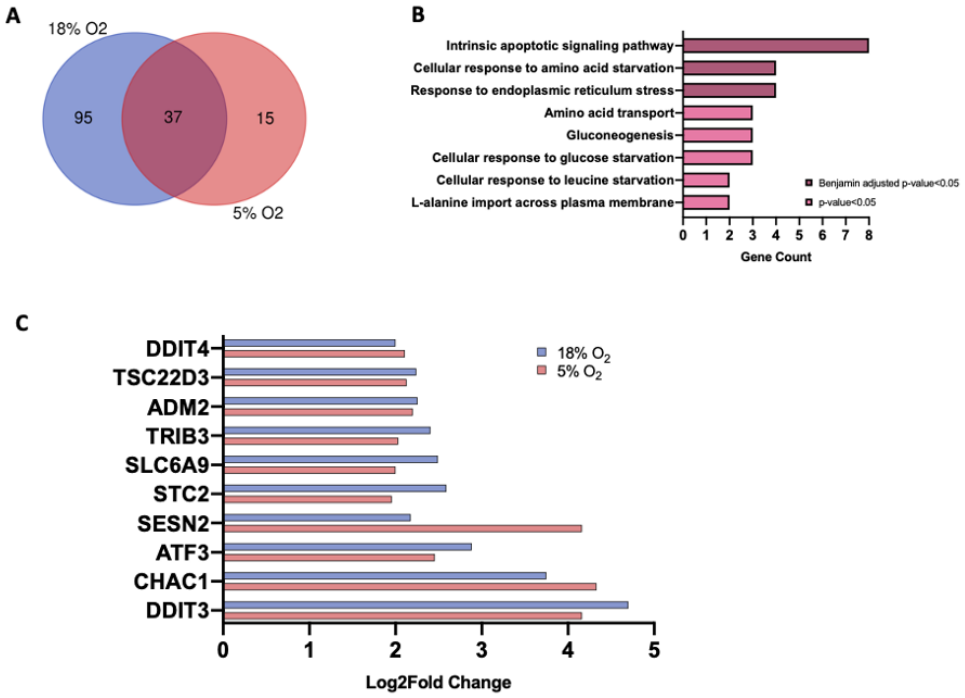

Supplemental Figure 2.5: Differentially expressed genes and GO terms in LNCaP cells cultured for 48h with no media exchange. (a) Venn diagram showing number of unique and shared DEGs at 18% O_2 and 5% O_2. (b) GO terms (biological process) of DEGs shared between oxygen conditions. GO terms were selected from lists reduced with Benjamin adjusted *p*-value<0.05 and *p*-value $\leq$ 0.05. (c) Top 10 most significantly enriched protein-coding genes (adjusted *p*-value $\leq$ 0.005) from shared 18% O_2 and 5% O_2 DEG list.

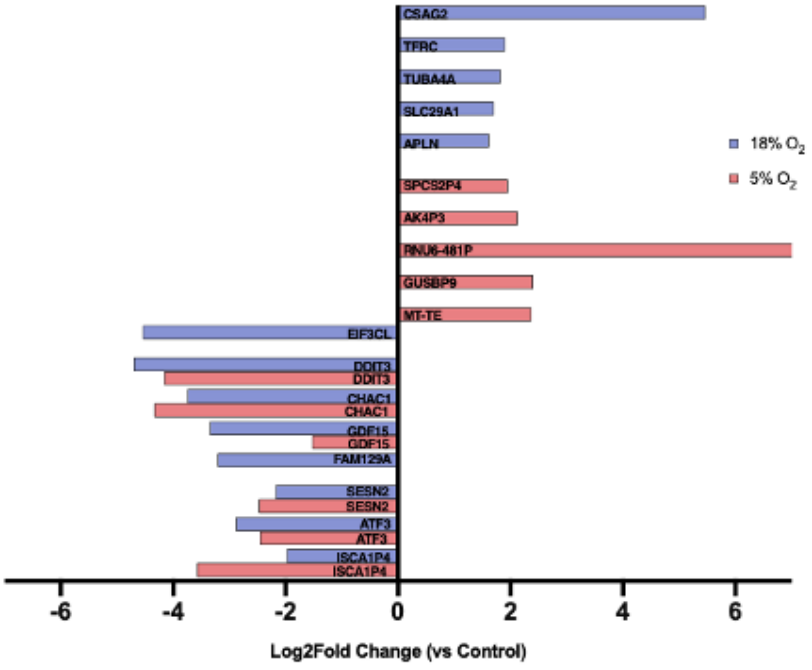

Supplemental Figure 2.6: Significantly differentially expressed genes in LNCaP cells left for 48h without media exchange versus cells with media exchanged at T24h. The top 5 most significant protein-coding DEGs were chosen from each reduced DEG list and compared with each oxygen condition. Log2Fold change is relative to the media exchange group as the 'control'. Negative Log2Fold is indicative of DEGs enriched when no media change is performed. Positive Log2Fold is indicative of DEGs enriched when media change is performed at T24h.

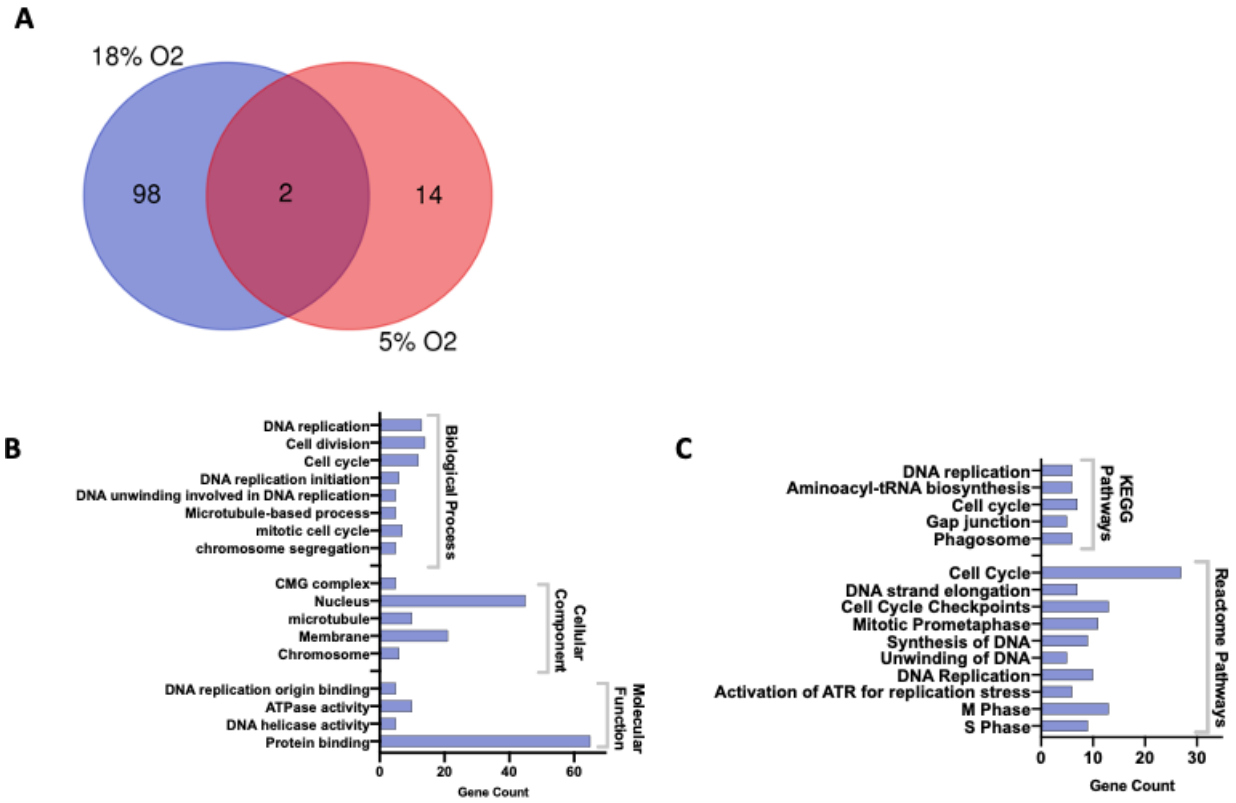

Supplemental Figure 2.7: Differentially expressed genes, GO terms and KEGG/Reactome pathways in LNCaP cells cultured for 48h with a media change performed at T24h. (a) Venn diagram showing number of unique and shared enriched DEGs at 18% O_2 and 5% O_2. (b) Enriched GO terms associated with media replacement at 18% O_2. (c) Enriched KEGG and Reactome pathways associated with media replacement at 18% O_2. DEG lists for this analysis were reduced to genes with a *p*-value ≤ 0.05

Chapter 3: Investigating the Importance of Physiological Tumour-like Conditions in Cultured Pancreatic Cancer Cells

Portions of this chapter are published as a Poster and Flash Talk abstract for the Mitochondria in Aging, Cancer and Cell Death 2023 conference. *Biochimica et Biophysica Acta – Molecular Basis of Disease.*

TMEM media preparation is published as a book chapter as: Gardner, G.L.*, Pinho, S.A.*, Alva, R., Stuart, J.A., Cunha-Oliveira, T. (2024) Creating Physiological Cell Environments *in vitro*: Adjusting Cell Culture Media Composition and Oxygen Levels to Investigate Mitochondrial Function and Cancer Metabolism. M*itochondrial Bioenergetics: Methods and Protocols, Third Edition.*
(*shared first authors)

Author contributions
Study conceptualization: GLG and JAS. I performed all experiments and draft manuscript writing. JAS contributed to manuscript editing.

3.1 ABSTRACT

The tumour microenvironment (TME) is complex and dynamic, characterized by poor vascularization, limited nutrient availability, hypoxia, and an acidic pH. This environment plays a critical role in cancer progression, driving hallmark changes in cancer cell metabolism, morphology, proliferation, and motility. Mammalian cell culture is a foundational tool used to study cancer cell biology *in vitro*. However, standard cell culture practices fail to replicate the *in vivo* cellular environment. Recently, 'physiologic' cell culture media that closely resemble human plasma (e.g., Plasmax, HPLM) have been developed, along with more frequent adoption of physiological oxygen conditions (2-8% O_2) rather than standard (~18% O_2). Nonetheless, further refinement of cell-specific culture conditions may be needed to better maintain the *in vivo* biology of cancer cells. In this study, I describe the development of a tumour microenvironment-like medium (TMEM) based on the metabolomic profile of murine pancreatic ductal adenocarcinoma tumour interstitial fluid (Sullivan et al., 2019). Using RNA-sequencing, I show that murine pancreatic ductal adenocarcinoma cells (KPCY) cultured in tumour-like conditions (TMEM, pH 7.0, 1.5% O_2) exhibit profound differential gene expression compared to those cultured under healthy plasma-like conditions (Mouse Plasma-like Medium, pH 7.4, 5% O_2). Specifically, the expression of genes associated with cell migration, amino acid biosynthesis, angiogenesis, and epithelial-to-mesenchymal transition was altered. Using functional assays to validate RNAseq data, I found that glucose uptake and lactate production rates were increased in tumour-like conditions compared to healthy plasma-like conditions, despite the lower initial glucose concentrations in TMEM (2.3 mM vs. 4.4 mM in Mouse Plasma-like Medium). Additionally, Seahorse Extracellular Flux Analysis showed an overall reduction in mitochondrial respiratory capacity and energy production in tumour microenvironment-adapted cells, suggesting that this shifts them toward glycolytic metabolism. Moreover, cell proliferation rates were lower in tumour-like conditions, while migration assays confirmed increased motility. Taken together, these findings demonstrate that growth in a medium designed to simulate the tumour microenvironment alters KPCY cell biology in ways that are hallmark to their pathology, highlighting the significance of maintaining tumour-like conditions in culture.

Keywords: Cancer Metabolism, Tumour Microenvironment, Cell Culture, Physiological, Metabolic Rewiring, Oxygen, Tumour Interstitial Fluid

3.2 INTRODUCTION

The microenvironment of solid tumours is a highly specialized niche that has been well characterized as being metabolically constrained. Inadequate and immature vascularization as a consequence of rapid tumour growth that exceeds the capacity for angiogenic signaling leads to regions of nutrient deprivation, hypoxia, waste accumulation, and increased acidity (Fukumura & Jain., 2007; Kamphorst et al., 2015; Pan et al., 2016; Pries et al., 2009; Schaaf et al., 2018; Vaupel et al., 2021). Survival of cancerous cells in such conditions requires significant metabolic flexibility, with cells adaptively rewiring in response to the dynamic and heterogenous environmental changes in order to maintain energy homeostasis, biomass requirements and redox homeostasis (Reviewed by DeBerardinis and Chandel 2016). Incidentally, many oncogenes and tumour suppressor genes are regulators of metabolic pathways (i.e. PI3K-AKT-mTOR deregulation), driving unregulated tumour growth regardless of metabolic constraints (Dey et al., 2020; Finicle et al., 2018; Furuta et al., 2010; Min & Lee, 2018). Rewiring of conventional metabolic pathways is thus accomplished by a combination of environmental cues, and intrinsic genetic factors. Ultimately, metabolic rewiring provides cancerous cells with a unique adaptive advantage that contributes to tumorigenesis, metastasis, and treatment evasion. Targeting these changes in metabolic activity and utilization thus represents a promising avenue for anti-cancer treatment.

Despite the role of nutrient availability in driving metabolic rewiring in tumours, the environment in which cancer cells are studied in culture fails to replicate the tumour microenvironment. Formulations of standard commercial media, such as DMEM and RPMI, frequently include constituents at concentrations that exceed physiological metabolite levels, or lack essential components altogether (Ackermann & Tardito, 2019; Golikov, Valuev-Elliston, et al., 2022). Moreover, the regulation of oxygen levels in cell culture is frequently overlooked, resulting in cultured cells being exposed to levels approaching atmospheric 18-20% O_2, rather than the 2-11% O_2 levels measured in healthy tissues (McKeown, 2014), or the 0-3% O_2 levels measured in solid tumours *in vivo* (Vaupel et al., 2021).

While recent efforts have been made to develop physiologic cell culture media representative of human plasma (i.e. Plasmax, HPLM) (Cantor et al., 2017; Vande Voorde et al., 2019), the plasma metabolome does not closely resemble the tumour microenvironment. Tumour interstitial fluid (TIF), i.e. the extracellular fluid that bathes the cells of the tumour, is metabolically

unique compared to plasma (Burgess & Sylven, 1962; Hirayama et al., 2009; Nierves et al., 2022; Reinfeld et al., 2021; Schroeder et al., 2013; Sullivan et al., 2019; Vecchio et al., 2021). While metabolite availability is generally limited in TIF, as is evident for glucose, oxygen and many amino acids, several metabolites can accumulate (i.e. lactate, glutamine, succinate, fumarate, and D-2-hydroxyglutarate) and serve as signaling molecules for angiogenic and metastatic pathways (Baryła et al., 2022; Liu & Yang, 2021). The specific metabolome of TIF may thus contribute to tumorigenesis within the tumour microenvironment (Y. Fu et al., 2022). Thus, to improve the ability of cell culture experiments to uncover key characteristics of cancer cells, media formulated based on TIF is desirable.

In Chapter 2.0 of this thesis, I observed that cancer cells cultured in nutrient-depleted Plasmax showed signs of metabolic remodelling and stress response in as little as 48 hours of continuous culture, which was absent in cells given fresh Plasmax at 24h (Gardner et al., 2022). While poorly representative of a homeostatic and well perfused tissue, we proposed that the nutrient replete culture environment established in exhausted Plasmax is more representative of the tumour microenvironment. In this chapter we explore this concept further by designing a reproducible cell culture model of the tumour microenvironment, and investigating the effect of our tumour-like culture conditions in modulating cancer hallmarks.

Herein, I describe the formulation of Tumour Microenvironment Medium (TMEM), a tumour-like culture medium designed using murine pancreatic ductal adenocarcinoma (PDAC) TIF metabolomics data (Sullivan et al., 2019). Using this formulation, I investigate the effect of culturing cancer cells in conditions representative of the tumour microenvironment by comparing murine PDAC cells (KPCY) adapted to our tumour-like culture model (TMEM and pericellular oxygen levels of ~0.7% O_2) (Koong et al., 2000), with 'standard' plasma-like physiological culture conditions (Mouse Plasma Medium (MPM) and pericellular oxygen levels of (~4% O_2) (Carlsson et al., 1998; Carlsson et al., 2001). Our findings reveal that by refining culture conditions to mimic the *in vivo* PDAC tumour microenvironment, numerous hallmark features of cancer cells are modulated including gene expression, cellular proliferation, migration, glucose uptake, and mitochondrial bioenergetics. This highlights the pivotal role of the tumour microenvironment in driving metabolic rewiring and metastatic phenotypes in cultured cells, exemplifying the importance of maintaining physiologically relevant tumour-like conditions when studying cancer biology *in vitro*.

3.3 MATERIALS AND METHODS

3.3.1 Tumour Microenvironment Medium Preparation

Tumour microenvironment medium (TMEM) was modelled after the nutrient composition of tumor interstitial fluid sampled from murine pancreatic ductal adenocarcinomas (PDAC) (Sullivan et al., 2019). All components that were measured and commercially available were included in the formulation (Table S3.1). For semi-quantitative metabolite measurements, the fold change from serum was calculated and applied to healthy murine plasma concentrations. This method assumed that serum metabolite concentrations in diseased mice were comparable to healthy murine serum. For glucose, tumour concentrations were approximately half that of paired plasma concentrations. I applied this conversion to healthy fasted mouse plasma levels to account for serum hyperglycemia otherwise managed clinically in PDAC patients (Cantor et al., 2017; Fontaine, 2019; Han et al., 2008). This assumed the relationship between plasma levels and tumour interstitial fluid availability is linear. The concentration of trace elements used were based on the trace element concentrations in DMEM F-12, as done for the Plasmax™ formulation (Vande Voorde et al., 2019). Salt components were based on *in vivo* murine measurements (Mckee and Komarova, 2017). To maximize the number of physiologically relevant metabolites and nutrients included in TMEM, if TIF measurements had not been performed but healthy murine concentrations were available, the healthy concentrations were used. This can be adapted in future formulations as more data on TIF metabolite concentrations become available.

To make TMEM, seven stock solutions were prepared according to metabolite concentration and solubility (Table S3.1) (See Gardner, Pinho et al., 2024 for preparation methods). The stock solutions were aliquoted at volumes appropriate for the preparation of 500 mL media bottles and stored at -80°C. To make a fresh bottle of TMEM, the seven stocks were combined with glucose, glutamine, sodium pyruvate, sodium L-lactate and salt components. After preparation, the pH was measured using an electronic pH meter and adjusted to 7.0 using 12 M HCl. Media made from stock solutions was prepared fresh bi-weekly and supplemented with 1% Penicillin/Streptomycin (P/S) (Sigma-Aldrich, P4333) and 2.5% Fetal Bovine Serum (FBS) (Sigma-Aldrich, F1051) to limit serum contributions.

3.3.2 Mouse Plasma Medium Preparation

Mouse plasma medium (MPM) was modeled after the nutrient composition of healthy mouse plasma sourced from metabolomics studies characterizing mouse plasma (**Table**

S3.1). All components included in TMEM were included in MPM at relevant murine plasma-like concentrations. As with TMEM, the concentration of trace elements were based on DMEM-F-12, and salt components were based on *in vivo* murine measurements (Mckee and Komarova, 2017). To make MPM, seven stock solutions were prepared according to metabolite concentration and solubility. The stock solutions were aliquoted at volumes appropriate for the preparation of 500 mL media bottles and stored at -80°C. To make a fresh bottle of MPM, the seven stocks were combined with glucose, glutamine, sodium pyruvate, sodium L-lactate and salt components. After preparation, the pH was measured using an electronic pH meter and adjusted to 7.4 using 12 M HCl. Media made from stock solutions was prepared fresh bi-weekly and supplemented with 1% P/S (Sigma-Aldrich, P4333) and 2.5% FBS (Sigma-Aldrich, F1051) to limit serum contributions.

3.3.3 Cell Culture

The pancreatic ductal adenocarcinoma cell line (KPCY) was purchased from Kerafast (MA, USA). Cells were initially thawed and expanded in growth conditions recommended by the supplier (DMEM, 10% FBS, Glutamax) in a 37 °C, humidified 5% CO_2 atmosphere, within a Forma 3110 Series water jacketed incubator (ThermoFisher, Waltham, MA, USA). Cells were then transitioned to either TMEM or MPM supplemented with 2.5% FBS and 1% P/S in humidified 5% CO_2 incubators at 37 °C with headspace oxygen set to 1.5% O_2 for TMEM (pericellular oxygen levels of ~0.7% O_2) and 5% O_2 for MPM (pericellular oxygen levels of ~4% O_2). Cells were adapted to their respective culture conditions for a minimum of two weeks prior to experimentation.

For standard maintenance of cells, daily media exchanges were performed to mitigate rapid depletion of nutrients in physiological media (Gardner et al., 2021). For initial adaptation, media volumes of 20mL in 100mm plates were used. However, volumes for adaption and standard maintenance were increased to 30mL in 100mm plates following glucose monitoring and pericellular oxygen measurement experiments to maintain target glucose and oxygen levels over a minimum of 24 hours. Cell passaging was performed every 3-4 days, or once plates reached ~80% confluency. For passaging, cells were washed with 1X phosphate buffered saline (PBS) and incubated with 0.25% trypsin/EDTA (Sigma-Aldrich, T4049) for 3 minutes at 37ºC. Following incubation, trypsin was neutralized by adding an equal volume of supplemented culture media to the plate. The cell suspension was then collected, pelleted, and a 1:4 subculture was performed.

3.3.4 Monitoring D-Glucose and L-Lactate Media Concentrations

For all glucose and lactate monitoring experiments, cells were counted using a hemocytometer and 1,000,000 cells were seeded per 100mm culture plate. Three plates were seeded per condition.

For preliminary analysis of fresh media metabolite concentrations and to monitor media replenishment requirements, media glucose and lactate levels were measured over 48 hours, with varied starting media volumes. Adapted KPCY cells were seeded with either, 20mL, 30mL, or 40mL media per 100mm plate, and cells were incubated for 48h. This was performed with KPCY cells under A) tumour-like conditions (1.5% O_2/TMEM) or B) plasma-like conditions (5% O_2/MPM). At 0h, two 1mL media samples were collected directly from the respective media bottle. At 24h and 48h, two 1mL media samples were collected from each plate. No media changes were performed throughout the 48-hour period. Immediately upon collection, samples were centrifuged at 200g for two minutes to separate cell debris from media. Supernatants were transferred to fresh Eppendorf tubes, snap frozen in liquid nitrogen, and stored at -80°C for later analysis. Glucose and lactate concentration of samples was determined using a YSI 2900 Biochemistry analyzer (Yellow Springs, OH, USA) fitted with enzyme-coated glucose and lactate membranes. Glucose and lactate standards, prepared in TMEM or MPM, were run alongside experimental samples. A standard curve was generated and used to calculate the concentration present in each experimental sample.

3.3.5 PreSens Oxodish Procedure

24-well disposable Oxodish™ plates (OD24; PreSens, Regensburg, Germany) were used to monitor pericellular oxygen levels in KPCY cells cultured under 1.5% O_2 or 5% O_2, in their respective media. Since pericellular oxygen varies with diffusion distance to cells (media height) and number of cells (oxygen consumption per cell), the volume of media used and seeding density was calculated to approximate typical experiments performed in a 100mm culture dish. Rather than vary headspace oxygen levels to achieve pericellular oxygen levels representative of *in vivo* PDAC tumours and healthy tissue, media volumes of 0.761mL, 1.141mL and 1.521mL were initially varied to approximate 20mL, 30mL and 40mL media in a 100mm Corning culture plate, respectively (**Sample Calculation 3.1**), mirroring volumes used for glucose monitoring experiments. 25,000 KPCY cells were seeded per well such that by the end of the measurement period, wells would near ~80% confluency. Cells were seeded 24 hours prior to measurement. The next day, just prior to the initiation of measurement, a media exchange was performed with

warmed, pre-equilibrated media. Pericellular O_2 levels were then measured at 15-minute intervals for 48 hours. 4-6 wells were seeded with KPCY cells per volume, and 6 wells were cell free controls.

Sample Calculation 3.1: Approximating media column height from 10cm plate to OD24 Well

$$Volume\ in\ 10cm\ plate = \pi(radius\ of\ 10cm\ plate)^2(Media\ height)$$

$$20mL = \pi(4.025)^2(Media\ height)$$

$$Media\ height = 0.3930cm$$

By substituting media column height from vessel 1 to equation for vessel 2, volume can be calculated.

$$Volume\ in\ OD24\ Well = \pi(radius\ of\ OD24\ Well)^2(Media\ height)$$

$$Volume\ in\ OD24\ Well = \pi(0.785cm)^2(0.3930cm)$$

$$Volume\ in\ OD24\ Well = 0.7607mL$$

Note: Radii used are based on growth area dimensions provided by Corning and Presens.

3.3.6 PreSens Hydrodish Procedure

24-well disposable Hydrodish plates (HD24; PreSens, Regensburg, Germany) were used to monitor pericellular pH levels in cells cultured under TMEM adjusted to a pH of 7.0. Cells were seeded one day prior to measurement in 1.141mL media, representative of the 30mL approximation. The next day, just prior to the initiation of measurement, a media exchange was performed with warmed, pre-equilibrated media. Pericellular pH levels were then measured at 15-minute intervals for 24 hours.

3.3.7 RNA Sample Preparation and Extraction

Total RNA was extracted from KPCY cells cultured in either A) tumour-like conditions (1.5% O_2/TMEM) or B) plasma-like conditions (5% O_2/MPM). Cells were adapted to their respective conditions for ~2 weeks, with daily 30mL media exchanges performed and cell passaging performed when plates reached ~80% confluency. After this two-week adaption period, cells were counted using a hemocytometer and 1,000,000 cells were seeded to three 100mm plates per culture condition, each with a final volume of 30mL of media. Plates were maintained with daily media exchanges until confluent, after which cells were trypsinized and the cell pellets were collected. Each pellet was washed twice with warm 1X PBS to remove remaining trypsin or serum-containing media. RNA extraction was then performed on each replicate per experimental condition using the Quagen RNAeasy Mini Plus Kit (Hilden, Germany). RNA sample replicates

(n=3) were pooled into one sample for sequencing. RNA purity and concentration were evaluated for the pooled samples using a 260/280 ratio measured using a Nanodrop spectrophotometer (ThermoFisher Scientific, MA, USA). RNA degradation and integrity was assessed using 1% Agarose Gel Electrophoresis. Pooled RNA samples were then snap frozen in liquid nitrogen and stored at -80˚C before being sent to Novogene Incorporated (Sacramento, CA, USA) for RNA sequencing.

3.3.8 Library Preparation and Sequencing

All RNA samples received by Novogene underwent additional in-house quality control (QC) tests prior to sequencing to assess RNA integrity and purity. These included Nanodrop spectrophotometry and Agarose Gel Electrophoresis. After successfully passing the initial QC assessment, the RNA library was constructed for the samples. mRNA within the total RNA samples were enriched using poly-T oligo-attached magnetic isolation beads that select for the polyA tails of mRNA, thus purifying the mRNA from total RNA. Fragmentation buffer was then added to the enriched mRNA to fragment the mRNA template. The cDNA was then synthesized from the mRNA template using random hexamer primers. Second-strand synthesis was initiated using custom second-strand synthesis buffer (Illumina), dNTPs, Rnase H and DNA polymerase I. A tailing, sequencing adaptor ligation and end-terminal repair was then performed, followed by size selection and PCR enrichment to produce the completed double-stranded cDNA library. QC was performed on the library using Qubit 2.0 for preliminary concentration measurements, Agilent 2100 for insert size analysis, and qPCR for precise library concentration quantification. Following library QC, sequencing of the completed cDNA library was performed using the Illumina NovaSec 6000 Sequencing System with a pair-end 150bp read length and a read-depth of >20 million reads per sample.

3.3.9 RNA Seq Data Analysis

To improve analysis quality and reliability, raw sequenced read filtering was performed in which reads containing adaptors, N>10% (N=bases that cannot be determined), and low quality Qscores of ≤ 5 in over 50% of the bases (Qscore=Quality value) were removed. Reads were aligned to the reference genome (*Mus musculus* GRCm38 – mm10) using Hisat2 v2.0.5. Gene expression was estimated using the FPKM (Fragments per Kilobase of transcript sequence per Millions base pairs sequenced) of each gene. Differential gene expression was assessed by analysing the group

means (per condition) and a global means (between conditions) of gene expression. Deviations of group means from global means was than calculated, presented as fold change and p-value.

Differentially expressed gene (DEG) lists were provided by Novogene, comparing gene expression in KPCY cells adapted to plasma-like conditions (5% O_2/MPM) or tumour-like conditions (1.5% O_2/TMEM). Once received, additional filtering was performed on DEG lists. These DEGs were reduced to genes with a Benjamini adjusted *p*-value < 0.05, log2(FC) ≥1 (equal to FC ≥ 2), and a minimum FPKM value of 5 in at least one of the two samples in the comparison to ensure the DEGs observed were strongly affected.

3.3.10 Functional Enrichment Analysis

Functional enrichment analysis was performed using the Database for Annotation, Visualization, and Integrated Discovery (DAVID) version 6.8 with default settings. The reduced DEG lists were imputed, using *Mus musculus* as the reference species. Enriched GO Terms, KEGG Pathways, and Reactome Pathways were reduced to terms with Benjamini adjusted *P*-value <0.05, or a *P*-value <0.05 as indicated. G:Profiler webserver g:GOSt was used to validate functional enrichment analysis using the 'ordered query' function. Similar to DAVID, DEG lists were imputed, using Mus musculus as the reference species, however the pre-ranked (by significance) order of the gene set was factored into the analysis (data not shown).

3.3.11 Cell Proliferation Analysis

Cellular proliferation rates of cells adapted to either A) tumour-like conditions (1.5% O_2/TMEM) or B) plasma-like conditions (5% O_2/MPM) was determined by hemocytometer cell counts of trypan blue stained cells. Briefly, a known number of viable cells were seeded in a 12-well plate on Day 0 of the assay. For the next four days, three wells per day were isolated by trypsinization and resuspended in PBS. At the time of trypsinization, the remaining wells underwent daily media exchanges with pre-equilibrated media. 50uL of 0.4% Trypan blue (Bioshop, TRY477) and 50uL of cell suspension were then mixed and incubated at room temperature for 3 minutes. The solution was then re-suspended and loaded onto a hemocytometer. The hemocytometer was viewed and counted using a Hund Wetzlar Wilovert A inverted microscope. The number of clear (viable) and blue (non-viable) cells were counted in four secondary squares. For each sample, hemocytometer counts were performed in triplicate and averaged to determine the cell density (cells/mL). The average cell density for each well was then multiplied by the total volume used to resuspend the isolated cell pellet to determine the final cell

count after the elapsed time. The Day 0 to Day 4 growth curves were then plotted and doubling time was calculated during exponential growth period of growth using the following formula (**Equation 3.1**) (Hayflick et al., 1973):

Equation 3.1: Doubling Time

$$Doubling\ Time = \frac{(T2 - T1) \cdot \ln(2)}{\ln\left(\frac{Cell\ count\ at\ T2}{Cell\ count\ at\ T1}\right)}$$

3.3.12 Cell Migration Scratch Assay

Cell migration was assessed using a scratch assay in which percent scratch closure was measured over 24 hours. KPCY cells adapted in either A) tumour-like conditions (1.5% O_2/TMEM) or B) plasma-like conditions (5% O_2/MPM) were seeded in six-well plates and cultured for 3 days until confluent. Each well was then scratched using a sterile 200uL pipette tip in a grid pattern previously drawn on the bottom of the plate. Once scratched, cells were washed with PBS twice to remove cell debris, and fresh equilibrated media was added to each well. Images were then captured at time 0h, 12h, and 24h using a Hund Wetzlar Wilovert A inverted microscope on a 4X objective with an OMAX A35 Series microscope camera. Four to six locations were imaged per well. To ensure the same location was imaged at each time point, a razorblade was used to mark the bottom of the plastic plate. Images were taken either directly above or below the mark in the plastic.

Migration and scratch closure were quantitatively evaluated using the Fiji/image J *Wound_healing_size_tool_update* plugin (https://github.com/AlejandraArnedo/Wound-healing-size-tool/wiki) that discriminates between regions of cell monolayer and cell-free regions based on pixel intensity variance and thresholding. Percent wound closure is calculated using the cell-free scratch area (um^2) inputted into the formula below (Equation 3.2):

Equation 3.2: Percent Wound Closure

$$Wound\ Closure\ \% = \left(\frac{Area_{t=0h} - Area_{t=\Delta t}}{Area_{t=0h}}\right) x\ 100\%$$

3.3.13 Cellular Respiration

Cellular respiration was evaluated in KPCY cells cultured in either A) tumour-like conditions (1.5% O_2/TMEM) or B) plasma-like conditions (5% O_2/MPM). Oxygen consumption

rate (OCR) and extracellular acidification rate (ECAR) were measured using a Seahorse Extracellular Flux Analyzer XFe24 Mito Stress test in Hypoxia Mode (Agilent, Santa Clara, CA). To regulate headspace oxygen levels to 1.5% and 5% O_2, the Seahorse Extracellular Flux Analyzer XFe24 was placed in a Coy Hypoxia Box (Coy Laboratory Products Inc, Grass Lake, MI, USA). A portable O_2 sensor, previously used to calibrate the oxygen regulating incubators, was used to validate O_2 levels.

The day prior to the assay, KPCY cells were seeded to an XFe24 microplate and placed in their respective incubator until the assay was initiated. Blank 'Background' and 'Hypoxia' wells were left cell free. Overnight, the Coy Hypoxia box containing the Seahorse Analyzer and all consumables was turned on, set to the appropriate oxygen level for the assay condition (1.5% O_2 or 5% O_2). Assay medium, that being either TMEM or MPM free of serum, sodium bicarbonate and antibiotic supplementation, was also equilibrated in the hypoxia box overnight, placed on a heating plate to warm the media to 37ºC.

On the day of the assay, one hour before the initiation of the Mito Stress Test, the XFe24 plate containing KPCY cells was quickly moved from the incubator to the Coy Hypoxia Box and each well was washed with the warmed, equilibrated assay medium. The plate was placed within the Seahorse Analyzer for 1 hour, serving as a 37ºC, CO_2 free 'incubator'. Following this wait period, a second wash using assay media was performed. For the Mito Stress Test, 1uM oligomycin A, 0.5 uM FCCP and 0.5uM rotenone/antimycin A were sequentially added by the Flux Analyzer, according to standard protocol and FCCP titrations. Hoechst 33342 (1ug/mL) nuclear staining dye (Sigma-Aldrich, MO, USA) was added after the assay was complete to normalize OCR/ECAR to total nuclei. Wells were imaged using a Cytation5 (Agilent, Santa Clara, CA) and counted using Gen5 fluorescent cell count.

3.3.14 Statistical Analysis

Statistical analyses were performed using Prism 8.4.3 (San Diego, CA). For glucose concentration experiments, a repeated measures two-way ANOVA was performed to test for effect of media volume (20mL, 30mL, 40mL) and time (24h, 48h) on media glucose concentration. Similarly, for scratch closure experiments, a repeated measures two-way ANOVA was performed to test for effect of time (12h, 24h) and culture condition (5% O_2/MPM vs 1.5% O_2/TMEM) on percent scratch closure. Tukey's and Sidak's multiple comparisons post-hoc tests were performed for either analysis, respectively. For all remaining experiments, unpaired t-tests between groups

were performed. Statistical significance was established at *p*-value ≤0.05 unless otherwise stated for RNA sequencing. All averaged data were presented as means ± standard error of means [SEM].

3.4 RESULTS

3.4.1 Formulation of a tumour microenvironment-like medium (TMEM) and mouse plasma medium (MPM)

To design a culture medium representative of *in vivo* tumour interstitial fluid (TIF), a thorough review of available publications quantifying *in vivo* TIF nutrient levels was performed (**Table 1.2**). Despite this extensive search, only one comprehensive study that provided absolute quantification of TIF metabolites was identified (Sullivan et al., 2019). In this study, 136 polar metabolites were quantified in TIF sampled from pancreatic ductal adenocarcinoma (PDAC) autochthonous $Kras^{G12D}$ $Trp53^{fl/fl}$ Pdx-1-cre (KP-/-C) mouse models. For this reason, I used this metabolomics TIF data alone to formulate a medium representative of the tumour microenvironment, called Tumour Microenvironment Medium (TMEM). For this formulation, all commercially available metabolites quantified by Sullivan et al. (2019) were included at averaged concentrations relevant to TIF, with minor adjustments calculated for semi-quantitative measurements and glucose (See Materials and Methods and Table S3.1). Trace element concentrations used were based on DMEM F-12 formulation, as done for the Plasmax™ formulation (Vande Voorde et al., 2019). Salt components were based on physiological murine measurements (McKee & Komarova, 2017). The pH was adjusted to 7.0 to mimic *in vivo* tumour acidification (Anderson et al., 2016; Gerweck & Seetharaman, 1996; Wike-Hooley et al., 1984). In total, Tumour Microenvironment Medium, hereafter referred to as TMEM, contains 89 metabolites total: 57 at concentrations relevant to TIF; 25 at concentrations relevant to murine plasma; and 7 at non-physiological levels (Table 3.1).

To assess the relevance of refining physiological culture media to be representative of the tumour microenvironment, I sought to compare PDAC cells cultured in TMEM to the current 'gold-standard' for physiological culture conditions, plasma-like medium, in addition to physiologically relevant oxygen levels. Since the nutrient levels used to formulate TMEM were sourced from mouse PDAC TIF, a mouse PDAC cell line was selected for this comparison (KPCY). Furthermore, to facilitate an appropriate comparison between physiological tumour-like and plasma-like conditions within a mouse model, I formulated a physiologically relevant Mouse Plasma Medium (MPM), as only human plasma-like media are currently available (Plasmax and HPLM) (Cantor et al., 2017; Vande Voorde et al., 2019).

MPM was formulated using health mouse plasma concentrations found in the literature (See Materials and Methods and Table S3.1). All metabolites included in the formulation of TMEM were included in MPM at concentrations relevant to mouse plasma to ensure any influence of media on cell response could be attributed to nutrient availability alone, rather than the absence or addition of unique metabolites. Similar to TMEM, the concentration of trace elements used were based on the trace element concentrations in DMEM F-12 (Vande Voorde et al., 2019), and salt components were based on physiological murine measurements (McKee & Komarova, 2017). The pH was adjusted to 7.4 to mimic normal tissue. In total, the Mouse Plasma Medium, from here on referred to as MPM contains 89 metabolites total: 83 at concentrations relevant to murine plasma; and 7 at non-physiological levels (Table 3.1).

Table 3.1: Metabolite concentrations (uM) in Tumour Microenvironment Medium (TMEM) and Mouse Plasma Medium (MPM). TMEM formulation is based on tumour interstitial fluid data from Sullivan et al. (2019). MPM formulation is based on literature mouse plasma metabolomics data from multiple sources.

	TMEM*	MPM**
Proteinogenic Amino Acids		
L-Alanine[1]	1122	691
L-Arginine[1]	2.1	66
L-Asparagine[1]	115	50
L-Aspartate[1]	399	7.3
L-Glutamate[1]	1054	19
L-Glutamine	821	934
L-Glycine[1]	483	217
L-Histidine[1]	94	76
L-Isoleucine[1]	130	138
L-Leucine[1]	289	270
L-Lysine[1]	139	176
L-Methionine[1]	74	53
L-Phenylalanine[1]	80	96
L-Proline[1]	122	71
L-Serine[1]	88	96
L-Threonine[1]	252	145
L-Tryptophan[1]	31	62
L-Tyrosine[1]	60	69
L-Valine[1]	150	262
Non-Proteinogenic Amino Acids		
α-Aminobutyrate[2]	2.93	4.90
Arginosuccinate[6]	0.75	0.23
Homocitrulline[2]	0.72	0.98
L-Citrulline[1]	73	38
L-Cystine[1]	51	30
L-Homocysteine[6]	3.34	3.34
Methionine Sulfoxide[2]	3.17	1.43
L-Ornithine[1]	312	23
N,N,N-Trimethyllysine[6]	1.20	1.93
Sarcosine[2]	0.22	1.93
Amino Acid Derivatives		
Acetyl carnitine[2]	25	45

Acetylglutamate[2]	1.40	1.24
N-Trimethylglycine (Betain)[2]	94	57
Glutathione (reduced)[2]	22	21
L-a-Aminoadipate[2]	15	4.53
L-Carnitine[2]	40	8.47
L-Carnosine[2]	0.49	0.37
N-Acetyl-L-aspartate[2]	1.13	4.02
N-Acetylglycine[2]	23	65
N,N-dimethyl-L-Arginine (ADMA)[6]	0.84	1.23
Taurine[6]	2326	763
Other Components		
Acetate[6]	350	350
Allantoin[7]	63	106
Carbamoyl aspartate[2]	0.78	3.19
cis Aconitate2	2.97	5.97
Citrate[6]	339	214
Creatine[6]	192	192
Creatinine[2]	13	10.05
Cytidine[2]	4.60	1.83
5'-Deoxy-5'-methylthioadenosine[2]	0.0612	0.0161
D-Glucose	2304	4381
Glycerol[6]	179	179
2-hydroxybutyrate[6]	84	84
3-hydroxybutyrate[6]	81	849
Hypoxanthine[6]	10	0.0232
L-Kynurenine[2]	1.01	1.09
Lactate[6]	3794	3088
Malate[2]	156	18
Orotate[7]	0.702	0.964
Pyruvate	42	150
Sorbitol[2]	1.34	0.92
Succinate[2]	106	14
Urea[2]	25	25
Urate[3]	14	14
Uridine[2]	61	4.33
Xanthine[7]	0.894	0.449
Vitamins		
Ascorbate[5]	361	63
Choline[5#]	7.16	7.16
D-Biotin[5#]	4.09	4.09
D-pantothenate[5#]	4.56	4.56
Folate[5#]	2.27	2.27
Myo-inositol[5#]	11.1	11.1
Niacinamide[5#]	8.19	8.19
Pyridoxal[5#]	4.91	4.91
Riboflavin[5#]	0.27	0.27
Thiamine[5##]	2.96	2.96
Vitamin B12[5]	0.00150	0.00150
Trace Elements		
Ammonium Metavanadate[3]	0.0026	0.0026
Cupric Sulfate[3]	0.0052	0.0052
Ferric Nitrate[3]	0.1238	0.1238
Ferric Sulfate[3]	1.0428	1.0428
Manganous Chloride[3]	0.0002	0.0002
Sodium Selenite[3]	0.0289	0.0289
Zinc Sulfate[3]	1.5000	1.5000
Inorganic Salts		
Ammonium Chloride[3]	50	50
Calcium Chloride	1125	1125
Magnesium Sulfate	475	475
Potassium Chloride	5050	5050
Sodium Bicarbonate	18400	18400

Sodium Chloride	91700	91700
Sodium Phosphate Monobasic	2045	2045

TIF=tumour interstitial fluid
PDAC=pancreatic ductal adenocarcinoma
Superscripts for each constituent refers to stock solution number
contributions approximated by BME Vitamix
† (For D-Calcium pantothenate)
*PDAC TIF metabolomics data source (Sullivan et al., 2019).
**Healthy mouse plasma metabolomics data sources (Cantor et al., 2017; Leeuwenburgh & Ji, 1995; N. Maeda et al., 2000; McKee & Komarova, 2017; Shubitowski et al., 2019; Z. Wang et al., 2020; Watanabe et al., 2014; L. Yao et al., 2019)

When comparing TIF and healthy mouse plasma concentration ranges (Table S3.1), as well as TMEM and MPM formulations (Table 3.1; Figure 3.1), the metabolic availability between the tumour microenvironment and healthy plasma is distinct, however not necessarily suggestive of total nutrient deprivation in the tumour. This agrees with observations made by Sullivan et al. (2019) when comparing TIF to paired plasma measurements from diseased mice, among numerous other studies that have quantified individual metabolites in TIF (Liu & Yang, 2021; Mei et al., 2022; Nierves et al., 2022; Roslin et al., 2003; Tiziani et al., 2013). Only a few select metabolites, including glucose, arginine, tryptophan, sarcosine, N-acetyl-L-aspartate, acetylglycine, carbomyl aspartate, cis aconitate, 3-hydroxybutyrate and pyruvate, are at least two-fold lower in TMEM, with arginine reduced by 30-fold compared to healthy mouse plasma. Rather, there is an accumulation of several unique essential, non-essential and derivative amino acids in TIF, and appropriately represented in TMEM (Figure 3.1 A; Table 3.1). Notably, many metabolites involved in the urea cycle, including ornithine, citrulline, glutamate, and arginosuccinate appear to accumulate within TIF when compared to healthy mouse plasma, thus contributing to increased metabolite contributions (mM) in TMEM versus MPM (Figure 3.1 B, C). Succinate, a proposed oncometabolite that accumulates due to succinate dehydrogenase deficiency or loss of function (Eijkelenkamp et al., 2020; Mu et al., 2017), is also increased in PDAC TIF by 7-fold, as reflected in TMEM. Furthermore, while glucose is the largest contributor in MPM, making up 31% of total metabolites concentrations, glucose contributions in TMEM are only 14%. Alternatively, lactate and taurine make up the greatest contributions in TMEM.

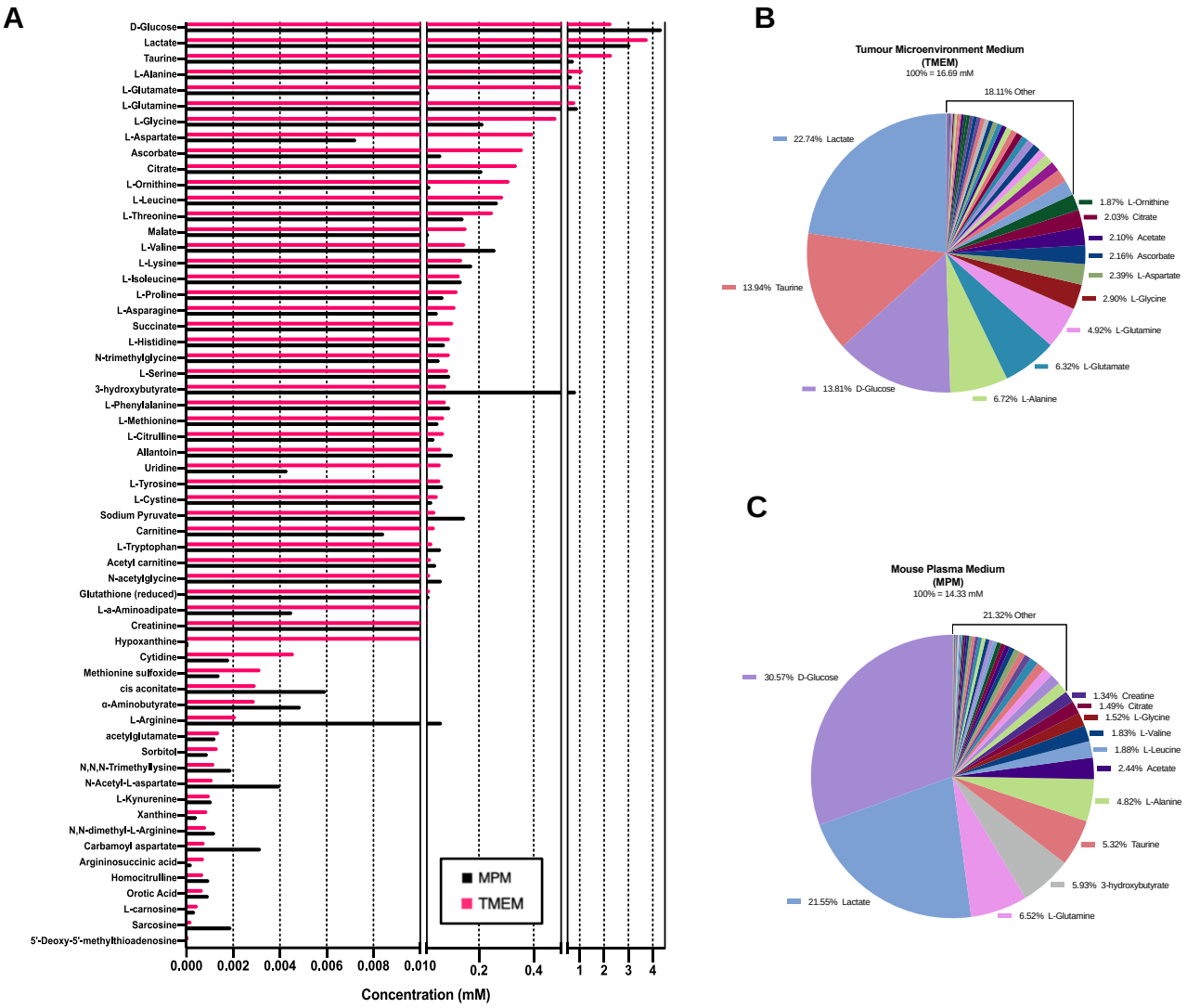

Figure 3.1: Metabolite contributions in Tumour Microenvironment Medium and Mouse Plasma Medium formulations. Tumour interstitial fluid and healthy mouse plasma metabolomic data were used to formulate novel murine cell culture mediums. **(A)** Comparison of concentration (mM) of metabolites used for TMEM and MPM formulations and (**B** and **C**) percent contributions of metabolites to total formulation. Metabolites with equal mM contributions in TMEM and MPM excluded from (A). Trace element and salts contributions excluded from all figures.

3.4.2 Establishing and maintaining PDAC tumour microenvironment conditions in culture

To establish a PDAC tumour-like culture model, PDAC cells were cultured in TMEM (pH 7.0) in incubators with headspace oxygen regulated to achieve relevant medium pericellular oxygen levels. A murine PDAC cell line (KPCY) was selected for culture. To validate the culture model as being representative of a PDAC tumour microenvironment, as well as to ensure

conditions remain within physiological targets for typical culture periods, glucose availability, pericellular oxygen, and media pH were monitored in adapted cells.

Target glucose concentrations representative of the PDAC tumour microenvironment are 2.3mM in TMEM. Given the rapid nutrient depletion that can be expected under physiological plasma-like conditions (Gardner et al., 2022), the more constrained conditions established in TMEM were expected to present exasperated risks. To address this, media volumes were increased and glucose availability was monitored over 48 hours. Since I previously observed that the depletion of several essential and non-essential amino acids follows a trend similar to that of glucose, glucose was used as a proxy metabolite to gauge nutrient depletion in this study. Cells were seeded on 100mm culture plates with 1,000,000 cells in 20mL, 30mL, or 40mL of TMEM, and media glucose levels measured at time 0h, 24h, and 48h (**Figure 3.2**).

Our 0h glucose measurement of 2.9mM, although higher than our formulation, is consistent with FBS contributions (~17mM) from 2.5% FBS supplementation (Owens and Kind, 2008).
Importantly, the results of repeated measures two-way ANOVA indicate a significant main effect of time ($F_{1.044,6.266}$ =5094, $P < 0.0001$), media volume ($F_{2,6} = 60.26$, $P = 0.0001$), and the interaction between time and media volume ($F_{4,12} = 67.79$, $P < 0.0001$) on glucose concentration. Thus, both factors must be considered in the establishment of culture practices that maintain TMEM glucose levels.
Post hoc analysis indicated significant glucose depletion in all media volumes over 24 and 48 hours such that following the first 24 hours, average glucose levels fell by 35-45%. Increased media volumes ameliorated glucose depletion at both 24h and 48h when compared to 20mL, however this was not sufficient to maintain glucose availability within target concentrations over the course of 48 hours. Alternatively, average glucose levels between 0h and 24h were 2.22mM, 2.34mM, and 2.375mM for increasing media volumes, respectively, suggesting appropriate glucose availability in TMEM only extends over the first 24 hours of culture. Since the glucose level was significantly increased with 30mL ($P = 0.0173$) and 40mL ($P = 0.0204$) media compared to 20mL, but no significant difference was measured between 30mL and 40mL ($P = 0.1185$), 30mL was selected as the optimal volume for further experiments to minimize glucose depletion over 24 hours. Conclusively, results were indicative of proceeding with 30mL daily media exchanges in 100mm plates, or ~1mL TMEM per 33,000 cells seeded, with appropriate adjustments made to maintain oxygen diffusion distance for alternative culture flasks.

A

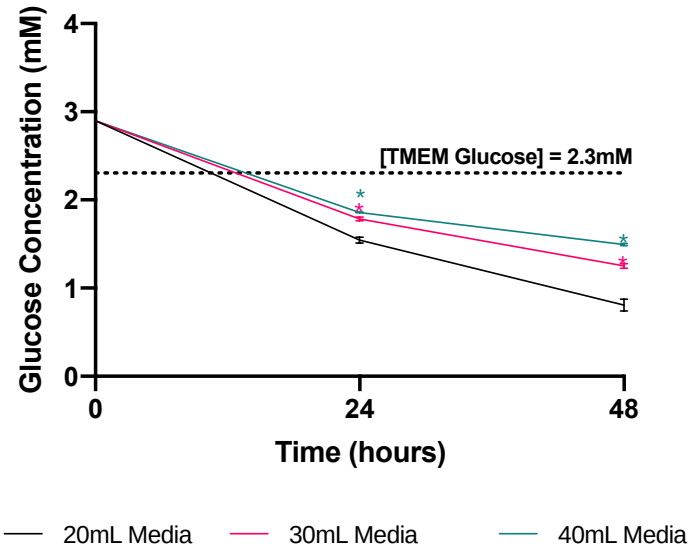

B

Glucose Concentration (mM)

	20 mL	30 mL	40 mL
T0	2.90	2.90	2.90
T24	1.54	1.78	1.85
T48	0.808	1.25	1.50

Figure 3.2: Mean glucose concentrations (mM) over 48 hours for KPCY cells cultured in 1.5% O_2/TMEM with increasing medium volumes. (A) Glucose measured over 48 hours at time 0h (fresh media), 24h and 48h. Media volumes of 20mL, 30mL and 40mL were used in 100mm plates to achieve target TMEM glucose concentration (2.3mM). (B) Averaged glucose concentrations (mM) at each measurement point and media volume. Graphical means expressed ± SEM. N=3 independent experiments. '*' represents significant difference compared to 20mL volume ($P \leq 0.05$). Statistical significance determined by repeated measures two-way ANOVA followed by Tukey's post-hoc analysis.

In vivo oxygen levels for PDAC are ~0.7% O_2 (Koong et al., 2000) (**Table 1.2**). Considering the poor diffusion of gas phase (headspace) oxygen to liquid phase in static cell culture (Place et al., 2017; Rogers et al., 2023), I monitored pericellular oxygen of KPCY cells cultured in TMEM to determine the conditions required to achieved tumour-like pericellular oxygen. While preliminary experiments initially varied headspace oxygen (1-2%) (data not shown), I found 1.5% O_2 best approximated pericellular targets of 0.7% O_2. Experimental conditions (media volumes, seeding densities) were thus manipulated and monitored at this oxygen level. Simultaneous to experiments quantifying glucose availability with varied media volumes, I measured the pericellular oxygen of cells cultured in a 24-well Oxodish with increasing media volumes that approximated the heights of volumes used in the 100mm plates (20mL, 30mL, 40mL), along with media only controls (**Figure 3.3A**). Media only wells equilibrated with headspace oxygen, with media oxygen levels averaging at 1.43% O_2 (± 0.031) over the 48 hours following equilibration. Cell containing wells showed a volume-dependent decrease in pericellular oxygen level between 0.47-0.88% O_2. Importantly, pericellular oxygen in wells approximating

30mL in a 100mm culture plate (1.141 mL) averaged at 0.61% O_2 (± 0.032) over 48 hours, and 0.67% O_2 (± 0.031) in the first 24 hours (**Figure 3.3B**). Thus, by regulating headspace oxygen to 1.5% O_2, pericellular oxygen levels representative of the PDAC microenvironment can be achieved in parallel to appropriate nutrient levels. For simplicity, and in alignment with how the field communicates cell culture oxygen levels, I will henceforth refer to this oxygen condition by the headspace oxygen level of 1.5% O_2. With that said, this result clearly illustrates the importance of controlling for impaired gas phase oxygen diffusion in static cell culture when establishing physiological oxygen levels.

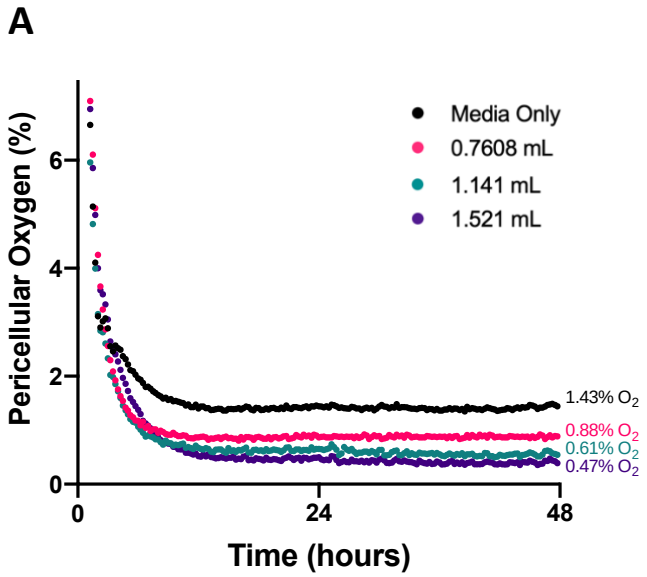

B

Pericellular Oxygen (%)

	Media Only	0.7608mL	1.141mL	1.521mL
First 24h	1.46	0.89	0.67	0.56
Second 24h	1.41	0.86	0.57	0.41

Figure 3.3: Pericellular oxygen of KPCY cells cultured in TMEM at 1.5% headspace O_2. (A) Presens Oxodish pericellular oxygen readings (%) in TMEM cultured KPCY cells at increasing media volumes and cell free 'media only' controls over 48 hours. Labeled O_2 values (%) are averages of the total 48 hours following stabilization. (B) Averaged pericellular oxygen readings (%) over the first and second 24 hours. Data shows the mean of 6 technical replicates per volume within one PreSens Oxodish.

The extracellular pH environment of solid tumours ranges from 5.5. to 7.2 (Anderson et al., 2016; Thistlethwaite et al., 2022). To achieve a pH representative of the tumour microenvironment in 5% CO_2 environment, a bicarbonate (HCO3-) buffering system was established, with TMEM adjusted to a pH of 7.0 upon preparation. Furthermore, I directly monitored the extracellular pH of TMEM cultured KPCY cells and media only control wells using a 24-well Hydrodish. The media volume (1.141 mL) and monitoring period (24 hours) used was continuous with the results from the glucose and oxygen experiments. Following equilibration, the

pH of TMEM stabilized to ~7.1 (± 0.002) at 5% CO_2 in media only wells (**Figure 3.4**). In KPCY containing wells, initial pH readings were similar to media controls, however acidification was observed over the 24 hours, averaging to ~7.05 (± 0.01). This was attributed to lactic acid production surpassing the buffering capacity of the media.

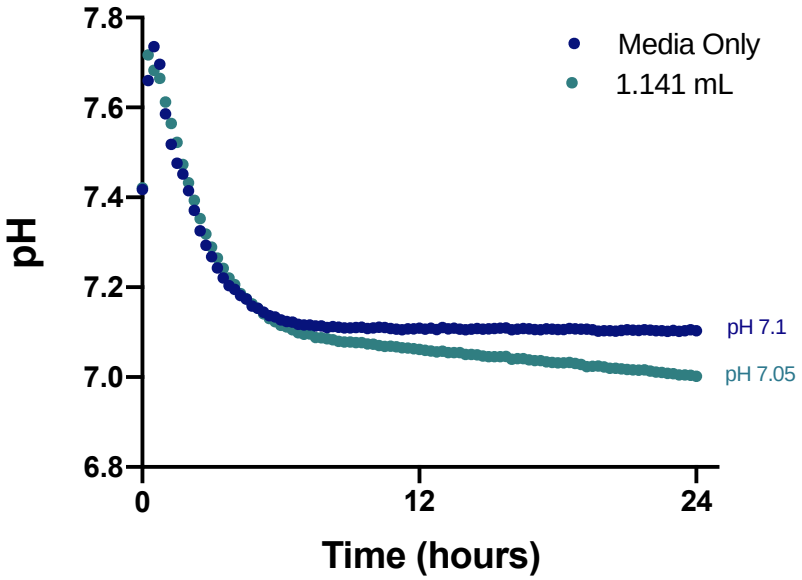

Figure 3.4: Extracellular pH of KPCY cells cultured in 1.5% O_2/TMEM. Presens Hydrodish pH readings in TMEM cultured KPCY cells and cell free 'media only' controls over 24 hours. Data shows the mean of 6 technical replicates within one PreSens Hydrodish.

Overall, through analysis of our glucose, pericellular oxygen, and pH monitoring data, I successfully determined the optimal culture conditions and practices to achieve PDAC tumour-like conditions in our KPCY model. Thus, for all subsequent experiments, daily media exchanges with a minimum of 1mL TMEM per 33,000 cells seeded were implemented. Additionally, the specific volume of media used for all other culture vessels was calculated to maintain the same media height (diffusion distance) as those monitored (**Table S3.2**). Furthermore, I maintained cell densities comparable those used for validation for remaining experiments, with some adjustments made for those experiments requiring longer culture periods. By doing so, I can ensure that relatively stable and reproducible tumour-like culture conditions are established.

Of note, glucose and pericellular oxygen monitoring was also performed for KPCY cells cultured in our physiological 'plasma-like' conditions (5% O_2/MPM) to validate the conditions prior to comparison with our tumour-like condition (1.5% O_2/TMEM) (**Figure S3.1**). Similar statistical analysis was performed on the glucose data as TMEM, with a significant main effect of

time ($F_{1.083,6.499}$ = 393.0, P < 0.0001) and media volume ($F_{2,6}$ = 16.84, P = 0.0035) on glucose concentration indicated. However, no effect was seen with increasing media volume in the first 24 hours (**Figure S3.1 A**). Nonetheless, to remain consistent with the tumour-like culture protocol, daily media exchanges with 1mL MPM per 33,000 cells seeded were maintained. Pericellular oxygen levels for MPM cultured KPCY cells at a headspace of 5% O_2 averaged to 3.67% O_2 (**Figure S3.1 B**), mimicking that of normal pancreatic tissue (~4% O_2) (Carlsson et al., 1998; Carlsson et al., 2001). This will be referred to as 5% O_2 hereafter.

3.4.3 Tumour-like culture conditions profoundly affect gene expression in KPCY cells compared to plasma-like conditions

Once initial experiments validated our PDAC tumour-like culture model in KPCY cells, the necessity for refining tumour-specific physiological condition was assessed by directly comparing KPCY cells adapted to our tumour-like culture condition (1.5% O_2/TMEM), to those adapted under physiological 'plasma-like' culture conditions (5% O_2/MPM).

To evaluate the global effect of tumour-like conditions (1.5% O_2/TMEM) versus plasma-like conditions (5% O_2/MPM) on cultured cells, differential gene expression was evaluated in cells adapted to their respective conditions using RNA sequencing. In total, 611 genes were differentially expressed between the two conditions: 247 up-regulated genes enriched in 1.5% O_2/TMEM vs. 5% O_2/MPM; and 364 down-regulated genes enriched in 1.5% O_2/TMEM vs. 5% O_2/MPM (**Figure 3.5 A**). The up-regulated differentially expressed genes (DEGs) in tumour-like conditions included transcripts involved in cytoskeletal network organization (Cdh22, Avil, Dynap, Tmem132c), metabolic transport (Slc7a3, Slc7a3), and biosynthesis (Ptgs2, Bcat1, Cth) (**Figure 3.5 B**). Alternatively, the top downregulated DEGs in tumour-like conditions included transcripts involved in cell adhesion (Tmidg1, Cdhr5, Lgals4, Tm4sf20), lipid metabolism (Pcsk9, Cyp2c65) and drug metabolism, (Cyp2c65, Tff2) (**Figure 3.5 B)**.

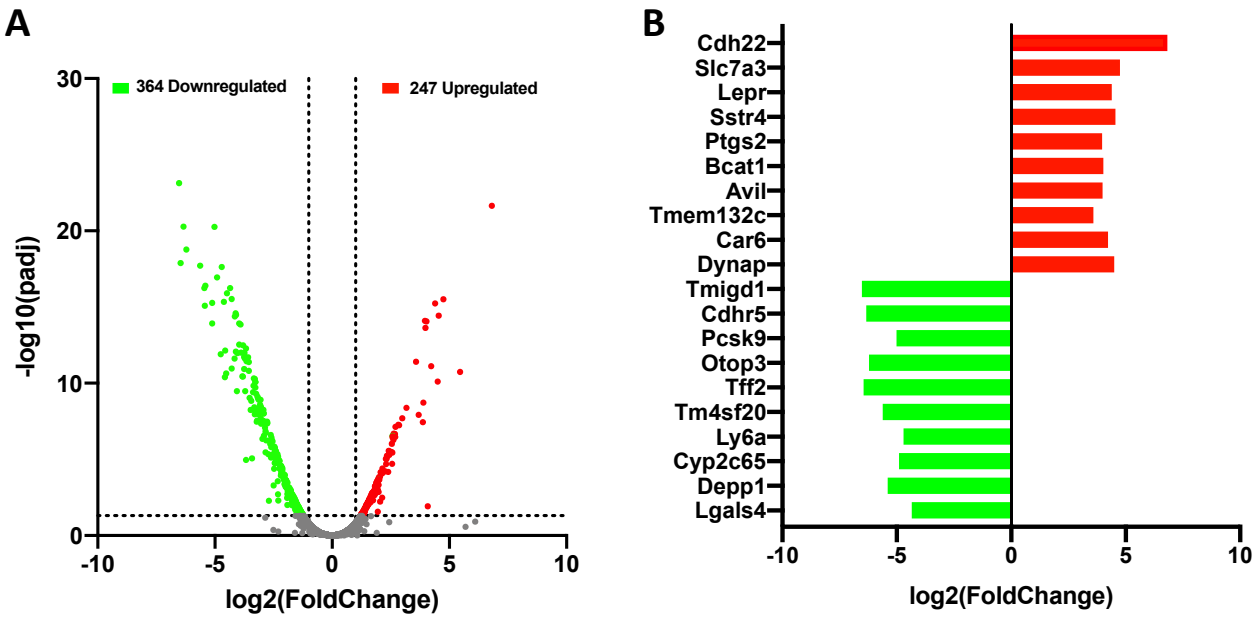

Figure 3.5: Differential gene expression in KPCY adapted to 1.5% O_2/TMEM versus 5% O_2/MPM. A) Volcano plot of the distribution of DEGs in 1.5% O_2/TMEM versus 5% O_2/MPM. Green and red data points show significant negatively (downregulated) and positively (upregulated) enriched DEGs, respectively, as defined by *P*-adj < 0.05, absolute log2(Fold Change) ≥ 1, and a minimum FPKM of 5 in at least one of the two samples compared. Grey data points show DEGs that did not make cut-off for significantly enriched genes. B) Top 10 protein coding DEGs down-regulated (green) and up-regulated (red) in 1.5% O_2/TMEM compared to 5% O_2/MPM. Significant DEGs sorted by log2(fold change) to determine top up- and down- regulated genes.

Over-representation analysis was performed on filtered DEG lists using DAVID to identify up- and down-regulated GO terms and KEGG/Reactome pathways associated with our culture conditions. GO term enrichment revealed several biological processes, cellular components, and molecular functions associated with either upregulated or downregulated enriched DEGs from our 1.5% O_2/TMEM vs. 5% O_2/MPM comparison. Upregulated DEGs enriched in cells adapted to 1.5% O_2/TMEM were associated with cell migration and motility, proliferation, protein synthesis, cytoskeletal dynamics, response to growth factors and cytokines (**Figure 3.6 A)**. Additional biological terms associated with vasculature development, angiogenesis, metabolic process, and regulation of apoptosis were also identified (**Table S3.3**). Cellular compartments included the extracellular region, plasma membrane, cytoplasm and actin filament.

Consistent with these findings, KEGG and Reactome pathway enrichment analysis showed significant enrichment of pathways involved in amino acid biosynthesis, regulation of proliferation, immune response, and apoptosis, including JAK-STAT, TNF, Hippo signaling

(**Figure 3.6 B**). Notably, terms related to axon guidance and neuronal processes also appeared enriched, potentially suggesting a role of the tumour microenvironment in establishing neuronal cross-talk and recruitment within the tumour niche.

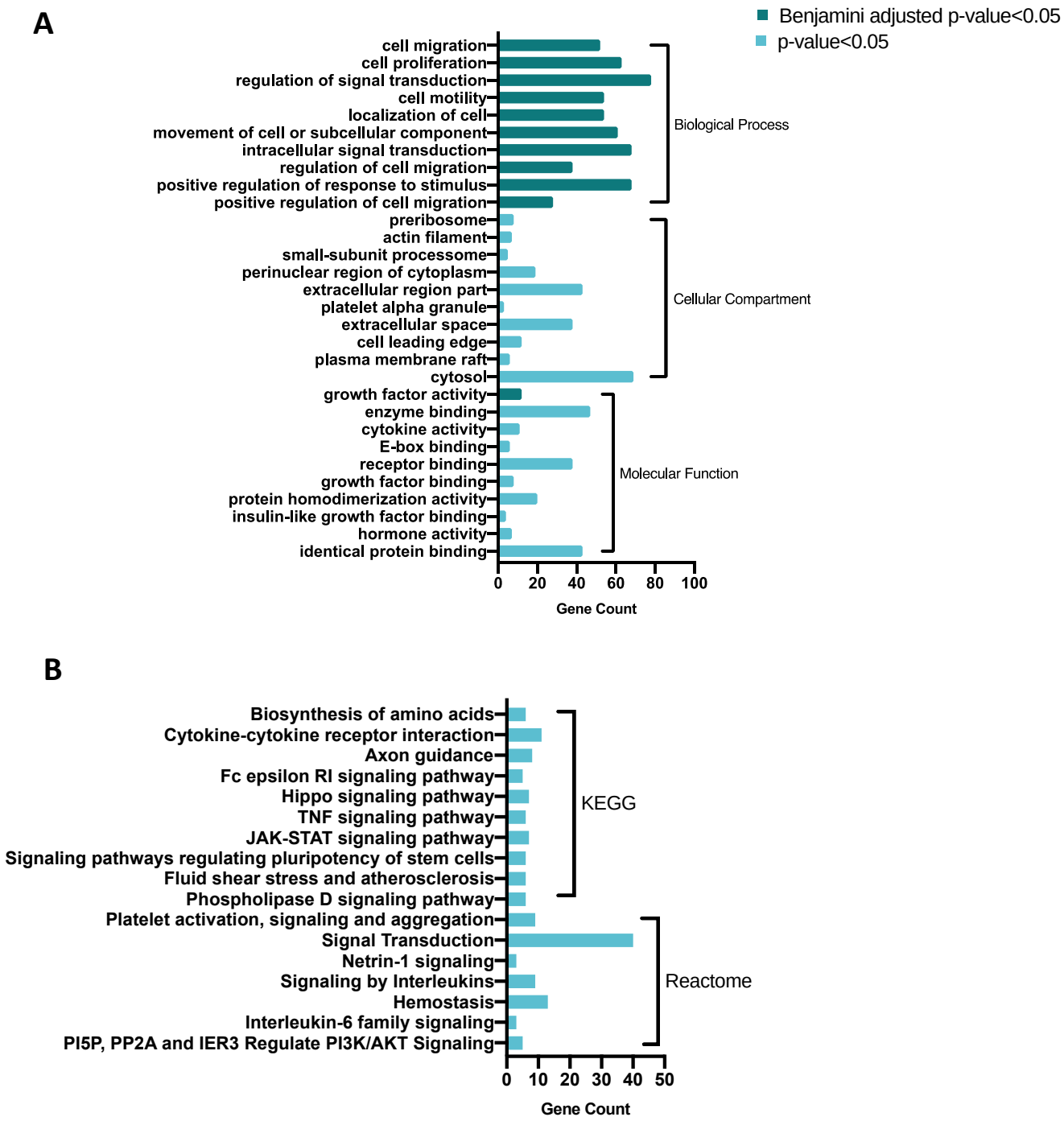

Figure 3.6: Top upregulated GO terms (A) and KEGG/Reactome (B) pathways enriched in KPCY adapted to 1.5% O_2/TMEM versus 5% O_2/MPM. DEG lists used for this analysis were positively enriched (positive fold change) filtered genes with *P* (adjusted) value ≤ 0.05, absolute log2(FC) ≥1, and a minimum FPKM of 5 in at least one of the two samples compared. Enrichment analysis terms were filtered to terms with a Benjamini adjusted *P* value ≤ 0.05, or *P* value ≤ 0.05, as indicated.

Downregulated DEGs enriched in cells adapted to 5% O_2/MPM were most significantly associated with metabolic and biosynthetic processes involving lipids, secondary alcohols, cholesterol, sterols, and steroids (**Figure 3.7 A**). Additional terms suggestive of cellular respiration and glutathione peroxidase/transferase activity were also identified (**Table S3.3**). Cellular compartments included the endoplasmic reticulum, plasma membrane, and peroxisome. KEGG and Reactome enrichment analysis confirmed pathways involved in fatty acid, steroid and cholesterol metabolism and biosynthesis (**Figure 3.7 B**).

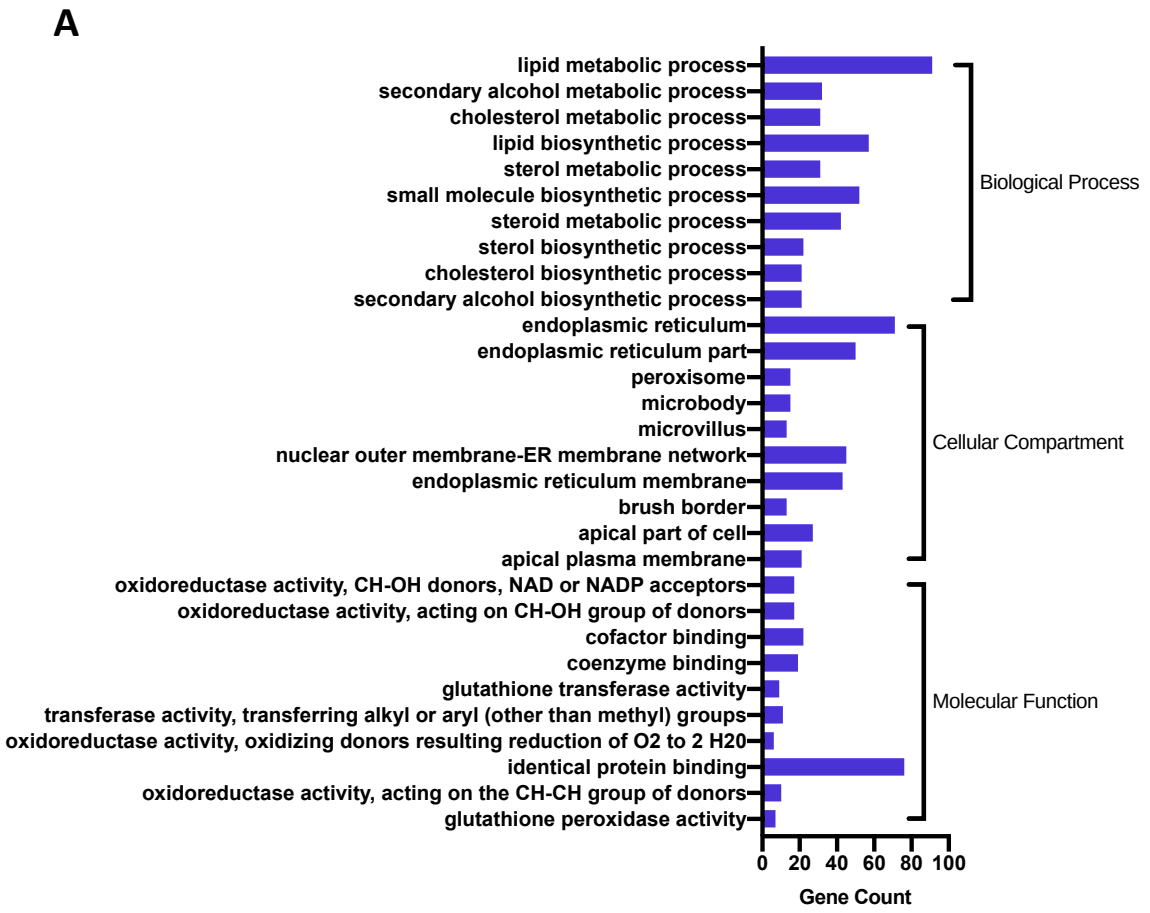

B

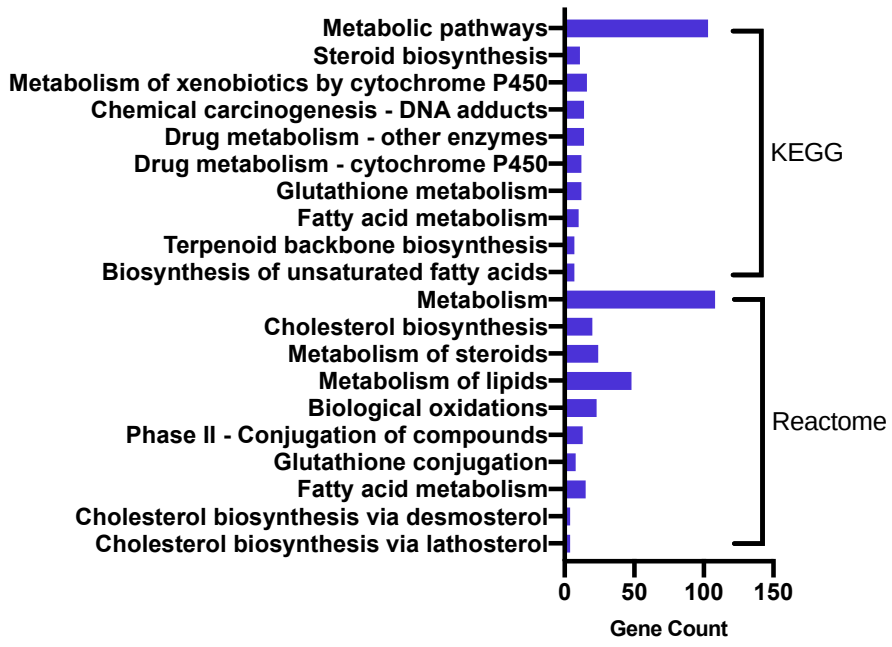

Figure 3.7: Top downregulated GO terms (A) and KEGG/Reactome (B) pathways enriched in KPCY adapted to 1.5% O_2/TMEM versus 5% O_2/MPM. DEG lists used for this analysis were negatively enriched (negative fold change) filtered genes with a *P* (adjusted) ≤ 0.05, absolute log2(FC) ≥1, and an minimum FPKM of 5 in at least one of the two samples compared. Enrichment analysis terms were filtered to terms with a Benjamini adjusted *P* value ≤ 0.05, or *P* value ≤ 0.05, as indicated.

Considering the enrichment analysis results suggesting that culture in 1.5% O_2/TMEM alters several metastatic and metabolic features in KPCY cells, I closely analyzed DEG lists for enrichment of hallmark gene targets contributing to these responses. Selecting for genes relevant to cancer biology, I identified several DEGs positively enriched in our tumour-like culture condition, implicated in tumorigenesis (**Table 3.2**). Alongside increased expression of Hif-1α (P_{adj} = 0.0463), several HIF-1/2 targets were significantly enriched, including genes involved in angiogenesis and vasculature remodelling (Serpine1, Adm2, Pdgfa, Edn1), cell cycle progression (Stc2, Pgf), glycolytic metabolism (*Pfkfb3),* and cell motility (*Ctfg*). Additionally, downstream gene targets of nutrient-responsive metabolic pathways were identified, including those specifically involved in amino acid biosynthesis (*Phgdh, Aldh18a. Psph),* and epithelial-mesenchymal-transition (EMT) (*Snai2, Inhba).* Importantly, several of these genes, including *Snai2* and *Pdgfa,* are established markers of cancer progression *in vivo*. Table 3.2 provides a brief

description of each of these genes and provides reference to their identification or role in cancer progression.

Table 3.2: Differentially expressed genes implicated in cancer hallmarks, selected from those upregulated in tumour-like culture conditions (1.5% O_2/TMEM).

Gene Symbol	Gene Name	Function	Ref	Log2FC
HIF 1/2 Targets				
Serpine1***	Serpin Family E Member 1 / Plasminogen activator Inhibitor 1	Inhibits fibrinolysis & enhances clot formation to maintain hemolysis	(Fink et al., 2002)	2.58
Stc2**	Stanniocalcin 2	Promotes cell cycle progression in metabolic stress, preventing apoptosis. Induces EMT.	(Law & Wong, 2010)	1.85
Pgf***	Placental growth factor	Promotes cell proliferation through growth factor activity. Member of VEGF family.	(Chaturvedi et al., 2012)	2.44
Pfkfb3**	6-Phosphofructo-2-kinase/Fructose-2,6-Biphosphatase 3	Catalyzes the synthesis and degradation of fructose-2,6-bisphosphate, promoting glycolysis. Positive regulator of cell proliferation via cyclin-dependent kinase 1.	(Minchenko et al., 2004)	1.73
Ctgf / Ccn2 **	Connective tissue growth factor / Cellular communication network factor 2	Mitoattractant – stimulates cell migration, adhesion, proliferation	(Higgins et al., 2004)	1.70
Hmox1*	Heme Oxygenase 1	Enzyme essential to heme catabolism. Roles in redox homeostasis.	(P. J. Lee et al., 1997)	1.41
Adm2*	Adrenomedullin 2	Promotes angiogenesis and vasodilation.	(Gu et al., 2020)	1.39
Edn1**	Endothelin 1	Vasoconstrictor preproprotein.	(J. Hu et al., 1998)	2.144
BhlheE41*	Basic Helix-Loop-Helix Family Member E41	Transcriptional regulator of genes implicated in cellular circadian rhythm (CLOCK* and BMAL1)	(Miyazaki et al., 2002)	1.30
Pdgfa**	Platelet Derived Growth Factor Subunit A	Implicated in promoting cell growth, EMT, and angiogenesis. Member of VEGF family.	(Y. Huang et al., 2004)	1.80
Metabolic Remodelling				
Phgdh**	Phosphoglycerate dehydrogenase	Enzyme involved in de novo serine synthesis; catalyzes conversion of 3PG to 3PHP	(Itoyama et al., 2021)	1.64

Aldh18a1***	Aldehyde dehydrogenase 18 family member A1	Enzyme involved in de novo proline, ornithine and arginine biosynthesis.	(Liu et al., 2012)	1.22
Aldh1l2***	Aldehyde dehydrogenase 1 family member L2	Regulatory mitochondrial enzyme involved in folate metabolism. Source of NADPH.	(C. Li et al., 2023)	2.58
Bcat1***	Branched chain amino acid transaminase 1	Catalyzes the reversible transamination of branched-chain alpha-keto acids to branched-chain L-amino acids essential for cell growth.	(Fox & Alvarez, 2020)	4.03
Psph**	Phosphoserine phosphatase	Enzyme involved in L-serine formation	(Ross et al., 2017)	1.98
Gpt2*	Glutamic-pyruvic transaminase 2	Mitochondrial alanine transaminase; Reversible transamination between alanine and 2-oxoglutarate to generate pyruvate and glutamate; gluconeogenesis and amino acid metabolism	(Hossain et al., 2021)	1.22
Invasion & Metastasis Markers				
Tc***	Tenascin C	Extracellular matrix protein. Induces migration and invasion via JNK/c-Jun.	(Paron et al., 2011)	2.62
Snai2*	Snail family transcriptional repressor 2	Transcription factor. Regulates expression of genes involved in EMT (i.e. CDH1) and proliferation.	(Gu et al., 2022)2024-05-23 2:32:00 PM	1.63
Inhba***	Inhibin β-A	Roles in EMT. Activates TFG- β signaling pathway	(Yu et al., 2021)	2.42
Avil***	Advillin	Actin-binding protein that regulates cytoskeleton assembly	(Hossain et al., 2021)	3.99

*P_{adj}<0.05, ** P_{adj}<0.005, *** P_{adj}<0.0005. Abbreviations: EMT, endothelial-mesenchymal-transition; VEGF, vascular endothelial growth factor; CLOCK, circadian locomotor output cycles kaput; BMAL1, Basic Helix-Loop-Helix ARNT Like 1; 3PG, 3-phosphoglycerate; 3PHP, phosphohydroxy pyruvate; JNL, Jun N-terminal kinase; CDH1, E-cadherin; TFG- β, transforming growth factor-β. Citations are evidence of gene targets or expression associated with tumorigenesis.

To directly determine whether our tumour-like culture condition elicits gene expression consistent with *in vivo* PDAC gene expression, I compared DEGs identified in this study to those enriched in human-derived PDAC tissue vs. matched adjacent tissue from a meta-analysis of The Cancer Genome Atlas Program (TCGA) Pan-Cancer microarray expression database (Atay, 2020). Of a total of 28 validated prognostic genes identified in this meta-analysis, two prognostic genes associated with poor PDAC survival were up-regulated in our tumour-like condition (*Frmd6,*

Dhrs9). Furthermore, two "hub" protein-coding genes considered to have a large number of protein-protein modulatory interactions in PDAC were identified, both of which were grouped within an extracellular matrix signaling gene cluster (*Tnc, Igfbp3*).

Overall, the gene expression results described here suggest that culture of KPCY cells in our 1.5% O_2/TMEM model alters the transcriptome of cells in a manner relevant to established cancer hallmarks. Further, our model appears to promote tumorigenesis and metastasis in cultured cells, consistent with aggressive cancer phenotypes *in vivo*.

3.4.4 Effect of tumour-like culture condition on cancer hallmarks in KPCY cells

Cell proliferation was evaluated in KPCY cells cultured in tumour-like culture conditions (1.5% O_2/TMEM) versus 'healthy' plasma-like culture conditions (5% O_2/MPM) to investigate the role of metabolic availability on replication. To determine proliferation rate during exponential growth, KPCY cells were counted over four days (**Figure 3.8 A**). In the first 24 hours, proliferation was comparable between either condition. However, following this lag period, KPCY cells cultured in 1.5% O_2/TMEM showed significantly slower proliferation such that by day 4, the final number of cells was 4-fold less than those cultured in 5% O_2/MPM ($P = 0.0044$) (**Figure 3.8 B**). Doubling time, calculated during exponential growth for each condition, was significantly increased in TMEM cultured cells ($P = 0.0076$) (**Figure 3.8 C**), averaging at 35.1 hours ± 3.7 for tumour-like conditions (1.5% O_2/TMEM) and 16.7 hours ± 0.4 for plasma-like conditions (5% O_2/MPM). This suggests that culture in 1.5% O_2/TMEM does not support proliferation to the same capacity as 5% O_2/MPM.

A

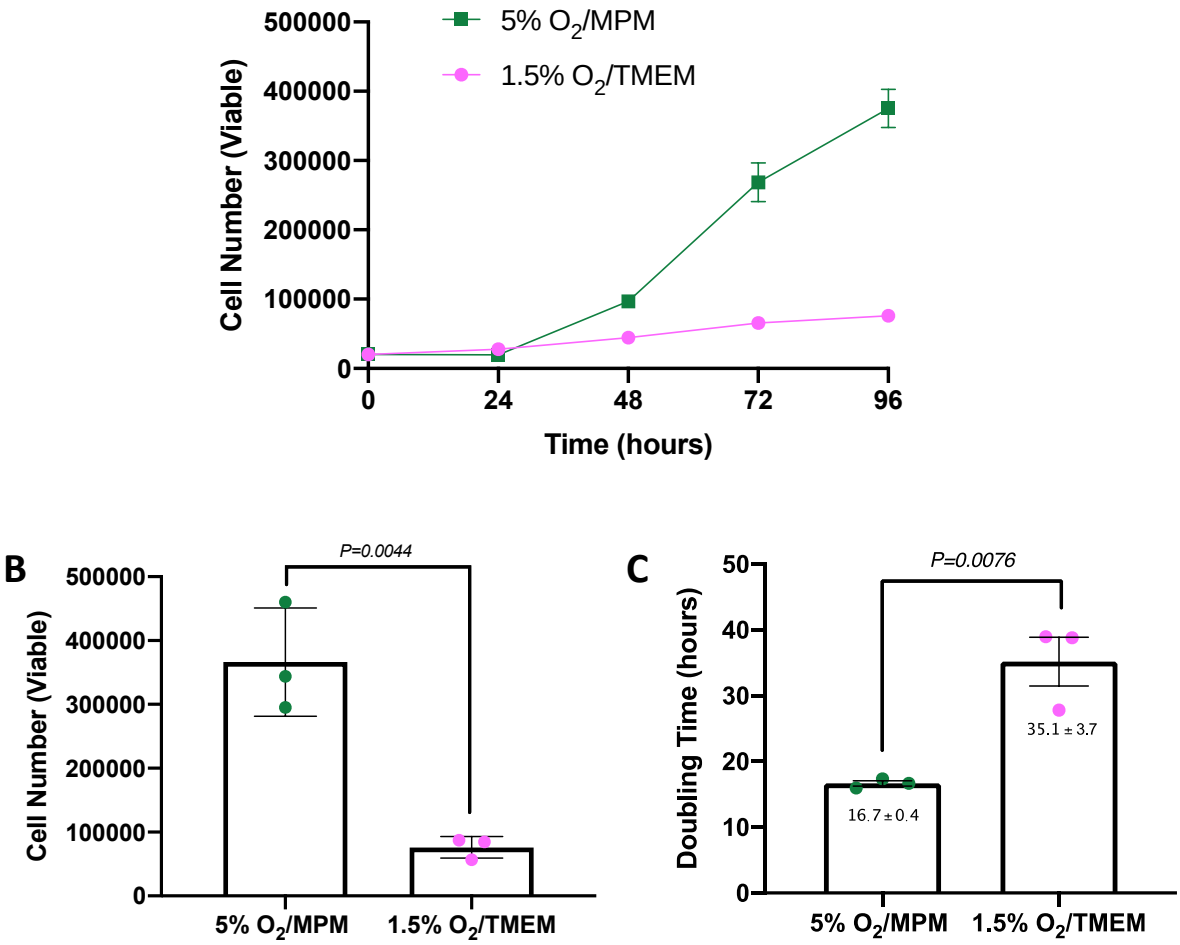

Figure 3.8: KPCY proliferation following culture in physiological plasma-like (5% O_2/MPM) or tumour-like conditions (1.5% O_2/TMEM). (A) Cell growth over 4-day proliferation assay and (B) final cell count on day 4 of assay. (C) Doubling time, calculated during exponential growth period of the 4-day assay for each experiment. Viable cells stained using trypan blue and counted manually on hemocytometer. Data shown as means ± SEM; N=3 independent experiments, with three wells counted in triplicate per experimental replicate. Statistical significance determined by unpaired two-tailed t-test, *P*-value ≤ 0.05.

Since over-representation analysis of KPCY cultured in tumour-like culture conditions (1.5% O_2/TMEM) was indicative of changes in motility and EMT, I next assessed cell migration using a scratch assay. Cells were seeded on 6-well plates and grown to confluency over 2-3 days, before a scratch was made through the cell monolayer using a micropipette tip. The size of the scratch was then monitored 12 and 24 hours post scratch (**Figure 3.9 A**). Results of repeated measures two-way ANOVA indicate a significant main effect of culture condition ($F_{1,4}$ =26.8, P = 0.0069), and time ($F_{1,4}$ = 439.8, P < 0.0001) on percent wound closure, but not the interaction

between the terms ($F_{1.4}$ = 0.6566 P = 0.4632). Post hoc analysis indicated that the extent of scratch closure was significantly greater in KPCY cells cultured in 1.5% O_2/TMEM at both 12h (P = 0.0044) and 24h (P = 0.022), such that by 24h, scratch percent closure from time 0h was ~80% (**Figure 3.9 B**). In comparison, in cells cultured in 5% O_2/MPM, scratch closure by 24h was ~63%. Thus, tumour-like culture conditions increased migratory behaviour of the cells, consistent with a metastatic phenotype.

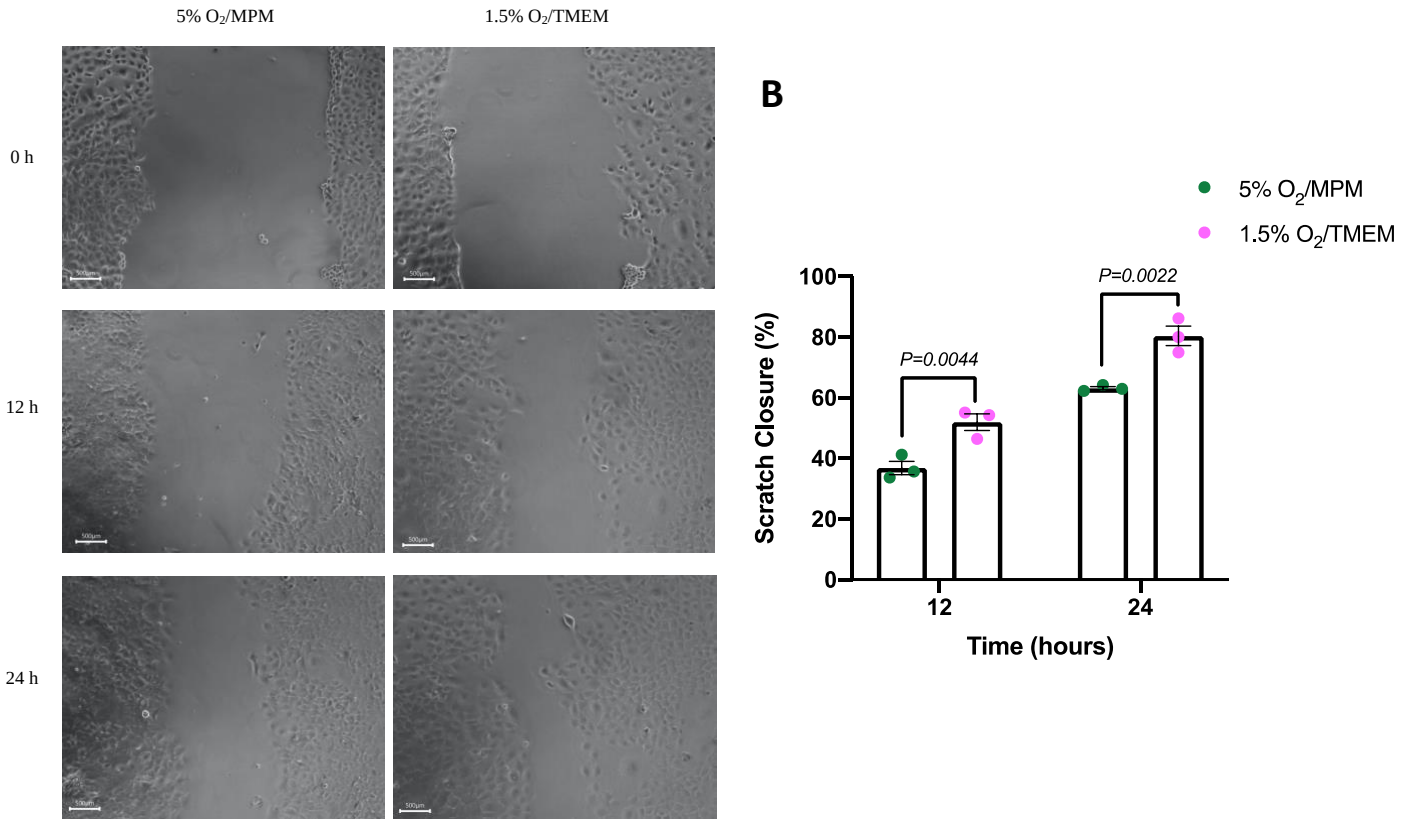

Figure 3.9: Migration of KPCY cells following culture under physiological plasma-like (5% O_2/MPM) or tumour-like conditions (1.5% O_2/TMEM). (A) Representative images of cell migration throughout scratch assay and (B) quantification of migration as percentage wound closure 12h and 24h following initiation of scratch assay. Data shown as means ± SEM; N=3 independent experiments, with three wells imaged per experimental replicate. For each well, multiple points along the scratch were imaged. Statistical significance determined by repeated measures two-way ANOVA followed by Sidak's post hoc test.

Increased glucose uptake, nutrient shunting through alternative metabolic pathways, and a shift in glucose utilization toward glycolysis are well noted as hallmark features in many cancers. Due to this rewiring hallmark, as well as the RNAseq metabolic hits, I next measured glucose

uptake and lactate production in KPCY cells cultured in tumour-like culture conditions (1.5% O_2/TMEM) versus plasma-like culture conditions (5% O_2/MPM). In agreement with these hallmark features, glucose uptake at 1.5% O_2/TMEM was significantly increased (1362.25 ± 60.89 fmol/cell*hour) compared to 5% O_2/MPM (825.13 ± 9.62 fmol/cell*hour) (**Figure 3.10 A**). Lactate production rate was also significantly greater at 1.5% O_2/TMEM (1143.78 ± 72.80 fmol/cell*hour) compared to 5% O_2/MPM (603.27 ± 8.65 fmol/cell*hour) (**Figure 3.10 B**). This suggests that glucose uptake and flux through glycolytic pathways to produce extracellular lactate is significantly increased in tumour-like conditions, consistent with increased rates of glycolysis.

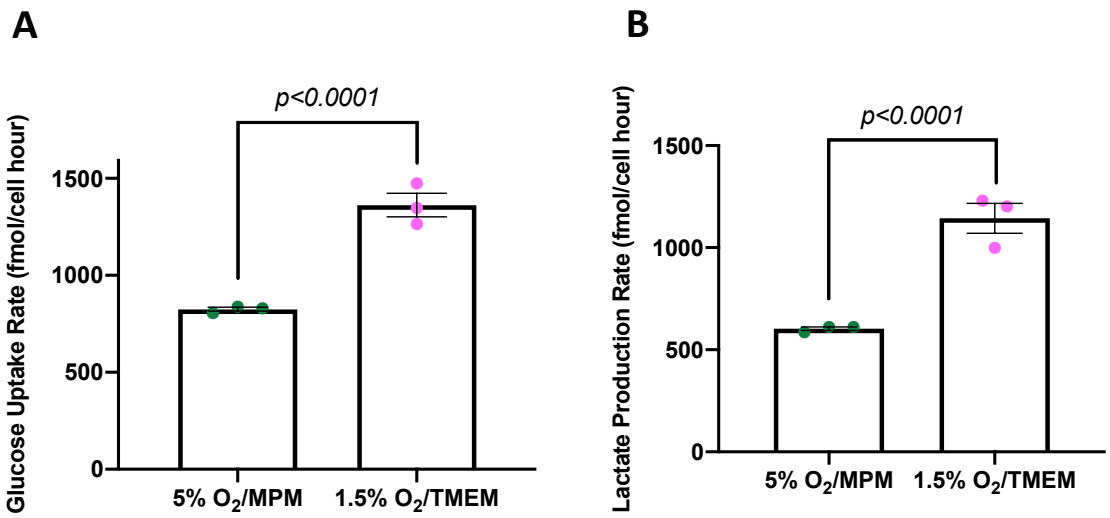

Figure 3.10: (A) Glucose uptake and (B) lactate production rate in KPCY cells cultured under physiological plasma-like (5% O_2/MPM) or tumour-like conditions (1.5% O_2/TMEM). Glucose uptake and lactate production was measured over 24 hour in KPCY cells. Data shown as means ± SEM; N=3 independent experiments, with 3 technical replicates (plates) per experimental replicate. Statistical significance determined by a unpaired two-tailed t-test, *p*-value ≤ 0.05

To further elucidate the effect of tumour-like culture conditions in modulating cellular bioenergetics and energy production, a Seahorse XF Cell Mito Stress Test was performed on KPCY cells cultured in their respective tumour-like (1.5% O_2/TMEM) or plasma-like (5% O_2/MPM) conditions. Hypoxic Seahorse extracellular flux analysis was performed within a hypoxia glovebox with headspace oxygen levels appropriate for either condition (1.5% or 5%), with all necessary considerations maintained to perform reliable 'hypoxia mode' Seahorse assays. In KPCY cells cultured in 1.5% O_2/TMEM, the OCR profile was ~3-fold lower

compared to OCR in cells cultured at 5% O_2/MPM following each injection (**Figure 11A**). Bioenergetic respiratory parameters calculated from basal OCR measurements, and OCR following injection of oligomycin, FCCP, and Rotenone/Antimycin A, were all significantly reduced in 1.5% O_2/TMEM cultured cells. Basal, maximal, and ATP-linked oxygen consumption were below 40 pmol/min/10,000 cells in 1.5% O_2/TMEM, whereas OCRs in 5% O_2/MPM cells were over 80 pmol/min/10,000 cells (**Figure 11B**). Similarly, OCR attributed to proton leak, spare respiratory capacity and non-mitochondrial oxygen consumption were below 10 pmol/min/10,000 cells in 1.5% O_2/TMEM, versus 15.8 (± 2.57), 70.96 (± 6.57), 14.92 (± 1.87) pmol/min/10,000 cells in 5% O_2/MPM cultured cells, respectively (**Figure 3.11C**). This suggests that mitochondrial respiration is reduced in cells cultured under tumour-like oxygen and nutrient conditions.

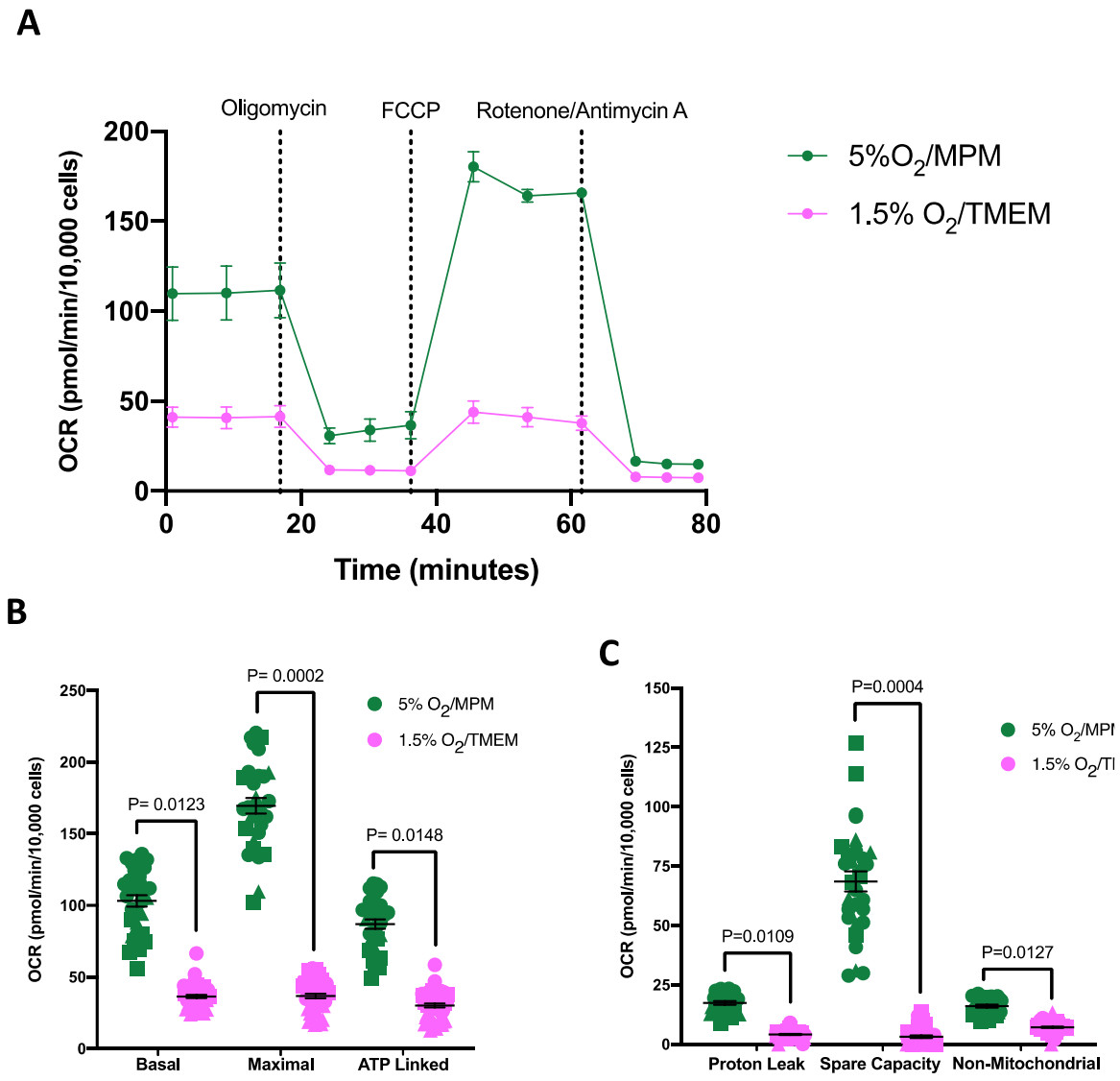

Figure 3.11: Oxygen consumption rate (OCR) for KPCY cells cultured under chronic physiological plasma-like (5% O_2/MPM) or tumour-like (1.5% O_2/TMEM) conditions. OCR profile (A) and bioenergetic respiratory parameters (B,C) calculated from OCR following injection of 1µM oligomycin, 0.5 µM FCCP and 0.5 µM rotenone/antimycin A. Data shown as means ± SEM. N=3 independent experiments, with 7-17 wells per condition for each experimental replicate. Different shapes for each condition represent technical replicates from independent experiments. Statistical significance determined by unpaired, two tailed t-test between culture conditions for each parameter, *P*-value ≤ 0.05.

3.5 DISCUSSION

Rewiring of metabolic pathways was among the key responses regulated in our tumour-like cell culture model. Consistent with glycolytic hallmarks, genes involved in the regulation of glycolysis and gluconeogenesis precursor synthesis were upregulated in 1.5% O_2/TMEM cultured cells. Functionally, both glucose uptake and lactate production rates were also significantly increased in tumour-like conditions. However, mitochondrial respiration was substantially decreased, indicating an increased glycolytic flux fated for fermentation. Additionally, genes implicated in amino acid biosynthesis and membrane transport were upregulated in 1.5% O_2/TMEM, despite similar or greater initial concentrations present in TMEM for those amino acids indicated (serine, proline, ornithine, glutamate, isoleucine, valine) (**Table 3.1 and 3.2**). Interestingly, this may suggest exogenous amino acid scavenging to support catabolic reprograming occurring in our tumour-like conditions (reviewed in (Wei et al., 2021); however, metabolomic uptake analysis and amino acid tracing must be performed to confirm this. Consistent with our results, numerous studies have shown that dysregulated glucose metabolism, and enhanced expression of amino acid synthetases (i.e. ASNS, ASS1), transferases (i.e. BCAT) and transporters (i.e. SLC7A11) are central to cancer cell survival under metabolic constraint (Crump et al., 2021; Cui et al., 2007; Koppula et al., 2018; Scalise et al., 2020; Shafei et al., 2020). Furthermore, PDAC cells specifically have been reported to increase amino acid utilization under reduced glucose and amino acid extracellular conditions both in vitro and *in vivo*, primarily through adaptive scavenging mechanisms including transaminase activity and macropinocytosis (Kamphorst et al., 2015; Tsai et al., 2021). Thus, our tumour-like model maintains features of metabolic remodelling hallmarks, promoting cellular adaptation in ways relevant to *in vivo* metabolism.

Environmental cues within the tumour microenvironment modulate cell migration, invasion, and metastasis through the coordination of several different signaling cascades. Metabolic availability is among these cues. Activation of AMPK, inhibition of mTOR, and HIF-1α signaling in response to metabolic stress coordinates downstream cytoskeletal remodelling, linking metabolite and energy homeostasis with cell motility (Crosas-Molist et al., 2023; L. Li et al., 2010; Rainero et al., 2015). Our finding that tumour-like culture conditions promote cell migration, both transcriptionally and functionally, is thus consistent with this mechanism. Furthermore, I identified several migratory terms enriched in 1.5% O_2/TMEM conditions that are

in vivo markers for EMT programming and metastasis (Carstens et al., 2021; Clere et al., 2020; Palamaris et al., 2021). Interestingly, while the downregulation of epithelial signatures (cytokeratins, claudins, mucin), and upregulation of mesenchymal signatures (extracellular matrix proteins, growth factors) were consistent with classical EMT mechanisms, hallmark differential gene expression of E-cadherin adhesion proteins was not identified. This observation may suggest an alternate 'partial-EMT' programming taking place, a mechanism that was recently characterized in murine PDAC tissue *in vivo* (Aiello et al., 2018). In this study, partial-EMT was associated with maintenance of E-cadherin mRNA expression, post translational protein re-localization of membrane adhesion molecules, and maintenance of epithelial capacities in PDAC cells. In breast, prostate and lung cancer, this mechanism of EMT is associated with increased metastatic potential, owing to the ability of cells to form intercellular junctions and migrate collectively (Armstrong et al., 2011; Lecharpentier et al., 2011; Yu et al., 2013). Our tumour-like condition seems to promote this phenotype at a transcriptomic level in KPCY cells, and may serve as an appropriate model to elucidate the mechanism by which the tumour microenvironment initiates 'partial-EMT' *in vivo*.

While rather substantial, it is not surprising that the proliferative capacity of KPCY cells was also affected in 1.5% O_2/TMEM conditions. Culture in human plasma-like media similarly slows proliferation in many cell lines compared to those measured in supraphysiological media (Cantor et al., 2017; Gardner et al., 2022; Golikov, Karpenko, et al., 2022; Vande Voorde et al., 2019). Additionally, chronic hypoxia exposure and HIF-1α stabilization have been shown to inhibit proliferation in various cultured cancer cells (Hubbi et al., 2013; Koshiji et al., 2004; Wilhelm et al., 2021). Given the metabolic constraint established in physiological media and hypoxia, the effect our tumour-like conditions have on proliferation is likely an adaptive response, mediated by AMPK and HIF-1α signaling, to coordinate replication with energy availability. This reduction in proliferation allows cells to maintain energy stores when nutrient and oxygen levels are limited. Moreover, while it is difficult to measure cellular proliferation rate *in vivo*, it is likely that replication is not as rapid as in standard culture, particularly in cell populations localized to poorly vascularized tumour regions. Notably, quiescent cancer cells, that being non-proliferative cells reversibly arrested in G0, have been reported to make up 80% of the total cells in established tumours, with their distribution within the tumour correlated with distance from blood vessels (Yano et al., 2014). While providing insight into the regulatory role of the tumour

microenvironment in proliferation, this finding exposes a limitation in current clinical therapeutic regimes that target cell cycle progression. Instead, targeting the adaptive mechanisms by which cancer cells dynamically modulate anabolic and catabolic pathways in response to environmental availability may offer more promising clinical outcomes.

Overall, the ability of our tumour-like culture conditions to maintain metabolic and metastatic phenotypes representative of *in vivo* adaptations is the most important result of this study (Atay, 2020; Kessler et al., 2008; van Pelt et al., 2023). Given the recent attention to metabolism-targeted anticancer drugs, it is imperative that pre-clinical experimental work is performed in culture models that maintain adaptive metabolic vulnerabilities characterized *in vivo*. As an example, lactate dehydrogenase (LDH), 6-phosphofructo-2-kinase/fructose-2,6-biphosphatase 3 (PFKFB3), and phosphoglycerate dehydrogenase (PHGDH) are critical enzymes enriched in PDAC tumours *in vivo* to promote glycolytic metabolism and serine biosynthesis in response to metabolic stress (Itoyama et al., 2021; Richardson et al., 2020; Xiao et al., 2017). Metabolic inhibitors of these enzymes are thus promising anti-cancer targets currently being investigated experimentally. In our tumour-like model, glucose fermentation through LHD was increased, and genes encoding PFKFB3 and PHGDH were upregulated as *in vivo*, making 1.5% O_2/TMEM a good model to screen for inhibitors. Conversely, plasma-like conditions in which these genes were not enriched may underestimate the therapeutic potential in a screening trial. Abbott et al. (2023) exemplify this effect of culture condition on screening outcomes, demonstrating the differential response of hundreds of metabolism-targeting drugs with culture in non-physiological (RPMI) versus serum-derived culture medium. Ultimately, culture conditions that poorly model metabolic or metastatic adaptations may limit the accuracy of pre-clinical drug screening studies in identifying successful therapeutics.

The metabolic and phenotypic landscape within solid tumours is heterogeneous and dynamic (Daemen et al., 2015; Tanaka et al., 2017; van Ineveld et al., 2021). Moreover, intertumoral differences in TIF exist depending on patient diet and tumour location (Sullivan et al., 2019). Thus, to illicit more oxidative and proliferative cancer phenotypes, future work may adjust the formulation of TMEM to be representative of well perfused tumours. In doing so, the need for combination anti-cancer drug therapies that target different sub-populations of cancerous cells may be revealed. Additionally, as more TIF quantification data becomes available, our formulation can be further adapted to model non-PDAC tumours. Ideally, a tumour-like media

such as TMEM should be developed using metabolomics data from several independent studies, with different formulations available for specific cancer types, given that TIF metabolomes differ substantially. However, without comprehensive metabolomics studies, this is not possible. Until then, TMEM may be used. Users may also choose to make adjustments to the formulation using whatever few metabolites of known concentrations are available for their specific cancer model (See Table 1.1 for summary of currently available TIF values).

Notably, during the formulation of TMEM and the research described in this study, a similar tumour-like medium, Tumour Interstitial Fluid Medium (TIFM), was developed by the same group that initially quantified murine PDAC TIF metabolites (Apiz-Saab et al., 2023). Although designed using the same TIF metabolomics data, these media differ slightly in formulation, owing to the following choices: 1) TMEM metabolite concentrations were selected using average TIF measurements, 2) In TMEM, semi-quantitative measurements were corrected using fold change applied to absolute literature plasma values, 3) Glucose was corrected using fold change applied to fasted glucose plasma values, 4) 2.5% FBS was used for serum supplementation, 5) pH was adjusted to 7.0. Moreover, while Apiz-Saab et al., (2023) investigate the effects of TIFM versus RPMI on cell metabolism at atmospheric oxygen, our work extends these observations. I show the importance of refined, microenvironment-specific culture conditions by comparing the effects of tumour-like and plasma-like media and oxygen conditions.

In summary, our results illustrate the importance of using physiological culture conditions in studying cell biology in vitro, and provides an example of how cancer biologists may implement tumour-like considerations into their research. Moreover, this work provides an appropriate model to study the mechanism of tumour microenvironment–mediated adaptations in vitro. Indeed, future studies should aim to better characterize this role in the metabolic adaptations implicated in this study, including specific amino acid rewiring pathways, and alternative nutrient uptake mechanisms (i.e. macropinocytosis). Additionally, the role of our tumour-like culture condition in modulating cellular responses to anti-cancer drugs should be investigated. This will provide evidence to the importance of tumour-like culture considerations in pre-clinical drug trials.

3.6 APPENDIX

Supplemental Table 3.1: Metabolite concentrations (uM) in PDAC TIF, Tumour Microenvironment Medium (TMEM), and Mouse Plasma Medium (MPM), compared to a commercially available Plasmax, and DMEM. TMEM formulation is based on tumour interstitial fluid data from Sullivan et al. (2019). MPM formulation based on mouse plasma metabolomics data listed (see supplementary excel sheet for specifics). A 3-point colour scale on concentration difference (log fold change) between TMEM and MPM was applied. A 3-point colour scale on concentration difference (log fold change) between Plasmax and MPM was also applied. Red colours represent increased concentration in each respective comparison (up to log fold change = 2). Blue colours represent decreased concentration in each respective comparison (up to log fold change = -2).

	PDAC TIFψ	TMEMψ	MPM**	Plasmax#	DMEM#
Proteinogenic Amino Acids					
L-Alanine	637.1 - 1458	1122	691	510	N/A
L-Arginine	0.9 - 5.2	2.1	66	64	398
L-Asparagine	62.9 - 145.5	115	50	41	N/A
L-Aspartate	246.5 - 519.1	399	7.3	6	N/A
L-Glutamate	789.1 - 1300.5	1054	19	98	N/A
L-Glutamine	434.4 - 1329.2	821	934	650	4000
L-Glycine	367.6 - 626.1	483	217	330	400
L-Histidine	53.1 - 117.4	94	76	120	200
L-Isoleucine	91.8 - 197.8	130	138	140	802
L-Leucine	204.5 - 425.7	289	270	170	802
L-Lysine	73.4 - 214.5	139	176	220	798
L-Methionine	35.4 - 106.7	74	53	30	201
L-Phenylalanine	54.2 - 105.6	80	96	68	400
L-Proline	70.7 - 164.2	122	71	360	N/A
L-Serine	54.6 - 115.3	88	96	140	400
L-Threonine	145 - 314.3	252	145	240	798
L-Tryptophan	18.4 - 71.3	31	62	78	78
L-Tyrosine	36.1 - 110.5	60	69	74	399
L-Valine	120.9 - 222.1	150	262	230	803
Non-Proteinogenic Amino Acids					
α-Aminobutyrate	4.7 – 13*	2.93	4.90	41	N/A
Arginosuccinate	0.2 - 1.3	0.75	0.23	N/A	N/A
Homocitrulline	0.4 - 2.2*	0.72	0.98	N/A	N/A

L-Citrulline	44.5 - 118.7	73	38	55	N/A
L-Cystine	16.1 - 110.6	51	30	65	201.3
L-Homocysteine	N/A	3.34	3.34	9	N/A
Methionine Sulfoxide	35.4 - 106.7	3.17	1.43	N/A	N/A
L-Ornithine	160.1 - 485.4	312	23	80	N/A
N,N,N-Trimethyllysine	0.9 - 1.7	1.20	1.93	N/A	N/A
Sarcosine	0.9 - 9.4*	0.22	1.93	N/A	N/A
Amino Acid Derivatives					
Acetyl carnitine	19.6 - 34.9*	25	45	N/A	N/A
Acetylglutamate	0.6 - 4.5	1.40	1.24	N/A	N/A
N-Trimethylglycine (Betain)	84 - 219.9*	94	57	72	N/A
Glutathione (reduced)	5.4 - 80.8*	22	21	37	N/A
L-a-Aminoadipate	10.7 - 21.9	15	4.53	N/A	N/A
L-Carnitine	27 - 54.6*	40	8.47	46	N/A
L-Carnosine	0.6 – 3*	0.49	0.37	6	N/A
N-Acetyl-L-aspartate	2.3 - 6.1*	1.13	4.02	N/A	N/A
N-Acetylglycine	0.1 - 1.8*	23	65	70	N/A
N,N-dimethyl-L-Arginine (ADMA)	1.4 - 2.4*	0.84	1.23	N/A	N/A
Taurine	1742 - 3070.4	2326	763	130	N/A
Other Components					
Acetate	N/A	350	350	42	N/A
Allantoin	59.7 - 191.2*	63	106	N/A	N/A
Carbamoyl aspartate	0.3 - 2.2	0.78	3.19		
cis Aconitate	1.4 - 5.5	2.97	5.97	N/A	N/A
Citrate	164.8 - 585.3	339	214	114	N/A
Creatine	N/A	192	192	37	N/A
Creatinine	5.5 - 27.3*	12.6	10.05	74	N/A
Cytidine	8.4 - 12.7*	4.60	1.83	N/A	N/A
5'-Deoxy-5'-methylthioadenosine	0.0429 – 0.0831	0.0612	0.0161	N/A	N/A
D-Glucose	808.2 - 10096.2	2304	4381	5560	25000
Glycerol	N/A	179	179	82	N/A

2-hydroxybutyrate	N/A	84	84	31	N/A
3-hydroxybutyrate	12 - 218.5	81	849	77	N/A
Hypoxanthine	50 - 152	10	0.0232	5	N/A
L-Kynurenine	0.3 - 1.9	1.01	1.09	N/A	N/A
Lactate	2009 - 6754.1	3794	3088	500	N/A
Malate	105.1 - 208.8	156	18	N/A	N/A
Orotate	0.5 - 1	0.702	0.964	N/A	N/A
Pyruvate	10.5 - 100.6	42	150	100	1000
Sorbitol	0.6 - 2	1.34	0.92	N/A	N/A
Succinate	69.7 - 164.9*	106	14	23	N/A
Urea	N/A	25	25	3000	N/A
Uric Acid	N/A	14	14	270	N/A
Uridine	25.8 - 102.5*	61	4.33	3	N/A
Xanthine	4.7 - 13.2*	0.894	0.449	N/A	N/A
Vitamins					
Ascorbate	117.8 - 182.5*	361	63	62	N/A
Choline	169.1 - 275.2	7.16	7.16	7.1	28.6
D-Biotin	0.028 - 0.089	4.09	4.09	4.2	0.53
D-pantothenate	1.7 - 5.8	4.56	4.56	2.1†	8.4
Folate	N/A	2.27	2.27	2.3	9.1
Myo-inositol	N/A	11.1	11.1	11.1	11.1
Niacinamide	N/A	8.19	8.19	8.2	32.8
Pyridoxal	0.1 - 0.3	4.91	4.91	4.9	19.4
Riboflavin	N/A	0.27	0.27	0.3	1.10
Thiamine	N/A	2.96	2.96	3.0	11.2
Vitamin B12	N/A	0.00150	0.00150	0.0050	N/A
Trace Elements					
Ammonium	N/A	0.0026	0.0026	0.0026	N/A
Metavanadate					
Cupric Sulfate	N/A	0.0052	0.0052	0.0052	N/A
Ferric Nitrate	N/A	0.1238	0.1238	0.1238	0.2475
Ferric Sulfate	N/A	1.0428	1.0428	1.0428	N/A
Manganous Chloride	N/A	0.0002	0.0002	0.0002	N/A
Sodium Selenite	N/A	0.0289	0.0289	0.0289	N/A

Zinc Sulfate	N/A	1.5000	1.5000	1.5000	N/A
Inorganic Salts					
Ammonium Chloride	N/A	50	50	50	N/A
Calcium Chloride	N/A	1125	1125	1800	1802
Magnesium Sulfate	N/A	475	475	813	N/A
Potassium Chloride	N/A	5050	5050	5330	5330
Sodium Bicarbonate	N/A	18400	18400	26191	44048
Sodium Chloride	N/A	91700	91700	118706	110345
Sodium Phosphate Monobasic	N/A	2045	2045	1010	906

TIF=tumour interstitial fluid
PDAC=pancreatic ductal adenocarcinoma
† (For D-Calcium pantothenate)
* Semi-quantitative quantification
ψ PDAC TIF metabolomics data source ((Sullivan et al., 2019)
**Healthy mouse plasma metabolomics data sources (Cantor et al., 2017; Leeuwenburgh & Ji, 1995; N. Maeda et al., 2000; McKee & Komarova, 2017; Shubitowski et al., 2019; Z. Wang et al., 2020; Watanabe et al., 2014; L. Yao et al., 2019)
#Plasmax and DMEM media formulations from (Ackermann & Tardito, 2019)

Supplemental Table 3.2: Volume (mL) used in cell culture vessels. Volumes calculated to maintain oxygen diffusion distance throughout experimentation

Cell Culture vessel	Volume Used (mL)
100-mm (Corning)	30
6-well plate	5.606
12-well plate	2.263
24-well plate (Presens)	1.141

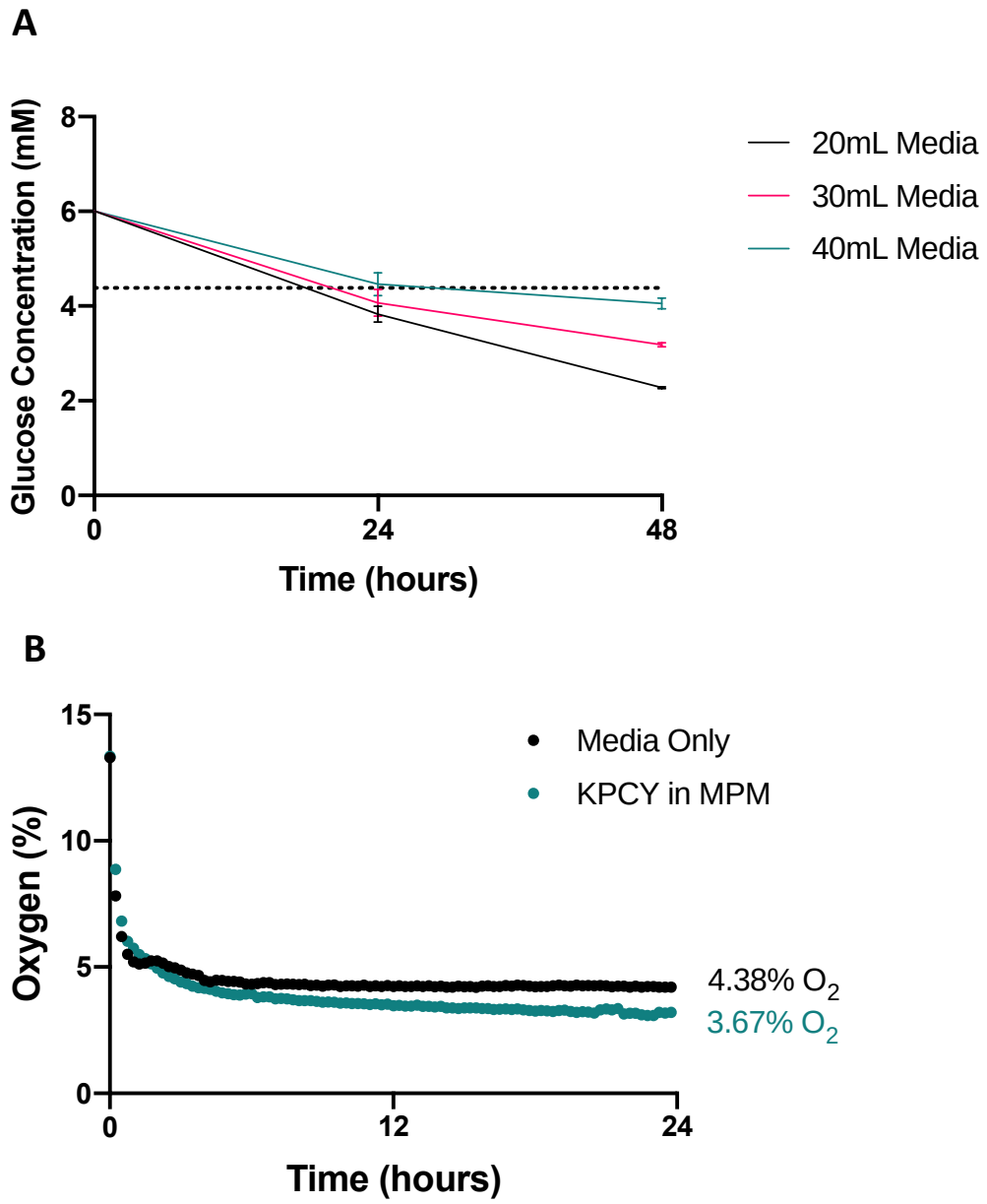

Supplemental Figure 3.1 Pericellular glucose concentration and oxygen levels of KPCY cells cultured in 5% O_2/MPM. (A) Glucose was measured over 48 hours at time 0h (fresh media), 24h and 48h. Media volumes of 20mL, 30mL and 40mL were used in 100mm plates. (B) Presens Oxodish pericellular oxygen readings (%) in MPM cultured KPCY cells and cell free 'media only' controls over 24 hours. Labeled O_2 values (%) are averages of the total 24 hours following stabilization. `Data shows the mean of 6 technical replicates per volume.

Supplemental Table 3.3: List of top 100 upregulated gene ontology terms enriched at 1.5% O_2/TMEM vs 5% O_2/MPM.

Biological Process	Gene Count
GO:0016477~cell migration	52
GO:0009966~regulation of signal transduction	79
GO:0008283~cell proliferation	63
GO:0048584~positive regulation of response to stimulus	70
GO:0035556~intracellular signal transduction	69
GO:0048870~cell motility	54
GO:0051674~localization of cell	54
GO:0006928~movement of cell or subcellular component	61
GO:0030334~regulation of cell migration	38
GO:0071310~cellular response to organic substance	70
GO:0030335~positive regulation of cell migration	28
GO:2000145~regulation of cell motility	38
GO:0048646~anatomical structure formation involved in morphogenesis	42
GO:0040011~locomotion	56
GO:0042127~regulation of cell proliferation	53
GO:0009967~positive regulation of signal transduction	50
GO:2000147~positive regulation of cell motility	28
GO:0010646~regulation of cell communication	81
GO:0051272~positive regulation of cellular component movement	28
GO:0023051~regulation of signaling	81
GO:1902531~regulation of intracellular signal transduction	52
GO:0040017~positive regulation of locomotion	28
GO:0070887~cellular response to chemical stimulus	78
GO:0040012~regulation of locomotion	38
GO:0008219~cell death	59
GO:0051270~regulation of cellular component movement	38
GO:0072359~circulatory system development	40
GO:0072358~cardiovascular system development	31
GO:0001944~vasculature development	31
GO:0001568~blood vessel development	30
GO:0022603~regulation of anatomical structure morphogenesis	37
GO:0010941~regulation of cell death	51
GO:1902533~positive regulation of intracellular signal transduction	37
GO:0048514~blood vessel morphogenesis	27
GO:0010647~positive regulation of cell communication	53
GO:0023056~positive regulation of signaling	53
GO:0009893~positive regulation of metabolic process	80
GO:0012501~programmed cell death	54
GO:0031401~positive regulation of protein modification process	39
GO:0010033~response to organic substance	79
GO:0010604~positive regulation of macromolecule metabolic process	74
GO:0071495~cellular response to endogenous stimulus	41
GO:0051240~positive regulation of multicellular organismal process	52
GO:0006915~apoptotic process	51
GO:0051094~positive regulation of developmental process	45
GO:0009719~response to endogenous stimulus	48
GO:0043067~regulation of programmed cell death	46

GO:0001525~angiogenesis	23
GO:0042327~positive regulation of phosphorylation	34
GO:0051246~regulation of protein metabolic process	65
GO:0010942~positive regulation of cell death	27
GO:0031399~regulation of protein modification process	48
GO:0016310~phosphorylation	54
GO:0008284~positive regulation of cell proliferation	34
GO:0051247~positive regulation of protein metabolic process	45
GO:0042325~regulation of phosphorylation	43
GO:0040007~growth	33
GO:0001667~ameboidal-type cell migration	20
GO:0007166~cell surface receptor signaling pathway	61
GO:0045937~positive regulation of phosphate metabolic process	35
GO:0010562~positive regulation of phosphorus metabolic process	35
GO:0042981~regulation of apoptotic process	44
GO:0043065~positive regulation of apoptotic process	25
GO:0019220~regulation of phosphate metabolic process	45
GO:0006468~protein phosphorylation	47
GO:0010634~positive regulation of epithelial cell migration	12
GO:0051174~regulation of phosphorus metabolic process	45
GO:0048585~negative regulation of response to stimulus	45
GO:0051128~regulation of cellular component organization	62
GO:0043068~positive regulation of programmed cell death	25
GO:0070848~response to growth factor	26
GO:0097191~extrinsic apoptotic signaling pathway	14
GO:0001934~positive regulation of protein phosphorylation	31
GO:0032270~positive regulation of cellular protein metabolic process	42
GO:0009968~negative regulation of signal transduction	36
GO:0071363~cellular response to growth factor stimulus	25
GO:0010632~regulation of epithelial cell migration	14
GO:0023014~signal transduction by protein phosphorylation	26
GO:0000165~MAPK cascade	26
GO:1901700~response to oxygen-containing compound	48
GO:0048608~reproductive structure development	21
GO:0061458~reproductive system development	21
GO:0032268~regulation of cellular protein metabolic process	59
GO:0051130~positive regulation of cellular component organization	39
GO:0009628~response to abiotic stimulus	35
GO:0001932~regulation of protein phosphorylation	38
GO:0006796~phosphate-containing compound metabolic process	63
GO:0001890~placenta development	12
GO:0060548~negative regulation of cell death	33
GO:0048589~developmental growth	26
GO:0070555~response to interleukin-1	10
GO:0006464~cellular protein modification process	72
GO:0036211~protein modification process	72
GO:0045595~regulation of cell differentiation	48
GO:0010648~negative regulation of cell communication	37
GO:0043410~positive regulation of MAPK cascade	20
GO:0023057~negative regulation of signaling	37
GO:0071347~cellular response to interleukin-1	9

GO:0007167~enzyme linked receptor protein signaling pathway	28
GO:0010631~epithelial cell migration	15

Supplemental Table 3.4: List of top 100 downregulated gene ontology terms enriched at 1.5% O_2/TMEM vs 5% O_2/MPM.

Biological Process	Gene Count
GO:0006629~lipid metabolic process	91
GO:1902652~secondary alcohol metabolic process	32
GO:0008203~cholesterol metabolic process	31
GO:0008610~lipid biosynthetic process	57
GO:0016125~sterol metabolic process	31
GO:0044283~small molecule biosynthetic process	52
GO:0008202~steroid metabolic process	42
GO:0016126~sterol biosynthetic process	22
GO:0006695~cholesterol biosynthetic process	21
GO:1902653~secondary alcohol biosynthetic process	21
GO:1901615~organic hydroxy compound metabolic process	49
GO:0006066~alcohol metabolic process	39
GO:0032787~monocarboxylic acid metabolic process	55
GO:0006694~steroid biosynthetic process	29
GO:0044255~cellular lipid metabolic process	66
GO:0046165~alcohol biosynthetic process	25
GO:1901617~organic hydroxy compound biosynthetic process	30
GO:0043436~oxoacid metabolic process	63
GO:0019752~carboxylic acid metabolic process	60
GO:0006082~organic acid metabolic process	63
GO:0006631~fatty acid metabolic process	36
GO:0006790~sulfur compound metabolic process	30
GO:0044712~single-organism catabolic process	48
GO:0006749~glutathione metabolic process	14
GO:0051186~cofactor metabolic process	30
GO:0072330~monocarboxylic acid biosynthetic process	21
GO:0019637~organophosphate metabolic process	48
GO:0006633~fatty acid biosynthetic process	18
GO:0006732~coenzyme metabolic process	26
GO:0006575~cellular modified amino acid metabolic process	19
GO:0046890~regulation of lipid biosynthetic process	20
GO:0033559~unsaturated fatty acid metabolic process	17
GO:0046394~carboxylic acid biosynthetic process	22
GO:0016053~organic acid biosynthetic process	22
GO:0006636~unsaturated fatty acid biosynthetic process	10
GO:0008299~isoprenoid biosynthetic process	8
GO:0044282~small molecule catabolic process	21
GO:0072329~monocarboxylic acid catabolic process	13
GO:0009410~response to xenobiotic stimulus	25

GO:0090181~regulation of cholesterol metabolic process	8
GO:0044724~single-organism carbohydrate catabolic process	13
GO:0019218~regulation of steroid metabolic process	12
GO:0072524~pyridine-containing compound metabolic process	14
GO:0006720~isoprenoid metabolic process	11
GO:0006644~phospholipid metabolic process	21
GO:0019216~regulation of lipid metabolic process	22
GO:0071466~cellular response to xenobiotic stimulus	15
GO:0045540~regulation of cholesterol biosynthetic process	6
GO:0006733~oxidoreduction coenzyme metabolic process	14
GO:0044723~single-organism carbohydrate metabolic process	24
GO:0090407~organophosphate biosynthetic process	25
GO:0050810~regulation of steroid biosynthetic process	10
GO:0006081~cellular aldehyde metabolic process	10
GO:0022600~digestive system process	11
GO:0042180~cellular ketone metabolic process	16
GO:0046490~isopentenyl diphosphate metabolic process	4
GO:0009240~isopentenyl diphosphate biosynthetic process	4
GO:0019362~pyridine nucleotide metabolic process	13
GO:0016052~carbohydrate catabolic process	13
GO:0046496~nicotinamide nucleotide metabolic process	13
GO:0005996~monosaccharide metabolic process	17
GO:0032933~SREBP signaling pathway	5
GO:0006793~phosphorus metabolic process	82
GO:0006805~xenobiotic metabolic process	11
GO:0071501~cellular response to sterol depletion	5
GO:0046395~carboxylic acid catabolic process	15
GO:0016054~organic acid catabolic process	15
GO:0007586~digestion	11
GO:0046889~positive regulation of lipid biosynthetic process	10
GO:0046365~monosaccharide catabolic process	7
GO:0044241~lipid digestion	5
GO:1904970~brush border assembly	4
GO:1901135~carbohydrate derivative metabolic process	38
GO:0006991~response to sterol depletion	5
GO:0005975~carbohydrate metabolic process	25
GO:0006796~phosphate-containing compound metabolic process	79
GO:0006690~icosanoid metabolic process	11
GO:1901568~fatty acid derivative metabolic process	11
GO:0006084~acetyl-CoA metabolic process	6
GO:0001889~liver development	12
GO:0008654~phospholipid biosynthetic process	12
GO:0061008~hepaticobiliary system development	12
GO:0051048~negative regulation of secretion	13
GO:1901136~carbohydrate derivative catabolic process	11
GO:0006692~prostanoid metabolic process	7

GO:0046486~glycerolipid metabolic process	17
GO:0006063~uronic acid metabolic process	5
GO:0019585~glucuronate metabolic process	5
GO:0019318~hexose metabolic process	14
GO:1901361~organic cyclic compound catabolic process	18
GO:0050892~intestinal absorption	6
GO:0060429~epithelium development	41
GO:0019287~isopentenyl diphosphate biosynthetic process, mevalonate pathway	3
GO:0019439~aromatic compound catabolic process	17
GO:0015850~organic hydroxy compound transport	15
GO:0097164~ammonium ion metabolic process	12
GO:0006767~water-soluble vitamin metabolic process	6
GO:0045834~positive regulation of lipid metabolic process	12
GO:1902930~regulation of alcohol biosynthetic process	6
GO:0030299~intestinal cholesterol absorption	4

Chapter 4: GENERAL DISCUSSION

4.1 DISCUSSION AND CONCLUSIONS

Cancerous cells exhibit remarkable adaptability, allowing them to thrive in diverse environments. *In vivo*, the tumour microenvironment plays a pivotal role in driving metabolic adaptation. Multiple studies have shown that enhanced expression of amino acid synthetases (i.e. ASNS, ASS1) (Crump et al., 2021; Cui et al., 2007), transferases (i.e. BCAT) (Shafei et al., 2020), and transporters (i.e. SLC7A11) (Koppula et al., 2018) is central to the adaptive response of cancer cells to nutrient deprivation and hypoxia *in vivo*. Moreover, an abundance of evidence suggests that non-physiological conditions *in vitro* alter a broad range of cellular processes, including proliferation, glucose utilization, oxygen consumption, mitochondrial morphology, redox states, and response to drugs. Conditions reflective of the tumour microenvironment must therefore be considered when modeling cancer biology in culture.

In this thesis, I sought to investigate the impact of physiological culture conditions, including those reflective of the tumor microenvironment, on cancer cell metabolism and behavior. The overall objective of this work was to enhance our understanding of how the nature of an *in vitro* model affects cancer cell biology and therefore experimental outcomes.

In Chapter 2, I evaluated rates of nutrient depletion and their concomitant effects on cancer cell biology by culturing four different cancer cell lines over 48 hours at both 5% and 18% O_2 in the physiological medium Plasmax. I found that depletion of glucose and amino acids occurred rapidly in all four cancer cell lines, such that the 'plasma-like' characteristic of Plasmax was substantially altered after just 24 hours and profoundly altered by 48 hours. This nutrient depletion from Plasmax evoked robust effects detected at the level of the transcriptome and mitochondrial bioenergetics assays. LNCAP cells cultured without a media exchange for 48 hours showed increased expression of transcripts related to ER stress, amino acid import and biosynthesis, and apoptosis. GO terms were consistent with GCN2/CHOP/AFT integrated stress response signaling. Interesting, this pathway is also regularly activated under low amino acid/glucose signaling in tumours, presumably as cancer cells adapt to nutrient-depleted environments by promoting amino acid metabolism to maintain growth (Horiguchi et al., 2012; Williams et al., 2020; Ye et al., 2010). Furthermore, this effect of nutrient depletion on OCR and ECAR was oxygen dependent, with nutrient depletion increasing oxidative metabolism at 5% O_2, and nutrient abundance increasing glycolytic flux at 5% O_2. No effect of nutrient depletion on OCR/ECAR was seen at 18% O_2. This is consistent with experiments performed in high vs low glucose DMEM, and DMEM vs Plasmax

that suggest increased glucose availability within media promotes glycolytic metabolism (Balsa et al., 2019; Moradi et al., 2021).

I observed that the nutrient-depleted culture environment established in exhausted Plasmax following 48h of continuous culture resembles a tumour microenvironment. In Chapter 3, I explored this further by creating a cell culture medium based on a tumour microenvironment. Using metabolomic data from a mouse pancreatic tumour I created TMEM. Mouse blood plasma metabolomic data was used to create MPM, a more nutrient replete medium resembling Plasmax. Interestingly, culturing murine PDAC cells (KPCY) in TMEM under hypoxic conditions representative of pancreatic tumours indeed elicited profound transcriptional and functional changes in the cells. These changes mirrored key aspects of *in vivo* cancer biology. Notably, cells cultured in 1.5%O_2/TMEM exhibited increased expression of genes associated with cell migration, amino acid biosynthesis, angiogenesis, and epithelial-to-mesenchymal transition. Functional assays showed increased glucose uptake and lactate production, with concomitant reduction in mitochondrial respiration in 1.5%O_2/TMEM. Furthermore, cell proliferation rates were attenuated, while migration assays demonstrated increased motility in response to tumor-like conditions. These results show that culture in 1.5% O_2/TMEM promotes metabolic and metastatic phenotypes typical of cancer cells in the context of a tumour *in vivo*. Future studies should investigate the specific utilization of TMEM carbon sources to identify novel metabolic vulnerabilities being promoted, which will help with future drug development. However, it is clearly critical that such research must be performed under hypoxic and nutrient constrained conditions to elicit the conditionally flexible nutrient acquisition strategies employed *in vivo*.

4.2 LIMITATIONS AND FUTURE PERSPECTIVES

While the cell culture tools and protocols used throughout this thesis aim to maintain physiologically relevant conditions in cultured cells, it is not yet feasible to control all environmental factors in one study. Thus, this presents some limitations to the studies described.

Firstly, at the time of this research, I did not have access to a sterile hypoxia work-station to perform media exchanges. Thus, in this thesis, cells were briefly re-exposed to atmospheric oxygen once daily. To mitigate fluctuation of oxygen during this time, culture work performed outside of the incubator was done quickly and media were pre-equilibrated overnight at appropriate O_2 levels. Future work may be performed using hypoxia work-stations to determine the effect of brief reoxygenation during cell maintenance. Moreover, the role of cyclical reoxygenation

representative of heterogenous tumour perfusion should also be determined in a similar line of experiments, since there is evidence that this occurs *in vivo*.

Furthermore, while most constituents of Plasmax, TMEM, and MPM are present at physiologically relevant concentrations, trace metals and lipids are not. Instead, trace metals are included at the same concentrations as in DMEM. Similarly, the lipid composition of the medium is achieved exclusively through serum supplementation and will not resemble the *in vivo* condition. While some physiological concentrations of trace elements (i.e. zinc) and lipids (i.e., DAGs, TAGs) have been quantified in plasma, others remain uncharacterized. Moreover, recent evidence suggests that there is significant variation in specific concentration of trace elements and FBS components between different batches of commercial media and FBS from the same provider (Else, 2020; Keenan et al., 2018), thus introducing variability into the cell culture conditions. Until more comprehensive quantification of these constituents are performed, however, available resources for trace metal and lipid contributions must be used.

Finally, while both data chapters in this thesis used transcriptomics for genome-wide gene expression analysis, differentially expressed genes were not validated with qRT-PCR. I recognize that transcriptomic changes do not always translate to proteomic or functional changes, thus validation of gene expression is important. Rather than validate gene expression directly, I instead performed several functional assays to confirm phenotypic changes indicated by the RNAseq results, including glucose uptake, cell migration, cell proliferation, and mitochondrial bioenergetics. Importantly, the results of the functional assays agreed with observations made through the functional enrichment analysis. Still, qRT-PCR validation may have enhanced these findings.

4.2 CONCLUSIONS AND FUTURE DIRECTIONS

Cancer cells are highly responsive to their metabolic environment in culture. Changes in nutrient availability promote adaptive phenotypes in cancer cells, whether following exhaustion of plasma-like media, or through the establishment of sustained tumour-like culture conditions. Critically, culture conditions designed to replicate the tumour microenvironment elicit cellular responses relevant to tumorigenesis, including those that contribute to poor clinical outcomes *in vivo*. Thus, while plasma-like medium represents a significant achievement in cell biology, refinement of culture conditions to specific cellular microenvironments is essential for maintaining the biological relevance of experimental models. While I exemplify this in a tumour context, this point is likely

true of other cellular microenvironments *in vivo*. Furthermore, I exemplify that when establishing physiologically relevant conditions in culture, careful monitoring of metabolite availability is necessary to ensure conditions achieve nutrient and oxygen levels desired. Finally, given that achieving and maintaining physiological culture conditions is readily achievable within standard cell culture workflows, I unequivocally argue that all cell biologists should transition to physiological culture conditions for future experimental work.

LITERATURE CITED

Abbas, M., Moradi, F., Hu, W., Regudo, K. L., Osborne, M., Pettipas, J., Atallah, D. S., Hachem, R., Ott-Peron, N., & Stuart, J. A. (2021). Vertebrate cell culture as an experimental approach—Limitations and solutions. *Comparative Biochemistry and Physiology. Part B, Biochemistry & Molecular Biology*, *254*, 110570. https://doi.org/10.1016/j.cbpb.2021.110570

Abbott, K. L., Ali, A., Casalena, D., Do, B. T., Ferreira, R., Cheah, J. H., Soule, C. K., Deik, A., Kunchok, T., Schmidt, D. R., Renner, S., Honeder, S. E., Wu, M., Chan, S. H., Tseyang, T., Greaves, D., Hsu, P. P., Ng, C. W., Zhang, C. J., … Heiden, M. G. V. (2023). *Screening in serum-derived medium reveals differential response to compounds targeting metabolism*. https://doi.org/10.1101/2023.02.25.529972

Ackermann, T., & Tardito, S. (2019). Cell culture medium formulation and its implications in cancer metabolism. *Trends in Cancer*, *5*(6), 329–332. https://doi.org/10.1016/j.trecan.2019.05.004

Aiello, N. M., Maddipati, R., Norgard, R. J., Balli, D., Li, J., Yuan, S., Yamazoe, T., Black, T., Sahmoud, A., Furth, E. E., Bar-Sagi, D., & Stanger, B. Z. (2018). EMT Subtype Influences Epithelial Plasticity and Mode of Cell Migration. *Developmental Cell*, *45*(6), 681-695.e4. https://doi.org/10.1016/j.devcel.2018.05.027

Allen, M. D., Luong, P., Hudson, C., Leyton, J., Delage, B., Ghazaly, E., Cutts, R., Yuan, M., Syed, N., Lo Nigro, C., Lattanzio, L., Chmielewska-Kassassir, M., Tomlinson, I., Roylance, R., Whitaker, H. C., Warren, A. Y., Neal, D., Frezza, C., Beltran, L., … Szlosarek, P. W. (2014). Prognostic and Therapeutic Impact of Argininosuccinate Synthetase 1 Control in Bladder Cancer as Monitored Longitudinally by PET Imaging. *Cancer Research*, *74*(3), 896–907. https://doi.org/10.1158/0008-5472.CAN-13-1702

Alva, R. (2024). *Investigating the Cellular Responses of Cancer Cells to Physiological and Hypoxic Oxygen Conditions*. Brock University.

Alva, R., Gardner, G. L., Liang, P., & Stuart, J. A. (2022). Supraphysiological Oxygen Levels in Mammalian Cell Culture: Current State and Future Perspectives. *Cells*, *11*(19), 3123. https://doi.org/10.3390/cells11193123

Alva, R., Moradi, F., Liang, P., & Stuart, J. A. (2022). Culture of Cancer Cells at Physiological Oxygen Levels Affects Gene Expression in a Cell-Type Specific Manner. *Biomolecules*, *12*(11), 1684. https://doi.org/10.3390/biom12111684

An, S., Lu, X., Zhao, W., Sun, T., Zhang, Y., Lu, Y., & Jiang, C. (2016). Amino Acid Metabolism Abnormity and Microenvironment Variation Mediated Targeting and Controlled Glioma Chemotherapy. *Small (Weinheim an Der Bergstrasse, Germany)*, *12*(40), 5633–5645. https://doi.org/10.1002/smll.201601249

Anderson, M., Moshnikova, A., Engelman, D. M., Reshetnyak, Y. K., & Andreev, O. A. (2016). Probe for the measurement of cell surface pH in vivo and ex vivo. *Proceedings of the National Academy of Sciences of the United States of America*, *113*(29), 8177–8181. https://doi.org/10.1073/pnas.1608247113

Ansari, R. E., Craze, M. L., Miligy, I., Diez-Rodriguez, M., Nolan, C. C., Ellis, I. O., Rakha, E. A., & Green, A. R. (2018). The amino acid transporter SLC7A5 confers a poor prognosis in the highly proliferative breast cancer subtypes and is a key therapeutic target in luminal B tumours. *Breast Cancer Research : BCR*, *20*. https://doi.org/10.1186/s13058-018-0946-6

Apiz Saab, J. J., Dzierozynski, L. N., Jonker, P. B., AminiTabrizi, R., Shah, H., Menjivar, R. E., Scott, A. J., Nwosu, Z. C., Zhu, Z., Chen, R. N., Oh, M., Sheehan, C., Wahl, D. R., Pasca

di Magliano, M., Lyssiotis, C. A., Macleod, K. F., Weber, C. R., & Muir, A. (2023). Pancreatic tumors exhibit myeloid-driven amino acid stress and upregulate arginine biosynthesis. *eLife*, *12*, e81289. https://doi.org/10.7554/eLife.81289

Armstrong, A. J., Marengo, M. S., Oltean, S., Kemeny, G., Bitting, R. L., Turnbull, J. D., Herold, C. I., Marcom, P. K., George, D. J., & Garcia-Blanco, M. A. (2011). Circulating Tumor Cells from Patients with Advanced Prostate and Breast Cancer Display Both Epithelial and Mesenchymal Markers. *Molecular Cancer Research*, *9*(8), 997–1007. https://doi.org/10.1158/1541-7786.MCR-10-0490

Atay, S. (2020). Integrated transcriptome meta-analysis of pancreatic ductal adenocarcinoma and matched adjacent pancreatic tissues. *PeerJ*, *8*, e10141. https://doi.org/10.7717/peerj.10141

Attwell, D., & Laughlin, S. B. (2001). An energy budget for signaling in the grey matter of the brain. *Journal of Cerebral Blood Flow and Metabolism: Official Journal of the International Society of Cerebral Blood Flow and Metabolism*, *21*(10), 1133–1145. https://doi.org/10.1097/00004647-200110000-00001

Auer, R. N., Wieloch, T., Olsson, Y., & Siesjö, B. K. (1984). The distribution of hypoglycemic brain damage. *Acta Neuropathologica*, *64*(3), 177–191. https://doi.org/10.1007/BF00688108

Baba, Y., Nosho, K., Shima, K., Irahara, N., Chan, A. T., Meyerhardt, J. A., Chung, D. C., Giovannucci, E. L., Fuchs, C. S., & Ogino, S. (2010). HIF1A Overexpression Is Associated with Poor Prognosis in a Cohort of 731 Colorectal Cancers. *The American Journal of Pathology*, *176*(5), 2292–2301. https://doi.org/10.2353/ajpath.2010.090972

Baker, L. E., & Carrel, A. (1926). EFFECT OF THE AMINO ACIDS AND DIALYZABLE CONSTITUENTS OF EMBRYONIC TISSUE JUICE ON THE GROWTH OF FIBROBLASTS. *The Journal of Experimental Medicine*, *44*(3), 397–407.

Balsa, E., Soustek, M. S., Thomas, A., Cogliati, S., García-Poyatos, C., Martín-García, E., Jedrychowski, M., Gygi, S. P., Enriquez, J. A., & Puigserver, P. (2019). ER and Nutrient Stress Promote Assembly of Respiratory Chain Supercomplexes Through PERK/eIF2α Axis. *Molecular Cell*, *74*(5), 877-890.e6. https://doi.org/10.1016/j.molcel.2019.03.031

Barnes, K., Ingram, J. C., Porras, O. H., Barros, L. F., Hudson, E. R., Fryer, L. G. D., Foufelle, F., Carling, D., Hardie, D. G., & Baldwin, S. A. (2002). Activation of GLUT1 by metabolic and osmotic stress: Potential involvement of AMP-activated protein kinase (AMPK). *Journal of Cell Science*, *115*(11), 2433–2442. https://doi.org/10.1242/jcs.115.11.2433

Baronzio, G., Schwartz, L., Kiselevsky, M., Guais, A., Sanders, E., Milanesi, G., Baronzio, M., & Freitas, I. (2012). Tumor Interstitial Fluid as Modulator of Cancer Inflammation, Thrombosis, Immunity and Angiogenesis. *Anticancer Research*, *32*(2), 405–414.

Bar-Peled, L., Schweitzer, L. D., Zoncu, R., & Sabatini, D. M. (2012). An expanded Ragulator is a GEF for the Rag GTPases that signal amino acid levels to mTORC1. *Cell*, *150*(6), 1196–1208. https://doi.org/10.1016/j.cell.2012.07.032

Baryła, M., Semeniuk-Wojtaś, A., Róg, L., Kraj, L., Małyszko, M., & Stec, R. (2022). Oncometabolites—A Link between Cancer Cells and Tumor Microenvironment. *Biology*, *11*(2), 270. https://doi.org/10.3390/biology11020270

Battaglioni, S., Benjamin, D., Wälchli, M., Maier, T., & Hall, M. N. (2022). mTOR substrate phosphorylation in growth control. *Cell*, *185*(11), 1814–1836. https://doi.org/10.1016/j.cell.2022.04.013

B'chir, W., Maurin, A.-C., Carraro, V., Averous, J., Jousse, C., Muranishi, Y., Parry, L., Stepien, G., Fafournoux, P., & Bruhat, A. (2013). The eIF2α/ATF4 pathway is essential for stress-induced autophagy gene expression. *Nucleic Acids Research*, *41*(16), 7683–7699. https://doi.org/10.1093/nar/gkt563

Bernabeu, M. O., Köry, J., Grogan, J. A., Markelc, B., Beardo, A., d'Avezac, M., Enjalbert, R., Kaeppler, J., Daly, N., Hetherington, J., Krüger, T., Maini, P. K., Pitt-Francis, J. M., Muschel, R. J., Alarcón, T., & Byrne, H. M. (2020). Abnormal morphology biases hematocrit distribution in tumor vasculature and contributes to heterogeneity in tissue oxygenation. *Proceedings of the National Academy of Sciences*, *117*(45), 27811–27819. https://doi.org/10.1073/pnas.2007770117

Blommaart, E. F., Luiken, J. J., Blommaart, P. J., van Woerkom, G. M., & Meijer, A. J. (1995). Phosphorylation of ribosomal protein S6 is inhibitory for autophagy in isolated rat hepatocytes. *The Journal of Biological Chemistry*, *270*(5), 2320–2326. https://doi.org/10.1074/jbc.270.5.2320

Boutilier, R. G., & St-Pierre, J. (2000). Surviving hypoxia without really dying. *Comparative Biochemistry and Physiology Part A: Molecular & Integrative Physiology*, *126*(4), 481–490. https://doi.org/10.1016/S1095-6433(00)00234-8

Brugarolas, J., Lei, K., Hurley, R. L., Manning, B. D., Reiling, J. H., Hafen, E., Witters, L. A., Ellisen, L. W., & Kaelin, W. G. (2004). Regulation of mTOR function in response to

hypoxia by REDD1 and the TSC1/TSC2 tumor suppressor complex. *Genes & Development*, *18*(23), 2893–2904. https://doi.org/10.1101/gad.1256804

Brurberg, K. G., Skogmo, H. K., Graff, B. A., Olsen, D. R., & Rofstad, E. K. (2005). Fluctuations in pO2 in poorly and well-oxygenated spontaneous canine tumors before and during fractionated radiation therapy. *Radiotherapy and Oncology: Journal of the European Society for Therapeutic Radiology and Oncology*, *77*(2), 220–226. https://doi.org/10.1016/j.radonc.2005.09.009

Budinger, G. R. S., Duranteau, J., Chandel, N. S., & Schumacker, P. T. (1998). Hibernation during Hypoxia in Cardiomyocytes: ROLE OF MITOCHONDRIA AS THE O2 SENSOR*. *Journal of Biological Chemistry*, *273*(6), 3320–3326. https://doi.org/10.1074/jbc.273.6.3320

Burgess, E. A., & Sylven, B. (1962). Glucose, lactate, and lactic dehydrogenase activity in normal interstitial fluid and that of solid mouse tumors. *Cancer Research*, *22*, 581–588.

Burr, S. P., Costa, A. S. H., Grice, G. L., Timms, R. T., Lobb, I. T., Freisinger, P., Dodd, R. B., Dougan, G., Lehner, P. J., Frezza, C., & Nathan, J. A. (2016). Mitochondrial Protein Lipoylation and the 2-Oxoglutarate Dehydrogenase Complex Controls HIF1α Stability in Aerobic Conditions. *Cell Metabolism*, *24*(5), 740–752. https://doi.org/10.1016/j.cmet.2016.09.015

Buttgereit, F., & Brand, M. D. (1995). A hierarchy of ATP-consuming processes in mammalian cells. *Biochemical Journal*, *312*(1), 163–167. https://doi.org/10.1042/bj3120163

Cantó, C., & Auwerx, J. (2010). AMP-activated protein kinase and its downstream transcriptional pathways. *Cellular and Molecular Life Sciences: CMLS*, *67*(20), 3407–3423. https://doi.org/10.1007/s00018-010-0454-z

Cantor, J. R., Abu-Remaileh, M., Kanarek, N., Freinkman, E., Gao, X., Louissaint, A., Lewis, C. A., & Sabatini, D. M. (2017). Physiologic Medium Rewires Cellular Metabolism and Reveals Uric Acid as an Endogenous Inhibitor of UMP Synthase. *Cell*, *169*(2), 258-272.e17. https://doi.org/10.1016/j.cell.2017.03.023

Carlsson, P. O., Liss, P., Andersson, A., & Jansson, L. (1998). Measurements of oxygen tension in native and transplanted rat pancreatic islets. *Diabetes*, *47*(7), 1027–1032. https://doi.org/10.2337/diabetes.47.7.1027

Carlsson, P. O., Palm, F., Andersson, A., & Liss, P. (2001). Markedly Decreased Oxygen Tension in Transplanted Rat Pancreatic Islets Irrespective of the Implantation Site. *Diabetes*, *50*(3), 489–495. https://doi.org/10.2337/diabetes.50.3.489

Carrel, A., & Baker, L. E. (1926). THE CHEMICAL NATURE OF SUBSTANCES REQUIRED FOR CELL MULTIPLICATION. *The Journal of Experimental Medicine*, *44*(4), 503–521.

Carstens, J. L., Yang, S., Correa de Sampaio, P., Zheng, X., Barua, S., McAndrews, K. M., Rao, A., Burks, J. K., Rhim, A. D., & Kalluri, R. (2021). Stabilized epithelial phenotype of cancer cells in primary tumors leads to increased colonization of liver metastasis in pancreatic cancer. *Cell Reports*, *35*(2), 108990. https://doi.org/10.1016/j.celrep.2021.108990

Chandel, N. S. (2021). Amino Acid Metabolism. *Cold Spring Harbor Perspectives in Biology*, *13*(4), a040584. https://doi.org/10.1101/cshperspect.a040584

Chantranupong, L., Wolfson, R. L., Orozco, J. M., Saxton, R. A., Scaria, S. M., Bar-Peled, L., Spooner, E., Isasa, M., Gygi, S. P., & Sabatini, D. M. (2014). The Sestrins interact with

GATOR2 to negatively regulate the amino-acid-sensing pathway upstream of mTORC1. *Cell Reports*, *9*(1), 1–8. https://doi.org/10.1016/j.celrep.2014.09.014

Chaturvedi, P., Gilkes, D. M., Wong, C. C. L., Kshitiz, Luo, W., Zhang, H., Wei, H., Takano, N., Schito, L., Levchenko, A., & Semenza, G. L. (2012). Hypoxia-inducible factor–dependent breast cancer–mesenchymal stem cell bidirectional signaling promotes metastasis. *The Journal of Clinical Investigation*, *123*(1). https://doi.org/10.1172/JCI64993

Chen, F., Chen, J., Yang, L., Liu, J., Zhang, X., Zhang, Y., Tu, Q., Yin, D., Lin, D., Wong, P.-P., Huang, D., Xing, Y., Zhao, J., Li, M., Liu, Q., Su, F., Su, S., & Song, E. (2019). Extracellular vesicle-packaged HIF-1α-stabilizing lncRNA from tumour-associated macrophages regulates aerobic glycolysis of breast cancer cells. *Nature Cell Biology*, *21*(4), Article 4. https://doi.org/10.1038/s41556-019-0299-0

Chen, R., Zou, Y., Mao, D., Sun, D., Gao, G., Shi, J., Liu, X., Zhu, C., Yang, M., Ye, W., Hao, Q., Li, R., & Yu, L. (2014). The general amino acid control pathway regulates mTOR and autophagy during serum/glutamine starvation. *The Journal of Cell Biology*, *206*(2), 173–182. https://doi.org/10.1083/jcb.201403009

Chen, S., Chen, J.-Z., Zhang, J.-Q., Chen, H.-X., Yan, M.-L., Huang, L., Tian, Y.-F., Chen, Y.-L., & Wang, Y.-D. (2016). Hypoxia induces TWIST-activated epithelial-mesenchymal transition and proliferation of pancreatic cancer cells in vitro and in nude mice. *Cancer Letters*, *383*(1), 73–84. https://doi.org/10.1016/j.canlet.2016.09.027

Chen, S., Giannakou, A., Wyman, S., Gruzas, J., Golas, J., Zhong, W., Loreth, C., Sridharan, L., Yamin, T.-T., Damelin, M., & Geles, K. G. (2018). Cancer-associated fibroblasts suppress SOX2-induced dysplasia in a lung squamous cancer coculture. *Proceedings of*

the National Academy of Sciences of the United States of America, *115*(50), E11671–E11680. https://doi.org/10.1073/pnas.1803718115

Chen, Z., Zhu, Y., Dong, Y., Zhang, P., Han, X., Jin, J., & Ma, X. (2017). Overexpression of TrpC5 promotes tumor metastasis via the HIF-1α-Twist signaling pathway in colon cancer. *Clinical Science (London, England: 1979)*, *131*(19), 2439–2450. https://doi.org/10.1042/CS20171069

Cheng, J.-C., Klausen, C., & Leung, P. C. K. (2013). Hypoxia-inducible factor 1 alpha mediates epidermal growth factor-induced down-regulation of E-cadherin expression and cell invasion in human ovarian cancer cells. *Cancer Letters*, *329*(2), 197–206. https://doi.org/10.1016/j.canlet.2012.10.029

Chhipa, R. R., Fan, Q., Anderson, J., Muraleedharan, R., Huang, Y., Ciraolo, G., Chen, X., Waclaw, R., Chow, L. M., Khuchua, Z., Kofron, M., Weirauch, M. T., Kendler, A., McPherson, C., Ratner, N., Nakano, I., Dasgupta, N., Komurov, K., & Dasgupta, B. (2018). AMP kinase promotes glioblastoma bioenergetics and tumour growth. *Nature Cell Biology*, *20*(7), 823–835. https://doi.org/10.1038/s41556-018-0126-z

Clere, N., Renault, S., & Corre, I. (2020). Endothelial-to-Mesenchymal Transition in Cancer. *Frontiers in Cell and Developmental Biology*, *8*, 747. https://doi.org/10.3389/fcell.2020.00747

Codogno, P., & Meijer, A. J. (2005). Autophagy and signaling: Their role in cell survival and cell death. *Cell Death and Differentiation*, *12 Suppl 2*, 1509–1518. https://doi.org/10.1038/sj.cdd.4401751

Connolly, J. L., Schnitt, S. J., Wang, H. H., Longtine, J. A., Dvorak, A., & Dvorak, H. F. (2003). Tumor Structure and Tumor Stroma Generation. In *Holland-Frei Cancer Medicine. 6th edition*. BC Decker. https://www.ncbi.nlm.nih.gov/books/NBK13447/

Cooper,P.D, Burt, A.M, & Wilson, J.N. (1958). Critical effect of oxygen tension on rate of growth of animal cells in continuous suspended culture—PubMed. *Nature*, *182*, 1508–1509.

Coronel, L., Häckes, D., Schwab, K., Riege, K., Hoffmann, S., & Fischer, M. (2022). P53-mediated AKT and mTOR inhibition requires RFX7 and DDIT4 and depends on nutrient abundance. *Oncogene*, *41*(7), 1063–1069. https://doi.org/10.1038/s41388-021-02147-z

Corradetti, M. N., Inoki, K., Bardeesy, N., DePinho, R. A., & Guan, K.-L. (2004). Regulation of the TSC pathway by LKB1: Evidence of a molecular link between tuberous sclerosis complex and Peutz-Jeghers syndrome. *Genes & Development*, *18*(13), 1533–1538. https://doi.org/10.1101/gad.1199104

Courtney, K. D., Bezwada, D., Mashimo, T., Pichumani, K., Vemireddy, V., Funk, A. M., Wimberly, J., McNeil, S. S., Kapur, P., Lotan, Y., Margulis, V., Cadeddu, J. A., Pedrosa, I., DeBerardinis, R. J., Malloy, C. R., Bachoo, R. M., & Maher, E. A. (2018). Isotope Tracing of Human Clear Cell Renal Cell Carcinomas Demonstrates Suppressed Glucose Oxidation In Vivo. *Cell Metabolism*, *28*(5), 793-800.e2. https://doi.org/10.1016/j.cmet.2018.07.020

Crosas-Molist, E., Graziani, V., Maiques, O., Pandya, P., Monger, J., Samain, R., George, S. L., Malik, S., Salise, J., Morales, V., Le Guennec, A., Atkinson, R. A., Marti, R. M., Matias-Guiu, X., Charras, G., Conte, M. R., Elosegui-Artola, A., Holt, M., & Sanz-Moreno, V. (2023). AMPK is a mechano-metabolic sensor linking cell adhesion and mitochondrial

dynamics to Myosin-dependent cell migration. *Nature Communications*, *14*(1), 2740. https://doi.org/10.1038/s41467-023-38292-0

Crump, N. T., Hadjinicolaou, A. V., Xia, M., Walsby-Tickle, J., Gileadi, U., Chen, J.-L., Setshedi, M., Olsen, L. R., Lau, I.-J., Godfrey, L., Quek, L., Yu, Z., Ballabio, E., Barnkob, M. B., Napolitani, G., Salio, M., Koohy, H., Kessler, B. M., Taylor, S., … Cerundolo, V. (2021). Chromatin accessibility governs the differential response of cancer and T cells to arginine starvation. *Cell Reports*, *35*(6), 109101. https://doi.org/10.1016/j.celrep.2021.109101

Cui, H., Darmanin, S., Natsuisaka, M., Kondo, T., Asaka, M., Shindoh, M., Higashino, F., Hamuro, J., Okada, F., Kobayashi, M., Nakagawa, K., Koide, H., & Kobayashi, M. (2007). Enhanced Expression of Asparagine Synthetase under Glucose-Deprived Conditions Protects Pancreatic Cancer Cells from Apoptosis Induced by Glucose Deprivation and Cisplatin. *Cancer Research*, *67*(7), 3345–3355. https://doi.org/10.1158/0008-5472.CAN-06-2519

Daemen, A., Peterson, D., Sahu, N., McCord, R., Du, X., Liu, B., Kowanetz, K., Hong, R., Moffat, J., Gao, M., Boudreau, A., Mroue, R., Corson, L., O'Brien, T., Qing, J., Sampath, D., Merchant, M., Yauch, R., Manning, G., … Evangelista, M. (2015). Metabolite profiling stratifies pancreatic ductal adenocarcinomas into subtypes with distinct sensitivities to metabolic inhibitors. *Proceedings of the National Academy of Sciences*, *112*(32), E4410–E4417. https://doi.org/10.1073/pnas.1501605112

Dan, H. C., Sun, M., Yang, L., Feldman, R. I., Sui, X.-M., Ou, C. C., Nellist, M., Yeung, R. S., Halley, D. J. J., Nicosia, S. V., Pledger, W. J., & Cheng, J. Q. (2002). Phosphatidylinositol 3-Kinase/Akt Pathway Regulates Tuberous Sclerosis Tumor

Suppressor Complex by Phosphorylation of Tuberin *. *Journal of Biological Chemistry*, *277*(38), 35364–35370. https://doi.org/10.1074/jbc.M205838200

Dang, C. V., O'Donnell, K. A., Zeller, K. I., Nguyen, T., Osthus, R. C., & Li, F. (2006). The c-Myc target gene network. *Seminars in Cancer Biology*, *16*(4), 253–264. https://doi.org/10.1016/j.semcancer.2006.07.014

DeBerardinis, R. J., & Chandel, N. S. (2016). Fundamentals of cancer metabolism. *Science Advances*, *2*(5), e1600200. https://doi.org/10.1126/sciadv.1600200

Dengler, V. L., Galbraith, M., & Espinosa, J. M. (2014). Transcriptional Regulation by Hypoxia Inducible Factors. *Critical Reviews in Biochemistry and Molecular Biology*, *49*(1), 1–15. https://doi.org/10.3109/10409238.2013.838205

Dey, P., Li, J., Zhang, J., Chaurasiya, S., Strom, A., Wang, H., Liao, W.-T., Cavallaro, F., Denz, P., Bernard, V., Yen, E.-Y., Genovese, G., Gulhati, P., Liu, J., Chakravarti, D., Deng, P., Zhang, T., Carbone, F., Chang, Q., … DePinho, R. A. (2020). Oncogenic KRAS-Driven Metabolic Reprogramming in Pancreatic Cancer Cells Utilizes Cytokines from the Tumor Microenvironment. *Cancer Discovery*, *10*(4), 608–625. https://doi.org/10.1158/2159-8290.CD-19-0297

Ding, C.-Z., Guo, X.-F., Wang, G.-L., Wang, H.-T., Xu, G.-H., Liu, Y.-Y., Wu, Z.-J., Chen, Y.-H., Wang, J., & Wang, W.-G. (2018). High glucose contributes to the proliferation and migration of non-small-cell lung cancer cells via GAS5-TRIB3 axis. *Bioscience Reports*, *38*(2), BSR20171014. https://doi.org/10.1042/BSR20171014

Dodd, K. M., Yang, J., Shen, M. H., Sampson, J. R., & Tee, A. R. (2015). mTORC1 drives HIF-1α and VEGF-A signalling via multiple mechanisms involving 4E-BP1, S6K1 and STAT3. *Oncogene*, *34*(17), 2239–2250. https://doi.org/10.1038/onc.2014.164

Dong, T., Liu, Z., Xuan, Q., Wang, Z., Ma, W., & Zhang, Q. (2017). Tumor LDH-A expression and serum LDH status are two metabolic predictors for triple negative breast cancer brain metastasis. *Scientific Reports*, *7*(1), 6069. https://doi.org/10.1038/s41598-017-06378-7

Downes, N. L., Laham-Karam, N., Kaikkonen, M. U., & Ylä-Herttuala, S. (2018). Differential but Complementary HIF1α and HIF2α Transcriptional Regulation. *Molecular Therapy: The Journal of the American Society of Gene Therapy*, *26*(7), 1735–1745. https://doi.org/10.1016/j.ymthe.2018.05.004

Ducommun, S., Deak, M., Sumpton, D., Ford, R. J., Núñez Galindo, A., Kussmann, M., Viollet, B., Steinberg, G. R., Foretz, M., Dayon, L., Morrice, N. A., & Sakamoto, K. (2015). Motif affinity and mass spectrometry proteomic approach for the discovery of cellular AMPK targets: Identification of mitochondrial fission factor as a new AMPK substrate. *Cellular Signalling*, *27*(5), 978–988. https://doi.org/10.1016/j.cellsig.2015.02.008

Dulbecco, R., & Freeman, G. (1959). Plaque production by the polyoma virus. *Virology*, *8*(3), 396–397. https://doi.org/10.1016/0042-6822(59)90043-1

Dumas, A. A., Pomella, N., Rosser, G., Guglielmi, L., Vinel, C., Millner, T. O., Rees, J., Aley, N., Sheer, D., Wei, J., Marisetty, A., Heimberger, A. B., Bowman, R. L., Brandner, S., Joyce, J. A., & Marino, S. (2020). Microglia promote glioblastoma via mTOR-mediated immunosuppression of the tumour microenvironment. *The EMBO Journal*, *39*(15), e103790. https://doi.org/10.15252/embj.2019103790

Eagle, H. (1955a). THE SPECIFIC AMINO ACID REQUIREMENTS OF A HUMAN CARCINOMA CELL (STRAIN HELA) IN TISSUE CULTURE. *Journal of Experimental Medicine*, *102*(1), 37–48. https://doi.org/10.1084/jem.102.1.37

Eagle, H. (1955b). THE SPECIFIC AMINO ACID REQUIREMENTS OF A MAMMALIAN CELL (STRAIN L) IN TISSUE CULTURE: Plate 1. *Journal of Biological Chemistry*, *214*(2), 839–852. https://doi.org/10.1016/S0021-9258(18)70932-0

Eagle, Harry. (1959). Amino Acid Metabolism in Mammalian Cell Cultures. *Science*, *130*(3373). https://www.science.org/doi/10.1126/science.130.3373.432

Earle, W. R., Ing, T. H. S., Straus, N. P., Brown, M. F., & Shelton, E. M. M. A. (1943). Changes Seen in the Living Cells. *Journal*, *4*, 165.

Efeyan, A., Comb, W. C., & Sabatini, D. M. (2015). Nutrient Sensing Mechanisms and Pathways. *Nature*, *517*(7534), 302–310. https://doi.org/10.1038/nature14190

Egan, D. F., Shackelford, D. B., Mihaylova, M. M., Gelino, S., Kohnz, R. A., Mair, W., Vasquez, D. S., Joshi, A., Gwinn, D. M., Taylor, R., Asara, J. M., Fitzpatrick, J., Dillin, A., Viollet, B., Kundu, M., Hansen, M., & Shaw, R. J. (2011). Phosphorylation of ULK1 (hATG1) by AMP-Activated Protein Kinase Connects Energy Sensing to Mitophagy. *Science*, *331*(6016), 456–461. https://doi.org/10.1126/science.1196371

Eijkelenkamp, K., Osinga, T. E., Links, T. P., & van der Horst-Schrivers, A. N. A. (2020). Clinical implications of the oncometabolite succinate in SDHx-mutation carriers. *Clinical Genetics*, *97*(1), 39–53. https://doi.org/10.1111/cge.13553

Eisenberg, L., Eisenberg-Bord, M., Eisenberg-Lerner, A., & Sagi-Eisenberg, R. (2020). Metabolic alterations in the tumor microenvironment and their role in oncogenesis. *Cancer Letters*, *484*, 65–71. https://doi.org/10.1016/j.canlet.2020.04.016

Elkalaf, M., Anděl, M., & Trnka, J. (2013). Low Glucose but Not Galactose Enhances Oxidative Mitochondrial Metabolism in C2C12 Myoblasts and Myotubes. *PLOS ONE*, *8*(8), e70772. https://doi.org/10.1371/journal.pone.0070772

El-Kenawi, A., Gatenbee, C., Robertson-Tessi, M., Bravo, R., Dhillon, J., Balagurunathan, Y., Berglund, A., Vishvakarma, N., Ibrahim-Hashim, A., Choi, J., Luddy, K., Gatenby, R., Pilon-Thomas, S., Anderson, A., Ruffell, B., & Gillies, R. (2019). Acidity promotes tumour progression by altering macrophage phenotype in prostate cancer. *British Journal of Cancer*, *121*(7), 556–566. https://doi.org/10.1038/s41416-019-0542-2

Else, P. L. (2020). The highly unnatural fatty acid profile of cells in culture. *Progress in Lipid Research*, *77*, 101017. https://doi.org/10.1016/j.plipres.2019.101017

Estrada, J. C., Albo, C., Benguría, A., Dopazo, A., López-Romero, P., Carrera-Quintanar, L., Roche, E., Clemente, E. P., Enríquez, J. A., Bernad, A., & Samper, E. (2012). Culture of human mesenchymal stem cells at low oxygen tension improves growth and genetic stability by activating glycolysis. *Cell Death and Differentiation*, *19*(5), 743–755. https://doi.org/10.1038/cdd.2011.172

Falk, S. J., Ward, R., & Bleehen, N. M. (1992). The influence of carbogen breathing on tumour tissue oxygenation in man evaluated by computerised p02 histography. *British Journal of Cancer*, *66*(5), 919–924.

Feng, W., Xue, T., Huang, S., Shi, Q., Tang, C., Cui, G., Yang, G., Gong, H., & Guo, H. (2018). HIF-1α promotes the migration and invasion of hepatocellular carcinoma cells via the IL-8–NF-κB axis. *Cellular & Molecular Biology Letters*, *23*(1), 26. https://doi.org/10.1186/s11658-018-0077-1

Fernandes, S. A., & Demetriades, C. (2021). The Multifaceted Role of Nutrient Sensing and mTORC1 Signaling in Physiology and Aging. *Frontiers in Aging*, *2*. https://www.frontiersin.org/articles/10.3389/fragi.2021.707372

Finicle, B. T., Jayashankar, V., & Edinger, A. L. (2018). Nutrient scavenging in cancer. *Nature Reviews Cancer*, *18*(10), Article 10. https://doi.org/10.1038/s41568-018-0048-x

Fink, T., Kazlauskas, A., Poellinger, L., Ebbesen, P., & Zachar, V. (2002). Identification of a tightly regulated hypoxia-response element in the promoter of human plasminogen activator inhibitor–1. *Blood*, *99*(6), 2077–2083. https://doi.org/10.1182/blood.V99.6.2077

Fischer, K., Hoffmann, P., Voelkl, S., Meidenbauer, N., Ammer, J., Edinger, M., Gottfried, E., Schwarz, S., Rothe, G., Hoves, S., Renner, K., Timischl, B., Mackensen, A., Kunz-Schughart, L., Andreesen, R., Krause, S. W., & Kreutz, M. (2007). Inhibitory effect of tumor cell-derived lactic acid on human T cells. *Blood*, *109*(9), 3812–3819. https://doi.org/10.1182/blood-2006-07-035972

Flickinger, K. M., Wilson, K. M., Rossiter, N. J., Hunger, A. L., Lee, T. D., Hall, M. D., & Cantor, J. R. (2023). *Conditional lethality profiling reveals anticancer mechanisms of action and drug-nutrient interactions*. https://doi.org/10.1101/2023.06.04.543621

Fonseca, J., Moradi, F., Valente, A. J. F., & Stuart, J. A. (2018). Oxygen and Glucose Levels in Cell Culture Media Determine Resveratrol's Effects on Growth, Hydrogen Peroxide Production, and Mitochondrial Dynamics. *Antioxidants*, *7*(11), Article 11. https://doi.org/10.3390/antiox7110157

Fontaine, D. (2019). 5 Common Questions for Diabetic Model. *The Jackson Laboratory*.

Forsythe, J. A., Jiang, B.-H., Iyer, N. V., Agani, F., Leung, S. W., Koos, R. D., & Semenza, G. L. (1996). Activation of Vascular Endothelial Growth Factor Gene Transcription by Hypoxia-Inducible Factor 1. *Molecular and Cellular Biology*, *16*(9), 4604–4613. https://doi.org/10.1128/MCB.16.9.4604

Fox, D. B., & Alvarez, J. V. (2020). *Epithelial-to-mesenchymal transition activates Bcat1 expression to promote recurrent tumor growth* (p. 2020.12.08.416479). bioRxiv. https://doi.org/10.1101/2020.12.08.416479

Fu, T., Dai, L.-J., Wu, S.-Y., Xiao, Y., Ma, D., Jiang, Y.-Z., & Shao, Z.-M. (2021). Spatial architecture of the immune microenvironment orchestrates tumor immunity and therapeutic response. *Journal of Hematology & Oncology*, *14*(1), 98. https://doi.org/10.1186/s13045-021-01103-4

Fu, Y., Yu, J., Li, F., & Ge, S. (2022). Oncometabolites drive tumorigenesis by enhancing protein acylation: From chromosomal remodelling to nonhistone modification. *Journal of Experimental & Clinical Cancer Research*, *41*(1), 144. https://doi.org/10.1186/s13046-022-02338-w

Fu, Y.-M., Lin, H., Liu, X., Fang, W., & Meadows, G. G. (2010). Cell death of prostate cancer cells by specific amino acid restriction depends on alterations of glucose metabolism. *Journal of Cellular Physiology*, *224*(2), 491–500. https://doi.org/10.1002/jcp.22148

Fukuda, R., Zhang, H., Kim, J., Shimoda, L., Dang, C. V., & Semenza, G. L. (2007). HIF-1 regulates cytochrome oxidase subunits to optimize efficiency of respiration in hypoxic cells. *Cell*, *129*(1), 111–122. https://doi.org/10.1016/j.cell.2007.01.047

Fukumura, D., & Jain, R. K. (2007). Tumor microenvironment abnormalities: Causes, consequences, and strategies to normalize. *Journal of Cellular Biochemistry*, *101*(4), 937–949. https://doi.org/10.1002/jcb.21187

Fukumura, D., & Jain., R. K. (2007). Tumor microvasculature and microenvironment: Targets for anti-angiogenesis and normalization. *Microvascular Research*, *74*(2–3), 72–84. https://doi.org/10.1016/j.mvr.2007.05.003

Furuta, E., Okuda, H., Kobayashi, A., & Watabe, K. (2010). Metabolic genes in cancer: Their roles in tumor progression and clinical implications. *Biochimica et Biophysica Acta*, *1805*(2), 141–152. https://doi.org/10.1016/j.bbcan.2010.01.005

Gan, L., Xiu, R., Ren, P., Yue, M., Su, H., Guo, G., Xiao, D., Yu, J., Jiang, H., Liu, H., Hu, G., & Qing, G. (2016). Metabolic targeting of oncogene MYC by selective activation of the proton-coupled monocarboxylate family of transporters. *Oncogene*, *35*(23), 3037–3048. https://doi.org/10.1038/onc.2015.360

Gao, X.-Z., Wang, G.-N., Zhao, W.-G., Han, J., Diao, C.-Y., Wang, X.-H., Li, S.-L., & Li, W.-C. (2019). Blocking OLFM4/HIF-1α axis alleviates hypoxia-induced invasion, epithelial–mesenchymal transition, and chemotherapy resistance in non-small-cell lung cancer. *Journal of Cellular Physiology*, *234*(9), 15035–15043. https://doi.org/10.1002/jcp.28144

Gao, Z.-J., Wang, Y., Yuan, W., Yuan, J., & Yuan, K. (2017). HIF-2α not HIF-1α overexpression confers poor prognosis in non–small cell lung cancer. *Tumor Biology*, *39*(6), 1010428317709637. https://doi.org/10.1177/1010428317709637

Garami, A., Zwartkruis, F. J. T., Nobukuni, T., Joaquin, M., Roccio, M., Stocker, H., Kozma, S. C., Hafen, E., Bos, J. L., & Thomas, G. (2003). Insulin activation of Rheb, a mediator of mTOR/S6K/4E-BP signaling, is inhibited by TSC1 and 2. *Molecular Cell*, *11*(6), 1457–1466. https://doi.org/10.1016/s1097-2765(03)00220-x

Gardner, G. L., Moradi, F., Moffatt, C., Cliche, M., Garlisi, B., Gratton, J., Mehmood, F., & Stuart, J. A. (2022). Rapid nutrient depletion to below the physiological range by cancer cells cultured in Plasmax. *American Journal of Physiology-Cell Physiology*, *323*(3), C823–C834. https://doi.org/10.1152/ajpcell.00403.2021

Gerlowski, L. E., & Jain, R. K. (1986). Microvascular permeability of normal and neoplastic tissues. *Microvascular Research*, *31*(3), 288–305. https://doi.org/10.1016/0026-2862(86)90018-x

Gerweck, L. E., & Seetharaman, K. (1996). *Cellular pH Gradient in Tumor versus Normal Tissue: Potential Exploitation for the Treatment of Cancer*.

Gey, G. (1952). Tissue culture studies of the proliferative capacity of cervical carcinoma and normal epithelium. *Cancer Research*, *12*, 264–265.

Ghashghaeinia, M., Köberle, M., Mrowietz, U., & Bernhardt, I. (2019). Proliferating tumor cells mimick glucose metabolism of mature human erythrocytes. *Cell Cycle (Georgetown, Tex.)*, *18*(12), 1316–1334. https://doi.org/10.1080/15384101.2019.1618125

Goetze, K., Walenta, S., Ksiazkiewicz, M., Kunz-Schughart, L. A., & Mueller-Klieser, W. (2011). Lactate enhances motility of tumor cells and inhibits monocyte migration and cytokine release. *International Journal of Oncology*, *39*(2), 453–463. https://doi.org/10.3892/ijo.2011.1055

Golikov, M. V., Karpenko, I. L., Lipatova, A. V., Ivanova, O. N., Fedyakina, I. T., Larichev, V. F., Zakirova, N. F., Leonova, O. G., Popenko, V. I., Bartosch, B., Kochetkov, S. N., Smirnova, O. A., & Ivanov, A. V. (2022). Cultivation of Cells in a Physiological Plasmax Medium Increases Mitochondrial Respiratory Capacity and Reduces Replication Levels of RNA Viruses. *Antioxidants*, *11*(1). https://doi.org/10.3390/antiox11010097

Golikov, M. V., Valuev-Elliston, V. T., Smirnova, O. A., & Ivanov, A. V. (2022). Physiological Media in Studies of Cell Metabolism. *Molecular Biology*, *56*(5), 629–637. https://doi.org/10.1134/S0026893322050077

Graveling, A. J., Deary, I. J., & Frier, B. M. (2013). Acute hypoglycemia impairs executive cognitive function in adults with and without type 1 diabetes. *Diabetes Care*, *36*(10), 3240–3246. https://doi.org/10.2337/dc13-0194

Gu, C., Park, S., Seok, J., Jang, H. Y., Bang, Y. J., & Kim, G. I. J. (2020). Altered expression of ADM and ADM2 by hypoxia regulates migration of trophoblast and HLA-G expression†. *Biology of Reproduction*, *104*(1), 159–169. https://doi.org/10.1093/biolre/ioaa178

Gu, J., Guo, Y., Du, J., Kong, L., Deng, J., Tao, B., Li, H., Jin, C., Fu, D., & Li, J. (2022). CDCA8/SNAI2 Complex Activates CD44 to Promote Proliferation and Invasion of Pancreatic Ductal Adenocarcinoma. *Cancers*, *14*(21), Article 21. https://doi.org/10.3390/cancers14215434

Gu, Y. Z., Moran, S. M., Hogenesch, J. B., Wartman, L., & Bradfield, C. A. (1998). Molecular characterization and chromosomal localization of a third alpha-class hypoxia inducible factor subunit, HIF3alpha. *Gene Expression*, *7*(3), 205–213.

Gui, D. Y., Sullivan, L. B., Luengo, A., Hosios, A. M., Bush, L. N., Gitego, N., Davidson, S. M., Freinkman, E., Thomas, C. J., & Vander Heiden, M. G. (2016). Environment Dictates Dependence on Mitochondrial Complex I for NAD+ and Aspartate Production and Determines Cancer Cell Sensitivity to Metformin. *Cell Metabolism*, *24*(5), 716–727. https://doi.org/10.1016/j.cmet.2016.09.006

Guo, Q. M., Malek, R. L., Kim, S., Chiao, C., He, M., Ruffy, M., Sanka, K., Lee, N. H., Dang, C. V., & Liu, E. T. (2000). Identification of c-myc responsive genes using rat cDNA microarray. *Cancer Research*, *60*(21), 5922–5928.

Guo, W., Li, K., Sun, B., Xu, D., Tong, L., Yin, H., Liao, Y., Song, H., Wang, T., Jing, B., Hu, M., Liu, S., Kuang, Y., Ling, J., Li, Q., Wu, Y., Wang, Q., Yao, F., Zhou, B. P., … Deng,

J. (2021). Dysregulated Glutamate Transporter SLC1A1 Propels Cystine Uptake via Xc− for Glutathione Synthesis in Lung Cancer. *Cancer Research*, *81*(3), 552–566. https://doi.org/10.1158/0008-5472.CAN-20-0617

Gurel, B., Iwata, T., Koh, C. M., Jenkins, R. B., Lan, F., Dang, C. V., Hicks, J. L., Morgan, J., Cornish, T. C., Sutcliffe, S., Isaacs, W. B., Luo, J., & Marzo, A. M. D. (2008). Nuclear MYC protein overexpression is an early alteration in human prostate carcinogenesis. *Modern Pathology*, *21*(9), 1156–1167. https://doi.org/10.1038/modpathol.2008.111

Gutmann, R., Leunig, M., Feyh, J., Goetz, A. E., Messmer, K., Kastenbauer, E., & Jain, R. K. (1992). Interstitial hypertension in head and neck tumors in patients: Correlation with tumor size. *Cancer Research*, *52*(7), 1993–1995.

Gwinn, D. M., Shackelford, D. B., Egan, D. F., Mihaylova, M. M., Mery, A., Vasquez, D. S., Turk, B. E., & Shaw, R. J. (2008). AMPK phosphorylation of raptor mediates a metabolic checkpoint. *Molecular Cell*, *30*(2), 214–226. https://doi.org/10.1016/j.molcel.2008.03.003

Han, B. G., Hao, C.-M., Tchekneva, E. E., Wang, Y.-Y., Lee, C. A., Ebrahim, B., Harris, R. C., Kern, T. S., Wasserman, D. H., Breyer, M. D., & Qi, Z. (2008). Markers of glycemic control in the mouse: Comparisons of 6-h- and overnight-fasted blood glucoses to Hb A1c. *American Journal of Physiology-Endocrinology and Metabolism*, *295*(4), E981–E986. https://doi.org/10.1152/ajpendo.90283.2008

Han, J., Zhang, L., Guo, H., Wysham, W. Z., Roque, D. R., Willson, A. K., Sheng, X., Zhou, C., & Bae-Jump, V. L. (2015). Glucose promotes cell proliferation, glucose uptake and invasion in endometrial cancer cells via AMPK/mTOR/S6 and MAPK signaling. *Gynecologic Oncology*, *138*(3), 668–675. https://doi.org/10.1016/j.ygyno.2015.06.036

Han, L., Ma, Q., Li, J., Liu, H., Li, W., Ma, G., Xu, Q., Zhou, S., & Wu, E. (2011). High Glucose Promotes Pancreatic Cancer Cell Proliferation via the Induction of EGF Expression and Transactivation of EGFR. *PLOS ONE*, *6*(11), e27074. https://doi.org/10.1371/journal.pone.0027074

Hara, K., Maruki, Y., Long, X., Yoshino, K., Oshiro, N., Hidayat, S., Tokunaga, C., Avruch, J., & Yonezawa, K. (2002). Raptor, a binding partner of target of rapamycin (TOR), mediates TOR action. *Cell*, *110*(2), 177–189. https://doi.org/10.1016/s0092-8674(02)00833-4

Hara, K., Yonezawa, K., Weng, Q. P., Kozlowski, M. T., Belham, C., & Avruch, J. (1998). Amino acid sufficiency and mTOR regulate p70 S6 kinase and eIF-4E BP1 through a common effector mechanism. *The Journal of Biological Chemistry*, *273*(23), 14484–14494. https://doi.org/10.1074/jbc.273.23.14484

Hara, S., Hamada, J., Kobayashi, C., Kondo, Y., & Imura, N. (2001). Expression and Characterization of Hypoxia-Inducible Factor (HIF)-3α in Human Kidney: Suppression of HIF-Mediated Gene Expression by HIF-3α. *Biochemical and Biophysical Research Communications*, *287*(4), 808–813. https://doi.org/10.1006/bbrc.2001.5659

Hardie, D. G., & Carling, D. (1997). The AMP-Activated Protein Kinase. *European Journal of Biochemistry*, *246*(2), 259–273. https://doi.org/10.1111/j.1432-1033.1997.00259.x

Hardie, D. G., Carling, D., & Sim, A. T. R. (1989). The AMP-activated protein kinase: A multisubstrate regulator of lipid metabolism. *Trends in Biochemical Sciences*, *14*(1), 20–23. https://doi.org/10.1016/0968-0004(89)90084-4

Hattori, A., Tsunoda, M., Konuma, T., Kobayashi, M., Nagy, T., Glushka, J., Tayyari, F., McSkimming, D., Kannan, N., Tojo, A., Edison, A. S., & Ito, T. (2017). Cancer

progression by reprogrammed BCAA metabolism in myeloid leukemia. *Nature*, *545*(7655), 500–504. https://doi.org/10.1038/nature22314

Hayflick, L, Kruse, P.F. Jr., & Patterson, M.K. Jr. (1973). *Tissue Culture Methods and Applications*. Academic Press.

Heichler, C., Scheibe, K., Schmied, A., Geppert, C. I., Schmid, B., Wirtz, S., Thoma, O.-M., Kramer, V., Waldner, M. J., Büttner, C., Farin, H. F., Pešić, M., Knieling, F., Merkel, S., Grüneboom, A., Gunzer, M., Grützmann, R., Rose-John, S., Koralov, S. B., … Neufert, C. (2020). STAT3 activation through IL-6/IL-11 in cancer-associated fibroblasts promotes colorectal tumour development and correlates with poor prognosis. *Gut*, *69*(7), 1269–1282. https://doi.org/10.1136/gutjnl-2019-319200

Higgins, D. F., Biju, M. P., Akai, Y., Wutz, A., Johnson, R. S., & Haase, V. H. (2004). Hypoxic induction of Ctgf is directly mediated by Hif-1. *American Journal of Physiology-Renal Physiology*, *287*(6), F1223–F1232. https://doi.org/10.1152/ajprenal.00245.2004

Hirayama, A., Kami, K., Sugimoto, M., Sugawara, M., Toki, N., Onozuka, H., Kinoshita, T., Saito, N., Ochiai, A., Tomita, M., Esumi, H., & Soga, T. (2009). Quantitative Metabolome Profiling of Colon and Stomach Cancer Microenvironment by Capillary Electrophoresis Time-of-Flight Mass Spectrometry. *Cancer Research*, *69*(11), 4918–4925. https://doi.org/10.1158/0008-5472.CAN-08-4806

Ho, C., Wang, C., Mattu, S., Destefanis, G., Ladu, S., Delogu, S., Armbruster, J., Fan, L., Lee, S. A., Jiang, L., Dombrowski, F., Evert, M., Chen, X., & Calvisi, D. F. (2012). AKT (v-akt murine thymoma viral oncogene homolog 1) and N-Ras (neuroblastoma ras viral oncogene homolog) coactivation in the mouse liver promotes rapid carcinogenesis by way of mTOR (mammalian target of rapamycin complex 1), FOXM1 (forkhead box

M1)/SKP2, and c-Myc pathways. *Hepatology*, *55*(3), 833–845. https://doi.org/10.1002/hep.24736

Hoekstra, A. S., & Bayley, J.-P. (2013). The role of complex II in disease. *Biochimica et Biophysica Acta (BBA) - Bioenergetics*, *1827*(5), 543–551. https://doi.org/10.1016/j.bbabio.2012.11.005

Hoffmann, C., Mao, X., Brown-Clay, J., Moreau, F., Al Absi, A., Wurzer, H., Sousa, B., Schmitt, F., Berchem, G., Janji, B., & Thomas, C. (2018). Hypoxia promotes breast cancer cell invasion through HIF-1α-mediated up-regulation of the invadopodial actin bundling protein CSRP2. *Scientific Reports*, *8*(1), 10191. https://doi.org/10.1038/s41598-018-28637-x

Horiguchi, M., Koyanagi, S., Okamoto, A., Suzuki, S. O., Matsunaga, N., & Ohdo, S. (2012). Stress-regulated transcription factor ATF4 promotes neoplastic transformation by suppressing expression of the INK4a/ARF cell senescence factors. *Cancer Research*, *72*(2), 395–401. https://doi.org/10.1158/0008-5472.CAN-11-1891

Hosios, A. M., Hecht, V. C., Danai, L. V., Johnson, M. O., Rathmell, J. C., Steinhauser, M. L., Manalis, S. R., & Vander Heiden, M. G. (2016). Amino Acids Rather than Glucose Account for the Majority of Cell Mass in Proliferating Mammalian Cells. *Developmental Cell*, *36*(5), 540–549. https://doi.org/10.1016/j.devcel.2016.02.012

Hossain, S. M. M., Halsana, A. A., Khatun, L., Ray, S., & Mukhopadhyay, A. (2021). Discovering key transcriptomic regulators in pancreatic ductal adenocarcinoma using Dirichlet process Gaussian mixture model. *Scientific Reports*, *11*, 7853. https://doi.org/10.1038/s41598-021-87234-7

Hou, Y., Zhou, M., Xie, J., Chao, P., Feng, Q., & Wu, J. (2017). High glucose levels promote the proliferation of breast cancer cells through GTPases. *Breast Cancer: Targets and Therapy*, *9*, 429–436. https://doi.org/10.2147/BCTT.S135665

Houten, S. M., & Wanders, R. J. A. (2010). A general introduction to the biochemistry of mitochondrial fatty acid β-oxidation. *Journal of Inherited Metabolic Disease*, *33*(5), 469–477. https://doi.org/10.1007/s10545-010-9061-2

Hu, J., Discher, D. J., Bishopric, N. H., & Webster, K. A. (1998). Hypoxia Regulates Expression of the Endothelin-1 Gene through a Proximal Hypoxia-Inducible Factor-1 Binding Site on the Antisense Strand. *Biochemical and Biophysical Research Communications*, *245*(3), 894–899. https://doi.org/10.1006/bbrc.1998.8543

Hu, X.-Q., & Zhang, L. (2021). Hypoxia and the integrated stress response promote pulmonary hypertension and preeclampsia: Implications in drug development. *Drug Discovery Today*, *26*(11), 2754–2773. https://doi.org/10.1016/j.drudis.2021.07.011

Huang, F., Zhang, Q., Ma, H., Lv, Q., & Zhang, T. (2014). Expression of glutaminase is upregulated in colorectal cancer and of clinical significance. *International Journal of Clinical and Experimental Pathology*, *7*(3), 1093–1100.

Huang, H.-Y., Wu, W.-R., Wang, Y.-H., Wang, J.-W., Fang, F.-M., Tsai, J.-W., Li, S.-H., Hung, H.-C., Yu, S.-C., Lan, J., Shiue, Y.-L., Hsing, C.-H., Chen, L.-T., & Li, C.-F. (2013). ASS1 as a novel tumor suppressor gene in myxofibrosarcomas: Aberrant loss via epigenetic DNA methylation confers aggressive phenotypes, negative prognostic impact, and therapeutic relevance. *Clinical Cancer Research: An Official Journal of the American Association for Cancer Research*, *19*(11), 2861–2872. https://doi.org/10.1158/1078-0432.CCR-12-2641

Huang, L. E., Gu, J., Schau, M., & Bunn, H. F. (1998). Regulation of hypoxia-inducible factor 1α is mediated by an O2-dependent degradation domain via the ubiquitin-proteasome pathway. *Proceedings of the National Academy of Sciences of the United States of America*, *95*(14), 7987–7992.

Huang, X., Li, X., & Guo, B. (2008). KLF6 induces apoptosis in prostate cancer cells through up-regulation of ATF3. *The Journal of Biological Chemistry*, *283*(44), 29795–29801. https://doi.org/10.1074/jbc.M802515200

Huang, Y., Hickey, R. P., Yeh, J. L., Liu, D., Dadak, A., Young, L. H., Johnson, R. S., & Giordano, F. J. (2004). Cardiac myocyte-specific HIF-1alpha deletion alters vascularization, energy availability, calcium flux, and contractility in the normoxic heart. *FASEB Journal: Official Publication of the Federation of American Societies for Experimental Biology*, *18*(10), 1138–1140. https://doi.org/10.1096/fj.04-1510fje

Huang, Y., Li, W., Keller, A., Barbara, S., & Anumol, T. (2018). Quantitative Analysis of Underivatized Amino Acids in Plant Matrix by Hydrophilic Interaction Chromatography (HILIC) with LC/MS Detection. *Agilent*.

Hubbi, M. E., Kshitiz, Gilkes, D. M., Rey, S., Wong, C. C., Luo, W., Kim, D.-H., Dang, C. V., Levchenko, A., & Semenza, G. L. (2013). A Nontranscriptional Role for HIF-1α as a Direct Inhibitor of DNA Replication. *Science Signaling*, *6*(262), ra10. https://doi.org/10.1126/scisignal.2003417

Huizing, M., Ruitenbeek, W., Thinnes, F. P., Depinto, V., Wendel, U., Trijbels, F. J. M., Smit, L. M. E., Ter Laak, H. J., & Van Den Heuvel, L. P. (1996). Deficiency of the Voltage-Dependent Anion Channel: A Novel Cause of Mitochondriopathy. *Pediatric Research*, *39*(5), Article 5. https://doi.org/10.1203/00006450-199605000-00003

Imamura, K., Ogura, T., Kishimoto, A., Kaminishi, M., & Esumi, H. (2001). Cell cycle regulation via p53 phosphorylation by a 5'-AMP activated protein kinase activator, 5-aminoimidazole- 4-carboxamide-1-beta-D-ribofuranoside, in a human hepatocellular carcinoma cell line. *Biochemical and Biophysical Research Communications*, *287*(2), 562–567. https://doi.org/10.1006/bbrc.2001.5627

Imran, S. A., Agarwal, G., Bajaj, H. S., & Ross, S. (2018). Targets for Glycemic Control. *Canadian Journal of Diabetes*, *42 Suppl 1*, S42–S46. https://doi.org/10.1016/j.jcjd.2017.10.030

Inoki, K., Li, Y., Xu, T., & Guan, K.-L. (2003). Rheb GTPase is a direct target of TSC2 GAP activity and regulates mTOR signaling. *Genes & Development*, *17*(15), 1829–1834. https://doi.org/10.1101/gad.1110003

Inoki, K., Li, Y., Zhu, T., Wu, J., & Guan, K.-L. (2002). TSC2 is phosphorylated and inhibited by Akt and suppresses mTOR signalling. *Nature Cell Biology*, *4*(9), 648–657. https://doi.org/10.1038/ncb839

International Hypoglycaemia Study Group. (2017). Glucose Concentrations of Less Than 3.0 mmol/L (54 mg/dL) Should Be Reported in Clinical Trials: A Joint Position Statement of the American Diabetes Association and the European Association for the Study of Diabetes. *Diabetes Care*, *40*(1), 155–157. https://doi.org/10.2337/dc16-2215

Isaacs, J. S., Jung, Y. J., Mole, D. R., Lee, S., Torres-Cabala, C., Chung, Y.-L., Merino, M., Trepel, J., Zbar, B., Toro, J., Ratcliffe, P. J., Linehan, W. M., & Neckers, L. (2005). HIF overexpression correlates with biallelic loss of fumarate hydratase in renal cancer: Novel role of fumarate in regulation of HIF stability. *Cancer Cell*, *8*(2), 143–153. https://doi.org/10.1016/j.ccr.2005.06.017

Itoyama, R., Yasuda-Yoshihara, N., Kitamura, F., Yasuda, T., Bu, L., Yonemura, A., Uchihara, T., Arima, K., Hu, X., Jun, Z., Okamoto, Y., Akiyama, T., Yamashita, K., Nakao, Y., Yusa, T., Kitano, Y., Higashi, T., Miyata, T., Imai, K., … Ishimoto, T. (2021). Metabolic shift to serine biosynthesis through 3-PG accumulation and PHGDH induction promotes tumor growth in pancreatic cancer. *Cancer Letters*, *523*, 29–42. https://doi.org/10.1016/j.canlet.2021.09.007

Iyer, N. V., Kotch, L. E., Agani, F., Leung, S. W., Laughner, E., Wenger, R. H., Gassmann, M., Gearhart, J. D., Lawler, A. M., Yu, A. Y., & Semenza, G. L. (1998). Cellular and developmental control of O2 homeostasis by hypoxia-inducible factor 1α. *Genes & Development*, *12*(2), 149–162. https://doi.org/10.1101/gad.12.2.149

Jacinto, E., Loewith, R., Schmidt, A., Lin, S., Rüegg, M. A., Hall, A., & Hall, M. N. (2004). Mammalian TOR complex 2 controls the actin cytoskeleton and is rapamycin insensitive. *Nature Cell Biology*, *6*(11), 1122–1128. https://doi.org/10.1038/ncb1183

Jadvar, H., Alavi, A., & Gambhir, S. S. (2009). 18F-FDG Uptake in Lung, Breast, and Colon Cancers: Molecular Biology Correlates and Disease Characterization. *Journal of Nuclear Medicine : Official Publication, Society of Nuclear Medicine*, *50*(11), 1820–1827. https://doi.org/10.2967/jnumed.108.054098

Jäger, S., Handschin, C., St.-Pierre, J., & Spiegelman, B. M. (2007). AMP-Activated Protein Kinase (AMPK) Action in Skeletal Muscle via Direct Phosphorylation of PGC-1α. *Proceedings of the National Academy of Sciences of the United States of America*, *104*(29), 12017–12022.

Jain, R. K. (1988). Determinants of tumor blood flow: A review. *Cancer Research*, *48*(10), 2641–2658.

Johannessen, C. M., Reczek, E. E., James, M. F., Brems, H., Legius, E., & Cichowski, K. (2005). The NF1 tumor suppressor critically regulates TSC2 and mTOR. *Proceedings of the National Academy of Sciences*, *102*(24), 8573–8578. https://doi.org/10.1073/pnas.0503224102

Johanns, M., Pyr dit Ruys, S., Houddane, A., Vertommen, D., Herinckx, G., Hue, L., Proud, C. G., & Rider, M. H. (2017). Direct and indirect activation of eukaryotic elongation factor 2 kinase by AMP-activated protein kinase. *Cellular Signalling*, *36*, 212–221. https://doi.org/10.1016/j.cellsig.2017.05.010

Johnson, M. A., Vidoni, S., Durigon, R., Pearce, S. F., Rorbach, J., He, J., Brea-Calvo, G., Minczuk, M., Reyes, A., Holt, I. J., & Spinazzola, A. (2014). Amino acid starvation has opposite effects on mitochondrial and cytosolic protein synthesis. *PloS One*, *9*(4), e93597. https://doi.org/10.1371/journal.pone.0093597

Jørgensen, S. B., Nielsen, J. N., Birk, J. B., Olsen, G. S., Viollet, B., Andreelli, F., Schjerling, P., Vaulont, S., Hardie, D. G., Hansen, B. F., Richter, E. A., & Wojtaszewski, J. F. P. (2004). The alpha2-5'AMP-activated protein kinase is a site 2 glycogen synthase kinase in skeletal muscle and is responsive to glucose loading. *Diabetes*, *53*(12), 3074–3081. https://doi.org/10.2337/diabetes.53.12.3074

Joseph, J. V., Conroy, S., Pavlov, K., Sontakke, P., Tomar, T., Eggens-Meijer, E., Balasubramaniyan, V., Wagemakers, M., den Dunnen, W. F. A., & Kruyt, F. A. E. (2015). Hypoxia enhances migration and invasion in glioblastoma by promoting a mesenchymal shift mediated by the HIF1α-ZEB1 axis. *Cancer Letters*, *359*(1), 107–116. https://doi.org/10.1016/j.canlet.2015.01.010

Kaira, K., Kawashima, O., Endoh, H., Imaizumi, K., Goto, Y., Kamiyoshihara, M., Sugano, M., Yamamoto, R., Osaki, T., Tanaka, S., Fujita, A., Imai, H., Kogure, Y., Seki, Y., Shimizu, K., Mogi, A., Shitara, Y., Oyama, T., Kanai, Y., & Asao, T. (2019). Expression of amino acid transporter (LAT1 and 4F2hc) in pulmonary pleomorphic carcinoma. *Human Pathology*, *84*, 142–149. https://doi.org/10.1016/j.humpath.2018.09.020

Kalinin, A., Zubkova, E., & Menshikov, M. (2023). Integrated Stress Response (ISR) Pathway: Unraveling Its Role in Cellular Senescence. *International Journal of Molecular Sciences*, *24*(24), Article 24. https://doi.org/10.3390/ijms242417423

Kamphorst, J. J., Nofal, M., Commisso, C., Hackett, S. R., Lu, W., Grabocka, E., Vander Heiden, M. G., Miller, G., Drebin, J. A., Bar-Sagi, D., Thompson, C. B., & Rabinowitz, J. D. (2015). Human pancreatic cancer tumors are nutrient poor and tumor cells actively scavenge extracellular protein. *Cancer Research*, *75*(3), 544–553. https://doi.org/10.1158/0008-5472.CAN-14-2211

Kaplan, O., Jaroszewski, J. W., Faustino, P. J., Zugmaier, G., Ennis, B. W., Lippman, M., & Cohen, J. S. (1990). Toxicity and effects of epidermal growth factor on glucose metabolism of MDA-468 human breast cancer cells. *The Journal of Biological Chemistry*, *265*(23), 13641–13649.

Kashiwagura, T., Wilson, D. F., & Erecińska, M. (1984). Oxygen dependence of cellular metabolism: The effect of O2 tension on gluconeogenesis and urea synthesis in isolated rat hepatocytes. *Journal of Cellular Physiology*, *120*(1), 13–18. https://doi.org/10.1002/jcp.1041200103

Kato, Y., Ozawa, S., Miyamoto, C., Maehata, Y., Suzuki, A., Maeda, T., & Baba, Y. (2013). Acidic extracellular microenvironment and cancer. *Cancer Cell International*, *13*(1), 89. https://doi.org/10.1186/1475-2867-13-89

Keeley, T. P., & Mann, G. E. (2019). Defining Physiological Normoxia for Improved Translation of Cell Physiology to Animal Models and Humans. *Physiological Reviews*, *99*(1), 161–234. https://doi.org/10.1152/physrev.00041.2017

Keenan, J., Horgan, K., Clynes, M., Sinkunaite, I., Ward, P., Murphy, R., & O'Sullivan, F. (2018). Unexpected fluctuations of trace element levels in cell culture medium in vitro: Caveat emptor. *In Vitro Cellular & Developmental Biology. Animal*, *54*(8), 555–558. https://doi.org/10.1007/s11626-018-0285-z

Kessler, R., Bleichert, F., Warnke, J.-P., & Eschrich, K. (2008). 6-Phosphofructo-2-kinase/fructose-2,6-bisphosphatase (PFKFB3) is up-regulated in high-grade astrocytomasri. *Journal of Neuro-Oncology*, *86*(3), 257–264. https://doi.org/10.1007/s11060-007-9471-7

Kim, D.-H., Sarbassov, D. D., Ali, S. M., King, J. E., Latek, R. R., Erdjument-Bromage, H., Tempst, P., & Sabatini, D. M. (2002). mTOR interacts with raptor to form a nutrient-sensitive complex that signals to the cell growth machinery. *Cell*, *110*(2), 163–175. https://doi.org/10.1016/s0092-8674(02)00808-5

Kim, E., Goraksha-Hicks, P., Li, L., Neufeld, T. P., & Guan, K.-L. (2008). Regulation of TORC1 by Rag GTPases in nutrient response. *Nature Cell Biology*, *10*(8), 935–945. https://doi.org/10.1038/ncb1753

Kim, J., Tchernyshyov, I., Semenza, G. L., & Dang, C. V. (2006). HIF-1-mediated expression of pyruvate dehydrogenase kinase: A metabolic switch required for cellular adaptation to hypoxia. *Cell Metabolism*, *3*(3), 177–185. https://doi.org/10.1016/j.cmet.2006.02.002

Kim, J., Zeller, K. I., Wang, Y., Jegga, A. G., Aronow, B. J., O'Donnell, K. A., & Dang, C. V. (2004). Evaluation of Myc E-Box Phylogenetic Footprints in Glycolytic Genes by Chromatin Immunoprecipitation Assays. *Molecular and Cellular Biology*, *24*(13), 5923–5936. https://doi.org/10.1128/MCB.24.13.5923-5936.2004

Kim, J.-H., Yoon, M.-S., & Chen, J. (2009). Signal transducer and activator of transcription 3 (STAT3) mediates amino acid inhibition of insulin signaling through serine 727 phosphorylation. *The Journal of Biological Chemistry*, *284*(51), 35425–35432. https://doi.org/10.1074/jbc.M109.051516

Kinoshita, Y., & Yokota, A. (1997). Absolute concentrations of metabolites in human brain tumors using in vitro proton magnetic resonance spectroscopy. *NMR in Biomedicine*, *10*(1), 2–12. https://doi.org/10.1002/(SICI)1099-1492(199701)10:1<2::AID-NBM442>3.0.CO;2-N

Knupp, J., Arvan, P., & Chang, A. (2019). Increased mitochondrial respiration promotes survival from endoplasmic reticulum stress. *Cell Death and Differentiation*, *26*(3), 487–501. https://doi.org/10.1038/s41418-018-0133-4

Konerding, M. A., Fait, E., & Gaumann, A. (2001). 3D microvascular architecture of pre-cancerous lesions and invasive carcinomas of the colon. *British Journal of Cancer*, *84*(10), 1354–1362. https://doi.org/10.1054/bjoc.2001.1809

Kontomanolis, E. N., Koutras, A., Syllaios, A., Schizas, D., Mastoraki, A., Garmpis, N., Diakosavvas, M., Angelou, K., Tsatsaris, G., Pagkalos, A., Ntounis, T., & Fasoulakis, Z.

(2020). Role of Oncogenes and Tumor-suppressor Genes in Carcinogenesis: A Review. *Anticancer Research*, *40*(11), 6009–6015. https://doi.org/10.21873/anticanres.14622

Koong, A. C., Mehta, V. K., Le, Q. T., Fisher, G. A., Terris, D. J., Brown, J. M., Bastidas, A. J., & Vierra, M. (2000). Pancreatic tumors show high levels of hypoxia. *International Journal of Radiation Oncology*Biology*Physics*, *48*(4), 919–922. https://doi.org/10.1016/S0360-3016(00)00803-8

Koppula, P., Zhang, Y., Zhuang, L., & Gan, B. (2018). Amino acid transporter SLC7A11/xCT at the crossroads of regulating redox homeostasis and nutrient dependency of cancer. *Cancer Communications*, *38*(1), 12. https://doi.org/10.1186/s40880-018-0288-x

Koshiji, M., Kageyama, Y., Pete, E. A., Horikawa, I., Barrett, J. C., & Huang, L. E. (2004). HIF-1α induces cell cycle arrest by functionally counteracting Myc. *The EMBO Journal*, *23*(9), 1949–1956. https://doi.org/10.1038/sj.emboj.7600196

Koukourakis, M. I., Giatromanolaki, A., Sivridis, E., Bougioukas, G., Didilis, V., Gatter, K. C., & Harris, A. L. (2003). Lactate dehydrogenase-5 (LDH-5) overexpression in non-small-cell lung cancer tissues is linked to tumour hypoxia, angiogenic factor production and poor prognosis. *British Journal of Cancer*, *89*(5), 877–885. https://doi.org/10.1038/sj.bjc.6601205

Koukourakis, M. I., Kontomanolis, E., Giatromanolaki, A., Sivridis, E., & Liberis, V. (2008). Serum and Tissue LDH Levels in Patients with Breast/Gynaecological Cancer and Benign Diseases. *Gynecologic and Obstetric Investigation*, *67*(3), 162–168. https://doi.org/10.1159/000183250

Koziel, A., Woyda-Ploszczyca, A., Kicinska, A., & Jarmuszkiewicz, W. (2012). The influence of high glucose on the aerobic metabolism of endothelial EA.hy926 cells. *Pflugers Archiv, 464*(6), 657. https://doi.org/10.1007/s00424-012-1156-1

Kurth-Kraczek, E. J., Hirshman, M. F., Goodyear, L. J., & Winder, W. W. (1999). 5' AMP-activated protein kinase activation causes GLUT4 translocation in skeletal muscle. *Diabetes, 48*(8), 1667–1671. https://doi.org/10.2337/diabetes.48.8.1667

Land, S. C., & Tee, A. R. (2007). Hypoxia-inducible factor 1alpha is regulated by the mammalian target of rapamycin (mTOR) via an mTOR signaling motif. *The Journal of Biological Chemistry*, *282*(28), 20534–20543. https://doi.org/10.1074/jbc.M611782200

Laplante, M., & Sabatini, D. M. (2013). Regulation of mTORC1 and its impact on gene expression at a glance. *Journal of Cell Science*, *126*(8), 1713–1719. https://doi.org/10.1242/jcs.125773

Law, A. Y. S., & Wong, C. K. C. (2010). Stanniocalcin-2 is a HIF-1 target gene that promotes cell proliferation in hypoxia. *Experimental Cell Research*, *316*(3), 466–476. https://doi.org/10.1016/j.yexcr.2009.09.018

Le Bacquer, O., Petroulakis, E., Paglialunga, S., Poulin, F., Richard, D., Cianflone, K., & Sonenberg, N. (2007). Elevated sensitivity to diet-induced obesity and insulin resistance in mice lacking 4E-BP1 and 4E-BP2. *The Journal of Clinical Investigation*, *117*(2), 387–396. https://doi.org/10.1172/JCI29528

Lecharpentier, A., Vielh, P., Perez-Moreno, P., Planchard, D., Soria, J. C., & Farace, F. (2011). Detection of circulating tumour cells with a hybrid (epithelial/mesenchymal) phenotype in patients with metastatic non-small cell lung cancer. *British Journal of Cancer*, *105*(9), Article 9. https://doi.org/10.1038/bjc.2011.405

Lee, E. Y. H. P., & Muller, W. J. (2010). Oncogenes and Tumor Suppressor Genes. *Cold Spring Harbor Perspectives in Biology*, *2*(10), a003236. https://doi.org/10.1101/cshperspect.a003236

Lee, P. J., Jiang, B. H., Chin, B. Y., Iyer, N. V., Alam, J., Semenza, G. L., & Choi, A. M. (1997). Hypoxia-inducible factor-1 mediates transcriptional activation of the heme oxygenase-1 gene in response to hypoxia. *The Journal of Biological Chemistry*, *272*(9), 5375–5381.

Leeuwenburgh, C., & Ji, L. L. (1995). Glutathione Depletion in Rested and Exercised Mice: Biochemical Consequence and Adaptation. *Archives of Biochemistry and Biophysics*, *316*(2), 941–949. https://doi.org/10.1006/abbi.1995.1125

Lewis, M. R. (1922). Wilhelm. *The Journal of Experimental Medicine*, *35*(3), 317–322.

Li, C., Teng, P., Sun, S., Cui, K., Yao, S., Fei, B., Ling, F., & Huang, Z. (2023). Acetylation of aldehyde dehydrogenase ALDH1L2 regulates cellular redox balance and the chemosensitivity of colorectal cancer to 5-fluorouracil. *The Journal of Biological Chemistry*, *299*(9), 105090. https://doi.org/10.1016/j.jbc.2023.105090

Li, J., Chekkoury, A., Prakash, J., Glasl, S., Vetschera, P., Koberstein-Schwarz, B., Olefir, I., Gujrati, V., Omar, M., & Ntziachristos, V. (2020). Spatial heterogeneity of oxygenation and haemodynamics in breast cancer resolved in vivo by conical multispectral optoacoustic mesoscopy. *Light: Science & Applications*, *9*(1), Article 1. https://doi.org/10.1038/s41377-020-0295-y

Li, L., Madu, C. O., Lu, A., & Lu, Y. (2010). HIF-1α Promotes A Hypoxia-Independent Cell Migration. *The Open Biology Journal*, *3*, 8–14. https://doi.org/10.2174/1874196701003010008

Li, S., Brown, M. S., & Goldstein, J. L. (2010). Bifurcation of insulin signaling pathway in rat liver: mTORC1 required for stimulation of lipogenesis, but not inhibition of gluconeogenesis. *Proceedings of the National Academy of Sciences of the United States of America*, *107*(8), 3441–3446. https://doi.org/10.1073/pnas.0914798107

Liu, P., Gan, W., Chin, Y. R., Ogura, K., Guo, J., Zhang, J., Wang, B., Blenis, J., Cantley, L. C., Toker, A., Su, B., & Wei, W. (2015). PtdIns(3,4,5)P3-dependent Activation of the mTORC2 Kinase Complex. *Cancer Discovery*, *5*(11), 1194–1209. https://doi.org/10.1158/2159-8290.CD-15-0460

Liu, Q., Stewart, J., Wang, H., Rashid, A., Zhao, J., Katz, M. H., Lee, J. E., Fleming, J. B., Maitra, A., Wolff, R. A., Varadhachary, G. R., Krishnan, S., & Wang, H. (2017). Reduced expression of argininosuccinate synthetase 1 has a negative prognostic impact in patients with pancreatic ductal adenocarcinoma. *PLoS ONE*, *12*(2), e0171985. https://doi.org/10.1371/journal.pone.0171985

Liu, W., Le, A., Hancock, C., Lane, A. N., Dang, C. V., Fan, T. W.-M., & Phang, J. M. (2012). Reprogramming of proline and glutamine metabolism contributes to the proliferative and metabolic responses regulated by oncogenic transcription factor c-MYC. *Proceedings of the National Academy of Sciences of the United States of America*, *109*(23), 8983–8988. https://doi.org/10.1073/pnas.1203244109

Liu, X., Wan, X., Kan, H., Wang, Y., Yu, F., Feng, L., Jin, J., Zhang, P., & Ma, X. (2018). Hypoxia-induced upregulation of Orai1 drives colon cancer invasiveness and angiogenesis. *European Journal of Pharmacology*, *832*, 1–10. https://doi.org/10.1016/j.ejphar.2018.05.008

Liu, Y., & Yang, C. (2021). Oncometabolites in Cancer: Current Understanding and Challenges. *Cancer Research*, *81*(11), 2820–2823. https://doi.org/10.1158/0008-5472.CAN-20-3730

Long, X., Lin, Y., Ortiz-Vega, S., Yonezawa, K., & Avruch, J. (2005). Rheb binds and regulates the mTOR kinase. *Current Biology: CB*, *15*(8), 702–713. https://doi.org/10.1016/j.cub.2005.02.053

Luengo, A., Li, Z., Gui, D. Y., Sullivan, L. B., Zagorulya, M., Do, B. T., Ferreira, R., Naamati, A., Ali, A., Lewis, C. A., Thomas, C. J., Spranger, S., Matheson, N. J., & Vander Heiden, M. G. (2021). Increased demand for NAD+ relative to ATP drives aerobic glycolysis. *Molecular Cell*, *81*(4), 691-707.e6. https://doi.org/10.1016/j.molcel.2020.12.012

Lugano, R., Ramachandran, M., & Dimberg, A. (2020). Tumor angiogenesis: Causes, consequences, challenges and opportunities. *Cellular and Molecular Life Sciences*, *77*(9), 1745–1770. https://doi.org/10.1007/s00018-019-03351-7

Lund, J., Ouwens, D. M., Wettergreen, M., Bakke, S. S., Thoresen, G. H., & Aas, V. (2019). Increased Glycolysis and Higher Lactate Production in Hyperglycemic Myotubes. *Cells*, *8*(9), Article 9. https://doi.org/10.3390/cells8091101

Lunt, S. Y., & Vander Heiden, M. G. (2011). Aerobic Glycolysis: Meeting the Metabolic Requirements of Cell Proliferation. *Annual Review of Cell and Developmental Biology*, *27*(1), 441–464. https://doi.org/10.1146/annurev-cellbio-092910-154237

Luo, J., Xiang, Y., Xu, X., Fang, D., Li, D., Ni, F., Zhu, X., Chen, B., & Zhou, M. (2018). High Glucose-Induced ROS Production Stimulates Proliferation of Pancreatic Cancer via Inactivating the JNK Pathway. *Oxidative Medicine and Cellular Longevity*, *2018*, e6917206. https://doi.org/10.1155/2018/6917206

Ma, L., Teruya-Feldstein, J., Behrendt, N., Chen, Z., Noda, T., Hino, O., Cordon-Cardo, C., & Pandolfi, P. P. (2005). Genetic analysis of Pten and Tsc2 functional interactions in the mouse reveals asymmetrical haploinsufficiency in tumor suppression. *Genes & Development*, *19*(15), 1779–1786. https://doi.org/10.1101/gad.1314405

MacPherson, S., Keyes, S., Kilgour, M. K., Smazynski, J., Chan, V., Sudderth, J., Turcotte, T., Devlieger, A., Yu, J., Huggler, K. S., Cantor, J. R., DeBerardinis, R. J., Siatskas, C., & Lum, J. J. (2022). Clinically relevant T cell expansion media activate distinct metabolic programs uncoupled from cellular function. *Molecular Therapy - Methods & Clinical Development*, *24*, 380–393. https://doi.org/10.1016/j.omtm.2022.02.004

Maddalena, L. A., Selim, S. M., Fonseca, J., Messner, H., McGowan, S., & Stuart, J. A. (2017). Hydrogen peroxide production is affected by oxygen levels in mammalian cell culture. *Biochemical and Biophysical Research Communications*, *493*(1), 246–251. https://doi.org/10.1016/j.bbrc.2017.09.037

Maeda, H., & Khatami, M. (2018). Analyses of repeated failures in cancer therapy for solid tumors: Poor tumor-selective drug delivery, low therapeutic efficacy and unsustainable costs. *Clinical and Translational Medicine*, *7*(1), 11. https://doi.org/10.1186/s40169-018-0185-6

Maeda, N., Hagihara, H., Nakata, Y., Hiller, S., Wilder, J., & Reddick, R. (2000). Aortic wall damage in mice unable to synthesize ascorbic acid. *Proceedings of the National Academy of Sciences*, *97*(2), 841–846. https://doi.org/10.1073/pnas.97.2.841

Mammucari, C., Milan, G., Romanello, V., Masiero, E., Rudolf, R., Del Piccolo, P., Burden, S. J., Di Lisi, R., Sandri, C., Zhao, J., Goldberg, A. L., Schiaffino, S., & Sandri, M. (2007).

FoxO3 Controls Autophagy in Skeletal Muscle In Vivo. *Cell Metabolism*, *6*(6), 458–471. https://doi.org/10.1016/j.cmet.2007.11.001

Mao, X., Xu, J., Wang, W., Liang, C., Hua, J., Liu, J., Zhang, B., Meng, Q., Yu, X., & Shi, S. (2021). Crosstalk between cancer-associated fibroblasts and immune cells in the tumor microenvironment: New findings and future perspectives. *Molecular Cancer*, *20*(1), 131. https://doi.org/10.1186/s12943-021-01428-1

Marsin, A.-S., Bertrand, L., Rider, M. H., Deprez, J., Beauloye, C., Vincent, M. F., Van den Berghe, G., Carling, D., & Hue, L. (2000). Phosphorylation and activation of heart PFK-2 by AMPK has a role in the stimulation of glycolysis during ischaemia. *Current Biology*, *10*(20), 1247–1255. https://doi.org/10.1016/S0960-9822(00)00742-9

Marsin, A.-S., Bouzin, C., Bertrand, L., & Hue, L. (2002). The Stimulation of Glycolysis by Hypoxia in Activated Monocytes Is Mediated by AMP-activated Protein Kinase and Inducible 6-Phosphofructo-2-kinase*. *Journal of Biological Chemistry*, *277*(34), 30778–30783. https://doi.org/10.1074/jbc.M205213200

Martinez, A. F., McCachren, S. S., Lee, M., Murphy, H. A., Zhu, C., Crouch, B. T., Martin, H. L., Erkanli, A., Rajaram, N., Ashcraft, K. A., Fontanella, A. N., Dewhirst, M. W., & Ramanujam, N. (2018). Metaboloptics: Visualization of the tumor functional landscape via metabolic and vascular imaging. *Scientific Reports*, *8*(1), 4171. https://doi.org/10.1038/s41598-018-22480-w

Mazurek, S., Michel, A., & Eigenbrodt, E. (1997). Effect of extracellular AMP on cell proliferation and metabolism of breast cancer cell lines with high and low glycolytic rates. *The Journal of Biological Chemistry*, *272*(8), 4941–4952. https://doi.org/10.1074/jbc.272.8.4941

McCommis, K. S., & Finck, B. N. (2015). Mitochondrial pyruvate transport: A historical perspective and future research directions. *The Biochemical Journal*, *466*(3), 443–454. https://doi.org/10.1042/BJ20141171

McKee, T. J., & Komarova, S. V. (2017). Is it time to reinvent basic cell culture medium? *American Journal of Physiology-Cell Physiology*, *312*(5), C624–C626. https://doi.org/10.1152/ajpcell.00336.2016

McKeown, S. R. (2014). Defining normoxia, physoxia and hypoxia in tumours—Implications for treatment response. *The British Journal of Radiology*, *87*(1035), 20130676. https://doi.org/10.1259/bjr.20130676

Mei, L., Ying, L., Wang, H., Xu, G., Ye, X., & Yang, G. (2022). 1H NMR-based metabolomics of skin squamous cell carcinoma and peri-tumoral region tissues. *Journal of Pharmaceutical and Biomedical Analysis*, *212*, 114643. https://doi.org/10.1016/j.jpba.2022.114643

Mihaylova, M. M., & Shaw, R. J. (2011). The AMP-activated protein kinase (AMPK) signaling pathway coordinates cell growth, autophagy, & metabolism. *Nature Cell Biology*, *13*(9), 1016–1023. https://doi.org/10.1038/ncb2329

Min, H.-Y., & Lee, H.-Y. (2018). Oncogene-Driven Metabolic Alterations in Cancer. *Biomolecules & Therapeutics*, *26*(1), 45–56. https://doi.org/10.4062/biomolther.2017.211

Minchenko, O., Opentanova, I., Minchenko, D., Ogura, T., & Esumi, H. (2004). Hypoxia induces transcription of 6-phosphofructo-2-kinase/fructose-2,6-biphosphatase-4 gene via hypoxia-inducible factor-1α activation. *FEBS Letters*, *576*(1–2), 14–20. https://doi.org/10.1016/j.febslet.2004.08.053

Miyazaki, K., Kawamoto, T., Tanimoto, K., Nishiyama, M., Honda, H., & Kato, Y. (2002). Identification of Functional Hypoxia Response Elements in the Promoter Region of the DEC1 and DEC2 Genes*. *Journal of Biological Chemistry*, *277*(49), 47014–47021. https://doi.org/10.1074/jbc.M204938200

Miyazaki, K., Togo, S., Okamoto, R., Idiris, A., Kumagai, H., & Miyagi, Y. (2020). Collective cancer cell invasion in contact with fibroblasts through integrin-α5β1/fibronectin interaction in collagen matrix. *Cancer Science*, *111*(12), 4381–4392. https://doi.org/10.1111/cas.14664

Mohtasham, N., Ayatollahi, H., Saghravanian, N., Zare, R., Shakeri, M.-T., Sahebkar, A., & Mohajertehran, F. (2019). Evaluation of Tissue and Serum Expression Levels of Lactate Dehydrogenase Isoenzymes in Patients with Head and Neck Squamous Cell Carcinoma. *Anti-Cancer Agents in Medicinal Chemistry- Anti-Cancer Agents)*, *19*(17), 2072–2078. https://doi.org/10.2174/1871520619666191014160818

Momcilovic, M., Bailey, S. T., Lee, J. T., Zamilpa, C., Jones, A., Abdelhady, G., Mansfield, J., Francis, K. P., & Shackelford, D. B. (2018). Utilizing 18F-FDG PET/CT Imaging and Quantitative Histology to Measure Dynamic Changes in the Glucose Metabolism in Mouse Models of Lung Cancer. *JoVE (Journal of Visualized Experiments)*, *137*, e57167. https://doi.org/10.3791/57167

Moradi, F., Fiocchetti, M., Marino, M., Moffatt, C., & Stuart, J. A. (2021). Media composition and O2 levels determine effects of 17β-estradiol and selective estrogen receptor modulators on mitochondrial bioenergetics and cellular reactive oxygen species. *American Journal of Physiology-Cell Physiology*, *321*(1), C72–C81. https://doi.org/10.1152/ajpcell.00080.2021

Moradi, F., Moffatt, C., & Stuart, J. A. (2021). The Effect of Oxygen and Micronutrient Composition of Cell Growth Media on Cancer Cell Bioenergetics and Mitochondrial Networks. *Biomolecules*, *11*(8), 1177. https://doi.org/10.3390/biom11081177

Movsas, B., Chapman, J. D., Horwitz, E. M., Pinover, W. H., Greenberg, R. E., Hanlon, A. L., Iyer, R., & Hanks, G. E. (1999). Hypoxic regions exist in human prostate carcinoma. *Urology*, *53*(1), 11–18. https://doi.org/10.1016/s0090-4295(98)00500-7

Mu, X., Zhao, T., Xu, C., Shi, W., Geng, B., Shen, J., Zhang, C., Pan, J., Yang, J., Hu, S., Lv, Y., Wen, H., & You, Q. (2017). Oncometabolite succinate to promote angiogenesis by upregulating VEGF expression through GPR91-mediated STAT3 and ERK activation. *Journal of Clinical Oncology*, *35*(15_suppl), e23000–e23000. https://doi.org/10.1200/JCO.2017.35.15_suppl.e23000

Muir, A., Danai, L. V., Gui, D. Y., Waingarten, C. Y., Lewis, C. A., & Vander Heiden, M. G. (2017). Environmental cystine drives glutamine anaplerosis and sensitizes cancer cells to glutaminase inhibition. *eLife*, *6*, e27713. https://doi.org/10.7554/eLife.27713

Mungrue, I. N., Pagnon, J., Kohannim, O., Gargalovic, P. S., & Lusis, A. J. (2009). CHAC1/MGC4504 is a novel proapoptotic component of the unfolded protein response, downstream of the ATF4-ATF3-CHOP cascade. *Journal of Immunology (Baltimore, Md.: 1950)*, *182*(1), 466–476. https://doi.org/10.4049/jimmunol.182.1.466

Neill, G., & Masson, G. R. (2023). A stay of execution: ATF4 regulation and potential outcomes for the integrated stress response. *Frontiers in Molecular Neuroscience*, *16*. https://doi.org/10.3389/fnmol.2023.1112253

Nierves, L., Guo, J., Chen, S., Tsui, J., Uzozie, A. C., Bush, J. W., Huan, T., & Lange, P. F. (2022). Multi-omic profiling of the leukemic microenvironment shows bone marrow

interstitial fluid is distinct from peripheral blood plasma. *Experimental Hematology & Oncology*, *11*(1), 56. https://doi.org/10.1186/s40164-022-00310-0

O'Donnell, A. F., & Schmidt, M. C. (2019). AMPK-Mediated Regulation of Alpha-Arrestins and Protein Trafficking. *International Journal of Molecular Sciences*, *20*(3), Article 3. https://doi.org/10.3390/ijms20030515

Ohoka, N., Yoshii, S., Hattori, T., Onozaki, K., & Hayashi, H. (2005). TRB3, a novel ER stress-inducible gene, is induced via ATF4-CHOP pathway and is involved in cell death. *The EMBO Journal*, *24*(6), 1243–1255. https://doi.org/10.1038/sj.emboj.7600596

Ong, L.-C., Jin, Y., Song, I.-C., Yu, S., Zhang, K., Ong, L.-C., Jin, Y., Song, I.-C., Yu, S., Zhang, K., & Chow, P. K. H. (2008). 2-[18F]-2-Deoxy-D-Glucose (FDG) Uptake in Human Tumor Cells is Related to the Expression of GLUT-1 and Hexokinase II. *Acta Radiologica*, *49*(10), 1145–1153. https://doi.org/10.1080/02841850802482486

Osthus, R. C., Shim, H., Kim, S., Li, Q., Reddy, R., Mukherjee, M., Xu, Y., Wonsey, D., Lee, L. A., & Dang, C. V. (2000). Deregulation of Glucose Transporter 1 and Glycolytic Gene Expression by c-Myc*. *Journal of Biological Chemistry*, *275*(29), 21797–21800. https://doi.org/10.1074/jbc.C000023200

Owens, Julie & Kind, Karen. (2008). *Nature and nurture impact on bioactives components – on farm manipulation – phase 1 | Meat & Livestock Australia*. MLA Corporate. https://www.mla.com.au/research-and-development/reports/2014/nature-and-nurture-impact-on-bioactives-components--on-farm-manipulation--phase-1/

Ozcan, S., & Senyuva, H. Z. (2006). Improved and simplified liquid chromatography/atmospheric pressure chemical ionization mass spectrometry method for

the analysis of underivatized free amino acids in various foods. *Journal of Chromatography. A*, *1135*(2), 179–185. https://doi.org/10.1016/j.chroma.2006.09.039

Packer, L., & Fuehr, K. (1977). Low oxygen concentration extends the lifespan of cultured human diploid cells. *Nature*, *267*(5610), 423–425. https://doi.org/10.1038/267423a0

Pahl, H. L., & Baeuerle, P. A. (1994). Oxygen and the control of gene expression. *BioEssays: News and Reviews in Molecular, Cellular and Developmental Biology*, *16*(7), 497–502. https://doi.org/10.1002/bies.950160709

Pajuelo Reguera, D., Čunátová, K., Vrbacký, M., Pecinová, A., Houštěk, J., Mráček, T., & Pecina, P. (2020). Cytochrome c Oxidase Subunit 4 Isoform Exchange Results in Modulation of Oxygen Affinity. *Cells*, *9*(2), Article 2. https://doi.org/10.3390/cells9020443

Pakos-Zebrucka, K., Koryga, I., Mnich, K., Ljujic, M., Samali, A., & Gorman, A. M. (2016). The integrated stress response. *EMBO Reports*, *17*(10), 1374–1395. https://doi.org/10.15252/embr.201642195

Palamaris, K., Felekouras, E., & Sakellariou, S. (2021). Epithelial to Mesenchymal Transition: Key Regulator of Pancreatic Ductal Adenocarcinoma Progression and Chemoresistance. *Cancers*, *13*(21), 5532. https://doi.org/10.3390/cancers13215532

Palm, W., & Thompson, C. B. (2017). Nutrient acquisition strategies of mammalian cells. *Nature*, *546*(7657), Article 7657. https://doi.org/10.1038/nature22379

Pan, M., Reid, M. A., Lowman, X. H., Kulkarni, R. P., Tran, T. Q., Liu, X., Yang, Y., Hernandez-Davies, J. E., Rosales, K. K., Li, H., Hugo, W., Song, C., Xu, X., Schones, D. E., Ann, D. K., Gradinaru, V., Lo, R. S., Locasale, J. W., & Kong, M. (2016). Regional

glutamine deficiency in tumours promotes dedifferentiation through inhibition of histone demethylation. *Nature Cell Biology*, *18*(10), Article 10. https://doi.org/10.1038/ncb3410

Pandkar, M. R., Dhamdhere, S. G., & Shukla, S. (2021). Oxygen gradient and tumor heterogeneity: The chronicle of a toxic relationship. *Biochimica Et Biophysica Acta. Reviews on Cancer*, *1876*(1), 188553. https://doi.org/10.1016/j.bbcan.2021.188553

Panek, R., Welsh, L., Baker, L. C. J., Schmidt, M. A., Wong, K. H., Riddell, A. M., Koh, D.-M., Dunlop, A., Mcquaid, D., d'Arcy, J. A., Bhide, S. A., Harrington, K. J., Nutting, C. M., Hopkinson, G., Richardson, C., Box, C., Eccles, S. A., Leach, M. O., Robinson, S. P., & Newbold, K. L. (2017). Non-invasive Imaging of Cycling Hypoxia in Head & Neck Cancer Using Intrinsic Susceptibility MRI. *Clinical Cancer Research : An Official Journal of the American Association for Cancer Research*, *23*(15), 4233–4241. https://doi.org/10.1158/1078-0432.CCR-16-1209

Papa, S., Francavilla, A., Paradies, G., & Meduri, B. (1971). The transport of pyruvate in rat liver mitochondria. *FEBS Letters*, *12*(5), 285–288. https://doi.org/10.1016/0014-5793(71)80200-4

Papandreou, I., Cairns, R. A., Fontana, L., Lim, A. L., & Denko, N. C. (2006). HIF-1 mediates adaptation to hypoxia by actively downregulating mitochondrial oxygen consumption. *Cell Metabolism*, *3*(3), 187–197. https://doi.org/10.1016/j.cmet.2006.01.012

Park, H.-W., Park, H., Ro, S.-H., Jang, I., Semple, I. A., Kim, D. N., Kim, M., Nam, M., Zhang, D., Yin, L., & Lee, J. H. (2014). Hepatoprotective role of Sestrin2 against chronic ER stress. *Nature Communications*, *5*, 4233. https://doi.org/10.1038/ncomms5233

Parmar, N., & Tamanoi, F. (2010). Rheb G-Proteins and the Activation of mTORC1. *The Enzymes*, *27*, 39–56. https://doi.org/10.1016/S1874-6047(10)27003-8

Paron, I., Berchtold, S., Vörös, J., Shamarla, M., Erkan, M., Höfler, H., & Esposito, I. (2011). Tenascin-C enhances pancreatic cancer cell growth and motility and affects cell adhesion through activation of the integrin pathway. *PloS One*, *6*(6), e21684. https://doi.org/10.1371/journal.pone.0021684

Pehmøller, C., Treebak, J. T., Birk, J. B., Chen, S., MacKintosh, C., Hardie, D. G., Richter, E. A., & Wojtaszewski, J. F. P. (2009). Genetic disruption of AMPK signaling abolishes both contraction- and insulin-stimulated TBC1D1 phosphorylation and 14-3-3 binding in mouse skeletal muscle. *American Journal of Physiology-Endocrinology and Metabolism*, *297*(3), E665–E675. https://doi.org/10.1152/ajpendo.00115.2009

Pelicano, H., Xu, R.-H., Du, M., Feng, L., Sasaki, R., Carew, J. S., Hu, Y., Ramdas, L., Hu, L., Keating, M. J., Zhang, W., Plunkett, W., & Huang, P. (2006). Mitochondrial respiration defects in cancer cells cause activation of Akt survival pathway through a redox-mediated mechanism. *The Journal of Cell Biology*, *175*(6), 913–923. https://doi.org/10.1083/jcb.200512100

Peng, H., Wang, Y., & Luo, W. (2020). Multifaceted role of branched-chain amino acid metabolism in cancer. *Oncogene*, *39*(44), 6747–6756. https://doi.org/10.1038/s41388-020-01480-z

Pettersen, E. O., Larsen, L. H., Ramsing, N. B., & Ebbesen, P. (2005). Pericellular oxygen depletion during ordinary tissue culturing, measured with oxygen microsensors. *Cell Proliferation*, *38*(4), 257–267. https://doi.org/10.1111/j.1365-2184.2005.00345.x

Pigott, K. H., Hill, S. A., Chaplin, D. J., & Saunders, M. I. (1996). Microregional fluctuations in perfusion within human tumours detected using laser Doppler flowmetry. *Radiotherapy*

and Oncology: Journal of the European Society for Therapeutic Radiology and Oncology, *40*(1), 45–50. https://doi.org/10.1016/0167-8140(96)01730-6

Place, T. L., Domann, F. E., & Case, A. J. (2017). Limitations of Oxygen Delivery to Cells in Culture: An Underappreciated Problem in Basic and Translational Research. *Free Radical Biology & Medicine*, *113*, 311–322. https://doi.org/10.1016/j.freeradbiomed.2017.10.003

Popova, N. V., & Jücker, M. (2022). The Functional Role of Extracellular Matrix Proteins in Cancer. *Cancers*, *14*(1), 238. https://doi.org/10.3390/cancers14010238

Poulsen, R. C., Knowles, H. J., Carr, A. J., & Hulley, P. A. (2014). Cell differentiation versus cell death: Extracellular glucose is a key determinant of cell fate following oxidative stress exposure. *Cell Death & Disease*, *5*(2), e1074. https://doi.org/10.1038/cddis.2014.52

Prado-Garcia, H., Campa-Higareda, A., & Romero-Garcia, S. (2020). Lactic Acidosis in the Presence of Glucose Diminishes Warburg Effect in Lung Adenocarcinoma Cells. *Frontiers in Oncology*, *10*, 807. https://doi.org/10.3389/fonc.2020.00807

Pries, A. R., Cornelissen, A. J. M., Sloot, A. A., Hinkeldey, M., Dreher, M. R., Höpfner, M., Dewhirst, M. W., & Secomb, T. W. (2009). Structural adaptation and heterogeneity of normal and tumor microvascular networks. *PLoS Computational Biology*, *5*(5), e1000394. https://doi.org/10.1371/journal.pcbi.1000394

Provenzano, P. P., Cuevas, C., Chang, A. E., Goel, V. K., Von Hoff, D. D., & Hingorani, S. R. (2012). Enzymatic targeting of the stroma ablates physical barriers to treatment of pancreatic ductal adenocarcinoma. *Cancer Cell*, *21*(3), 418–429. https://doi.org/10.1016/j.ccr.2012.01.007

Psychogios, N., Hau, D. D., Peng, J., Guo, A. C., Mandal, R., Bouatra, S., Sinelnikov, I., Krishnamurthy, R., Eisner, R., Gautam, B., Young, N., Xia, J., Knox, C., Dong, E., Huang, P., Hollander, Z., Pedersen, T. L., Smith, S. R., Bamforth, F., … Wishart, D. S. (2011). The Human Serum Metabolome. *PLoS ONE*, *6*(2), e16957. https://doi.org/10.1371/journal.pone.0016957

Qian, X., Li, X., Tan, L., Lee, J.-H., Xia, Y., Cai, Q., Zheng, Y., Wang, H., Lorenzi, P. L., & Lu, Z. (2018). Conversion of PRPS Hexamer to Monomer by AMPK-Mediated Phosphorylation Inhibits Nucleotide Synthesis in Response to Energy Stress. *Cancer Discovery*, *8*(1), 94–107. https://doi.org/10.1158/2159-8290.CD-17-0712

Qiu, F., Chen, Y.-R., Liu, X., Chu, C.-Y., Shen, L.-J., Xu, J., Gaur, S., Forman, H. J., Zhang, H., Zheng, S., Yen, Y., Huang, J., Kung, H.-J., & Ann, D. K. (2014). Arginine Starvation Impairs Mitochondrial Respiratory Function in ASS1-Deficient Breast Cancer Cells. *Science Signaling*, *7*(319), ra31–ra31. https://doi.org/10.1126/scisignal.2004761

Qu, J., Zhao, X., Wang, J., Liu, X., Yan, Y., Liu, L., Cai, H., Qu, H., Lu, N., Sun, Y., Wang, F., Wang, J., & Zhang, J. (2017). MYC overexpression with its prognostic and clinicopathological significance in breast cancer. *Oncotarget*, *8*(55), 93998–94008. https://doi.org/10.18632/oncotarget.21501

Rainero, E., Howe, J. D., Caswell, P. T., Jamieson, N. B., Anderson, K., Critchley, D. R., Machesky, L., & Norman, J. C. (2015). Ligand-Occupied Integrin Internalization Links Nutrient Signaling to Invasive Migration. *Cell Reports*, *10*(3), 398–413. https://doi.org/10.1016/j.celrep.2014.12.037

Rauschner, M., Lange, L., Hüsing, T., Reime, S., Nolze, A., Maschek, M., Thews, O., & Riemann, A. (2021). Impact of the acidic environment on gene expression and functional

parameters of tumors in vitro and in vivo. *Journal of Experimental & Clinical Cancer Research*, *40*(1), 10. https://doi.org/10.1186/s13046-020-01815-4

Reinfeld, B. I., Madden, M. Z., Wolf, M. M., Chytil, A., Bader, J. E., Patterson, A. R., Sugiura, A., Cohen, A. S., Ali, A., Do, B. T., Muir, A., Lewis, C. A., Hongo, R. A., Young, K. L., Brown, R. E., Todd, V. M., Huffstater, T., Abraham, A., O'Neil, R. T., … Rathmell, W. K. (2021). Cell-programmed nutrient partitioning in the tumour microenvironment. *Nature*, *593*(7858), Article 7858. https://doi.org/10.1038/s41586-021-03442-1

Reznik, E., Luna, A., Aksoy, B. A., Liu, E. M., La, K., Ostrovnaya, I., Creighton, C. J., Hakimi, A. A., & Sander, C. (2018). A Landscape of Metabolic Variation across Tumor Types. *Cell Systems*, *6*(3), 301-313.e3. https://doi.org/10.1016/j.cels.2017.12.014

Ribeiro Franco, P. I., Rodrigues, A. P., de Menezes, L. B., & Pacheco Miguel, M. (2020). Tumor microenvironment components: Allies of cancer progression. *Pathology, Research and Practice*, *216*(1), 152729. https://doi.org/10.1016/j.prp.2019.152729

Richardson, D., Sritangos, P., James, A., Sultan, A., & Bruce, J. (2020). Metabolic regulation of calcium pumps in pancreatic cancer: Role of phosphofructokinase-fructose-bisphosphatase-3 (PFKFB3). *Cancer & Metabolism*, *8*. https://doi.org/10.1186/s40170-020-0210-2

Ricketts, C., Woodward, E. R., Killick, P., Morris, M. R., Astuti, D., Latif, F., & Maher, E. R. (2008). Germline SDHB Mutations and Familial Renal Cell Carcinoma. *JNCI: Journal of the National Cancer Institute*, *100*(17), 1260–1262. https://doi.org/10.1093/jnci/djn254

Rogers, Z. J., Colombani, T., Khan, S., Bhatt, K., Nukovic, A., Zhou, G., Woolston, B. M., Taylor, C. T., Gilkes, D. M., Slavov, N., & Bencherif, S. A. (2023). *Controlling*

pericellular oxygen tension in cell culture reveals distinct breast cancer responses to low oxygen tensions. https://doi.org/10.1101/2023.10.02.560369

Roh, H. D., Boucher, Y., Kalnicki, S., Buchsbaum, R., Bloomer, W. D., & Jain, R. K. (1991). Interstitial hypertension in carcinoma of uterine cervix in patients: Possible correlation with tumor oxygenation and radiation response. *Cancer Research*, *51*(24), 6695–6698.

Rong, Y., Wu, W., Ni, X., Kuang, T., Jin, D., Wang, D., & Lou, W. (2013). Lactate dehydrogenase A is overexpressed in pancreatic cancer and promotes the growth of pancreatic cancer cells. *Tumor Biology*, *34*(3), 1523–1530. https://doi.org/10.1007/s13277-013-0679-1

Roslin, M., Henriksson, R., Bergström, P., Ungerstedt, U., & Bergenheim, A. T. (2003). Baseline levels of glucose metabolites, glutamate and glycerol in malignant glioma assessed by stereotactic microdialysis. *Journal of Neuro-Oncology*, *61*(2), 151–160. https://doi.org/10.1023/a:1022106910017

Ross, K. C., Andrews, A. J., Marion, C. D., Yen, T. J., & Bhattacharjee, V. (2017). Identification of the serine biosynthesis pathway as a critical component of BRAF inhibitor resistance of melanoma, pancreatic, and non-small cell lung cancer cells. *Molecular Cancer Therapeutics*, *16*(8), 1596–1609. https://doi.org/10.1158/1535-7163.MCT-16-0798

Rossiter, N. J., Huggler, K. S., Adelmann, C. H., Keys, H. R., Soens, R. W., Sabatini, D. M., & Cantor, J. R. (2021). CRISPR screens in physiologic medium reveal conditionally essential genes in human cells. *Cell Metabolism*, *33*(6), 1248-1263.e9. https://doi.org/10.1016/j.cmet.2021.02.005

Roux, W. (1885). Beiträge zur Entwickelungsmechanik des Embryo: III. Ueber die Bestimmung der Hauptrichtungen des Froschembryo im Ei und über die erste Theilung des Froscheies. *Breslauer Ärztl Z.*

Sancak, Y., Bar-Peled, L., Zoncu, R., Markhard, A. L., Nada, S., & Sabatini, D. M. (2010). Ragulator-Rag complex targets mTORC1 to the lysosomal surface and is necessary for its activation by amino acids. *Cell*, *141*(2), 290–303. https://doi.org/10.1016/j.cell.2010.02.024

Sancak, Y., Peterson, T. R., Shaul, Y. D., Lindquist, R. A., Thoreen, C. C., Bar-Peled, L., & Sabatini, D. M. (2008). The Rag GTPases bind raptor and mediate amino acid signaling to mTORC1. *Science (New York, N.Y.)*, *320*(5882), 1496–1501. https://doi.org/10.1126/science.1157535

Sanchez-Vega, F., Mina, M., Armenia, J., Chatila, W. K., Luna, A., La, K. C., Dimitriadoy, S., Liu, D. L., Kantheti, H. S., Saghafinia, S., Chakravarty, D., Daian, F., Gao, Q., Bailey, M. H., Liang, W.-W., Foltz, S. M., Shmulevich, I., Ding, L., Heins, Z., … Schultz, N. (2018). Oncogenic Signaling Pathways in The Cancer Genome Atlas. *Cell*, *173*(2), 321-337.e10. https://doi.org/10.1016/j.cell.2018.03.035

Sarbassov, D. D., Ali, S. M., Kim, D.-H., Guertin, D. A., Latek, R. R., Erdjument-Bromage, H., Tempst, P., & Sabatini, D. M. (2004). Rictor, a novel binding partner of mTOR, defines a rapamycin-insensitive and raptor-independent pathway that regulates the cytoskeleton. *Current Biology: CB*, *14*(14), 1296–1302. https://doi.org/10.1016/j.cub.2004.06.054

Saxena, M., Balaji, S. A., Deshpande, N., Ranganathan, S., Pillai, D. M., Hindupur, S. K., & Rangarajan, A. (2018). AMP-activated protein kinase promotes epithelial-mesenchymal

transition in cancer cells through Twist1 upregulation. *Journal of Cell Science*, *131*(14), jcs208314. https://doi.org/10.1242/jcs.208314

Saxton, R. A., & Sabatini, D. M. (2017). mTOR Signaling in Growth, Metabolism, and Disease. *Cell*, *168*(6), 960–976. https://doi.org/10.1016/j.cell.2017.02.004

Scaffa, A. M., Peterson, A. L., Carr, J. F., Garcia, D., Yao, H., & Dennery, P. A. (2021). Hyperoxia causes senescence and increases glycolysis in cultured lung epithelial cells. *Physiological Reports*, *9*(10), e14839. https://doi.org/10.14814/phy2.14839

Scalise, M., Console, L., Rovella, F., Galluccio, M., Pochini, L., & Indiveri, C. (2020). Membrane Transporters for Amino Acids as Players of Cancer Metabolic Rewiring. *Cells*, *9*(9), Article 9. https://doi.org/10.3390/cells9092028

Scalise, M., Pochini, L., Galluccio, M., Console, L., & Indiveri, C. (2017). Glutamine Transport and Mitochondrial Metabolism in Cancer Cell Growth. *Frontiers in Oncology*, *7*, 306. https://doi.org/10.3389/fonc.2017.00306

Schaaf, M. B., Garg, A. D., & Agostinis, P. (2018). Defining the role of the tumor vasculature in antitumor immunity and immunotherapy. *Cell Death & Disease*, *9*(2), Article 2. https://doi.org/10.1038/s41419-017-0061-0

Schaffer, B. E., Levin, R. S., Hertz, N. T., Maures, T. J., Schoof, M. L., Hollstein, P. E., Benayoun, B. A., Banko, M. R., Shaw, R. J., Shokat, K. M., & Brunet, A. (2015). Identification of AMPK phosphorylation sites reveals a network of proteins involved in cell invasion and facilitates large-scale substrate prediction. *Cell Metabolism*, *22*(5), 907–921. https://doi.org/10.1016/j.cmet.2015.09.009

Schmidt, A., Li, L., Lv, Z., Yan, S., & Großhans, J. (2021). Dia- and Rok-dependent enrichment of capping proteins in a cortical region. *Journal of Cell Science*, *134*(21), jcs258973. https://doi.org/10.1242/jcs.258973

Schroeder, U., Himpe, B., Pries, R., Vonthein, R., Nitsch, S., & Wollenberg, B. (2013). Decline of lactate in tumor tissue after ketogenic diet: In vivo microdialysis study in patients with head and neck cancer. *Nutrition and Cancer*, *65*(6), 843–849. https://doi.org/10.1080/01635581.2013.804579

Selak, M. A., Armour, S. M., MacKenzie, E. D., Boulahbel, H., Watson, D. G., Mansfield, K. D., Pan, Y., Simon, M. C., Thompson, C. B., & Gottlieb, E. (2005). Succinate links TCA cycle dysfunction to oncogenesis by inhibiting HIF-alpha prolyl hydroxylase. *Cancer Cell*, *7*(1), 77–85. https://doi.org/10.1016/j.ccr.2004.11.022

Semenza, G. L., Jiang, B.-H., Leung, S. W., Passantino, R., Concordet, J.-P., Maire, P., & Giallongo, A. (1996). Hypoxia Response Elements in the Aldolase A, Enolase 1, and Lactate Dehydrogenase A Gene Promoters Contain Essential Binding Sites for Hypoxia-inducible Factor 1*. *Journal of Biological Chemistry*, *271*(51), 32529–32537. https://doi.org/10.1074/jbc.271.51.32529

Semenza, G. L., & Wang, G. L. (1992). A nuclear factor induced by hypoxia via de novo protein synthesis binds to the human erythropoietin gene enhancer at a site required for transcriptional activation. *Molecular and Cellular Biology*, *12*(12), 5447–5454.

Sengupta, S., Peterson, T. R., Laplante, M., Oh, S., & Sabatini, D. M. (2010). mTORC1 controls fasting-induced ketogenesis and its modulation by ageing. *Nature*, *468*(7327), 1100–1104. https://doi.org/10.1038/nature09584

Shafei, M., Forshaw, T., Davis, J., Flemban, A., Qualtrough, D., Dean, S., Perks, C., Dong, M., Newman, R., & Conway, M. (2020). BCATc modulates crosstalk between the PI3K/Akt and the Ras/ERK pathway regulating proliferation in triple negative breast cancer. *Oncotarget*, *11*. https://doi.org/10.18632/oncotarget.27607

Shaw, R. J. (2008). mTOR signaling: RAG GTPases transmit the amino acid signal. *Trends in Biochemical Sciences*, *33*(12), 565–568. https://doi.org/10.1016/j.tibs.2008.09.005

Shubitowski, T. B., Poll, B. G., Natarajan, N., & Pluznick, J. L. (2019). Short-chain fatty acid delivery: Assessing exogenous administration of the microbiome metabolite acetate in mice. *Physiological Reports*, *7*(4), e14005. https://doi.org/10.14814/phy2.14005

Sinkala, M. (2023). Mutational landscape of cancer-driver genes across human cancers. *Scientific Reports*, *13*, 12742. https://doi.org/10.1038/s41598-023-39608-2

Sjöblom, T., Jones, S., Wood, L. D., Parsons, D. W., Lin, J., Barber, T. D., Mandelker, D., Leary, R. J., Ptak, J., Silliman, N., Szabo, S., Buckhaults, P., Farrell, C., Meeh, P., Markowitz, S. D., Willis, J., Dawson, D., Willson, J. K. V., Gazdar, A. F., … Velculescu, V. E. (2006). The consensus coding sequences of human breast and colorectal cancers. *Science (New York, N.Y.)*, *314*(5797), 268–274. https://doi.org/10.1126/science.1133427

Stamatelos, S. K., Bhargava, A., Kim, E., Popel, A. S., & Pathak, A. P. (2019). Tumor Ensemble-Based Modeling and Visualization of Emergent Angiogenic Heterogeneity in Breast Cancer. *Scientific Reports*, *9*(1), 5276. https://doi.org/10.1038/s41598-019-40888-w

Sullivan, M. R., Danai, L. V., Lewis, C. A., Chan, S. H., Gui, D. Y., Kunchok, T., Dennstedt, E. A., Vander Heiden, M. G., & Muir, A. (2019). Quantification of microenvironmental

metabolites in murine cancers reveals determinants of tumor nutrient availability. *eLife*, *8*, e44235. https://doi.org/10.7554/eLife.44235

Sun, H., Chen, L., Cao, S., Liang, Y., & Xu, Y. (2019). Warburg Effects in Cancer and Normal Proliferating Cells: Two Tales of the Same Name. *Genomics, Proteomics & Bioinformatics*, *17*(3), 273–286. https://doi.org/10.1016/j.gpb.2018.12.006

Sun, Y., Wang, H., Qu, T., Luo, J., An, P., Ren, F., Luo, Y., & Li, Y. (2023). mTORC2: A multifaceted regulator of autophagy. *Cell Communication and Signaling*, *21*(1), 4. https://doi.org/10.1186/s12964-022-00859-7

Sung, Y., Yu, Y. C., & Han, J. M. (2023). Nutrient sensors and their crosstalk. *Experimental & Molecular Medicine*, *55*(6), Article 6. https://doi.org/10.1038/s12276-023-01006-z

Syed, N., Langer, J., Janczar, K., Singh, P., Lo Nigro, C., Lattanzio, L., Coley, H. M., Hatzimichael, E., Bomalaski, J., Szlosarek, P., Awad, M., O'Neil, K., Roncaroli, F., & Crook, T. (2013). Epigenetic status of argininosuccinate synthetase and argininosuccinate lyase modulates autophagy and cell death in glioblastoma. *Cell Death & Disease*, *4*(1), e458–e458. https://doi.org/10.1038/cddis.2012.197

Tanaka, N., Kanatani, S., Tomer, R., Sahlgren, C., Kronqvist, P., Kaczynska, D., Louhivuori, L., Kis, L., Lindh, C., Mitura, P., Stepulak, A., Corvigno, S., Hartman, J., Micke, P., Mezheyeuski, A., Strell, C., Carlson, J. W., Fernández Moro, C., Dahlstrand, H., … Uhlén, P. (2017). Whole-tissue biopsy phenotyping of three-dimensional tumours reveals patterns of cancer heterogeneity. *Nature Biomedical Engineering*, *1*(10), 796–806. https://doi.org/10.1038/s41551-017-0139-0

Tardito, S., Oudin, A., Ahmed, S. U., Fack, F., Keunen, O., Zheng, L., Miletic, H., Sakariassen, P. Ø., Weinstock, A., Wagner, A., Lindsay, S. L., Hock, A. K., Barnett, S. C., Ruppin, E.,

Mørkve, S. H., Lund-Johansen, M., Chalmers, A. J., Bjerkvig, R., Niclou, S. P., & Gottlieb, E. (2015). Glutamine Synthetase activity fuels nucleotide biosynthesis and supports growth of glutamine-restricted glioblastoma. *Nature Cell Biology*, *17*(12), 1556–1568. https://doi.org/10.1038/ncb3272

Teske, B. F., Fusakio, M. E., Zhou, D., Shan, J., McClintick, J. N., Kilberg, M. S., & Wek, R. C. (2013). CHOP induces activating transcription factor 5 (ATF5) to trigger apoptosis in response to perturbations in protein homeostasis. *Molecular Biology of the Cell*, *24*(15), 2477–2490. https://doi.org/10.1091/mbc.e13-01-0067

Thistlethwaite, L. R., Li, X., Burrage, L. C., Riehle, K., Hacia, J. G., Braverman, N., Wangler, M. F., Miller, M. J., Elsea, S. H., & Milosavljevic, A. (2022). Clinical diagnosis of metabolic disorders using untargeted metabolomic profiling and disease-specific networks learned from profiling data. *Scientific Reports*, *12*(1), Article 1. https://doi.org/10.1038/s41598-022-10415-5

Thomson, D. M., & Winder, W. W. (2009). AMPK Control of Fat Metabolism in Skeletal Muscle. *Acta Physiologica (Oxford, England)*, *196*(1), 147–154. https://doi.org/10.1111/j.1748-1716.2009.01973.x

Tian, H., McKnight, S. L., & Russell, D. W. (1997). Endothelial PAS domain protein 1 (EPAS1), a transcription factor selectively expressed in endothelial cells. *Genes & Development*, *11*(1), 72–82. https://doi.org/10.1101/gad.11.1.72

Tiede, L. M., Cook, E. A., Morsey, B., & Fox, H. S. (2011). Oxygen matters: Tissue culture oxygen levels affect mitochondrial function and structure as well as responses to HIV viroproteins. *Cell Death & Disease*, *2*(12), e246. https://doi.org/10.1038/cddis.2011.128

Timpano, S., Guild, B. D., Specker, E. J., Melanson, G., Medeiros, P. J., Sproul, S. L. J., & Uniacke, J. (2019). Physioxic human cell culture improves viability, metabolism, and mitochondrial morphology while reducing DNA damage. *FASEB Journal: Official Publication of the Federation of American Societies for Experimental Biology*, *33*(4), 5716–5728. https://doi.org/10.1096/fj.201802279R

Tiziani, S., Kang, Y., Harjanto, R., Axelrod, J., Piermarocchi, C., Roberts, W., & Paternostro, G. (2013). Metabolomics of the Tumor Microenvironment in Pediatric Acute Lymphoblastic Leukemia. *PLOS ONE*, *8*(12), e82859. https://doi.org/10.1371/journal.pone.0082859

Tokunaga, M., Kami, K., Ozawa, S., Oguma, J., Kazuno, A., Miyachi, H., Ohashi, Y., Kusuhara, M., & Terashima, M. (2018). Metabolome analysis of esophageal cancer tissues using capillary electrophoresis-time-of-flight mass spectrometry. *International Journal of Oncology*, *52*(6), 1947–1958. https://doi.org/10.3892/ijo.2018.4340

Tomlinson, I. P. M., Alam, N. A., Rowan, A. J., Barclay, E., Jaeger, E. E. M., Kelsell, D., Leigh, I., Gorman, P., Lamlum, H., Rahman, S., Roylance, R. R., Olpin, S., Bevan, S., Barker, K., Hearle, N., Houlston, R. S., Kiuru, M., Lehtonen, R., Karhu, A., … Group 3. (2002). Germline mutations in FH predispose to dominantly inherited uterine fibroids, skin leiomyomata and papillary renal cell cancer. *Nature Genetics*, *30*(4), 406–410. https://doi.org/10.1038/ng849

Tönjes, M., Barbus, S., Park, Y. J., Wang, W., Schlotter, M., Lindroth, A. M., Pleier, S. V., Bai, A. H. C., Karra, D., Piro, R. M., Felsberg, J., Addington, A., Lemke, D., Weibrecht, I., Hovestadt, V., Rolli, C. G., Campos, B., Turcan, S., Sturm, D., … Radlwimmer, B. (2013). BCAT1 promotes cell proliferation through amino acid catabolism in gliomas

carrying wild-type IDH1. *Nature Medicine*, *19*(7), 901–908. https://doi.org/10.1038/nm.3217

Torres-Quesada, O., Doerrier, C., Strich, S., Gnaiger, E., & Stefan, E. (2022). Physiological Cell Culture Media Tune Mitochondrial Bioenergetics and Drug Sensitivity in Cancer Cell Models. *Cancers*, *14*(16), Article 16. https://doi.org/10.3390/cancers14163917

Toyama, E. Q., Herzig, S., Courchet, J., Lewis, T. L., Losón, O. C., Hellberg, K., Young, N. P., Chen, H., Polleux, F., Chan, D. C., & Shaw, R. J. (2016). AMP-activated protein kinase mediates mitochondrial fission in response to energy stress. *Science*, *351*(6270), 275–281. https://doi.org/10.1126/science.aab4138

Tsai, P.-Y., Lee, M.-S., Jadhav, U., Naqvi, I., Madha, S., Adler, A., Mistry, M., Naumenko, S., Lewis, C. A., Hitchcock, D. S., Roberts, F. R., DelNero, P., Hank, T., Honselmann, K. C., Morales Oyarvide, V., Mino-Kenudson, M., Clish, C. B., Shivdasani, R. A., & Kalaany, N. Y. (2021). Adaptation of pancreatic cancer cells to nutrient deprivation is reversible and requires glutamine synthetase stabilization by mTORC1. *Proceedings of the National Academy of Sciences*, *118*(10), e2003014118. https://doi.org/10.1073/pnas.2003014118

Tsun, Z.-Y., Bar-Peled, L., Chantranupong, L., Zoncu, R., Wang, T., Kim, C., Spooner, E., & Sabatini, D. M. (2013). The Folliculin tumor suppressor is a GAP for RagC/D GTPases that signal amino acid levels to mTORC1. *Molecular Cell*, *52*(4), 10.1016/j.molcel.2013.09.016. https://doi.org/10.1016/j.molcel.2013.09.016

van Ineveld, R. L., Kleinnijenhuis, M., Alieva, M., de Blank, S., Barrera Roman, M., van Vliet, E. J., Martínez Mir, C., Johnson, H. R., Bos, F. L., Heukers, R., Chuva de Sousa Lopes, S. M., Drost, J., Dekkers, J. F., Wehrens, E. J., & Rios, A. C. (2021). Revealing the

spatio-phenotypic patterning of cells in healthy and tumor tissues with mLSR-3D and STAPL-3D. *Nature Biotechnology*, *39*(10), 1239–1245. https://doi.org/10.1038/s41587-021-00926-3

van Pelt, J., Meeusen, B., Derua, R., Guffens, L., Van Cutsem, E., Janssens, V., & Verslype, C. (2023). Human pancreatic cancer patients with Epithelial-to-Mesenchymal Transition and an aggressive phenotype show a disturbed balance in Protein Phosphatase Type 2A expression and functionality. *Journal of Translational Medicine*, *21*(1), 317. https://doi.org/10.1186/s12967-023-04145-z

Vande Voorde, J., Ackermann, T., Pfetzer, N., Sumpton, D., Mackay, G., Kalna, G., Nixon, C., Blyth, K., Gottlieb, E., & Tardito, S. (2019). Improving the metabolic fidelity of cancer models with a physiological cell culture medium. *Science Advances*, *5*(1), eaau7314. https://doi.org/10.1126/sciadv.aau7314

Vander Heiden, M. G., Cantley, L. C., & Thompson, C. B. (2009). Understanding the Warburg Effect: The Metabolic Requirements of Cell Proliferation. *Science*, *324*(5930), 1029–1033. https://doi.org/10.1126/science.1160809

Vaupel, P., Flood, A. B., & Swartz, H. M. (2021). Oxygenation Status of Malignant Tumors vs. Normal Tissues: Critical Evaluation and Updated Data Source Based on Direct Measurements with pO2 Microsensors. *Applied Magnetic Resonance*, *52*(10), 1451–1479. https://doi.org/10.1007/s00723-021-01383-6

Vaupel, P., Höckel, M., & Mayer, A. (2007). Detection and characterization of tumor hypoxia using pO2 histography. *Antioxidants & Redox Signaling*, *9*(8), 1221–1235. https://doi.org/10.1089/ars.2007.1628

Vaupel, P., Kallinowski, F., & Okunieff, P. (1989). *Blood Flow, Oxygen and Nutrient Supply, and Metabolic Microenvironment of Human Tumors: A Review*.

Vaupel, P., & Mayer, A. (2012). Availability, not respiratory capacity governs oxygen consumption of solid tumors. *The International Journal of Biochemistry & Cell Biology*, *44*(9), 1477–1481. https://doi.org/10.1016/j.biocel.2012.05.019

Vaupel, P., Mayer, A., Briest, S., & Höckel, M. (2003). Oxygenation Gain Factor: A Novel Parameter Characterizing the Association between Hemoglobin Level and the Oxygenation Status of Breast Cancers. *Cancer Research*, *63*(22), 7634–7637.

Vaz, C. V., Alves, M. G., Marques, R., Moreira, P. I., Oliveira, P. F., Maia, C. J., & Socorro, S. (2012). Androgen-responsive and nonresponsive prostate cancer cells present a distinct glycolytic metabolism profile. *The International Journal of Biochemistry & Cell Biology*, *44*(11), 2077–2084. https://doi.org/10.1016/j.biocel.2012.08.013

Vecchio, E., Caiazza, C., Mimmi, S., Avagliano, A., Iaccino, E., Brusco, T., Nisticò, N., Maisano, D., Aloisio, A., Quinto, I., Renna, M., Divisato, G., Romano, S., Tufano, M., D'Agostino, M., Vigliar, E., Iaccarino, A., Mignogna, C., Andreozzi, F., … Fiume, G. (2021). Metabolites Profiling of Melanoma Interstitial Fluids Reveals Uridine Diphosphate as Potent Immune Modulator Capable of Limiting Tumor Growth. *Frontiers in Cell and Developmental Biology*, *9*. https://www.frontiersin.org/articles/10.3389/fcell.2021.730726

Verma, S., Shankar, E., Chan, E. R., & Gupta, S. (2020). Metabolic Reprogramming and Predominance of Solute Carrier Genes during Acquired Enzalutamide Resistance in Prostate Cancer. *Cells*, *9*(12), 2535. https://doi.org/10.3390/cells9122535

Vicente-Dueñas, C., Romero-Camarero, I., Cobaleda, C., & Sánchez-García, I. (2013). Function of oncogenes in cancer development: A changing paradigm. *The EMBO Journal*, *32*(11), 1502–1513. https://doi.org/10.1038/emboj.2013.97

Vogelaar, J. P., & Erlichman, E. (1933). A feeding solution for cultures of human fibroblasts. *The American Journal of Cancer*, *18*(1), 28–38.

Voutouri, C., Polydorou, C., Papageorgis, P., Gkretsi, V., & Stylianopoulos, T. (2016). Hyaluronan-Derived Swelling of Solid Tumors, the Contribution of Collagen and Cancer Cells, and Implications for Cancer Therapy. *Neoplasia (New York, N.Y.)*, *18*(12), 732–741. https://doi.org/10.1016/j.neo.2016.10.001

Wagner, M., & Wiig, H. (2015). Tumor Interstitial Fluid Formation, Characterization, and Clinical Implications. *Frontiers in Oncology*, *5*. https://doi.org/10.3389/fonc.2015.00115

Wang, G. L., Jiang, B. H., Rue, E. A., & Semenza, G. L. (1995). Hypoxia-inducible factor 1 is a basic-helix-loop-helix-PAS heterodimer regulated by cellular O2 tension. *Proceedings of the National Academy of Sciences*, *92*(12), 5510–5514. https://doi.org/10.1073/pnas.92.12.5510

Wang, J., Peng, W., Yu, A., Fokar, M., & Mechref, Y. (2022a). Comparative Transcriptomics and Proteomics of Cancer Cell Lines Cultivated by Physiological and Commercial Media. *Biomolecules*, *12*(11), Article 11. https://doi.org/10.3390/biom12111575

Wang, J., Peng, W., Yu, A., Fokar, M., & Mechref, Y. (2022b). Glycome Profiling of Cancer Cell Lines Cultivated in Physiological and Commercial Media. *Biomolecules*, *12*(6), 743. https://doi.org/10.3390/biom12060743

Wang, K., Yorke, E., Nehmeh, S. A., Humm, J. L., & Ling, C. C. (2009). Modeling acute and chronic hypoxia using serial images of 18F-FMISO PET. *Medical Physics*, *36*(10), 4400–4408. https://doi.org/10.1118/1.3213092

Wang, W., Shen, T., Dong, B., Creighton, C. J., Meng, Y., Zhou, W., Shi, Q., Zhou, H., Zhang, Y., Moore, D. D., & Yang, F. (2019). MAPK4 overexpression promotes tumor progression via noncanonical activation of AKT/mTOR signaling. *The Journal of Clinical Investigation*, *129*(3), 1015–1029. https://doi.org/10.1172/JCI97712

Wang, Y., Stancliffe, E., Fowle-Grider, R., Wang, R., Wang, C., Schwaiger-Haber, M., Shriver, L. P., & Patti, G. J. (2022). Saturation of the mitochondrial NADH shuttles drives aerobic glycolysis in proliferating cells. *Molecular Cell*, *82*(17), 3270-3283.e9. https://doi.org/10.1016/j.molcel.2022.07.007

Wang, Z., Bian, L., Mo, C., Shen, H., Zhao, L. J., Su, K.-J., Kukula, M., Lee, J. T., Armstrong, D. W., Recker, R., Lappe, J., Bonewald, L. F., Deng, H.-W., & Brotto, M. (2020). Quantification of aminobutyric acids and their clinical applications as biomarkers for osteoporosis. *Communications Biology*, *3*(1), Article 1. https://doi.org/10.1038/s42003-020-0766-y

Warburg, O. (1956). On the Origin of Cancer Cells. *Science*, *123*(3191), 309–314. https://doi.org/10.1126/science.123.3191.309

Watanabe, T., Tomioka, N. H., Watanabe, S., Tsuchiya, M., & Hosoyamada, M. (2014). False in vitro and in vivo elevations of uric acid levels in mouse blood. *Nucleosides, Nucleotides & Nucleic Acids*, *33*(4–6), 192–198. https://doi.org/10.1080/15257770.2013.865742

Wei, Z., Liu, X., Cheng, C., Yu, W., & Yi, P. (2021). Metabolism of Amino Acids in Cancer. *Frontiers in Cell and Developmental Biology*, *8*. https://www.frontiersin.org/articles/10.3389/fcell.2020.603837

Wibom, C., Surowiec, I., Mörén, L., Bergström, P., Johansson, M., Antti, H., & Bergenheim, A. T. (2010). Metabolomic Patterns in Glioblastoma and Changes during Radiotherapy: A Clinical Microdialysis Study. *Journal of Proteome Research*, *9*(6), 2909–2919. https://doi.org/10.1021/pr901088r

Wiig, H., & Swartz, M. A. (2012). Interstitial Fluid and Lymph Formation and Transport: Physiological Regulation and Roles in Inflammation and Cancer. *Physiological Reviews*, *92*(3), 1005–1060. https://doi.org/10.1152/physrev.00037.2011

Wike-Hooley, J. L., Haveman, J., & Reinhold, H. S. (1984). The relevance of tumour pH to the treatment of malignant disease. *Radiotherapy and Oncology: Journal of the European Society for Therapeutic Radiology and Oncology*, *2*(4), 343–366. https://doi.org/10.1016/s0167-8140(84)80077-8

Wilhelm, C., Hackenberg, S., Bregenzer, M., Meyer, T., Gehrke, T., Kleinsasser, N., Hagen, R., & Scherzad, A. (2021). Effect of Hypoxia on Proliferation and the Expression of the Genes HIF-1α and JMJD1A in Head and Neck Squamous Cell Carcinoma Cell Lines. *Anticancer Research*, *41*(1), 113–122. https://doi.org/10.21873/anticanres.14756

Williams, R. T., Guarecuco, R., Gates, L. A., Barrows, D., Passarelli, M. C., Carey, B., Baudrier, L., Jeewajee, S., La, K., Prizer, B., Malik, S., Garcia-Bermudez, J., Zhu, X. G., Cantor, J., Molina, H., Carroll, T., Roeder, R. G., Abdel-Wahab, O., Allis, C. D., & Birsoy, K. (2020). ZBTB1 Regulates Asparagine Synthesis and Leukemia Cell Response to L-Asparaginase. *Cell Metabolism*, *31*(4), 852. https://doi.org/10.1016/j.cmet.2020.03.008

Wishart, D. S., Feunang, Y. D., Marcu, A., Guo, A. C., Liang, K., Vázquez-Fresno, R., Sajed, T., Johnson, D., Li, C., Karu, N., Sayeeda, Z., Lo, E., Assempour, N., Berjanskii, M., Singhal, S., Arndt, D., Liang, Y., Badran, H., Grant, J., … Scalbert, A. (2018). HMDB 4.0: The human metabolome database for 2018. *Nucleic Acids Research*, *46*(D1), D608–D617. https://doi.org/10.1093/nar/gkx1089

Wishart, D. S., Lewis, M. J., Morrissey, J. A., Flegel, M. D., Jeroncic, K., Xiong, Y., Cheng, D., Eisner, R., Gautam, B., Tzur, D., Sawhney, S., Bamforth, F., Greiner, R., & Li, L. (2008). The human cerebrospinal fluid metabolome. *Journal of Chromatography B*, *871*(2), 164–173. https://doi.org/10.1016/j.jchromb.2008.05.001

Wolfson, R. L., Chantranupong, L., Saxton, R. A., Shen, K., Scaria, S. M., Cantor, J. R., & Sabatini, D. M. (2016). Sestrin2 is a leucine sensor for the mTORC1 pathway. *Science (New York, N.Y.)*, *351*(6268), 43–48. https://doi.org/10.1126/science.aab2674

Wu, Q.-R., Zheng, D.-L., Liu, P.-M., Yang, H., Li, L.-A., Kuang, S.-J., Lai, Y.-Y., Rao, F., Xue, Y.-M., Lin, J.-J., Liu, S.-X., Chen, C.-B., & Deng, C.-Y. (2021). High glucose induces Drp1-mediated mitochondrial fission via the Orai1 calcium channel to participate in diabetic cardiomyocyte hypertrophy. *Cell Death & Disease*, *12*(2), 1–15. https://doi.org/10.1038/s41419-021-03502-4

Xiao, L., Zhu, H., Shu, J., Gong, D., Zheng, D., & Gao, J. (2022). Overexpression of TGF-β1 and SDF-1 in cervical cancer-associated fibroblasts promotes cell growth, invasion and migration. *Archives of Gynecology and Obstetrics*, *305*(1), 179–192. https://doi.org/10.1007/s00404-021-06137-0

Xiao, Y., Chen, W., Xie, Z., Shao, Z., Xie, H., Qin, G., & Zhao, N. (2017). Prognostic relevance of lactate dehydrogenase in advanced pancreatic ductal adenocarcinoma patients. *BMC Cancer*, *17*, 25. https://doi.org/10.1186/s12885-016-3012-8

Xu, W., Yang, H., Liu, Y., Yang, Y., Wang, P., Kim, S.-H., Ito, S., Yang, C., Wang, P., Xiao, M.-T., Liu, L., Jiang, W., Liu, J., Zhang, J., Wang, B., Frye, S., Zhang, Y., Xu, Y., Lei, Q., … Xiong, Y. (2011). Oncometabolite 2-hydroxyglutarate is a competitive inhibitor of α-ketoglutarate-dependent dioxygenases. *Cancer Cell*, *19*(1), 17–30. https://doi.org/10.1016/j.ccr.2010.12.014

Yamaguchi, H., & Wang, H.-G. (2004). CHOP is involved in endoplasmic reticulum stress-induced apoptosis by enhancing DR5 expression in human carcinoma cells. *The Journal of Biological Chemistry*, *279*(44), 45495–45502. https://doi.org/10.1074/jbc.M406933200

Yang, H., Jiang, X., Li, B., Yang, H. J., Miller, M., Yang, A., Dhar, A., & Pavletich, N. P. (2017). Structural Mechanisms of mTORC1 activation by RHEB and inhibition by PRAS40. *Nature*, *552*(7685), 368–373. https://doi.org/10.1038/nature25023

Yang, S., Zhang, Z., Hao, Y., Zhao, Y., Qian, F., Shi, Y., Li, P., Liu, C., & Yu, P. (2017). HIF-1α induces the epithelial-mesenchymal transition in gastric cancer stem cells through the Snail pathway. *Oncotarget*, *8*(6), 9535–9545. https://doi.org/10.18632/oncotarget.14484

Yang, X., & Potts, P. R. (2020). CSAG2 is a cancer-specific activator of SIRT1. *EMBO Reports*, *21*(9), e50912. https://doi.org/10.15252/embr.202050912

Yano, S., Zhang, Y., Miwa, S., Tome, Y., Hiroshima, Y., Uehara, F., Yamamoto, M., Suetsugu, A., Kishimoto, H., Tazawa, H., Zhao, M., Bouvet, M., Fujiwara, T., & Hoffman, R. M. (2014). Spatial–temporal FUCCI imaging of each cell in a tumor demonstrates locational

dependence of cell cycle dynamics and chemoresponsiveness. *Cell Cycle*, *13*(13), 2110–2119. https://doi.org/10.4161/cc.29156

Yao, L., Cao, B., Cheng, Q., Cai, W., Ye, C., Liang, J., Liu, W., Tan, L., Yan, M., Li, B., He, J., Hwang, S. H., Zhang, X., Wang, C., Ai, D., Hammock, B. D., & Zhu, Y. (2019). Inhibition of soluble epoxide hydrolase ameliorates hyperhomocysteinemia-induced hepatic steatosis by enhancing β-oxidation of fatty acid in mice. *American Journal of Physiology-Gastrointestinal and Liver Physiology*, *316*(4), G527–G538. https://doi.org/10.1152/ajpgi.00148.2018

Yao, S. Y. M., Ng, A. M. L., Cass, C. E., Baldwin, S. A., & Young, J. D. (2011). Nucleobase transport by human equilibrative nucleoside transporter 1 (hENT1). *The Journal of Biological Chemistry*, *286*(37), 32552–32562. https://doi.org/10.1074/jbc.M111.236117

Ye, J., Kumanova, M., Hart, L. S., Sloane, K., Zhang, H., De Panis, D. N., Bobrovnikova-Marjon, E., Diehl, J. A., Ron, D., & Koumenis, C. (2010). The GCN2-ATF4 pathway is critical for tumour cell survival and proliferation in response to nutrient deprivation. *The EMBO Journal*, *29*(12), 2082–2096. https://doi.org/10.1038/emboj.2010.81

Yu, M., Bardia, A., Wittner, B. S., Stott, S. L., Smas, M. E., Ting, D. T., Isakoff, S. J., Ciciliano, J. C., Wells, M. N., Shah, A. M., Concannon, K. F., Donaldson, M. C., Sequist, L. V., Brachtel, E., Sgroi, D., Baselga, J., Ramaswamy, S., Toner, M., Haber, D. A., & Maheswaran, S. (2013). Circulating Breast Tumor Cells Exhibit Dynamic Changes in Epithelial and Mesenchymal Composition. *Science*, *339*(6119), 580–584. https://doi.org/10.1126/science.1228522

Yu, Y., Wang, W., Lu, W., Chen, W., & Shang, A. (2021). Inhibin β-A (INHBA) induces epithelial-mesenchymal transition and accelerates the motility of breast cancer cells by

activating the TGF-β signaling pathway. *Bioengineered*, *12*(1), 4681–4696. https://doi.org/10.1080/21655979.2021.1957754

Yuan, F., Salehi, H. A., Boucher, Y., Vasthare, U. S., Tuma, R. F., & Jain, R. K. (1994). Vascular permeability and microcirculation of gliomas and mammary carcinomas transplanted in rat and mouse cranial windows. *Cancer Research*, *54*(17), 4564–4568.

Zhang, D., Tang, Z., Huang, H., Zhou, G., Cui, C., Weng, Y., Liu, W., Kim, S., Lee, S., Perez-Neut, M., Ding, J., Czyz, D., Hu, R., Ye, Z., He, M., Zheng, Y. G., Shuman, H. A., Dai, L., Ren, B., … Zhao, Y. (2019). Metabolic regulation of gene expression by histone lactylation. *Nature*, *574*(7779), 575–580. https://doi.org/10.1038/s41586-019-1678-1

Zhang, L., & Han, J. (2017). Branched-chain amino acid transaminase 1 (BCAT1) promotes the growth of breast cancer cells through improving mTOR-mediated mitochondrial biogenesis and function. *Biochemical and Biophysical Research Communications*, *486*(2), 224–231. https://doi.org/10.1016/j.bbrc.2017.02.101

Zhang, P., Yao, Q., Lu, L., Li, Y., Chen, P.-J., & Duan, C. (2014). Hypoxia-Inducible Factor 3 Is an Oxygen-Dependent Transcription Activator and Regulates a Distinct Transcriptional Response to Hypoxia. *Cell Reports*, *6*(6), 1110–1121. https://doi.org/10.1016/j.celrep.2014.02.011

Zhang, Y., Ren, S., Liu, Y., Gao, K., Liu, Z., & Zhang, Z. (2017). Inhibition of Starvation-Triggered Endoplasmic Reticulum Stress, Autophagy, and Apoptosis in ARPE-19 Cells by Taurine through Modulating the Expression of Calpain-1 and Calpain-2. *International Journal of Molecular Sciences*, *18*(10), 2146. https://doi.org/10.3390/ijms18102146

Zhong, H., De Marzo, A. M., Laughner, E., Lim, M., Hilton, D. A., Zagzag, D., Buechler, P., Isaacs, W. B., Semenza, G. L., & Simons, J. W. (1999). Overexpression of hypoxia-

inducible factor 1alpha in common human cancers and their metastases. *Cancer Research, 59*(22), 5830–5835.

Zou, Z., Tao, T., Li, H., & Zhu, X. (2020). mTOR signaling pathway and mTOR inhibitors in cancer: Progress and challenges. *Cell & Bioscience, 10*(1), 31. https://doi.org/10.1186/s13578-020-00396-1